DOE/ET/23007-80/1
(DE81024093)

PLANETARY BOUNDARY LAYER WIND MODEL EVALUATION AT A MID-ATLANTIC COASTAL SITE

By
H. W. Tieleman

October 1980

Work Performed Under Contract No. AC06-79ET23007

Virginia Polytechnic Institute and
State University
Blacksburg, Virginia

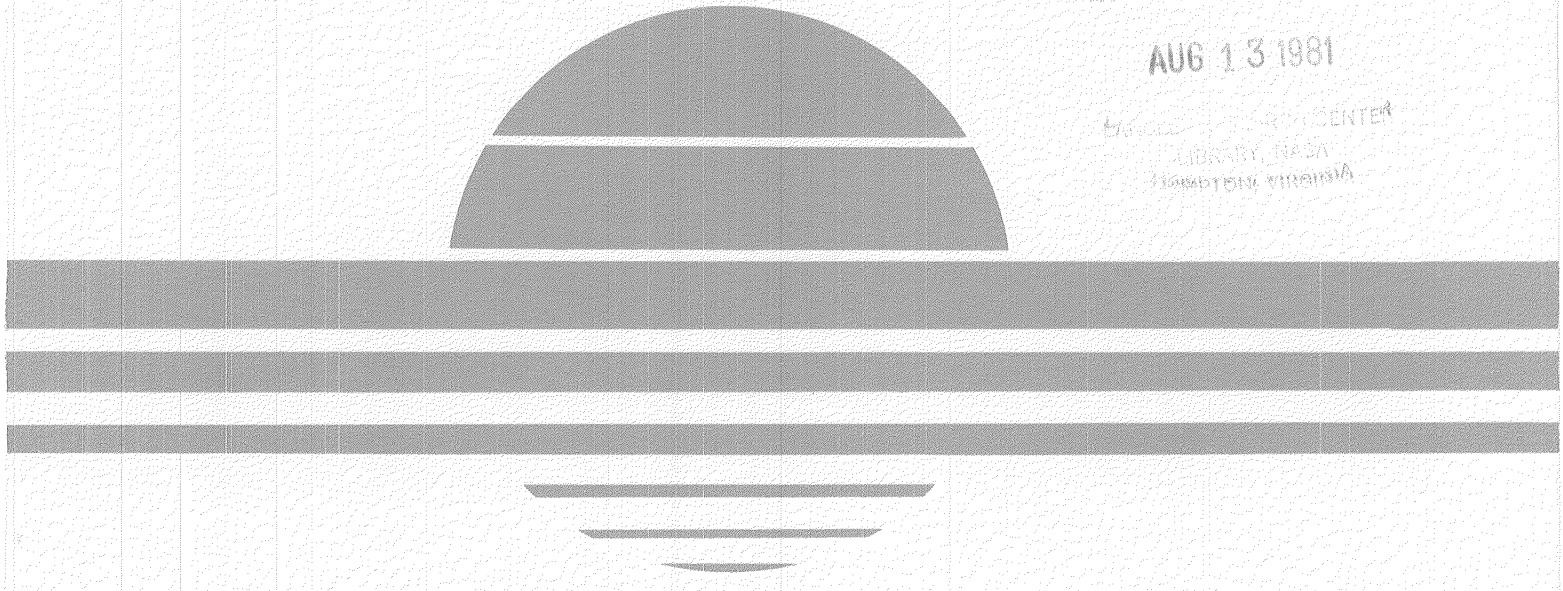

U.S. Department of Energy

Solar Energy

DISCLAIMER

DOE/ET/23007-80/1
(DE81024093)
Distribution Category UC-60

PLANETARY BOUNDARY LAYER WIND MODEL EVALUATION AT A MID-ATLANTIC COASTAL SITE

H. W. Tieleman
Department of Engineering Science and Mechanics
Virginia Polytechnic Institute and State University
Blacksburg, Virginia 24061

October 1980

Prepared for the

U.S. Department of Energy
Office of Solar Power Applications

FEDERAL WIND ENERGY PROGRAM

DOE Contract No. DE-AC06-79ET23007

This Page Intentionally Left Blank

ACKNOWLEDGEMENTS

Financial assistance for preparation of this report from the U. S. Department of Energy through Contract DE-AC06-79 ET 23007 is gratefully acknowledged. The development of the instrumentation, data acquisition and data handling systems and the actual data acquisition and data analysis was supported by the National Aeronautics and Space Administration, Grant NGL 47-004-067.

The continuous support of the grant officers Mr. J. F. Spurling, W. H. West, R. E. Carr, F. Schmidlin and the Director of Wallops Space Flight Center Mr. R. L. Krieger is greatly appreciated. In particular my thanks go to the technical assistance of Mr. C. A. Lewis, J. Van Overeem, P. H. Randall and R. L. Kelley without their help the success of this research program would have been impossible. A special thanks goes to Ms. E. Jane Harrison for her willing cooperation and perseverance in the typing of this report.

This Page Intentionally Left Blank

EXECUTIVE SUMMARY

Detailed measurements of the mean flow and turbulence have been made with the use of a micrometeorological facility consisting of an instrumented 76-m tall tower located within a 100-m distance from the Atlantic Ocean at Wallops Island, Virginia. An interpretation of the experimental results demonstrates that under moderately strong wind conditions (hourly mean wind speed between 10 m/s and 20 m/s at a height of 10 m), the popular neutral boundary-layer flow model fails to provide an adequate description of the actual flow.

For daytime westerly winds the convective boundary layer, which has been previously observed at sites on the continent, provides an adequate model for the surface flow at the Wallops Island site. However variations from this model have been observed for certain wind directions and under certain atmospheric conditions such as low altitude cloud cover combined with precipitation. The observed low-frequency velocity fluctuations give rise to increased turbulent intensities and larger turbulence integral scales. These low-frequency fluctuations also occur in the surface layer where the observed mean velocity profiles generally fit the logarithmic law quite well.

For on-shore winds the surface flow is complicated as the result of the development of an internal boundary layer (IBL) as the air crossing the beach generally experiences a change in surface roughness and surface temperature. The internal boundary layer has a height between 15 m and 30 m at the tower location depending on wind direction and change in surface conditions. For southerly winds the warmer air

flows over the cooler water allowing the existence of a surface-based inversion of variable depth. Under these conditions a low-altitude maximum velocity (surface jet), occasionally below the highest observation level of 76 m, has been observed. Under extreme stable conditions at hourly mean velocities in excess of 10 m/s the turbulence has been observed to vanish completely. In addition, low-frequency internal gravity waves have been observed to co-exist with the turbulence.

In addition to detailed flow information for all wind directions, averages of the important flow parameters used for design such as vertical distribution of mean velocity, turbulence intensities and turbulence integral scales have been presented for wind-direction sectors with near-uniform upstream terrain. Power spectra of the three velocity components for the prevailing northwesterly and southerly winds are presented and discussed in detail.

The experimental results indicate clearly that the non-uniformity of the upstream surface conditions, the non-neutral thermal stratification and the presence of appreciable low-frequency velocity fluctuations have a pronounced effect on the surface flow. Consequently it is impossible to find a simple and single PBL model to describe the flow at this site even under moderately strong wind conditions. Moreover, there is no evidence that under still stronger wind conditions (hourly mean wind speed at z=10 m over 20 m/s) the surface flow will alter sufficiently as to conform to the neutral boundary-layer model whose turbulence is of purely mechanical origin.

TABLE OF CONTENTS

LIST OF SYMBOLS

Symbol	Definition
C	Constant
c_p	Specific heat
f	Reduced frequency f=nz/U
$(f_o)_i$	Reduced frequency at the point of intersection of the extrapolated inertial subrange of the velocity spectra and the line $nS_i(n)/\sigma_i^2=1$ for i=u,v and w.
g	Gravitational constant
K	Von Karman's constant
k	Wave number
k_e	Wave number range of energy-containing eddies
k_1	One-dimensional wave number
L	Monin-Obukhov length scale (4)
L_i^x	Streamwise turbulence integral scale for i=u,v,w (1)
L_i^z	Vertical turbulence integral scale for i=u and v (8)
n	Frequency
Q_o	Surface heat flux
R_u	Autocorrelation function
R_{ii}^z	Vertical correlation coefficient for i=u and v (9)
Ri	Gradient Richardson number (5)
S	Three-dimensional power spectral density function
$S_i(n)$	One-dimensional power spectral density function for i=u,v and w
T	Time of integration and absolute temperature
T_1	Maximum time delay
t	Time
U	Mean Velocity

Symbol	Definition
U^*	Local friction (shear) velocity, $U^* = [\overline{uw}^2 + \overline{vw}^2]^{1/4}$
U^*_o	Friction (shear) velocity obtained from the logarithmic velocity profile (2)
U_R	Reference velocity
u,v,w	Turbulence velocity components in x,y and z directions respectively
V	Magnitude of mean velocity
x,y,z	Mean wind coordinates
z'	Vertical separation distance
z_o	Roughness length (2)
z_R	Reference height
α	Power law exponent of mean velocity profile (6)
γ_a	Adiabatic lapse rate
Θ	Absolute temperature
θ	Temperature fluctuations
λ	Wavelength
λ_m	Wavelength associated with spectral peak
λ_o	Wavelength associated with f_o
ρ	Air density
σ_i	Standard deviation of the fluctuating velocity compoent i=u,v and w
τ	Time delay
τ_o	Surface stress
ϕ	Wind direction
ψ	Universal function of z/L (3)
$\uparrow$	Upward integration for one-sided integral scales (8, 9)
$\downarrow$	Downward integration for one-sided integral scales (8,9)
$\updownarrow$	Two-sided integration for two-sided integral scales (10, 11)

LIST OF FIGURES

FIGURE PAGE

FIGURE PAGE

LIST OF TABLES

This Page Intentionally Left Blank

1. INTRODUCTION

The purpose of this report is to provide information on the local wind climate at a mid-Atlantic coastal site. The acquired information can be used for the design of wind-turbine generators at similar sites. Since wind is a very important design parameter for these generators, information is provided in this report on wind speed, wind direction, wind shear and wind turbulence.

The data presented in this report were collected from an instrumented meteorological tower, 76.2 m (250 feet) tall and located at Wallops Island. This island is one of the barrier islands at the Atlantic coast along the Eastern Shore of Virginia and is used by the National Aeronautics and Space Administration as a sounding rocket launch facility. The results acquired from this facility should be typical for any Atlantic coastal site, although local effects such as upstream buildings and obstacles and changes in surface roughness and surface temperature modify the flow near the surface. At Wallops Island, the surrounding terrain beyond a distance of 100-300 m from the tower can be considered as homogeneous and uniform, so that the flow above a height of approximately 10-30 m should not be affected by local terrain nonuniformities.

The wind and temperature data from this site were acquired under moderately strong wind conditions with an hourly mean velocity of at least 10 m/s at the 76.2 m (250 ft) level. For wind directions between northeast and southwest this requirement had to be reduced to approximately 8 m/s, since strong winds from this sector occur very seldom.

Mean wind and turbulence measurements were made with two types of instrumentation consisting of cup-vanes and resistance temperature probes primarily used for mean profile measurements of velocity and temperature respectively. In addition, the cup-vane instruments were used for turbulence intensities of the two horizontal velocity components and horizontal and vertical turbulence integral scales. The hot-film and thermocouple system was used for measurement of turbulence intensities, turbulence fluxes and velocity spectra in all three directions. The cup-vane system was used to acquire wind data from all directions, while the hot-film system was only used for turbulence measurements from the two prevailing wind directions, south and northwest.

The results of this experimental research are presented in a form suitable for design purposes. Where ever possible the results are also compared with previously published results and with existing empirical models for near-neutrally stratified low-level winds.

2. SITE DESCRIPTION

Wallops Island consists of a narrow strip of dunes, approximately 3 meters above sea level, and is situated in a northeast-southwest direction. The island is separated from the "Delmarva" peninsula by a tidal marsh on the west side, and with the Atlantic Ocean on the east.

Winds with directions varying between west and north are usually encountered following the passage of a cold front. Winds from this sector will have crossed in succession (Fig. 1) the mainland, the Chesapeake Bay (20-50 km), the "Delmarva" peninsula (20-50 km) and the tidal marsh (3-5 km). Depending on the wind direction, for the last

200-300 m the air travels over land before it arrives at the tower location (Fig. 2). The tidal marsh between the island and the peninsula consists of shallow areas of water interchanged with swamp vegetation, mostly grass of a maximum height of 1 m. Some taller vegetation consisting of bushes and brush of a maximum height of 5 m exists in several upstream directions. For wind directions between 255° and 270°, a 6.5 m high rocket fuel storage bunker is approximately 90 m upstream (Fig. 2). An elevated roadway (levee) 2 m above the surrounding terrain passes the tower on the west side within 200 m. Winds with directions varying between north-east and south approach the island from the Atlantic Ocean.

Sectors with approximately the same immediate upstream roughness have been established as shown in Fig. 3. Between 0° (north) and 30° the upstream terrain features two bunkers within a distance of 100 m from the tower. In addition, a few small buildings and intermittent patches of brush are upstream as far as 750 m. Between 30° and 45° (wind direction parallel to the island) many buildings are upstream and winds in this sector should encounter the roughest terrain at this site over a distance of approximately 4 km. For wind directions between 45° and 210° the winds approach the island over water, and cross the beach at varying distances from the tower depending on the direction. For wind directions between 140° and 170° a one-story rocket assembly building is about 100 m upstream of the tower. The prevailing southerly winds vary in direction between 170° and 210°, however in the sector between 195° and 210° the 45-m tall Aerobee tower and associated buildings are about 300 m upstream. For directions between 210° and 230°, the wind direction is approximately parallel to the island

with part of the Aerobee tower complex approximately 300 m upstream. In this same sector a few other buildings, levees and sand dunes are upstream at greater distances. Between 230° and 330° the upstream terrain is very uniform with no big obstacles other than the aforementioned bunker and roadway. For the sector between 330° and 360°, several patches of brush, 2 levees and one radar building are upstream of the tower within a distance of 500 m with marsh at further upstream distances.

3. INSTRUMENTATION

3.1 Cup-Vane Instruments

The 76 m (250 ft) micrometeorological tower is a self-standing non-guyed tower with working platforms at 15.2 m (50 ft) intervals (Fig. 4). The cup-vane velocity-direction instruments and aspirated temperature probes both primarily used for profile measurements are mounted at 5 levels near each platform. Two sets of cup-vane instruments are mounted at each level on 2m booms on opposite sites of the tower (Fig. 4). An automatic electronic switching circuit ensures that data are taken only with the instruments on the upwind side of the tower. The electronics associated with this instrumentation system, together with a digital readout panel of all instruments from one side of the tower, are located in a small instrumentation building at the base of the tower (Fig. 4). From this location the digitized data are transmitted to the NASA control center at the main base on the peninsula about 13 km to the northwest. Here the data from each level sampled at a rate of 1 sample each 2 seconds are recorded on digital tape. At this sample rate, data can be acquired without interruption for about

8 hours. This instrumentation system is used by NASA in conjunction with its rocket launching operations. Regularly scheduled maintenance and calibration of this system are performed by personnel under NASA's supervision.

3.2 Hot-film Anemometers

Six three-dimensional split-film anemometers (TSI-1080D) are used for turbulence measurements, which include turbulence intensities, turbulence fluxes, spectra and cross spectra of all three turbulence components and temperature. These anemometer systems were chosen for this research program since they have the advantage of small physical size, fast response and high sensitivity over a wide range of velocities. The instruments are mounted on 1.8 m booms at the same levels as the cup-vane instruments and also at the 9 m (30 ft) level. Each hot-film probe is mounted on a rotor, which is capable of rotating the probe about a vertical axis so as to align the probe axis approximately into the mean wind direction. The probe-rotor combination is mounted on a 1.8 m-boom, which in turn is mounted on the railing at each platform. The probes were mounted on the south side of the tower for measurement of the prevailing south winds during the summer and on the north side of the tower for measurement of the prevailing northwest winds during the winter and spring. The electronics as well as the data-acquisition and data-handling system for this instrumentation system are located in an instrumentation trailer parked at the base of the tower (Fig. 4).

Each hot-film probe consists of three split-film sensors used for measurement of wind speed and direction and a copper-constantan thermocouple used for temperature measurements. Each sensor consists of a 0.15 mm diameter quartz rod coated with a platinum film of about

1000 angstrom in thickness. The platinum film on each rod consists of two segments, separated from each other by two longitudinal splits 180° apart. The active elements on each rod are electrically heated to the same constant temperature by separate anemometer circuits. The total sensor length is about 5 mm, and the three sensors are mounted mutually perpendicular to form a Cartesian coordinate system. When the instruments are not used for data acquisition, the three sensors and thermocouple are protected by an aluminum shield which can be moved pneumatically to cover the sensors. As an added precaution, dry filtered air is allowed to blow across the sensors when the shield covers the sensors. This is done to protect the sensors from contamination in the salt-air environment and moisture while not in operation. For a more detailed review of the hot-film anemometer system the reader is advised to consult Reference 1.

Calibration of the hot-film anemometers is carried out in a low-speed wind tunnel located at the main base. In order to obtain data of a desired accuracy from the hot-film instrumentation system, a new calibration and operating procedure was developed. Instead of using the calibration constants supplied by the manufacturer, all constants were obtained from calibration procedures carried out in the low-speed wind tunnel and thermal chamber. This procedure proved to be both time consuming and complicated but necessary. Calibration of each instrument in the wind tunnel was carried out for 11 wind approach angles between plus and minus 50° and for 13 velocities in a range varying between 0.3 and 15 m/s. The best accuracy of the data was obtained for wind

directions parallel to the axes of the instrument, and consequently the tower mounted instruments were rotated in the direction of the mean wind before the data acquisition was started. For details of the calibration procedure and the relations for the conversion from output voltage to velocity components it is suggested that the reader consult References 1 and 2.

4. DATA HANDLING AND DATA ANALYSIS

4.1 Cup-vane Instruments

The output signals from the cup-vane instruments and temperature sensing probes are sampled and digitized at a rate of 1 sample per second. This information is transmitted to the control center of the main base, where every other sample is recorded on digital tape. The data from these tapes, each capable of storing up to 8 hours of data, are then analyzed on the HW-625 computer at NASA, Wallops Flight Center. The data are analyzed in blocks of 2^8=256 samples, representing a data record of 512 seconds. For each sample the east-west and north-south velocity components are calculated and averaged over 256 samples from which the mean velocity and the mean direction for each block are obtained. Also a block mean for the temperature is calculated. Reasonably stationary sample records of 5 to 10 blocks in length are selected for further analysis. This selection is based on the inspection of the printout of the block means of velocity, direction and temperature for all five levels.

Next the east-west and north-south velocity components and temperature are averaged for the selected sample, from which the sample mean velocity and sample mean direction are calculated. This direction

defines the mean-wind coordinate system with the x-axis parallel to the direction of the sample mean wind, the y-axis in the horizontal plane perpendicular to the x-axis and the z-axis vertically upward. For all the data points in each block the velocity components in the mean-wind coordinate system are calculated and averaged to obtain the block means. After the block means were removed from each set of components, variances and covariances are calculated for each block. Sample variances and covariances are obtained by averaging of the block variances and covariances over the total number of blocks. The covariances calculated in this manner include all the combinations of like velocity components at the different levels, allowing for the calculation of the vertical turbulence integral scales of both the u and v components. In addition, the autocorrelation function, $R_u(\tau)$ of the streamwise velocity is calculated from which the turbulence integral scale, L_u^x, is obtained as follows:

$$L_u^x = \frac{U}{(\sigma_u)^2} \int_0^{T_1} R_u(\tau)d\tau, \qquad (1)$$

where T_1 is the time delay for which the first zero-crossing of the calculated autocorrelation function occurs. The turbulence data acquired with the cup-vane system are analyzed in a limited frequency range of 0.00195-0.25 Hz.

A total of 195 digital data tapes were generated during the period of July 1974 and December 1978. Approximately 300 data samples were

analyzed each varying between 43 and 85 minutes. Initially data were acquired with the cup-vane system only, it was not until February 1976 that the temperature system came on line. However this system is not too reliable and often temperature at one or two levels is missing as the result of the equipment being down or out of calibration. Before a lightning-arrester system was installed on the tower, excessive amount of damage was inflicted on all systems during thunderstorms as a result of line power surges and voltage induction in the cables that connect the instruments on the tower to the electronics at the base of the tower. During the summer of 1976 a thermograph for recording the air temperature at ground level was added to the system.

Occasionally when the equipment on the 76m (250 ft) tower was down, data-acquisition was switched to the 91 m (300 ft) tower located at the north end of the island. This tower is instrumented with cup-vane systems at six levels but has no temperature instruments. Its location from the beach is 280 m as compared to the 76 m (250 ft) tower which is approximately 150 m from the beach. No major buildings or other obstacles exist between the 91 m (300 ft) tower and the beach. However, for ocean winds the overland distance is longer and more modification of the undisturbed ocean winds can be expected at the 91 m (300 ft) tower.

4.2 Hot-film Anemometers

The data-acquisition and data-handling system is designed to handle output from six split-film anemometer systems, sampled at a rate of 200 samples per second for a period of approximately one hour. This system consists of two main parts: (a) the multiplexing and analog recording system and (b) the demultiplexing, digitizing and

digital recording system. The seven output voltages from each anemometer are frequency modulated by voltage-controlled oscillators each with a different center frequency. There is one set of voltage-controlled oscillators for each probe. The seven frequency-modulated signals together with a 100 kHz reference signal are fed into a summing amplifier to produce one single multiplexed signal. The multiplexed signals from each instrument are recorded on separate channels of an analog tape recorder together with time-of-day, which serves as a reference for the recorded data.

At a later time, each of the multiplexed signals is demultiplexed into its seven analog components after passage through seven discriminators. In order to avoid aliasing of the velocity spectra the six output voltages corresponding to the six split films are passed through a 100 Hz low-pass filter. Next the analog voltages are sampled at a rate of 200 Hz, digitized and recorded on digital tape.
A mini-computer (DEC Model PDP 11/20) controls the multiplexing analog-to-digital conversion and the digital recording. Access to the mini-computer is obtained with a teletypewriter. The data conversion starts at a time-of-day prescribed by the operator, and the analog-to-digital converter performs successive scans and conversions of seven analog voltages into 16 bit words at a rate of one scan each 5 milliseconds. These words are stored in one of the buffers of the mini-computer which in turn transfers the data to a 9-track digital magnetic tape. Each buffer has a capacity of 209 scans representing 1.05 seconds of data. A total of 3300 records make up a single sample record over a time period of slightly less than one hour. The tapes with the digitized

data are taken to VPI and SU where the data are analyzed on an IBM-370 computer. Four separate computer programs have been developed to calculate the following major statistical parameters: mean values, variances, covariance spectra and cross spectra.

The first step in the data-analysis procedure is to convert the seven output voltages from each film to three velocity components in the sensor-oriented coordinate system and temperature, using the constants obtained from the calibration data. The converted data are transferred on another magnetic tape to await the next step of the data reduction.

In the second program velocity and temperature data are analyzed in blocks of $N=2^{13}=8192$ data points, representing nearly 41 seconds of data. For each of these blocks of data mean velocity components, mean velocity and direction, mean temperature and the four standard deviations are calculated. A total of 80 data blocks (almost 55 minutes) are analyzed in this manner. A stationarity trend test is performed on each of the calculated parameters to check for unacceptable nonstationarities. Also inspection af the printout of the block parameters helps in the decision whether or not to continue with the statistical anlaysis. At this point blocks with unrealistic data can be recognized and omitted from the data sample in future analysis. The sample mean velocity components are obtained by averaging the block means, allowing the calculation of the horizontal angle between the sample mean-wind direction and the probe axis. In the following step this angle is needed to tranfer the original velocity components in the sensor-oriented coordinate system into u, v and w velocity components of the mean-wind coordinate system as defined previously.

Block means are calculated for the temperature and for the velocity components in the mean-wind coordinates system and removed from the data in each block. The resulting fluctuating components are recorded on magnetic tape for further analysis. Also variances and all covariances for each block are calculated and averaged over 80 blocks to obtain the sample variances and covariances. The statistical parameters, including the spectra to be calculated in the next step, contain only contributions from the fluctuations in the frequency range of 0.0244-100 Hz. In order to include contributions from frequencies below 0.0244 Hz, sixteen consecutive data points are averaged into one data point to form a new data record, which is also recorded on magnetic tape. This averaging is performed after the data are transformed into the mean-wind coordinates and before the block means are removed. In this way only 5 blocks, each 10.92 minutes long, are analyzed allowing for data analysis in the frequency range of 0.00153-6.25 Hz. For these new data records, block variances and covariances and sample variances and covariances are also calculated. For the lowest frequency range the data, after transformation into the mean-wind cooordinates, are subjected to an 80-point non-overlapping averaging for analysis in the frequency range between 0.00031-1.25 Hz.

The last step of the data analysis is the spectral analysis of the high, middle and low frequency data in the frequency range of 0.0244-100 Hz, 0.00153-6.25 Hz and 0.00031-1.25 Hz respectively. Spectral estimates are calculated for each block using a specially developed Fast Fourier Transform algorithm [4]. The combined averaging technique is employed, averaging first all the block estimates at a given frequency (ensemble averaging) and then averaging these results

over appropriate frequency intervals (frequency averaging).

In total, 24 one-hour data records were generated with the hot-film system. Nine runs were generated during warm summer afternoons of the year 1976. This set of data was acquired for southerly winds only, and the detailed results are presented in Reference 3. The remaining 15 runs were acquired during the spring of 1977 for winds of northwesterly direction. For some of these data records, data were acquired simultaneously with the cup-vane system.

The hot-film system is extremely delicate. Lightning and powerline fluctuations have often caused difficulties with the operation of the system. It is very seldom that the entire system is fully operational at one particular time. The hot-films also have a tendency to undergo resistance shifts. If an appreciable shift is detected, the probes are recalibrated. Corrections have to be made for changes in cable resistance due to changes in ambient temperature. Similarly, heat transfer corrections have to be made for changes in temperature. Because of the uncertainties in these corrections and other variations, the mean velocity and mean temperature measured with this system are not reliable. Resistance shifts in the active part of the system (films and cables) result in a parallel shift of the heat transfer (voltage)/velocity calibration curve. This shift of course will affect the mean quantities a great deal but should not affect the calculated turbulence quantitites as much. As pointed out in Reference 5, the results from these instruments become less accurate for wind directions of $\pm 40°$ and $\pm 90°$ with respect to the probe axis. Consequently, the probes are rotated in the direction of the mean wind prior to data acquisition. For southerly winds this is no problem

since these winds especially at the higher elevations are very steady and have low turbulence levels. For northwest winds the alignment with the mean wind is more of a problem because of the presence of long-period fluctuations in direction. Precautions were made as much as possible to ensure that data of the highest quality were acquired, and it is believed that the measured turbulence quantities fall within an accuracy level of less than 10%.

5. PLANETARY BOUNDARY LAYER (PBL)

The planetary boundary layer (PBL) may be defined as that part of the atmosphere where the effect of the earth's surface is directly felt. The flow structure of the boundary layer is extremely complex due to the variability of surface roughness changes in terrain, changes in surface temperature, variability of water vapor, presence of clouds and the fact that the flow is turbulent. Consequently, a simple model describing all the variables in the PBL such as velocity, wind direction, temperature and humidity, and covering all possible conditions is still not available.

The unstable or convective PBL is characterized by a strong upward heat flux from the surface and by strong vertical mixing due to positive buoyancy forces. Under these conditions above the surface layer, a well-mixed layer exists with an almost uniform potential temperature and an almost constant wind speed and direction. Due to the convective mixing a relatively sharp inversion is created on top of the mixed layer that delineates the depth of the PBL. Above this inversion the atmosphere is relatively undisturbed by the presence of the earth's surface and only gravity waves are generated. During the course of a sunny day

the convective PBL increases in depth as the land surface heats up and extends up to the inversion layer, which is the result of the convective mixing of unstable air below with warmer stable air above. Under these conditions the convective PBL can be characterized by three different layers, which are, starting from the earth's surface:
1) a surface layer, 2) a mixed layer, and 3) a capping inversion. The existence of this model for the convective PBL is based on theoretical considerations [6], numerical flow modeling [7,8,9,10], laboratory flow modeling [11] and actual observations [12,13,14].

In the case a layer of stable air is present at the surface, and/or one or more stable layers exist at higher altitudes, no capping inversion exists. In stable air, turbulence is suppressed and may vanish completely under extremely stable conditions, and the air in the different layers becomes uncoupled as a result of reduced mechanical mixing. No simple model is available to describe this situation. A surface-based inversion with or without one or more stable layers at higher elevations has been observed over water surfaces, as warm air flows over the cooler water during either day or night [3,18]. Under these conditions a low-level wind maximum (surface jet) is usually observed and the interpretation of the wind fluctuations near the surface is often complicated as a result of the co-existence of turbulence and internal gravity waves. These two phenomena have quite different properties although a non-linear interaction may exist between them.

More complications are introduced in the flow analysis of the PBL when clouds are present and condensation of water vapor occurs within the PBL. As condensation takes place in the layer where the clouds are located, latent heat is released and an inversion layer develops below

the cloud base that is responsible for some degree of suppression of the turbulence. Under these conditions the large-scale plume structure, normally present in the convective PBL, does not develop resulting in a considerable suppression and reduction in low-frequency velocity fluctuations. This phenomenon in turn results in reduced velocity variances and an increased roll-off in the low-frequency range of the spectra of the horizontal velocity components.

Just above the earth's surface the shear-production of turbulence dominates the buoyant production or suppression of turbulence. However the importance of the shear-produced turbulence diminishes with height as the effect of buoyancy on the turbulence gains importance. In the layer just above the earth's surface where shear-produced turbulence dominates and the Reynolds stress is nearly constant, the velocity is adequately expressed by the well-known logarithmic law, provided the roughness of the terrain is uniform. As buoyant production or buoyant suppression of turbulence gains importance with height relative to shear production, modification of the logarithmic velocity profile will result. The buoyant production of turbulence is associated with the upward heat flux of sensible and latent heat, which usually occurs when the atmosphere near the earth's surface is unstably stratified ($\frac{d\theta}{dz} < 0$). The buoyant suppression of turbulence is associated with the downward heat flux which usually occurs when the atmosphere is stably stratified ($\frac{d\theta}{dz} > 0$), where θ is the local potential temperature.

Under strong-wind conditions on a sunny day, the layer in which the shear-produced turbulence dominates increases in height, and the logarithmic velocity profile exists to higher elevations before it is eventually

modified as a result of convective activity, even under the strongest wind conditions.

Following this discussion of the PBL, it is unlikely that its flow characteristics are based exclusively on mechanically or shear-produced turbulence. Experimental results describing the mean flow and turbulence in the PBL, under a variety of stability conditions ranging from unstable via near-neutral to stable conditions, clearly indicate that some basic differences exist between the PBL and the typical zero-pressure gradient wind-tunnel boundary layer. The most noticeable differences are observed in the evolving convective PBL on a sunny day with the mixed layer occupying about 90% of the height and the surface layer consisting of the lower 10% of the PBL. In the mixed layer the velocity and wind direction are practically uniform [12,13]. Also, the downward entrainment of heat and momentum at the base of the capping inversion is a phenomenon that makes the assumption of vanishing turbulence at the edge of the boundary layer untenable [12,13,14].

The entrainment of heat and momentum of different magnitude and direction into the mixed layer is mainly responsible for the low-frequency fluctuations observed in the horizontal velocity components down to near ground level [19,20]. These low-frequency fluctuations are not present under stable conditions, although as mentioned before, low-frequency fluctuations associated with gravity waves have been observed under stable conditions [15,18].

An abrupt discontinuity (increase) in low-frequency content has been observed in the spectra of the horizontal velocity components as the thermal stratification changes from stable to unstable [19,20].

Similarly, the variances of the u and v velocity components and the reduced peak frequencies of these spectra increase abruptly as the stratification changes from stable to unstable. These abrupt changes have been observed in the horizontal velocity components u and v only, and do not occur in the vertical velocity component w. Experimental evidence of the abrupt increase in variance of the u velocity component and of the total velocity variance as the flow changes from slightly stable to slightly unstable is clearly presented by Busch [21]. For slightly stable stratifications the ratio of the standard deviations of the vertical and longitudinal velocities $\sigma_w/\sigma_u = 0.36$ and for slightly unstable stratifications this ratio is reduced to 0.25.

It has been observed that shortly before sunset the convective boundary layer disintegrates suddenly in a matter of minutes as a surface-based inversion begins to develop [22,23]. During the night (or when there is a heavy cloud cover and water-vapor condensation in the PBL) the large-scale turbulence structure of the convective PBL is suppressed and no low-frequency components are present in the u and v velocity spectra near the earth's surface.

Some of the experimental evidence, used previously in support of the flow description of the PBL, was obtained under relatively strong wind conditions. For example, during the Minnesota experiment [12] two data records (2A1 and 2A2) were acquired each with an hourly mean velocity of approximately 10 m/s at a height of 10 m. For these two data records the mean velocity is practically uniform above 60 m, which is typical for the mixed layer. Also the standard deviations

of the three velocity components do not change appreciably with elevation up to an elevation of 1220 m, indicating that there is little evidence of vanishing turbulence at the edge of the PBL. In addition, the horizontal turbulence stresses $\overline{uw}$ and $\overline{vw}$ exhibit minima near the surface and a considerable upward heat flux is observed up to the top of the mixed layer where the heat flux changes direction due to entrainment of warm air at the base of the capping inversion. The gradient-Richardson numbers for these two records of Reference 12 are approximately -0.30 and -0.46 respectively, which excludes these records from the near-neutral stability category.

In another example, extremely strong winds with mean velocities up to 28 m/s have been observed at 10 m heights over water [24]. The turbulence intensities of the u and v components show an abrupt increase for mean velocities in excess of 12 m/s (σ_u/U from 8% to 15%, σ_v/U from 8% to 11.5% and σ_w/U remains constant at 5%). There is strong evidence that helical vortices, which form over the ocean under near-neutral conditions, are responsible for this increase in turbulence intensity of the horizontal velocity components. Also nocturnal jets near the earth's surface with a jet velocity of approximately 20 m/s and a gradient Richardson number of +0.5 have been observed in Nebraska [16].

Based on these examples and other experimental evidence presented in the cited references, there is no basis for the assumptions that under strong wind conditions the turbulence in the PBL is purely of mechanical origin and that the PBL flow-structure is similar to that of a zero-pressure gradient wind-tunnel boundary layer with vanishing turbulence at the free stream.

For the benefit of structural engineers and wind engineers who deal with a large number of problems requiring the knowledge of the mean flow and turbulence in the atmosphere, the atmospheric flow characteristics near the earth's surface under strong wind conditions have been reviewed and summarized in several review papers [References 25 through 31]. The input data to most of these review papers were obtained from many different sources and include multi-level tower data and airplane data usually taken over horizontal terrain with near-uniform roughness. The results from these strong-wind experiments have formed the basis for empirical models of the wind structure near the earth's surface and of the atmospheric flows at higher elevations. In many of the review papers it is assumed that under strong wind conditions the turbulence is purely mechanically generated, and that buoyant production and suppression of the turbulence can be neglected. Under these conditions it is then assumed that the atmosphere is neutrally stable and the mean and turbulent flow behave similar to the flow in a zero-pressure gradient turbulent boundary layer developed in a low-speed wind tunnel.

The review papers generally indicate tht the PBL under strong wind conditions is neutrally stable but may be modified as the result of thermal effects. However, it is generally assumed that under strong wind conditions there is sufficient mixing that thermal effects can be completely ignored. The neutrally stable PBL-flow model, which is generally assumed in the review papers, has never been experimentally verified at different sites for a large variety of strong wind conditions. Nevertheless, it is widely assumed by many engineers and

scientists in the field on wind engineering that this model provides an adequate description of the flow in the PBL under strong wind conditions.

Upon reading of the review papers one does not always get a clear picture when neutral conditions exist. Deaves and Harris [30] do not give any conditions for the existence of neutrally stable flow in the PBL other then the mean velocity has to be strong enough. Counihan [26] considers only those data which specifically indicate adiabatic or near adiabatic conditions, or which have wind speeds in excess of 5 m/s at a height of z = 10 m. ESDU [27,28,29] considers neutral stability to exist when the hourly mean wind at a height of 10 m is greater than 10 m/s. Using the gradient Richardson number as a measure for the degree of thermal stability in the PBL, near-neutral conditions are suggested to exist by Teunissen [25] for $|Ri| < 0.03$ and by Panofsky [31] for $|Ri| < 0.01$ for flow near the surface.

Panofsky [31] also states that wind shear, and therefore mechanical production of turbulence, decreases rapidly with height and that the effect of buoyancy becomes progressively more important. Consequently thermal effects can no longer be neglected even under strong wind conditions for heights above approximately 50 m.

Most of the observations at Wallops Island presented in this report have been made with the mean wind speed at the 76 m (250 ft) level between 10 m/s and 20 m/s and therefore can be considered to belong to the strong-wind category. However the results of these observations will be presented and discussed in the framework of non-neutral PBL-flow.

6. RESULTS AND DISCUSSION

This chapter deals with the discussion of the mean flow and turbulence measurements obtained with the two instrumentation systems mounted on the 76 m (250 ft) meteorological tower at Wallops Island, Virginia.

Data were acquired with the cup-vane and resistance temperature probes during a period of more than 4 years (August 1974 - December 1978). Most of these data records were taken during daytime, although some night records are included. The prevailing wind directions at this site are southerly during the summer and fall, and between west and north during winter and spring. Consequently, for these two direction sectors many data records are available but the data base for on-shore winds in the sector between northwest and south is limited. For this set of data, mean velocity U, mean direction ϕ, mean temperature T, the turbulence variances σ_u and σ_v*, and the turbulence integral scales L_u^x, L_u^z, L_v^z were obtained for each data record, based on the measurements from 5 levels at 15.3 m (50 ft) intervals on the 76 m (250 ft) tower.

A second set of data was taken with the hot-film instrument system. Nine data records, each one hour long and for southerly wind directions, were acquired during 3 days in July and August of 1976 [3]. In addition 14 data records for winds from northwesterly directions were acquired during several days in March, May and June of 1977 [23].

---

*The symbol σ refers to the standard deviation, but for simplicity the word variance will be used in the text.

For these data records the following parameters were obtained: variances and covariances of the three turbulence components and temperature, spectra and cospectra, and longitudinal integral scales L_u^x, L_v^x and L_w^x, all measured at the same levels as the cup-vane instruments and at 9.1 m (30 ft). For some of these records data were acquired simultaneously with the cup-vane system, allowing direct comparison of the measurements with the two instrument systems.

6.1 Mean Wind and Mean Temperature Profiles

For near-neutral stratification the wind profiles over homogeneous terrain obeys the relation

$$U = (U_o^*/K)\ \ln(z/z_o) \qquad (2)$$

where U_o^* is the friction or shear velocity, which is ideally equal to $\sqrt{\tau_o}/\rho$, where τ_o is the surface stress and p the air density, K is Von Karman's constant taken at 0.4 and z_o is the roughness length. The height z below which the log-law (2) is valid depends on the stability of the flow or on the relative importance of the buoyant production or suppression of the turbulence with respect to the mechanically produced turbulence. The height where the measured velocity profile starts to deviate from the logarithmic profile varies a great deal and the deviation increases progressively for increasing heights. Under strong convective conditions and under extreme stable conditions the near neutral part of the surface layer is well below 15.2 m (50 ft), the height of the lowest mean-velocity measurement. Consequently under these conditions it is incorrect to fit the log-law (2) to the measured mean-velocity data in order to obtain values of z_o and U_o^*.

The theoretical velocity profile over uniform terrain for the upper part of the surface layer where non-neutral stratification exists, is based on the Monin-Obukhov similarity theory and is given by [32]

$$U = (U_o^*/U)\ [\ln(z/z_o - \psi] \tag{3}$$

where ψ is a universal function of the stability parameter z/L and L is the Monin-Obukhov length defined (in the absence of moisture) as [32]

$$L = \frac{c_p \rho}{K}\ \frac{\theta}{g}\ \frac{U^{*3}}{Q_o} \tag{4}$$

where T is the absolute temperature, $U^* = \sqrt{\tau_o/\rho}$ and Q_o is the surface heat flux, which can be approximated by $c_p \rho\ \overline{w\theta}$ measured in the surface layer. The stability parameter, z/L, depends on the gradient Richardson number [32]

$$Ri = \frac{g}{T}\ \frac{\gamma_a + dT/dz}{(dU/dz)^2}\ , \tag{5}$$

where γ_a is the adiabatic lapse rate (0.01°C/m for dry air and 0.0065°C/m for air saturated with moisture). With the use of the expressions relating Ri, z/L and ψ as given by Panofsky [31], the departure from the logarithmic profile due to buoyancy effects in the surface layer can be obtained so that (3) can be used to obtain estimates of z_o and U^*.

This approach can be taken for velocity profiles measured in the surface layer, which is loosely defined as that part of the PBL where the horizontal stress and vertical heat flux are nearly constant. The height of the surface layer is frequently estimated as

the lower 10% of the convective PBL depth, z_i, and is limited to a height $z<L$ [13].

For stable conditions L varies a great deal and is relatively small [17]. The surface layer is not well defined and often is only a few meters high [33]. Under these conditions the velocity profile for non-neutral conditions cannot be used for estimation of z_o and U_o^*, with velocity measurements taken well above the surface layer.

In general, Monin-Obukhov (M-O) similarity theory can only be applied in the surface layer, when the flow conditions are stationary, when surface conditions are uniform (roughness and temperature), and over level terrain without major topographical features such as mountains etc. If the measured velocity data are linear with ln z, then this observation does not automatically guarantee that the profile is truly logarithmic. For the majority of sites including the Wallops Island site the above conditions are not met, and application of the M-O similarity concepts such as the empirical flux-profile relationships, which are based on data with the above conditions satisfied, is questionable and should probably be avoided.

For neutral conditions the temperature profile should follow the adiabatic lapse rate of either 0.01 or 0.0065°C/m for dry and saturated air respectively. It is very seldom, even under the strongest wind conditions, that a truly neutral stratification is encountered for any length of time. The usual daytime thermal stratification near the surface is $-\frac{dT}{dz} > \gamma_a$ (unstable stratification) and $-\frac{dT}{dz} < \gamma_a$ (stable stratification) for nighttime. There is a short time around sunrise and in the late afternoon before sunset when a neutrally stable stratification is observed near the surface in the first 10 or 20 m. The

stratification of the air at higher elevations varies a great deal with time of day, cloud cover and season. For southerly flows over the ocean the air temperature is usually higher than the water temperature and a surface-based inversion ($-dT/dz < \gamma_a$) exists day and night.

Changes in temperature and velocity profile occur also as the flow experiences a sudden change in surface roughness and surface temperature, and an internal boundary layer (IBL) develops as the flow adjusts itself to the new surface conditions. On-shore winds at Wallops Island usually experience an increase in roughness and an increase in surface temperature in daytime as they cross the beach. For westerly winds the surface temperature changes as the wind moves from the wet marsh over the warm land surface during daytime. Within the observation height of 76m at the Wallops Island site, temperature gradients vary greatly with height and even change from positive to negative or vice versa. Under these conditions the local Richardson number is not a true indicator of the overall thermal stratification of the observed flow and M-O similarity does not apply.

Typical temperature profiles for southerly winds on a summer afternoon are shown in Figure 5. These temperature profiles clearly indicate the stable conditions above the IBL in the early afternoon, and the surface cooling in the late afternoon. Daytime and nighttime temperature profiles for strong westerly winds are shown in Figure 6. During daytime the surface temperature is maximum and gradually decreases with height. On a rainy day with low cloud cover a stable stratification is observed above 40 m. Neutral temperature profiles throughout the tower height are seldom observed; the second temperature profile shown in Figure 6 is the closest to an observed neutral temperature profile. Typical nighttime temperature profiles show a stable stratification near the surface with near neutral

conditions above 15 m.

Ratios of mean velocities at the 15.2 m (50 ft), 30.5 m (100 ft), 45.7 m (150 ft) and 61 m (200 ft) levels with respect to the mean velocity at the 76.2 m (250 ft) level are shown in Figure 7. The plotted data in this figure represent the mean and the plus and minus standard deviation from the mean, as well as the maximum and minimum values of the velocity ratios for the data records acquired in each 15-degree sector. Because the mean velocity at higher elevations is less disturbed by local surface obstacles and is outside the developing IBL, the mean velocity at the 76.2 m (250 ft) level was chosen as the reference velocity. For the one sector between 0° and 15° and the 5 sectors between 90° and 165° (east-southeast) the number of data records available in each sector was four or less, an insufficent number for determination of the standard deviation, and only the average velocity ratios are presented.

Between 230° and 360° (southwest-north) the variation in mean wind speed between the different elevations is relatively minor under moderately strong wind conditions. Conversely, for southerly winds in the sector $160° < \phi < 230$, large variations in mean wind speeds relative to the mean velocity at the 76.2 m (250 ft) level are observed. For example in the sector between 180° and 195° the mean wind-speed ratio, V50/V250, varies from 0.4 to 0.8, clearly indicating the great variability of mean velocity distribution near the surface. Relatively large variations of the mean velocity ratios are also observed for wind directions approximately parallel to the island for sectors 30°-45° and 210°-225°. For winds from these two sectors a small change in wind direction gives rise to a large variation in upstream terrain roughness. Generally the variations of the mean velocity distribution near the surface for on-shore winds are

much larger than for westerly winds. For on-shore winds, the changing development length of the IBL, the thermal stratification and other atmospheric conditions have a great effect on the velocity distribution near the surface as the data indicate. For southerly winds, a surface-based inversion exists during the daytime as the result of warmer air flowing over the colder water [3]. Under these conditions the existence of a surface jet with a maximum mean velocity (jet velocity) within a few hundred meters from the surface has been observed. The jet velocity has been observed as low as 45.7 m (150 ft) as shown by the maximum values of the velocity ratio V150/V250 of larger than one for wind directions between 170° and 210°, and by one of the velocity profiles of Figure 8.

Typical strong-wind velocity profiles for wind directions between southwest and north are shown in Figure 9. The stronger wind profile is linear over the entire observation height when presented in semi-logarithmic coordinates. In the second profile with somewhat lower velocities, a distinct "kink" is observed. The majority of the measured velocity profiles for westerly wind directions shows similar "kinks". The values of z_o obtained from the velocity profiles above the "kink" are much too small for the upstream terrain. Moreover the two velocity profiles of Figure 9 are approximately from the same direction. Therefore the "kinks" in the profiles cannot be the result of an upstream change in roughness, but must be interpreted as the beginning of the transition from the surface-layer flow to the uniform mixed-layer flow [13].

6.2 Velocity Profile Parameters z_o and α

The roughness length, z_o, can be evaluated from fitting of either the logarithmic law (2) or the non-neutral profile law (3) to the measured mean velocities in the surface layer. The height of the

surface layer in which (2) and (3) are valid is roughly defined as the layer near the surface which the fluxes $\overline{uw}$ and $\overline{w\theta}$ are approximately constant and not less than 80% of the surface stress, $\sqrt{\tau_o/\rho}$, and surface heat flux, $Q_o/c_p\rho$, respectively. Measurement of the turbulent fluxes at Wallops Island indicate that the thickness of the surface layer varies a great deal with wind speed, wind direction and thermal stratification.

For on-shore winds the top of the surface layer is generally below the lowest observation level of 9.1 m (30 ft) and for the strongest westerly winds the surface layer extends above the height of the tower. For on-shore winds when an IBL develops as the air crosses the beach, turbulent heat-flux measurements show an upward flux at the lower levels and a downward flux at the higher elevations [3]. Transition usually occurs between the 15.2 m (50 ft) and 30.5 m (100 ft) levels, which should correspond to the height of the IBL at the tower location. The flow above the IBL is still associated with the ocean surface, but is well above the surface layer, which for southerly winds extends only a few meters above the water surface. Consequently no values of the roughness length, z_o, for either the land or ocean surface can be obtained from the measured velocity profiles. Despite the fact that two velocity profiles of Figure 8 show a linear variation of velocity with lnz, fitting of the log-law (2) to the velocity data leads to values of z_o of the order of 1m, which are much too high for either the existing upstream terrain or the ocean. The parameters describing the on-shore turbulent flow depend in part on the roughness of the underlying surface (ocean) but also to a great extent on the stability of the flow. Consequently, knowledge of the roughness length, z_o, for flows over the ocean is not sufficient for the prediction of the turbulence

parameters for higher elevations as presented by ESDU [28,34].

For westerly winds the local shear velocity $U^*=[\overline{uw}^2 + \overline{vw}^2]^{1/4}$ is approximately constant over most of the observation height, indicating that the surface layer extends well above the lowest observation level of 9.1 m (30 ft). Also the values of the local shear velocity, U*, compare quite well with the profile friction velocity U_o^*, obtained from mean velocity measurements below the profile "kink". The roughness length, z_o, obtained from fitting of the log-law (2) to the measured mean velocities below the profile "kink", vary with upstream roughness and thermal stability of the flow in the surface layer.

Figure 10 shows the variation of z_o with wind direction, clearly indicating the effect of the 6.5 m high storage bunker for mean wind directions of 270°. In the sector between 350° and 30° the upstream terrain is much rougher which results in higher values of z_o. For the sectors between 230° and 260°, and 280° and 340°, the terrain is reasonably uniform and the average value of the roughness length, z_o=0.034 m , corresponds quite well to the predicted values of ESDU [28,29] for similar terrain. In Figure 11 all values for z_o, obtained for wind directions in the before-mentioned sectors, are shown as a function of the gradient Richardson number evaluated at z=15.2 m (Ri_{15}). The values of z_o were obtained by fitting of the log-law to the velocity measurements below the profile "kink". The scatter of the data is appreciable for $Ri_{15}>-0.15$, however the values of z_o decrease rapidly for $Ri_{15}<-0.15$. At this point the mean velocity profile in the surface layer can no longer be estimated with the log-law (2), as stability effects start to dominate. An attempt was made to estimate the roughness length by fitting the non-neutral profile (3) to the mean velocity data above the "kink" as outlined by Panofsky [31].

However, this correction technique leads to unrealistic estimates of z_o, which seem to indicate that the velocity profile above the "kink" is not part of the surface-layer profile but instead is the transition of the surface layer profile to the mixed layer profile.

In Table I mean profile parameters and turbulence parameters are presented for strong-wind data records with wind directions in the above-mentioned sectors with near-uniform upstream terrain and measured with the cup-vane system and the hot-film anemometers. For the data records with a thermal stratification close to neutral the semilogarithmic velocity profiles (S) are generally linear throughout, and for the records for which the flow is more unstable, kinks (K) start to appear in the profile.

Engineers generally favor the power law as an expression for the velocity profile through the entire PBL over uniform terrain

$$U/U_R = (z/z_R)^{\alpha} \tag{6}$$

Although under certain conditions this law has fitted observed profiles over uniform terrain quite well, it is now generally accepted that the log-law (2) is preferable over the power law (6) for flow in the surface layer. Also the power law (6) cannot be expected to be a good approximation for wind profiles in the convective PBL. The latter seems to be prevalent over the North American continent even under the strongest wind conditions.

The mean velocity profiles of records 2A1 and 2A2 acquired during the Minnesota 1973 atmospheric boundary layer experiment [12] as well as the velocity profile acquired at the Boulder Atmospheric Observatory (300 m mast [35]) on the morning of the 11th of September 1978 under

extremely strong wind conditions (20-minute average velocity of 18.67 m/s at z=10 m) show clearly that the power law with one constant exponent does not fit the velocity measurements. The measured strong-wind velocity profile at the Boulder site starts to deviate from the log-law (2) at z=22m and becomes more or less uniform above 200 m.

On the other hand mean-velocity measurements made at 3 levels (10m, 80 m and 200 m) of the 213-m mast at Cabauw, the Netherlands, under extremely strong westerly winds (30-minute average velocity of 22.2 m/s at z =10 m) [36] indicate that the power law (6) fits these data quite well. The Cabauw tower is operated by the Royal Netherlands Meteorological Institute and is located about 50 km east from the North Sea coastline. For westerly winds the upstream terrain is flat low-lying pastureland with a very shallow water table. Simultaneous temperature measurements made at 8 levels between 2 m and 200 m indicate a near- neutral thermal stratification with possibly a minimal upward heat flux from the mostly wet upstream terrain that inhibits the formation of a convective PBL, which is typical for the observations of the two North American sites.

As Panofsky [31] has pointed out the power law can be expected to fit the velocity data in the surface layer only over a limited height range. In the near-neutral surface layer where the logarithmic law applies the power-law exponent can be approximated by [31]

$$\alpha = [\ln(\sqrt{z_1 z_2}/z_o)]^{-1} \qquad (7)$$

clearly showing the variation of α with roughness, z_o, and geometric mean height, $\sqrt{z_1 z_2}$ where z_1 and z_2 represent the elevation boundaries of the layer over which a near constant α may be expected. Near the surface α has a relative large value depending on the value of z_o, but

decreases with height and should approach zero outside the surface layer as transition to the mixed layer takes place.

For westerly winds at the Wallops Island site, power law exponents based on the mean velocities of the three lower levels (z_1=15.2 m, z_2=45.7 m) are shown in Figure 12 as a function of the roughness length, z_o. Similarly, power law exponents based on the mean velocity measurements under strong-wind conditions (no "kinks") at all five levels and the three highest levels are shown versus roughness length, z_o, in Figures 13 and 14 respectively. Panofsky's relation (7) fits the measurements extremely well except for the results based on the mean velocities of the three highest levels (Figure 14). The reason for this is that on a semi-logarithmic plot of U vs. ln z, the results of the higher levels fall close together and may seem to vary in a linear fashion. However in reality the data already deviate from the log-law (2) and all three prediction methods, which are based on known roughness lengths, overestimate the power law exponents obtained from the measured velocity profiles. No attempt was made to obtain power law exponents for the velocity profiles of on-shore winds, because of the variability of the profiles, the presence of an IBL and the absence of values for z_o.

6.3 Turbulence Intensities

Average turbulence intensities of the horizontal velocity components u and v measured with the cup-vane instruments at 5 levels, are shown in Figures 15 and 16 for each 15-degree sector. In addition to the average turbulence intensities, the maximum and the minimum observed turbulence intensities for each sector and the mean intensity plus and minus the

standard deviation are shown. In the sector 0°-15° and the 5 sectors between 90° and 165° only average turbulence intensities are shown, because the number of data records available in each of these sectors is four or less. For on-shore winds σ_u/U is approximately 10% at z=15.2 m decreasing to 5% or less at the highest observation level (z=76.2 m). For westerly winds the σ_u/U decreases from about 20% at the lowest level to about 14% at the highest level (Fig. 17). In general the variation of the turbulence intensity, σ_u/U, in each section is relatively small, except for the two sectors between 195° and 225°.

The turbulence intensity of the v component, σ_v/U, shows much the same pattern, although some differences can be observed. For on-shore winds the average value of σ_v/U at the lowest observation level (in the IBL) is about 8%, decreasing to about 4% at the highest level (above the IBL). For southerly winds in the three sectors between 165° and 210° turbulence intensities for both u and v components of less than 2% have been observed at the highest observation levels above the IBL. These observations have been made under stable conditions, and on several occasions the mechanical turbulence has been observed to vanish completely at these elevations at mean velocities of 10 m/s and higher.

The average turbulence intensity σ_u/U is nearly constant at each level for wind directions between 240° and 345°. The average turbulence intensity σ_v/U at each level increases with wind direction from 240° to about 300° where a maximum is reached and decreases gradually with wind directions from 300° to about 50°. Figure 17 shows the variation of the average turbulence intensities of the u and v components with height in the two sectors 240°-255° and 300°-315°. The averaged results are also compared with the estimates of Teunissen [25] and ESDU [28] both

based on the roughness length, z_o, whose average is 0.037 m for either one of these sectors [Fig. 10]. Although the upstream terrain for the two sectors is about identical, the values of σ_v/U in the sector between 300° and 315° are considerably higher than those for the sector between 240° and 255°. The average values of σ_v/U for the latter sector correspond extremely well with the Teunissen estimate, but for the sector between 300° and 315° the average values of σ_v/U are about 3 to 4% higher. On the other hand the average values of σ_u/U for these two sectors are about identical and fall between the estimates of Teunissen [25] and ESDU [28].

A possible explanation for this unusual behavior of σ_v/U can be derived from the visual inspection of several years of strip-chart recordings of wind speed and direction obtained continously from a propeller-vane anemometer located about 1 km northeast from the tower on Wallops Island. These recordings clearly show that for northwesterly winds the instantaneous wind direction experiences frequently large fluctuations toward the north (Fig. 18). These direction fluctuations are larger than usual and are not normally distributed as shown in (Fig. 19), which explains the large values of both σ_v/U and the covariance $\overline{vw}$ measured in this sector.

The turbulence intensity, σ_u/U, which is constant over near-uniform terrain for westerly wind directions (Fig. 17), instead varies with time of day. Nighttime measurements are systematically 1% higher than the daytime results (Fig. 20). The vertical distribution of the vertical turbulence intensity, σ_w/U, based on five strong-wind data records obtained with the hot-film system, is shown in comparison with the ESDU [28] and Teunissen estimates in Figure 21.

The vertical distributions of the turbulence intensity of all three components for southerly winds are shown in Figures 22, 23 and 24. For these wind directions an internal boundary layer (IBL) develops as the air crosses the beach. Based on the change in direction of the daytime vertical heat flux $\overline{w\theta}$, which is expected to be positive in the IBL and negative above it [3], the height of the IBL at the tower must be between the 15.2 m (50 ft) level and 30.5 m (100 ft) level. This observation agrees with the relationship given by Elliot [37], which predicts a height of the IBL of approximately 26 m, based on an upwind roughness length over the ocean of z_o'=0.001 m and a downwind roughness length of z_o''=0.01 m and a development length of 300 m. The average turbulence intensities of the u and v components from nine data records, obtained with the hot-film instrumentation during summer afternoons, compare surprisingly well with the average turbulence intensities from 29 data records, obtained during winter and early spring under strong wind conditions with the cup-vane system (Figs. 22,23,24). The turbulence intensities in the IBL compare reasonably well with the ESDU [28] predictions based on a roughness length of z_o=0.01 m. However above the IBL the ESDU [28] predicted values of the turbulence intensities, based on a roughness length z_o=0.001 m, overestimate the actual measured values by a factor of two. The turbulence intensites for run 7 [3] obtained under extremely stable conditions (R_f=+25.5, U=10.7 m/s at z=61 m), which are included in Figures 22 through 24, show lower than average values above the IBL. Under similar conditions it has been observed that the turbulence vanishes completely for some time. The variation of the ratios of average turbulence intensities, σ_v/σ_u and σ_w/σ_u, for all wind directions is shown in Figure 25. The measurements indicate that the values of

these ratios are more or less independent of height, and the data shown in Figure 25 are not only the ratios of the average turbulence intensities of all data records in each sector but are also averaged over all observation levels. For most wind directions the values of σ_v/σ_u are between 0.75 and 0.85 in comparison with the predictions of 0.75 and 0.80 by Counihan [26] and Teunissen [25]. The estimates of ESDU [28] are not single valued but are dependent on height and roughness length. Smaller values than 0.75 for σ_v/σ_u are observed for wind directions approximately parallel to the island at $\phi \simeq 40°$ and $\phi \simeq 230°$. Values of σ_v/σ_u higher than 0.85 are observed for southerly winds for $\phi \simeq 170°$ and for northwesterly winds in the sector $280° < \phi < 350°$. That the values of σ_v/σ_u are relatively high in this last sector is no big surprise since often large direction fluctuations have been observed in this sector (Fig. 18). Values of σ_v/σ_u and σ_w/σ_u obtained from the hot-film data records are also shown in Figure 25. The values of σ_v/σ_u obtained with this system compare quite well with the cup-vane results. The values of the ratio, σ_w/σ_u, for winds from the sector between south and southwest and northwesterly winds fall between 0.55 and 0.60 as compared to values of 0.50 and 0.52 as predicted by Counihan [26] and Teunissen [25] respectively.

The results discussed so far in this report show clearly that at the Wallops site large variations in mean as well as turbulent flow occur varying with wind direction. The important observed deviations from the simple neutral boundary-layer models are:

1. The development of an internal boundary layer (IBL) for on-shore winds as they cross the beach.
2. The existence of a surface jet for southerly winds with extremely low turbulence intensities (2% or less and occasionally

vanishing under stable conditions) coexisting with gravity waves.

3. Large direction fluctuations towards the north for northwesterly winds, observed during the daytime, which are responsible for higher than usual lateral turbulence intensities.

These observations were made under strong wind conditions and there is no reason to believe that for still stronger wind speeds (maximum observed speeds) these deviations from the neutrally stable boundary-layer model will suddenly vanish.

6.4 Turbulence Integral Scales

6.4.1 Integral Scales, L_u^x, L_u^z and L_v^z from cup-vane data

In this section the distribution of the turbulence integral scales obtained from measurements with the cup-vane system will be discussed and compared with the estimates from several review papers [25,26,28,29]. The streamwise turbulence integral scale of the u component, L_u^x, is calculated from the autocorrelation function (1), $R_u(\tau)$, assuming that Taylor's hypothesis is valid. Averages of all scales, L_u^x, obtained from the data records in each 15-degree sector, are plotted along with the maximum and minimum and plus and minus the standard deviation from the average value in Figure 26 for each observation level. Averages only are plotted in the sector 0°-15° and between 90° and 160° because of the limited number of available data records in these sectors. The integral scales, L_u^x, increase systematically with height and show a great deal of variability for all wind directions. In general the magnitude of these integral scales is larger for westerly winds than for on-shore winds except for southerly wind directions. At the highest observation level two distinct extremes for the maxima can be observed in the two sectors between 180° and 210°, and between 300° and 330°. For southerly winds between 180° and 210°

the air is frequently stably stratified which under certain conditions may lead to the coexistence of turbulence and low-frequency gravity waves. If gravity waves are present the integral scale obtained from the autocorrelation function can be expected to be high [3], a maximum value of 800 m at the 76.2 m (250 ft) level has been observed. On the other hand, if the low-frequency gravity waves are absent and only turbulence of less than 5% intensity is present (Fig. 15), minimum turbulence integral scales of less than 100 m have been observed for the southerly winds. In the sector between 300° and 330° large variations in L_u^x are also present, which are the result of either the presence or absence of low-frequency velocity fluctuations as can be observed from measured u-spectra.

Vertical integral scales of the horizontal velocity components obtained from the measurements with the cup-vane system can be calculated by integration of the vertical correlation coefficients of either the u or v components.

$$L_i^z = \int_0^\infty R_{ii}^z(z')dz' \tag{8}$$

where

$$R_{ii}^z(z') = \frac{1}{\{\sigma_i(z)\}^2} \frac{1}{T} \int_0^T u_i(t,z)\, u_i(t,z+z')dt \tag{9}$$

and i = u or v

$R_{ii}^z(z')$ is the vertical correlation coefficient of either the u or v velocity fluctuations measdured at two different levels separated by a distance z'. For this research program with the Wallops Island tower the separation distance, z', can be either 0, 15.2 m (50 ft),

30.5 m (100 ft), 45.7 m (150 ft) and 61 m (200 ft). The integration (8) should be performed to the point where the correlation coefficient $R_{uu}^{z}(z')$ changes for the first time from positive to negative. However only a maximum of five values of the correlation coefficients are available for either upward or downward integration according to expression 8, and often the correlation coefficient has still a large positive value for the maximum separation distance z'.

In order to arrive at a reasonable estimate of the vertical scales, it is assumed that the vertical correlation coefficients of the horizontal velocity components u and v decay exponentially in the same manner as has been observed by Dryden et al. [38] for high Reynolds-number grid turbulence, according to

$$R_{ii}^{z}(z') = \exp[-z'/L_i^z] \tag{10}$$

Vertical integral scales of either the u or v velocity components can then be obtained from a least-squares fit of (10) to the available measured correlation coefficients.

Because of the non-symmetric flow in the boundary layer, integral scales obtained from upward and downward integration of the correlation coefficients with the origin at a common point cannot be expected to be the same. Instead a slightly different definition for the vertical integral scale is used as suggested by ESDU [29], where the correlation coefficient is defined as

$$R_{ii}^{z}(z') = \frac{1}{\{\sigma_i(z)\}^2} \frac{1}{T} \int_0^T v_i(t,z+z')v_i(t,z-z')dt \tag{11}$$

where i = u or v.

With the use of this definition only one vertical integral scale is defined for each height z. However this definition can be used for the evaluation of the integral scales of the u or v component at the 45.7 m (150 ft) level only.

The distribution of the vertical turbulence integral scales of the horizontal velocity fluctuations and obtained with the cup-vane system is shown in Figure 27 and 28 respectively. Calculation of these scales is based on expression (10). Integral scales obtained from upward integration of the correlation coefficients are shown as LUZ↑ or LVZ↑ on the figures and as $L_u^{z}\uparrow$ or $L_v^{z}\uparrow$ in the text. For the integral scales obtained from downward integration the direction of the arrow is reversed. The two-sided integral scales obtained according to the definition (11) are shown as LUZ$\updownarrow$ or LVZ$\updownarrow$ on the figures and as $L_u^{z}\updownarrow$ or $L_v^{z}\updownarrow$ in the text. Averages of all the integral scales for each sector as well as the maximum and minimum, and the mean plus and minus the standard deviations for each each sector are shown in these figures. In the sectors 0°-15° and between 90° and 165° not enough data records were available to calculate a standard deviation and only average values are plotted.

The integral scales L_u^{z} for on-shore winds are generally smaller than those for westerly winds by less than a factor of two. The integral scale $L_u^{z}\uparrow$ measured at the 15.2 m (50 ft) level and the scale $L_u^{z}\downarrow$ measured at the 76.2 (250 ft) level are of the same magnitude. The smallest observed value of L_u^{z} is about 10 m for southerly winds without the presence of gravity waves. The larger values of L_u^{z} are also observed for southerly winds when gravity waves are present.

Large values of L_u^z are also observed for northwesterly wind directions between 300° and 320°. The upward integrated scales, $L_u^{z\uparrow}$, obtained from the lower three levels for wind directions between 0° and 100° show much less variation than the downward integrated scales, $L_u^{z\downarrow}$, from the upper three levels in the same sector. Comparison of the three different scales, $L_u^{z\uparrow}$, $L_u^{z\downarrow}$ and $L_u^{z\updownarrow}$ of the measurements at the 45.7 m (150 ft) level shows that for winds between 0° and 100° the upward and downward integrated scales are of the same magnitude (37 m) with the scale $L_u^{z\updownarrow}$ having an average value of approximately 43 m. For westerly winds between 250° and 360°, $L_u^{z\uparrow}$ is about 20 m larger than $L_u^{z\downarrow}$.

The vertical integral scale of the v-component, L_v^z, behaves in a similar fashion as the scale L_u^z, but the latter is generally twice as large. The magnitude of L_v^z for winds from westerly directions is about twice the value of L_v^z for on-shore winds. Minimum values of just a few meters are observed for on-shore winds. Maximum values of these integral scales are associated with winds from northwesterly directions ($\phi \simeq 310°$) for which large direction fluctuations have been observed (Fig. 18). For southerly winds ($\phi \simeq 180°$) no large maximum values for L_v^z have been observed as for L_u^z. For on-shore winds the magnitude of the three different scales at the 45.7 m (150 ft) level are about the same but for westerly winds $L_v^{z\uparrow} > L_v^{z\downarrow}$ with the value of $L_v^{z\updownarrow}$ in between.

Figures 29 and 30 show the variation of the relative magnitude of the average turbulence integral scales L_u^x/L_u^z with wind direction for each observation level. For southerly winds between 135° and 225°, the ratio L_u^x/L_u^z increases with height from about 3.7 at the lowest

level to values between 10 and 15 at the three highest observation levels. For all wind directions outside this sector the ratio L_u^x/L_u^z is 3.3 and 3.7 at the 15.3 m (50 ft) level and the 76.2 m (250 ft) level respectively. The magnitude of the ratio of average integral scales, L_u^z/L_v^z, is 1.9, generally independent of height and wind direction.

6.4.2 Comparison of the Cup-Vane Scales with Predicted Values from References 25, 26 and 29

From the above discussion it is clear that the measured turbulence integral scales L_u^x, L_u^z and L_v^z vary significantly with terrain roughness, wind direction, time of day, thermal stability and other atmospheric conditions. In this section the measured integral scales are compared with the predicted scales from either Teunissen [25], Counihan [26] and ESDU [29].

In Figure 31 the averaged turbulence integral scales, L_u^x, obtained from the cup-vane data are shown for two westerly wind-direction sectors over near-identical terrain and are compared with the estimates of References 25, 26 and 29. At the higher elevations the values of L_u^x in the sector $300° < \phi < 315°$ are approximately 100 m larger than those in the sector $240° < \phi < 255°$. The Counihan [26] predictions match the measurements below 30 m but for higher elevations all three references under-estimate the measured integral scales. Averaged values of L_u^z and L_v^z for the same two wind direction sectors are shown in Figures 32 and 33 and compared with predicted values from Counihan [26] and ESDU [29]. The results show the decrease in magnitude when the change is made from upward to downward integration.

Values of L_v^z in the sector $300°<\phi<315°$ are about twice as large as those in the sector $240°<\phi<255°$, which is in contrast with the values of L_u^z which are approximately identical in the two wind-direction sectors. The ESDU [29] predictions of both L_u^z and L_v^z match the measured data in the wind sector $240°<\phi<255°$ reasonably well, but underestimate the scales for wind directions between 300° and 315° for which large wind-direction fluctuations have been observed [Fig. 18].

Figures 34, 35 and 36 show the averaged values of L_u^x, L_u^z and L_v^z obtained from the cup-vane data, in comparison with the predicted values for southerly winds. Since no measured values of roughness length are available for this wind direction, values of z_o were selected in accordance with the nature of the upstream terrain and Table 1 of Reference 28. Below 20 m, for the flow in the IBL, a roughness length z_o=0.01 m is appropriate and for the flow above the IBL a roughness length of z_o=0.001 m was selected. The measured longitudinal scales, L_u^x, are generally larger than the ESDU [29] predicted values, while the measured vertical scales L_u^z and L_v^z are generally smaller than the ESDU [29] predictions. These results support the likelihood that internal gravity waves exist in the surface-based inversion over the ocean. The extent of the waves is much longer in the direction of the flow than in the vertical direction because of the suppression of vertical velocity fluctuations by buoyancy forces in stable air. The results of Figure 30 show clearly the large extent of the streamwise integral scale, L_u^x, relative to the vertical scale, L_u^z for southerly winds only. For these winds the scale ratio L_u^x/L_u^z above the IBL varies between 10 and 15, for all

other wind directions the magnitude of this ratio is of the order of 4.

Longitudinal integral scales, L_u^x, obtained for westerly winds over near-uniform terrain are dependent on time of day (Fig. 37). The scales acquired during nighttime are approximately 50% longer than those obtained from morning records with the scales from afternoon data falling in between. The increase of the scales during daytime can be explained with the increase of the height of the mixed layer (See Fig. 5, Reference 13). However, no definite explanation for the large integral scales observed during nighttime is available.

In Figures 38 and 39 individual values of the turbulence integral scales, L_u^x, at the 15.2 m (50 ft) and the 45.7 m (150 ft) levels are plotted versus roughness length, z_o. These results are for near-neutral strong wind data records for wind directions varying between ϕ=250° and ϕ=30°. The scatter of the data is appreciable as is to be expected since the previously discussed results also indicate variation of L_x^u with wind direction (Fig. 31) and time of day (Fig. 37). The ESDU [29] and Teunissen [25] predictions are consistently lower than the measurements, while the Counihan predictions [26] fit the measured integral scales reasonably well. Similarly, the corresponding vertical scales $L_{u\downarrow}^{z\uparrow}$ and $L_{v\downarrow}^{z\uparrow}$ are shown versus roughness length, z_o, in Figures 40 and 41. The ESDU [29] predictions for $L_{v\downarrow}^{z\uparrow}$ match the measured results quite well, while the predictions for $L_{u\downarrow}^{z\uparrow}$ of the same source fall generally below the measured data except in the range 0.1 m<z_o<1.0 m.

6.4.3 The Direct and Spectral Methods for Obtaining Turbulence Integral Scales

Integral scales of turbulence are defined for any correlation coefficient as the integral over the entire range of the independent variable, which can be either time or space as previously discussed. In practice the integration process is carried out between the origin and the first zero-crossing. Time scales are related to the length scales in the direction of the flow by assuming the existence of Taylor's frozen turbulence hypothesis. The magnitude of the time scales varies significantly depending on the presence of low-frequency fluctuations and or trends. In order to omit these fluctuations from the time-correlation coefficients, the data should be high-pass filtered at some low frequency. The filtering of the cup-vane data takes place as a result of the block averaging, excluding trends and low-frequency fluctuations below 0.00195 Hz from the sample. Similarly, the hot-film data are high-pass filtered at either 0.0244 Hz or at 0.00153 Hz depending on whether the data are analyzed in the high-frequency range (0.0244-100 Hz) or middle-frequency range (0.00153-6.25 Hz) (See section 4.2). Turbulence integral scales calculated in this way are said to be obtained by the direct method.

An estimate of the size of the energy-containing eddies can also be obtained from the Von Karman interpolation formula for the three-dimensional power spectrum covering the wavenumber-range from the energy containing eddies to the inertial subrange [39].

$$S(k/k_e) = \frac{C(k/k_e)^4}{[1+(k/k_e)^2]^{17/6}} \qquad (12)$$

where k_e corresponds to wavenumbers in the range of the energy-containing eddies. With the assumption of isotropic turbulence, expressions for the physical realizable one-dimensional spectrum functions $S_u(k_1)$, $S_v(k_1)$ and $S_w(k_1)$ can be obtained (see expressions 3-72 and 3-73, Hinze [40]). The wavenumber of the energy-containing eddies, k_e, can be replaced by the inverse of the turbulence integral scales, L_i^x, in the appropriate spectrum functions and the constants can be adjusted to fit the measured spectra. The one-dimensional Von Karman spectrum functions obtained in this manner and presented by Teunissen [25] fit the measured spectra of mechanically produced wind tunnel turbulence quite well [41,42]. The spectral expressions for the streamwise and lateral velocity components are given by

$$\frac{nS_u(n)}{\sigma_u^2} = \frac{4(nL_u^x/U)}{[1+70.7(nL_u^x/U)^2]^{5/6}} \tag{13}$$

and

$$\frac{nS_i(n)}{\sigma_i^2} = 4\left(\frac{nL_i^x}{U}\right) \frac{1+188.4(2nL_i^x/U)^2}{\{1+70.7(2nL_i^x/U)^2\}^{11/6}} \tag{14}$$

where i = v and w.

For the comparison of these wind tunnel spectra with the normalized spectrum functions, the turbulence integral scales, L_i^x, were determined independently using the previously discussed direct method. The Von Karmon spectral equations show the correct $n^{-5/3}$-dependence in the inertial subrange. Integration of these expressions over the entire

frequency range leads to unity. At vanishing wavenumbers these spectral equations also predict the proper integral scale $L_i^x = S_i(0)U/4\sigma_i^2$. At low frequencies the logarithmic spectra vary as n^{+1}, which also fits the wind tunnel spectra quite well.

However, caution must be taken with the automatic adaption of the Von Karman spectral functions to atmospheric turbulence under near neutral thermal stratification. The work of Kaimal et al [20] clearly points out that under near-neutral conditions the low-frequency content in the spectra of the horizontal velocity components can vary appreciably. In the convective boundary layer spectral data approach a definite shape when near neutral conditions are approached from the stable regime. Under these conditions significant low-frequency velocity fluctuations in the u and v components are absent and the spectral shape of these components is similar to the Von Karman model. On the other hand no unique spectral shape for the u and v component exists for near neutral conditions approached from the unstable regime. Under these conditions, the low-frequency spectral content is much higher and the Von Karman model does not represent the spectral data well.

In order to check the validity of the Von Karman spectral functions, it will be necessary to check these relations against measured spectra, where the frequency is normalized with the local mean velocity and the turbulence integral scale obtained independently via the direct method. In Figures 42 and 43 logarithmic spectra of the u-component measured at 5 different elevations for data record 19 (Table 1) are compared with the Von Karman spectral function. The difference in those two illustrations is that variances and integral scales used in Figure 42

were obtained in the middle-frequency range (0.00153-6.25 Hz) while for Figure 43 the variances and integral scales were obtained in the high-frequency range (0.0244-100 Hz) filtering out the low-frequency fluctuations. In the latter case the Von Karman expression fits the measured spectra quite well in the -2/3 region but in the low-frequency range the measured spectral values are considerably higher than the predicted values. Consequently no distinct spectral peak at the predicted value of the reduced frequency of $nL_u^x/U=0.146$ is present. Similarly, the measured v spectra follow the Von Karman spectrum in the -2/3 region only if variances and integral scales are used from which the low-frequency components are filtered out. Figures 44 and 45 show the w-spectra for run #19 in comparison with the Von Karman spectrum function for variances and integral scales obtained in the middle and high frequency range respectively. In the latter case the measured spectra fit the theoretical Von Karman spectrum function much better especially for the spectra from the higher elevations.

Based on these results the conclusion can be drawn that the theoretical Von Karman spectrum functions do not represent the spectra of atmospheric turbulence in the low-frequency range or in the high-frequency range when turbulence integral scales are used that are obtained via the direct method when low-frequency fluctuations are included. Better fit of the measured spectra in the -2/3 region is achieved when variances and turbulence integral scales are used that are obtained from data records from which the low-frequency fluctuations have been removed. Inversely, if the theoretical Von Karman spectrum functions are used to obtain streamwise turbulence integral scales,

L_i^x, as is suggested in references 25 and 28, then these scales are not equivalent to the integral scales obtained via the direct method. The integral scales obtained via the Von Karman method must be interpreted as integral scales associated with velocity records from which all low-frequency fluctuations with periods longer than approximately 40 seconds have been filtered out.

The expressions for the streamwise turbulence integral scales, L_i^x for i=u,v and w, listed in references 25 and 29 are based on scales obtained via the Von Karman method by either matching of the measured spectra at the peak reduced frequency or by using a best overall fit of the spectra. Consequently the predicted integral scales from these sources must be interpreted as integral scales associated with the high-frequency content of the turbulence components.

6.4.4 Comparison of Integral Scales Obtained Via the Direct and Spectrum Methods With Predicted Values from References 25, 26 and 29.

The turbulence integral scales, L_u^x, obtained from the cup-vane data are obtained via the direct method in the frequency range from 0.00195 Hz to 0.25 Hz. Integral scales obtained from the hot-film data and discussed in this section, are obtained by one of the following three methods:

1. The direct method in the middle-frequency (MF) range (0.00153-6.25 Hz).

2. The Von Karman method, with the spectra and variances obtained from filtered data in the middle-frequency range (VK-MF).

3. The Von Karman method, with the spectra and variances obtained from filtered data in the high-frequency range (0.0244-100 Hz) (VK-HF).

For method 2 and 3 values of L_i^x were obtained by matching the measured logarithmic spectra ($nS_i(n)/\sigma_i^2$ versus nz/U) at nz/U=10 to the Von Karman spectrum functions in the -2/3 range. Averaged and single-record streamwise integral scales, L_i^x, obtained from the cup-vane data or from the hot-film data, the latter derived through one of the above three methods, are shown for the two basic wind directions (south and northwest) in Figures 46 through 57 and are compared with the predicted values of references 25, 26 and 29.

Figures 46, 47 and 48 show the variation of the averaged integral scales, L_i^x with i=u,v and w, obtained from the hot-film data (methods 2 and 3) versus height for southerly winds. The predicted values are based on a roughness length, z_o=0.01 m in the IBL below 20 m and on a roughness length z_o=0.001 m above the IBL. The values of L_u^x from the cup-vane data match the ESDU [29] predictions and the scales obtained from the hot-film data via the Von Karman method in the middle-frequency range match the Teunissen [25] predictions. Values of L_v^x and L_x^x obtained with the use of the Von Karman method in either frequency range fall well below the predictions. Of course, as previously discussed, the ratio of longitudinal scales and lateral scales is much higher for southerly winds than for the other wind directions (Figs. 29, 30). The effect of buoyancy in the inversion layer tends to suppress the vertical motion and consequently the measured scales L_w^x are much smaller than the predicted scales. It must be assumed that the predicted scales are based on data records taken under conditions where buoyancy had very little effect on the turbulence. The lateral scales, L_v^x and L_w^x obtained via the Von Karman method in the middle-frequency range are about twice as long as the scales obtained from the same data in the high-frequency range.

Figures 49, 50 and 51 show the averaged integral scales, L_i^x for i=u, v and w, obtained from the hot-film data and analyzed according to methods 1 and 2 for northwesterly wind directions. In Figure 49 comparison of L_u^x is also made with the cup-vane data. The scales obtained via the direct method from the cup-vane data are generally smaller than the scales from the hot-film data via the direct method in the middle-frequency range. The scales obtained with the Von Karman method in the middle-frequency range are systematically smaller than the scales obtained with the direct method from either the cup-vane or hot-film data in the same frequency range. The Teunissen [25] and ESDU [29] predictions only fit the measured scales obtained via the Von Karman method below a height of 20 m. Above this height the predicted values are systematically lower than the measured values. The Counihan [26] predicted scales of L_u^x fit the observed scales obtained via the direct method below 20 m, however above the height of 20 m the Counihan prediction falls between the measured scales obtained via the direct method and those obtained via the von Karman method.

The measured lateral scales L_w^x and L_v^x obtained via the direct method in the middle-frequency range are three to four times as large as those obtained via the Von Karman method in the same frequency range (Figs. 50, 51). The latter scales match the Teunissen [25] and ESDU [29] predictions very well.

In Figures 52, 53 the integral scales, L_u^x, obtained from a single early-evening record are compared with the predicted scales and with the average scales from the daytime records all analyzed in the middle-frequency range. It has been observed [13, 23] that just before sunset the convective boundary layer dissolves abruptly and the low-frequency velocity fluctuations normally associated with the convective

PBL suddenly disappear as can be clearly seen from the comparison of the plotted records of the horizontal velocity components of record 16 (evening run) and record 19 (afternoon run) (Fig. 54). The results indicate much smaller scales if the low-frequency fluctuations of the horizontal components are absent. For record 16 the scales obtained via the direct method are systematically larger than those obtained via the Von Karman method, although the difference is less significant for this early evening run than for the daytime records, which contain low-frequency fluctuations (Figs. 49-51).

Figures 55 through 58 show the averaged integral scales, L_v^x and L_w^x, from the daytime records and those for record 16 obtained via the Von Karman method in either the high-frequency range or the middle-frequency range. The Von Karman method for obtaining integral scales provides near-identical results independent of the frequency range if large low-frequency fluctuations are absent (e.g. record 16) or if the low-frequency fluctuations are removed from the data records. If the large low-frequency fluctuations are present (e.g. u and v components of daytime records Fig. 54) and are not removed from the daytime records the Von Karman method leads to much larger integral scales. If no appreciable low-frequency velocity fluctuations are present in the data records, the integral scales obtained via either the direct or the Von Karman method are about the same in magnitude. However, if low-frequency components are present the magnitude of the scales depends on the method by which they were calculated and also depends on the frequency range in which the data are analyzed.

When the integral scales, L_u^x, obtained via the two-methods in either one of the frequency ranges, for data records with or without low-frequency content are compared with predicted values (Figs. 49, 52 and 53) one observes appreciable variation. In general, the Teunissen [25] predicted values correspond to scales obtained from data records for which the large low-frequency fluctuations are absent or are filtered out, and obtained via either method. On the other hand the Counihan [26] predicted values correspond more to the scales obtained from data records with low-frequency fluctuations and obtained via the Von Karman method in the middle-frequency range and to the scales obtained from the cup-vane data. The magnitude of the scales obtained from the same data records via the direct method are generally larger than those predicted by Counihan [26]. The ESDU [29] predicted scales fall between the two previously mentioned predictions. The scales obtained from data records of north-west winds with low-frequency fluctuations vary almost linearly with height, while the predicted scales show more a tendency toward independency with height at higher elevations.

Similarly the lateral integral scales, L_v^x (Figs. 50, 55 and 57) also show appreciable variation. The Teunissen [25] and ESDU [29] predictions correspond reasonably well to the scales obtained during daytime via the Von Karman method in the middle-frequency range. The scales obtained from the same daytime records via the direct method are significantly larger than the predictions. On the other hand if low-frequency components are absent or filtered from the data records the measured values for the lateral integral scales, L_v^x, fall well below the predicted values.

The integral scales, L_w^x, (Figs. 51, 57 and 58) show a similar pattern, the ESDU [29] and Teunissen [25] predictions correspond best

to the scales obtained via the Von Karman method in the middle frequency range. The scales obtained via the direct method in the same frequency range are considerably larger than the predicted values. If low-frequency components are absent or removed from the data records the measured scales are generally lower than the ESDU [29] and Teunissen [25] predictions.

In general it can be concluded that the ESDU [29] and the Teunissen [25] predicted L_v^x and L_w^x scales should be interpreted as scales obtained via the Von Karman method for turbulence with low-frequency fluctuations. On the other hand the Teunissen [25] predicted L_u^x scales should be interpreted as scales obtained from data records from which the large low-frequency fluctuations are absent or are filtered out. In general the horizontal scales L_u^x and L_v^x obtained from the daytime data records via the Von Karman method in the middle-frequency range vary linearly with height, while the predicted scales show a tendency of independnece with height at the higher elevations.

6.5 Power Spectra

In this section the power spectra of the three velocity components obtained from the hot-film data are discussed for the two basic wind directions, south and northwest. Ample discussion of the spectra in the previous section has indicated that the spectral shape in the low-frequency range depends greatly on the absence or presence of large low-frequency velocity fluctuations.

The logarithmic spectra obtained from south-wind records generally show very little variation in shape and vary as $f^{-2/3}$ in the high-frequency range and approximately as f^{+1} in the low-frequency range. These two ranges

are separated by a distinct spectral peak. Kaimal (43) suggests that under stable conditions in the absence of appreciable low-frequency fluctuations all spectra can be brought in coincidence and approximated by the empirical relation

$$\frac{nS_i(n)}{\sigma_i^2} = \frac{0.164(f/f_o)}{1+0.164(f/f_o)^{5/3}} \tag{15}$$

with i=u, v and w,

where $f=nz/U$ is the reduced frequency and f_o is the reduced frequency at the point of intersection of the extrapolation of the inertial subrange of the spectra and the line $nS_i(n)/\sigma_i^2=1$. Kaimal's spectra and variances are obtained from data in the frequency range $0.005 \leq n \leq 10$ Hz.

The Von Karman spectrum functions (13, 14) can be modified into similar expressions

$$\frac{nS_u(n)}{\sigma_u^2} = \frac{0.156f/f_o}{[1+0.108(f/f_o)^2]^{5/6}} \tag{16}$$

and

$$\frac{nS_i(n)}{\sigma_i^2} = 0.12(f/f_o)\left[\frac{1+0.679(f/f_o)^2}{\{1+0.255(f/f_o)^2\}^{11/6}}\right] \tag{17}$$

with i=v and w.

In this set of equations the reduced frequency is defined as $f=nL_i^x/U$. However the parameter f/f_o for either the Kaimal or the Von Karman expressions represents the wavelength ratio λ_o/λ, where λ_o is the wavelength associated with the reduced frequency, f_o. In both spectral expressions the parameter f/f_o is independent of the length scale which is either the elevation or the turbulence integral scale L_i^x.

The Kaimal (15) and the Von Karman (16,17) spectrum functions are nearly identical in the inertial subrange, but the Kaimal spectrum predicts a slightly smaller spectral peak. In the low-frequency range the u-spectra again are about identical, but the Von Karman v and w spectra fall slightly below the Kaimal spectrum.

In Figures 59, 60 and 61 the normalized logarithmic u, v and w spectra ($nS_i(n)/\sigma_i^2$) are plotted as a function of the modified reduced-frequency f/f_o. The spectra were taken from different data records for winds from southerly directions, which were classified according to the local stability parameter z/L. The spectral data and the variances were obtained from data analyzed in the high-frequency range $0.0244 \leq n \leq 100$ Hz. The velocity spectra obtained from stable-air records above the IBL do not differ from those obtained in the unstable air in the IBL and all fit the Von Karman and the Kaimal spectral functions remarkably well.

The empirical spectrum functions (15,16,17) for estimation of the velocity spectra in the case low-frequency fluctuations are absent can be extremely useful if values of f_o can be predicted. Based on the experimental results it is obvious that f_o varies with height and with the presence or absence of appreciable low-frequency velocity fluctuations. The results did not indicate any systematic variation of f_o with stability as suggested by Kaimal [43]. Averaged values of $f_o=(nz/U)_o$ for each velocity component and obtained from normalized logarithmic spectra in the high-frequency range are shown as a function of height in Figure 62. However, values for f_o obtained from the same data records but analyzed in the middle-frequency range ($0.00153 \leq n \leq 6.25$ Hz) depend greatly on the presence of low-frequency velocity fluctuations. If no appreciable low-

frequency fluctuations are present, the values f_o are independent of the frequency range the data are analyzed.

For all u-spectra investigated low-frequency fluctuations are present between the low cut-off frequencies for the middle- and high-frequency ranges, 0.00153 Hz and 0.0244 Hz respectively. These spectra do not exhibit a distinct spectral peak but instead values of the logarithmic spectra are approximately the same for $f<0.1$. Values of f_o obtained from the u-spectra analyzed in the middle-frequency range are generally smaller than those obtained from the same data records but analyzed in the high-frequency range and seem to converge to a general value in the range $0.02<f_o<0.03$, independent of height.

For those records where internal gravity waves affect the spectra above a frequency of n=0.00153 Hz, the frequency range for which spectral values are increased varies with elevation. At the lowest elevation (z=9.1 m) only the spectral values at the lowest frequencies are affected and an appreciable range where the normalized logarithmic spectrum varies as f^{+1} is still present (Fig. 63). However for spectra from higher elevations the f^{+1}-range becomes gradually smaller as the effect of the waves is felt at increasing frequencies until no appreciable frequency range with a f^{+1} spectral distribution is present (Fig. 64). For those cases values of f_o for the u-spectra seem to vary between the lower limit of $f_o=0.02\sim0.03$ and the values of f_o obtained in the high-frequency range as shown in Figure 62. Similar observations can be made for the v and w spectra. The values of f_o obtained from spectra analyzed in the middle-frequency range are generally lower than those obtained from the same spectra analyzed in the high-frequency range.

Spectra obtained from data records for westerly winds exhibit significant low-frequency content for all elevations and the spectral data fit the Kaimal or the Von Karman spectrum functions (15,16,17) in the inertial subrange (-2/3 region) only (Figs. 65,66,67). The v-spectra (Fig. 66) show a peculiar shape which is typical for spectra of the lateral velocity component in the surface layer of a convective boundary layer [19]. Kaimal's explanation for this shape is based on the fact that in the inertial subrange the spectral values of the v-component are 4/3 times larger than the u-spectra, a requirement for isotropy in this range. (A similar situation exits for the w-spectra.) As the w-spectra reach their peak and start to roll off with lower frequencies, the v-spectra instead continue to increase and start to follow the u-spectra. The result of this is the peculiar shape of the v-spectra in the transition between the -2/3 range and the low-frequency range where the u and v spectra both are independent with elevation but instead vary with the height, z_i, of the convective boundary layer.

In the case the low-frequency fluctuations are absent as is the case just before sunset, as the convective boundary layer disintegrates rapidly, the u, v and w spectra (Figs. 68,69,70) and specifically the v-spectra (Fig. 69) have a completely different character. The v-spectra show a distinct spectral peak and a rapid roll-off at lower frequencies although the spectra values fall above the Von Karman prediction in this range. However in comparison with the spectra of the daytime run 19 [figs. 65, 66,67], the spectra of the evening run 16 show much lower spectra values in the low-frequency range and the peculiar shape of the daytime v-spectra as discussed above has disappeared and the v-spectra resemble the Von Karman

prediction.

Values of the reduced frequency, f_o, defined as the intersection of the extrapolation of the spectra in the inertial subrange and the line $nS_i(n)/\sigma_i^2=1$, were obtained from spectra analyzed in both the high- and middle-frequency range. For the daytime u and v-spectra for which appreciable low-frequency velocity fluctuations are present, the values of f_o obtained in the high-frequency range are systematically three times as large as the corresponding values obtained from the spectra analyzed in the middle frequency range, while for the w-spectra the ratio $(f_o)_{HF}/(f_o)_{MF}$ is approximately 1.6, indicating that the low-frequency content is larger in the u and v spectra than in the w-spectra. For run 16 this ratio for the u-spectra is 1.9 and for the v and w spectra 1.25. These results clearly indicate the effect of the low-frequency fluctuations on the location of the inertial subrange when the spectra are presented in the logarithmic form with $nS_i(n)/\sigma_i^2$ and $f=nz/U$ as coordinates. The distribution of f_o with elevation for daytime spectra and evening spectra analyzed in the middle-frequency range are shown in Figure 71. The results from the daytime spectra show that the values of f_o for each velocity component are approximately independent with height and are $(f_o)_u \simeq 0.01$, $(f_o)_v \simeq 0.02$ and $(f_o)_w \simeq 0.07$. This observation is in agreement with some of the results obtained for southerly winds although the values are somewhat higher because of less low-frequency content. If no low-frequency fluctuations are present in the velocity components, the values of f_o generally increase with height (Figs. 62,71).

The values of f_o can be used to obtain the wavelengths corresponding to the spectral peaks associated with either the Kaimal or the Von Karman spectral functions. Since for both empirical relations the logarithmic

spectral peak is approximately located at $f/f_o \simeq 3.8$, then $f_m \simeq 3.8 f_o$ and

$$(\lambda_m)_i = 0.26z/(f_o)_i \quad \text{for } i=u,v,w. \tag{18}$$

Here the wavelength, $\lambda_m=(U/n)_m$, corresponds to the peak of the Kaimal and Von Karman spectrum functions and to the peak of the measured spectra if no appreciable low-frequency fluctuations are present in the data records. The peak wavelengths, $(\lambda_m)_i$, are often used in micrometeorology as measures of the energy containing eddies, or they can be slightly modified to fit the original Von Karman spectrum functions (13,14) from which values of L_i^x can be predicted as proposed by Teunissen [25]

$$L_u^x = 0.146\ (\lambda_m)_u$$

and

$$L_i^x = 0.106\ (\lambda_m)_i \text{ for } i=u,w \tag{19}$$

However it must be realized that these predicted scales associated with the empirical spectrum functions are equivalent to the turbulence integral scale obtained from correlation functions only if no large low-frequency velocity fluctuations are present. In the case large low-frequency velocity fluctuations are present and not filtered from the data records, the scales obtained from correlation functions are generally larger in magnitude (see section 6.4).

7. SUMMARY AND CONCLUSIONS

A rather detailed description has been given of a micrometeorological facility consisting of an instrumented 76 m (250 ft) tower located within a 100 m distance from the shore at Wallops Island, Virginia. The instrumentation system consists of cup-vane and temperature instruments mainly used for profile measurements and a hot-film system for turbulence measurements. The data acquisition and handling system for the hot-film instruments is located in an instrumentation trailer located at the base of the tower. The heart of this system is a PDP 11/20 DEC minicomputer which controls the digitization of the data (200 Hz sample rate) and the data transfer onto digital tape. The digitized data have been analyzed on an IBM-370 computer located on the VPI and SU campus.

Data have been acquired with the cup-vane system under moderately strong wind conditions for all wind directions during a 4 1/2-year period. From this data-base mean velocity and mean temperature profiles and associated parameters (roughness length, z_o, and powerlaw exponent, α) have been derived as well as turbulence intensities, σ_u/U and σ_v/U, and turbulence integral scales, L_u^x, L_u^z and L_v^z. Averages of the calculated flow parameters from all data records in each 15-degree sector have been presented. In addition averaged mean velocity ratios V/V_{250}, turbulence intensities, σ_u/U, σ_v/U, and turbulence integral scales, L_u^x, have been obtained for 11 sectors each with near-uniform upstream terrain. The results provide information about the microclimate at this site under moderately strong wind conditions. This information is graphically presented in

Figures 72 through 75 from which average wind design data for this coastal site can be established. In addition, data have been acquired with the hot-film system for the southerly and northwesterly prevailing wind directions. With this system turbulence parameters such as turbulence intensities, Reynolds stresses, turbulence heat fluxes, integral scales (L_u^x, L_v^x and L_w^x) and power spectra of the three velocity components have been obtained.

For all observations made at this site under moderately strong wind conditions, truly neutral thermal stratifications have never been encountered throughout the observation height of 76.2 m for any length of time. For westerly wind direction under sunny daytime conditions the measured velocity and temperature profiles suggest that the surface flow at the Wallops Island site is similar to the surface flow observed during the Minnesota experiment [12]. The observed PBL flow at Minnesota is an example of a typical convective boundary layer, a model of which is described in detail in Reference 13. In addition to mechanical and convective turbulence generated in this atmospheric boundary layer, large-scale turbulence due to the interaction of the mixed layer and the capping inversion (entrainment) affects the mean and turbulent surface flow regardless of the wind velocity. However, appreciable deviations from the convective boundary-layer model may occur depending on atmospheric conditions, time of day and wind direction.

It has been observed that just before sunset the daytime boundary-layer flow is modified drastically as a result of the

disappearance of the large-scale turbulence and appearance of a surface-based inversion. Similarly under conditions of low cloud cover combined with precipitation, an inversion below the cloud cover may develop, impeding the regular development of the daytime convective boundary layer. Under these conditions the influence of the large-scale turbulent motions on the flow below the inversion is reduced, resulting in an appreciable reduction in turbulence intensities and turbulence integral scales. Large negative lateral velocity fluctuations or large wind direction fluctuations towards the north have been observed for northwesterly wind directions specifically between 300° and 315°. For winds in this sector larger values of the lateral turbulence intensity and larger turbulence integral scales have been observed than for winds outside this sector but with the same upstream terrain. In addition, turbulence intensities and turbulence integral scales vary during the daytime as the convective boundary layer develops. The above observations have been made under moderately strong wind conditions with hourly mean-wind speeds between 10 m/s and 20 m/s at z=9.1 m. Based on all the observations made for westerly winds at Wallops Island, there is no evidence that similar flow variations in the surface layer would not exist under extreme and potentially damaging wind conditions with velocities in excess of 20 m/s. Consequently at this point in time it cannot automatically be assumed that for extremely strong winds from westerly directions, the PBL flow at the Wallops Island site is similar to the purely shear-generated,

neutrally-stratified boundary-layer flow model, which is so often advocated by wind engineers.

The mean and turbulent flow for southerly winds also differs appreciably from that predicted by the neutral boundary-layer model. During the summertime the warm air blowing over the cooler ocean water gives rise to a surface-based inversion of variable height. Depending on the thermal stability, a low-level jet with a maximum velocity occasionally below the highest observation level has been observed. Under extreme stable conditions the turbulence at the two highest observation levels has been observed to vanish completely and generally internal gravity waves may co-exist with the turbulence. Under these conditions the surface layer is very shallow, well below the lowest observation level. Moreover, the flow near the surface will also undergo a modification as soon as the ocean air crosses the beach and experiences an increase in surface roughness and surface temperature. These modifications of the surface flow manifest themselves in the form of a developing internal boundary layer (IBL) which at the tower location is between 15 m and 30 m in height, depending on the change in surface temperature and the overland development distance which varies with wind direction.

The conclusions of the boundary-layer experiment at Wallops Island can be summarized as follows:

I. Westerly wind directions

1. The observed daytime flow below 76m at Wallops Island is described better by the convective boundary-layer model [13] than by the neutral boundary-layer model.

2. The height at which transition occurs from the logarithmic velocity profile to the mixed-layer velocity profile varies with wind velocity surface roughness and thermal stability.

3. The roughness length, z_o, obtained from velocity profiles below the transition are in agreement with predicted values from PBL-flow review papers.

4. The Panofsky relation, $\alpha = z_o / \ln \sqrt{z_1 z_2}$, is only useful for predicting values of powerlaw exponents for velocity profiles in the surface layer below the elevation where transition to the mixed-layer profile starts.

5. Measured turbulence intensities are generally in agreement with predicted values, except for the lateral turbulence intensities, σ_v/U, in the northwesterly wind-direction sector $300° < \phi < 315°$. In this sector the turbulence intensities of the horizontal velocity components (u and v) are of the same magnitude.

6. Turbulence intensities of the horizontal components also vary with time of day and atmospheric conditions, or in general with the absence or presence of appreciable low-frequency velocities fluctuating in the frequency range between 0.0015 Hz and 0.02 Hz.

7. The magnitude of the turbulence integral scales depends on the method (direct method or spectral method) by which they are calculated and also on the presence or absence of appreciable low-frequency velocity fluctuations.

8. If appreciable low-frequency content is present and is not filtered from the data records, the turbulence integral scales obtained via the direct method are larger than the predicted values.

9. The turbulence integral scales vary also with time of day, wind direction, surface roughness, and atmospheric conditions such as cloud cover combined with precipitation.

10. The measured vertical integral scales, L_u^z and L_v^z vary with direction of integration but are generally in agreement with predicted values.

11. The ratio L_u^x/L_v^z varies generally between 3 and 4 and the ratio L_u^z/L_v^z has an approximate value of 2.

12. The daytime turbulence spectra follow the Kaimal model [19] and deviate appreciably from the Von Karman model especially in the low-frequency range.

13. The Von Karman spectral model does not fit the measured spectra if appreciable low-frequency velocity fluctuations are present and are included in the spectral analysis and in the calculation of the variance, σ_i, and integral scale (direct method).

II. Southerly wind Directions

1. For on-shore winds an IBL develops as the surface air passes the beach and experiences an increase in surface roughness and an increase in surface temperature especially in the summer during daytime.

2. For southerly wind directions warmer air flows over the cooler water creating a surface based inversion which is characterized by a very shallow surface layer, low-level maximum velocity (surface jet), low turbulence intensities, occasional vanishing of the turbulence under extreme stable conditions and co-existence of turbulence and low-frequency internal gravity waves.

3. No simple boundary-layer flow model is available to describe the on-shore flow at the Wallops Island site. Variations in observed velocity and temperature profiles, turbulence intensities and turbulence integral scales are extremely high and can occur within a very short time.

4. Measured velocity spectra (excluding the low-frequency gravity waves) are independent of thermal stability and seem to fit the modified Von Karman spectrum model (16,17) and the Kaimal stable spectrum model (15) extremely well.

As the above conclusions clearly indicate, there is no single and no simple PBL-flow model available to describe the mean and turbulent flow near the surface under moderately strong wind conditions at the Wallops Island site. The presence or absence of appreciable low-frequency velocity fluctuations causes the parameters describing this flow to vary a great deal. The non-uniform surface conditions

and the presence of the low-frequency fluctuations, either in the convective boundary layer or in the on-shore winds in the form of internal gravity waves, cause the observed surface flow to be quite different from the neutral boundary layer flow model. For the prevailing winds from either the south or westerly directions the experimental results do not show any evidence for the PBL flow to approach the neutral boundary-layer model as the wind speed increases from moderately strong to extreme.

It is assumed that engineers, already aware of uncertainty in modeling the PBL flow, use safety factors in the design of wind turbines to allow for differences in the actual wind environment in comparison with the predictions from the neutral PBL model. The variation of the turbulence intensities and turbulence integral scales, measured under moderately strong wind conditions at the Wallops site, is appreciable. Consequently a great deal of difference may exist between actual measurements and the neutral PBL model. Experimental evidence does not indicate that mean wind and turbulence parameters will conform closer to the neutral PBL-model under higher wind-speed and slightly unstable conditions. The observed differences appear at the lower frequencies which are pertinent to the response characteristics of the larger machines. Therefore, the design of large wind turbines may need an increased safety factor with respect to turbulence at frequencies below about 0.01 Hz.

REFERENCES

REFERENCES

1. H. W. Tieleman and S. C. Tavoularis, "A Method for the Measurement and the Statistical Analysis of Atmospheric Turbulence," NASA-CR-140586, 1974. Also Virginia Polytechnic Institute and State University, VPI-E-74-26, October 1974.

2. H. W. Tieleman and S. C. Tavoularis, "An Instrumentation System for the Measurement of Atmospheric Turbulence," Journal Industrial Aerodynamics, 2(1) (1977) 49-63.

3. H. W. Tieleman and D. B. Derrington, "An Experimental Study of the Atmospheric Boundary Layer Modified by a Change in Surface Roughness and Surface Temperature," Virginia Polytechnic Institute and State University, VPI-E-77-17, May 1977.

4. H. W. Tieleman and W. W. L. Chen, "Statistical Analysis of Low-Level Atmospheric Turbulence," NASA-CR-137456, 1974. Also Virginia Polytechnic Institute and State University, VPI-E-74-3, January 1974.

5. H. W. Tieleman, K. P. Fewell and H. L. Wood, "An Evaluation of the Three-Dimensional Split-Film Anemometer for Measurements of Atmospheric Turbulence," NASA-CR-62093, 1973. Also Virginia Polytechnic Institute and State University, VPI-E-73-9, March 1973.

6. H. Tennekes, "A Model for the Dynamics of the Inversion above a Convective Boundary Layer," Journal Atmospheric Sciences, 30(1973), 558-567.

7. J. W. Deardorff, "Numerical Investigation of Neutral and Unstable Planetary Boundary Layers," Journal Atmospheric Sciences, 29 (1972) 91-115.

8. J. W. Deardorff, "Three-Dimensional Numerical Study of the Height and Mean Structure of a Heated Planetary Boundary- Layer," Boundary-Layer Meteorology, 7 (1974) 81-106.

9. J. W. Deardorff, "Three-Dimensional Numerical Study of Turbulence in an Entraining Mixed Layer," Boundary-Layer Meteorology, 7 (1974) 199-226.

10. J. C. Wyngaard and O. R. Coté, "The Evolution of a Convective Planetary Boundary Layer- A Higher-Order-Closure Model Study," Boundary-Layer Meteorology, 7 (1974) 289-308.

11. G. E. Willis and J. W. Deardorff, "A Laboratory Model of the Unstable Planetary Boundary Layer," Journal Atmospheric Sciences, 31 (1974) 1449-1452.

12. Y. Izumi and S. J. Caughey, "Minnesota 1973 Atmospheric Boundary Layer Experiment Data Report," AFCRL-TR-76-0038, Air Force Cambridge Research Labratories, Hanscom AFB, January 1976.

13. J. C. Kaimal et al., "Turbulence Structure in the Convective Boundary Layer," Journal Atmospheric Sciences, 33(1976) 2152-2169.

14. S. J. Caughey and J. C. Wyngaard, "The Turbulence Kinetic Energy Budget in Convective Conditions," Quarterly Journal of the Royal Meteorological Society, 105 (1979) 231-239.

15. S. J. Caughey, "Boundary-Layer Turbulence Spectra in Stable Conditions," Boundary-Layer Meteorology, 11 (1977) 3-14.

16. L. Mahrt et al., "An Observational Study of the Structure of the Nocturnal Boundary Layer," Boundary-Layer Meteorology, 17 (1979) 247-264.

17. S. J. Caughey, J. C. Wyngaard and J. C. Kaimal, "Turbulence in the Evolving Stable Boundary Layer," Journal Atmospheric Sciences, 36 (1979) 1041-1052.

18. S. Sethuraman, "The Observed Generation and Breaking of Atmospheric Internal Gravity Waves Over the Ocean," Boundary-Layer Meteorology, 12 (1977) 331-349.

19. J. C. Kaimal, "Horizontal Velocity Spectra in an Unstable Surface Layer," Journal Atmospheric Sciences, 35 (1978) 18-24.

20. J. C. Kaimal et al., "Spectral Characteristics of Surface-Layer Turbulence," Quarterly Journal of the Royal Meteorological Society, 98 (1972) 563-589.

21. N. E. Busch, "The Surface Boundary Layer," Boundary-Layer Meteorology, 4 (1973) 213-240.

22. S. J. Caughey and J. C. Kaimal, "Vertical Heat Flux in the Convective Boundary Layer," Quarterly Journal of the Royal Meteorological Society, 103 (1977) 811-815.

23. H. W. Tieleman and S. E. Mullins, "Atmospheric Turbulence Below 75 m in the Convective Boundary Layer (Strong Wind Conditions)," Proceedings, Third Colloquium on Industrial Aerodynamics, Aachen, Department of Aeronautics, Fachhochschule Aachen, (1978) 1-23.

24. S. Sethuraman, "Structure of Turbulence over Water During High Winds," Journal Applied Meteorology, 18 (1979) 324-328.

25. H. W. Teunissen, "Characteristics of the Mean Wind and Turbulence in the Planetary Boundary Layer," UTIAS Review No. 32, University of Toronto, October 1970.

26. J. Counihan, "Adiabatic Atmospheric Boundary Layers: A Review and Analysis of Data from the Period 1880-1972," Atmospheric Environment, 9 (1975) 871-905.

27. Engineering Sciences Data Unit, "Characteristics of Wind Speed in the Lower Layers of the Atmosphere near the Ground: Strong Winds (Neutral Atmosphere)," ESD Item No. 72026, 1972.

28. Engineering Sciences Data Unit, "Characteristics of Atmospheric Turbulence near the Ground, Part II: Single Point Data for Strong Winds (Neutral Atmosphere)," ESD Item No. 74031, 1974.

29. Engineering Sciences Data Unit, "Characteristics of Atmospheric Turbulence near the Ground, Part III: Variations in Space and Time for Strong Wind Conditions (Neutral Atmosphere)," ESD Item No. 75001, 1975.

30. D. M. Deaves and R. I. Harris, "A Mathematical Model of the Structure of Strong Winds," ESRU Report No. 24, Environmental Sciences Research Unit, Cranfield, England, December 1976.

31. H. A. Panofsky, "Wind Structure in Strong Winds Below 150 m", Wind Engineering, 1 (1977) 91-103.

32. J. L. Lumley and H. A. Panofsky, "The Structure of Atmospheric Turbulence," John Wiley, New York, 1974.

33. H. A. Panofsky, "The Atmospheric Boundary Layer Below 150 Meters," Annual Review of Fluid Mechanics, Volume 6, Annual Reviews Inc., Palo Alto, California, 1974.

34. H. W. Tieleman and S. E. Mullins, "The Structure of Moderately Strong Winds at a Mid-Atlantic Coastal Site (Below 75 m)," Proceedings Fifth International Conference on Wind Engineering, Colorado State University, (1979), II-5, 1-15.

35. J. C. Kaimal, "NOAA Instrumentation at the Boulder Atmospheric Observatory," Proceedings Fourth Symposium on Meteorological Observations and Instrumentation, Denver, Colorado, (1978) 35-40.

36. A. P. van Ulden, J. G. van der Vliet and J. Wieringa, "Temperature and Wind Observations at Heights from 2 m to 200 m at Cabauw in 1973," Royal Netherlands Meteorological Institute, De Bilt, W. R. 76-7, 1976.

37. W. P. Elliott, "The Growth of the Atmospheric Internal Boundary Layer," Transaction American Geophysical Union, 39 (1958) 1048-1054.

38. H. L. Dryden et al., "Measurements of Intensity and Scale of Wind-Tunnel Turbulence and Their Relation to the Critical Reynolds number of Spheres," NACA TR No. 581, 1937.

39. T. Von Karman, "Progress in the Statistical Theory of Turbulence," Turbulence, Classic Papers on Statistical Theory, S. K. Friedlander and L. Topper editors, Interscience Publishers, Inc. New York, 1961.

40. J. O. Hinze, Turbulence, 2nd edition, McGraw-Hill, New York, 1975.

41. T. A. Reinhold, H. W. Tieleman and F. J. Maher, "Investigation of a Grid-Induced Turbulent Environment for Wind Tunnel Testing," Virginia Polytechnic Institute and State University, VPI-E-74-30, December 1974.

42. T. A. Reinhold, H. W. Tieleman and F. J. Maher, "Simulation of the Urban Neutral Boundary Layer for the Model Study of Wind Loads on Tall Buildings," Virginia Polytechnic Institute and State University, VPI-E-77-12, March 1978.

43. J. C. Kaimal, "Structure Parameters in the Stable Surface Layer," Boundary-Layer Meteorology, 4 (1973) 289-309.

FIGURES

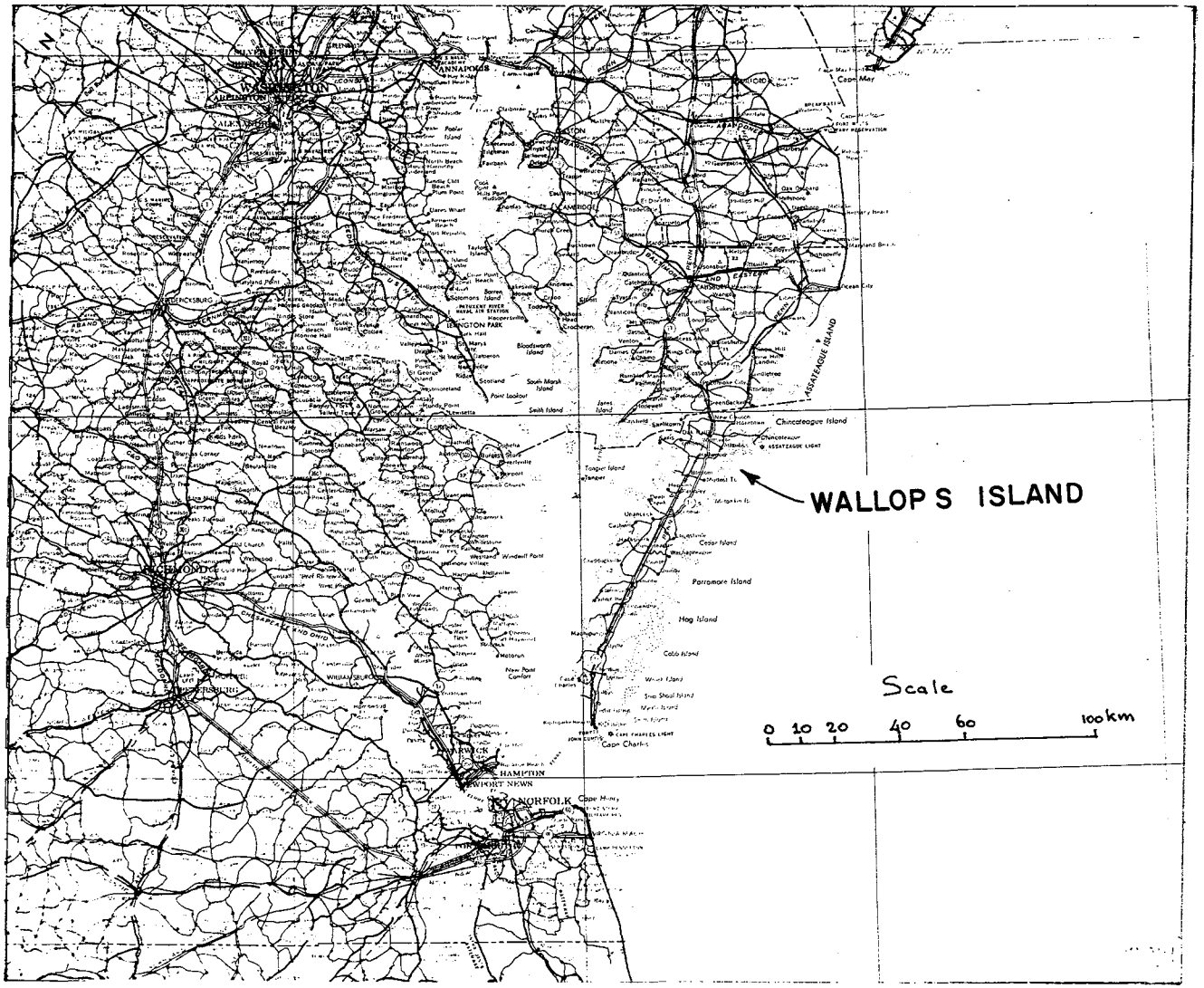

Figure 1. Map of Chesapeake Bay and Delmarva Peninsula

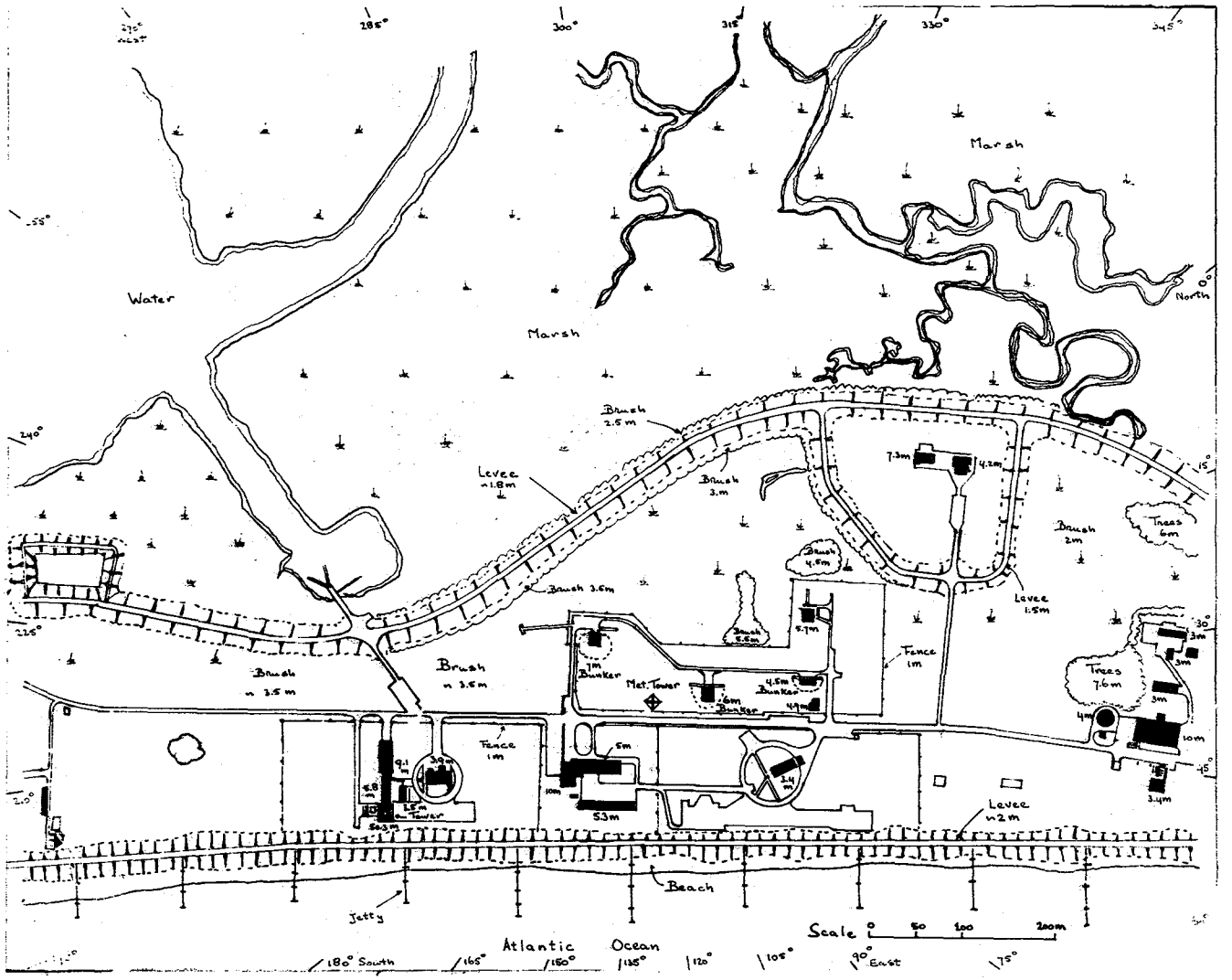

Figure 2. Wallops Island, Immediate Surroundings of the Meteorological Tower

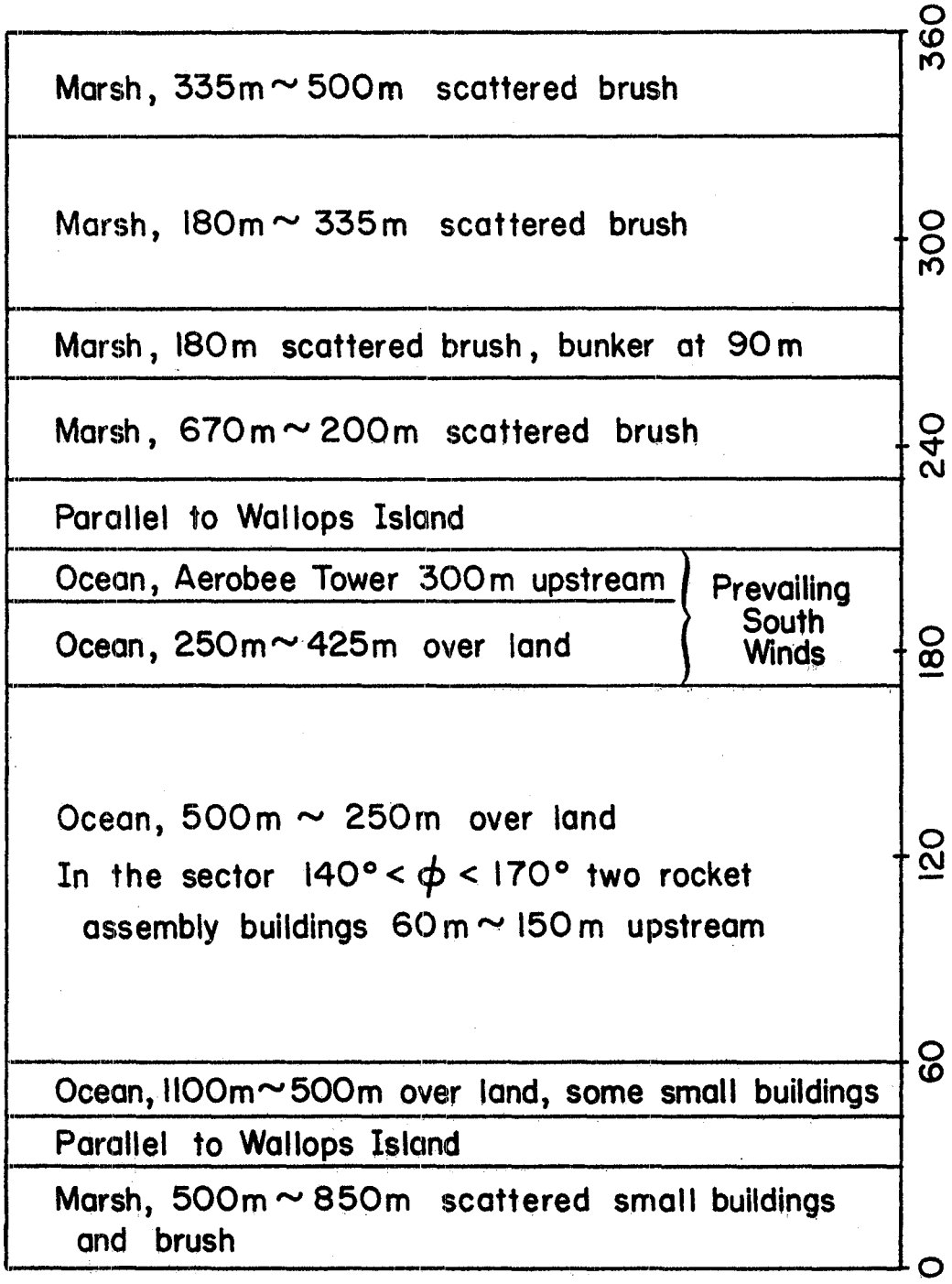

Figure 3. Wind Direction Sectors with Upstream Terrain Features

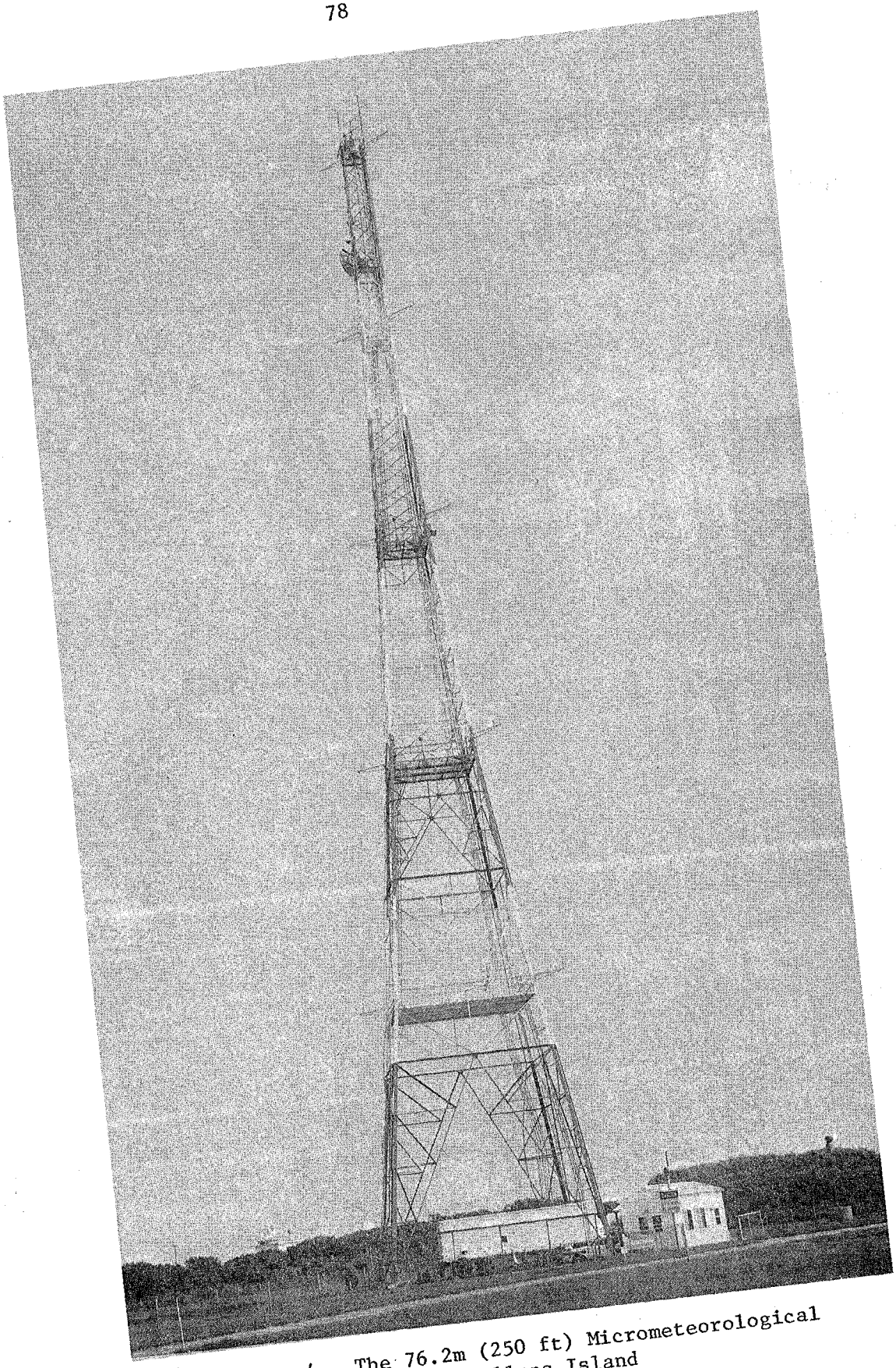

Figure 4. The 76.2m (250 ft) Micrometeorological tower at Wallops Island

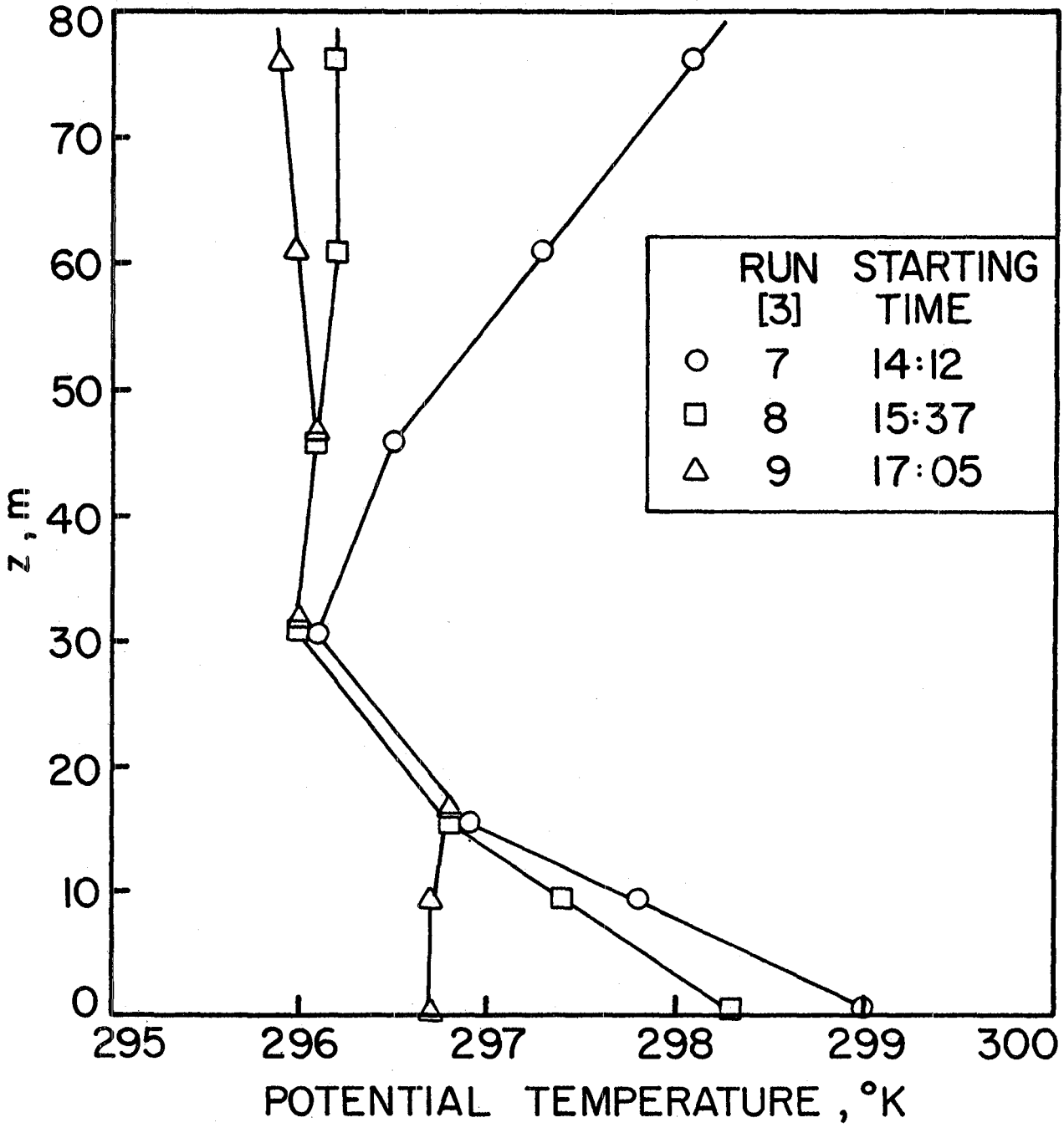

Figure 5. Afternoon Temperature Profiles for Southerly Winds

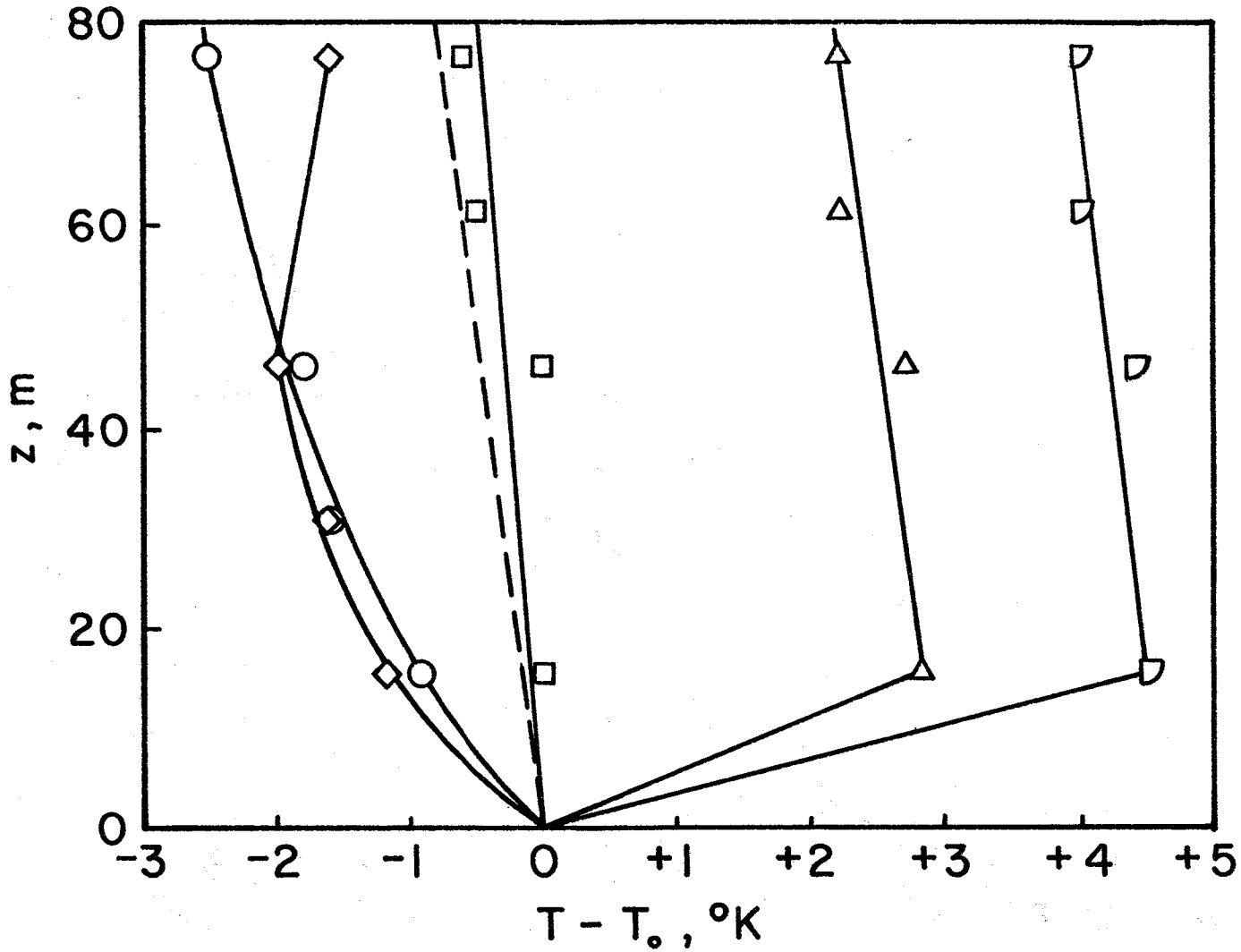

Figure 6. Temperature Profiles for Westerly Winds.
– – – Dry adiabatic lapse rate.

○ $U_{76.2}$ = 16.7 m/s, 12-21-'76, 12:22-13:39
□ $U_{76.2}$ = 16.6 m/s, 1-26-'78, 18:52-19:43
◇ $U_{76.2}$ = 20.9 m/s, 8-9-'76, 17:07-18:07
△ $U_{76.2}$ = 15.9 m/s, 1-27-'78, 01:09-02:09
▽ $U_{76.2}$ = 13.8 m/s, 1-27-'78, 05:42-06:58

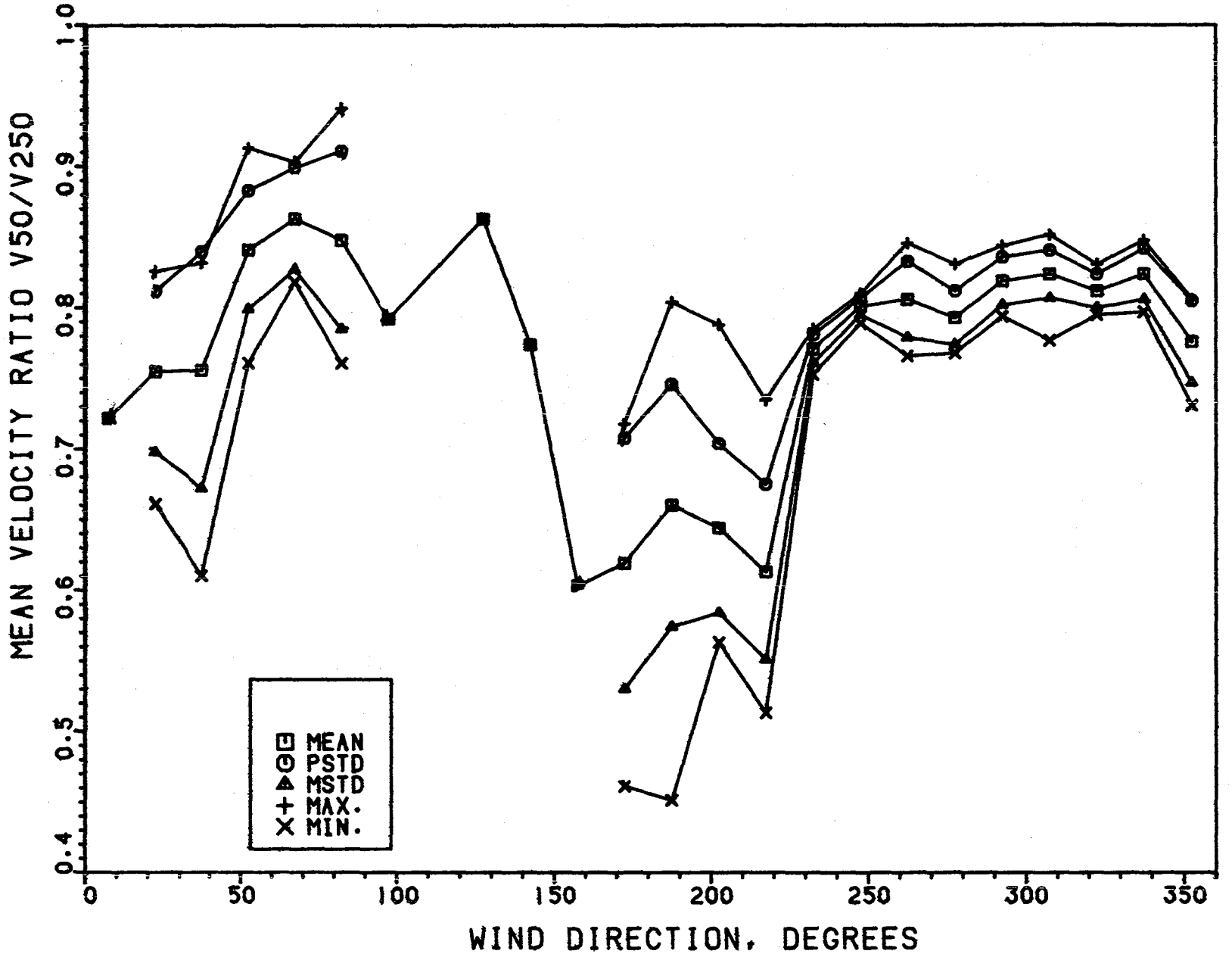

Figure 7a. Variation of Mean-Velocity Ratio, V(15.2)/V(76.2) with Wind Direction

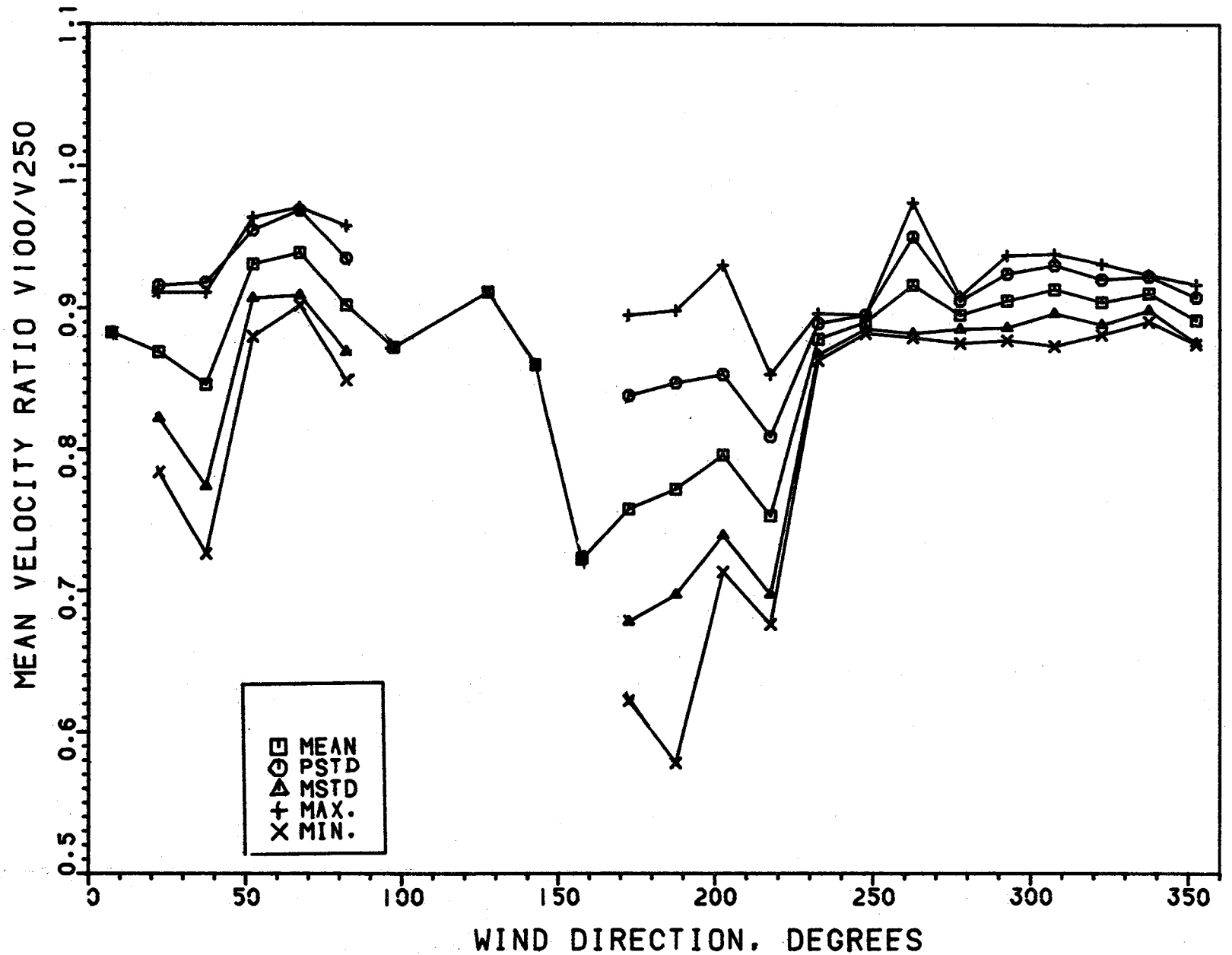

Figure 7b. Variation of Mean-Velocity Ratio, V(30.5)/V(76.2) with Wind Direction

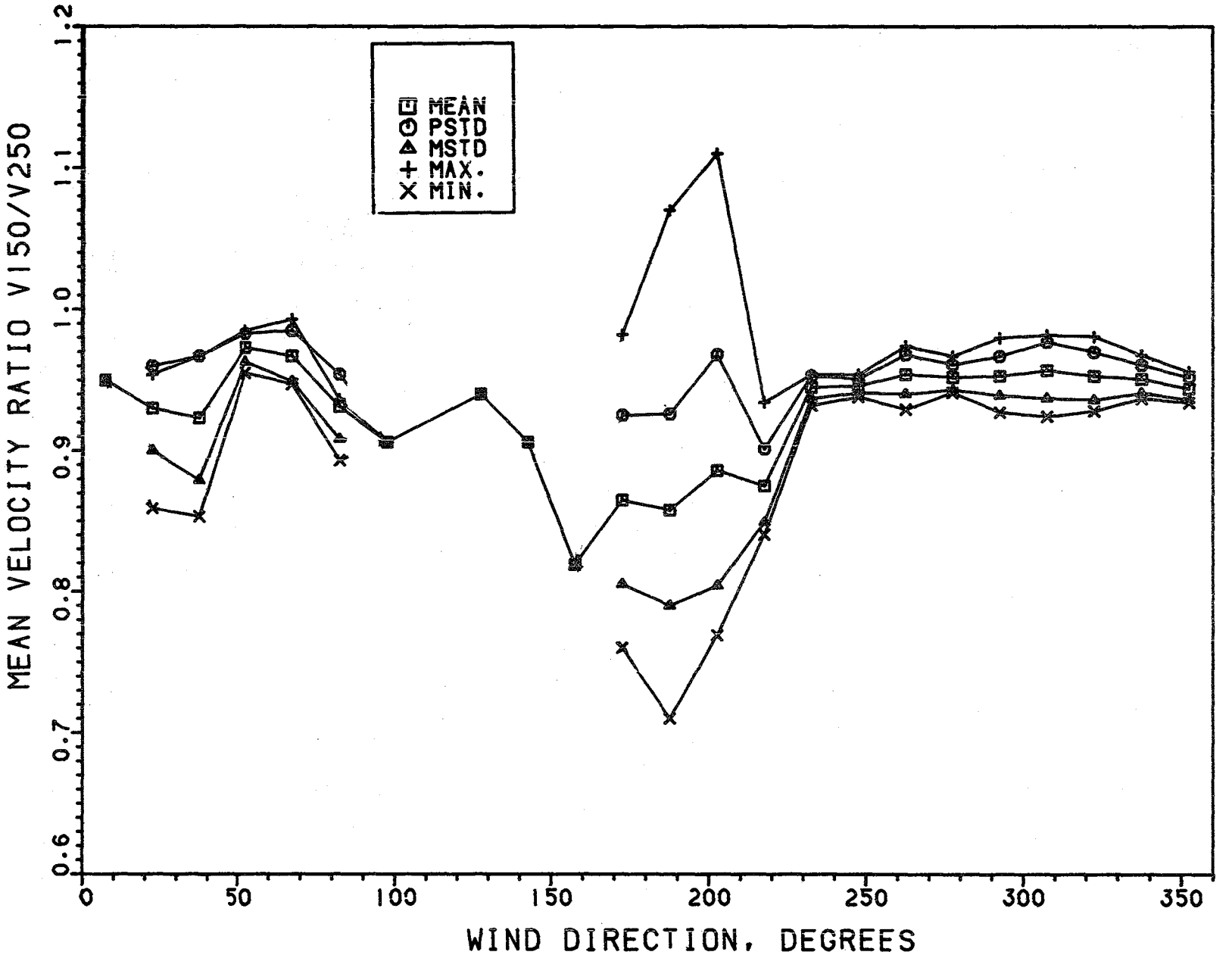

Figure 7c. Variation of Mean-Velocity Ratio, V(45.7)/V(76.2) with Wind Direction

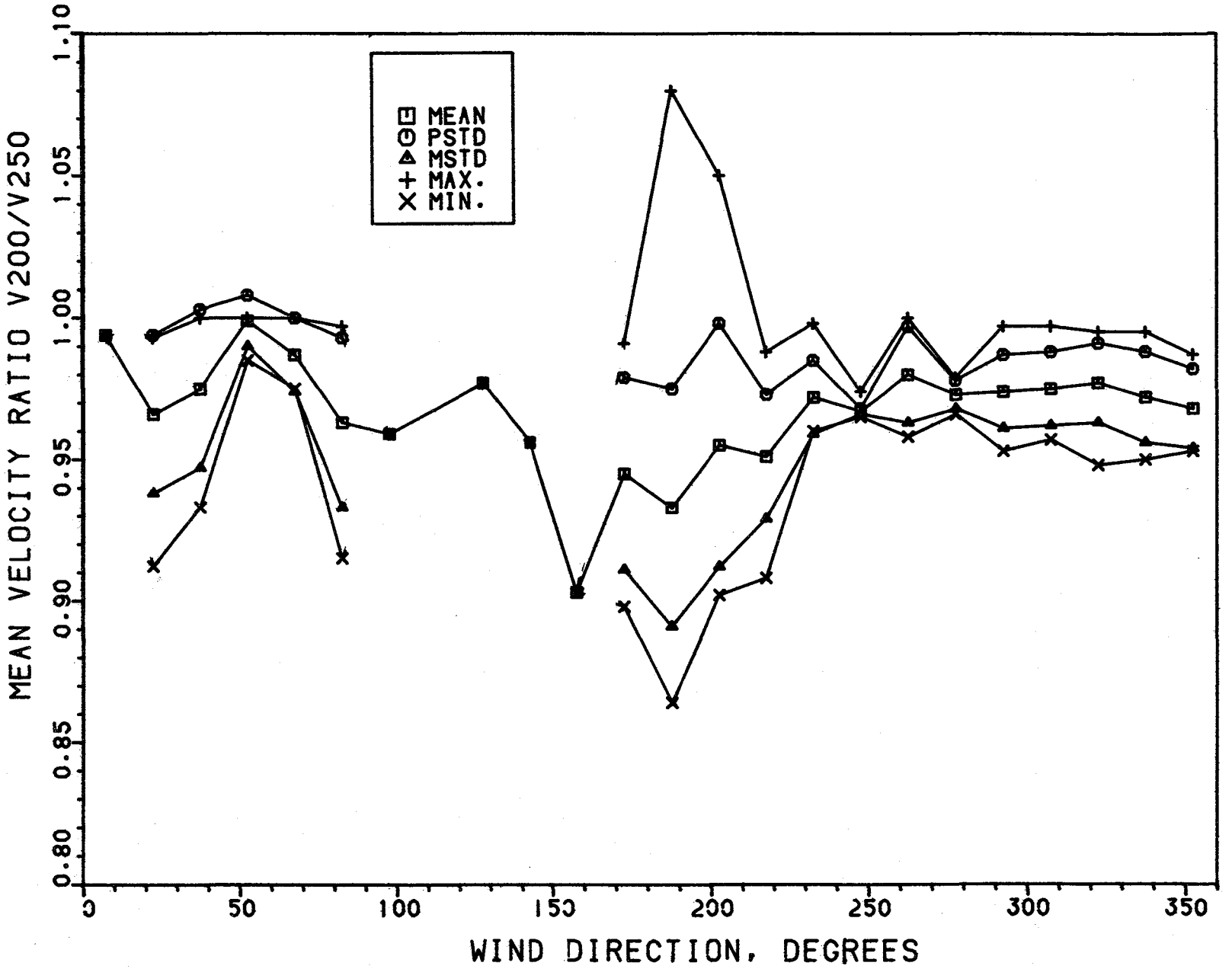

Figure 7d. Variation of Mean-Velocity Ratio, V(61.0)/V(76.2) with Wind Direction

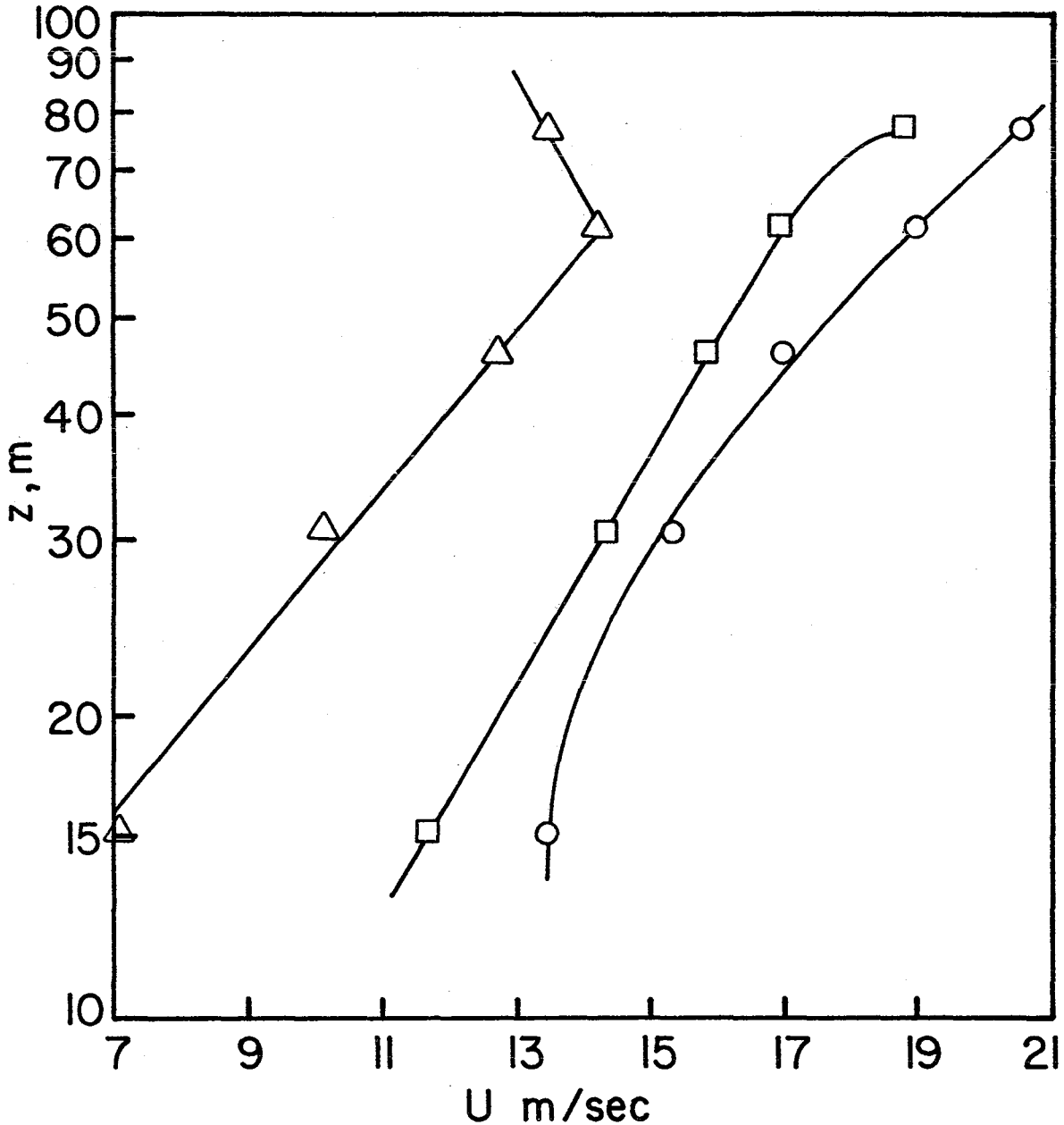

Figure 8. Typical Strong-Wind Profiles for Southerly Wind Directions

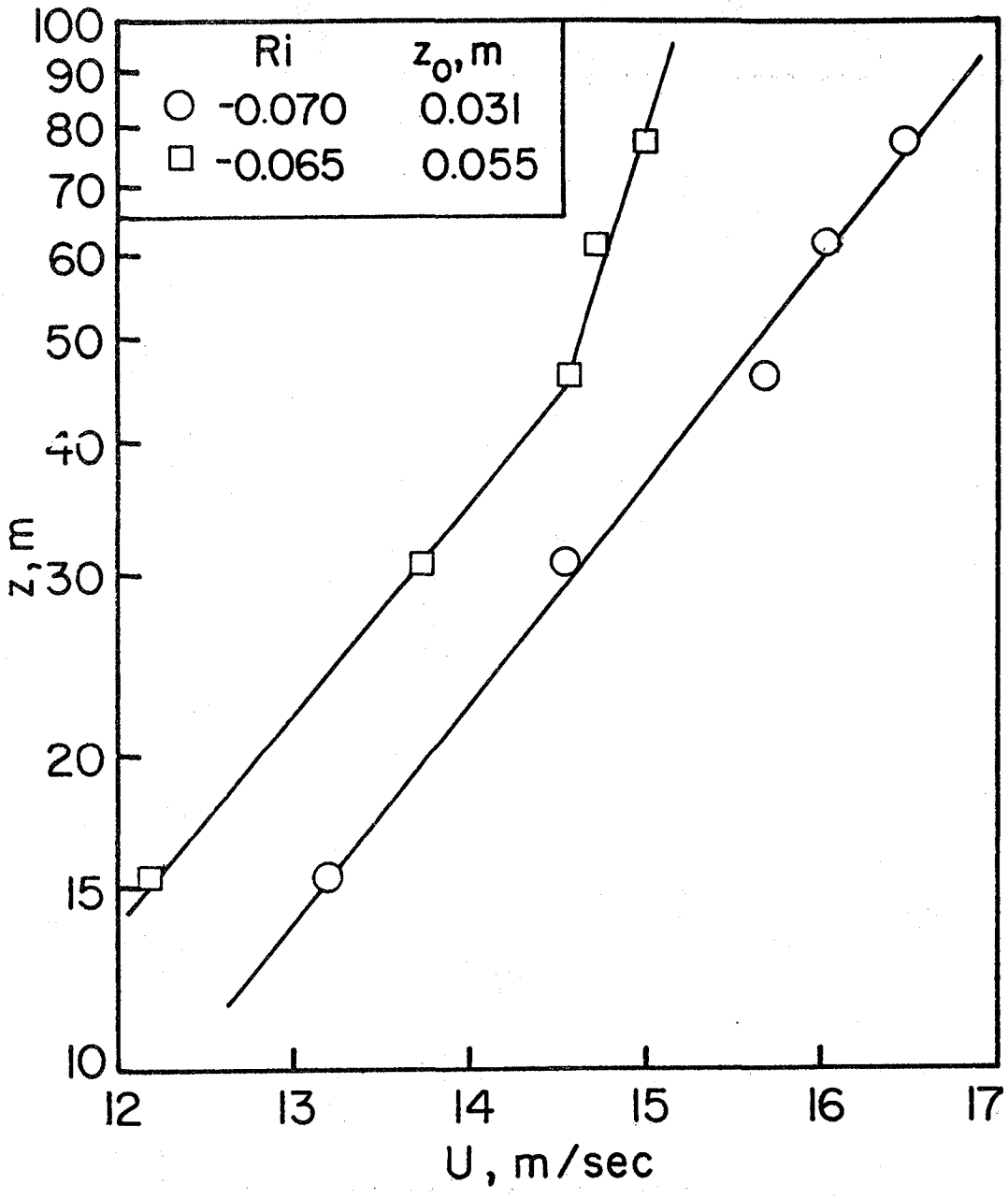

Figure 9. Typical Strong-Wind Profiles for Westerly Wind Directions Gradient Richardson Number (5) Evaluated at z=15.2m.

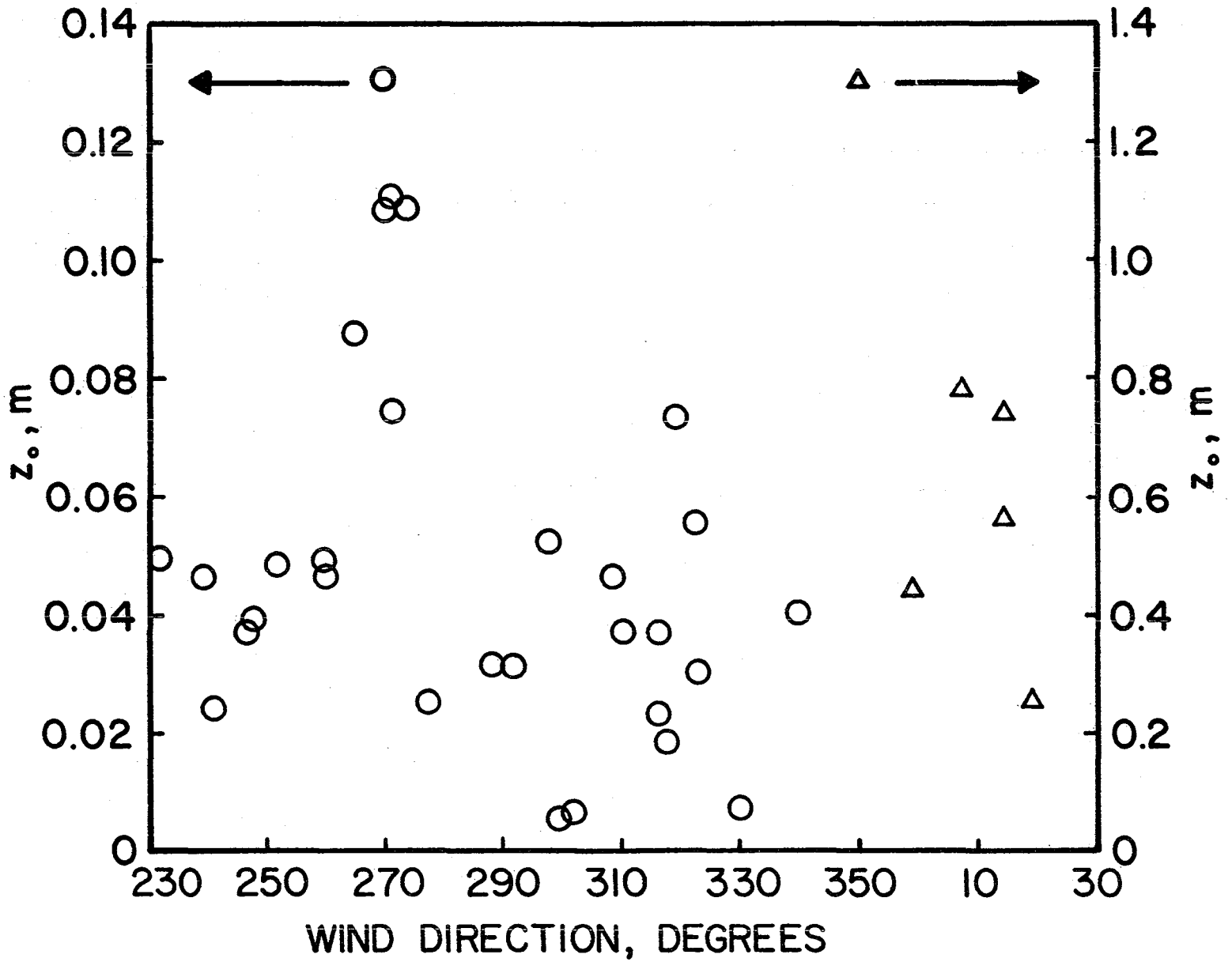

Figure 10. Variation of the Roughness Length, z_o, Versus Wind Direction
Note the larger roughness lengths in the sector $350° < \phi < +30°$.

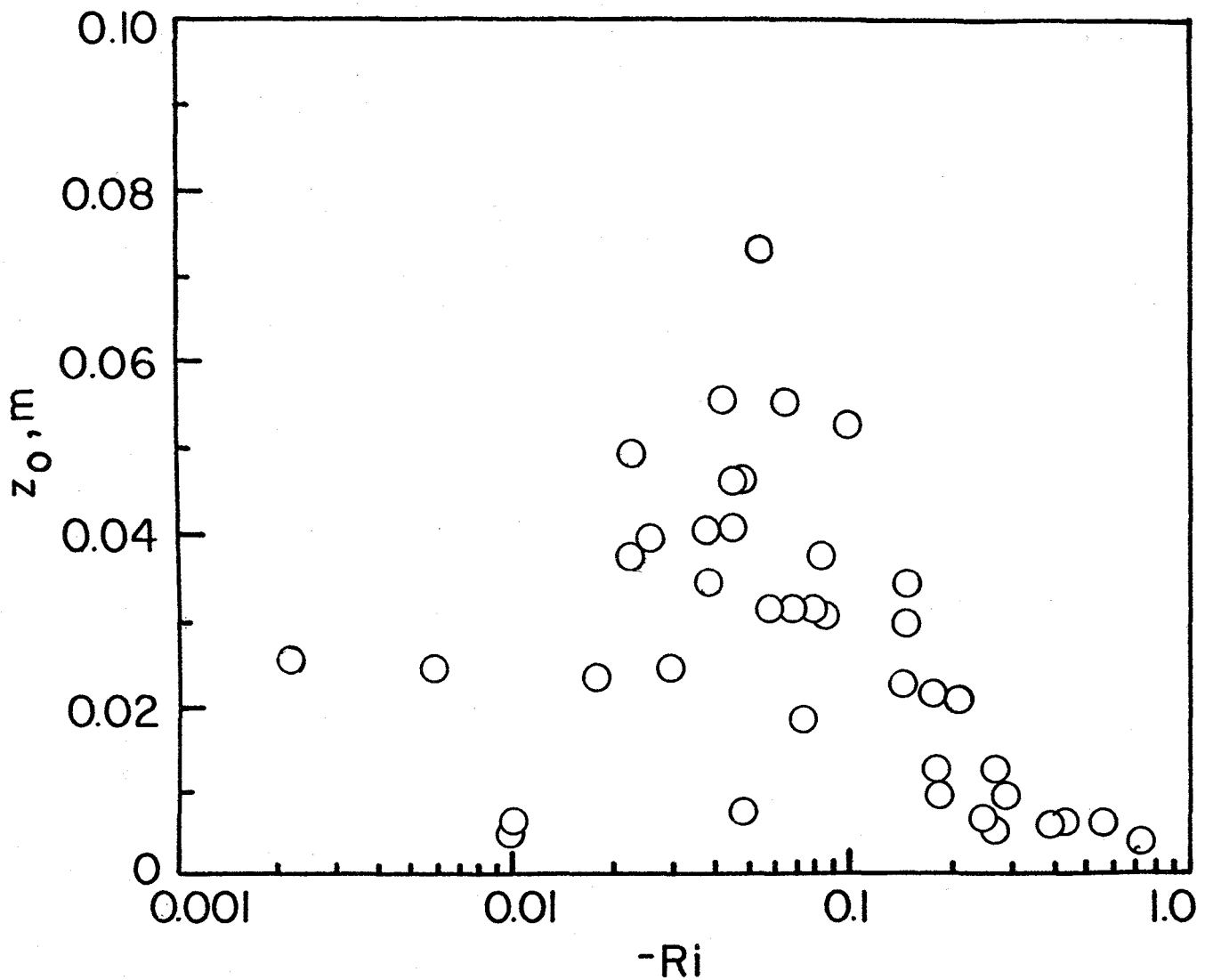

Figure 11. Variation of the Roughness Length, z_o, with the Gradient Richardson Number (5) Evaluated at z=15.2m

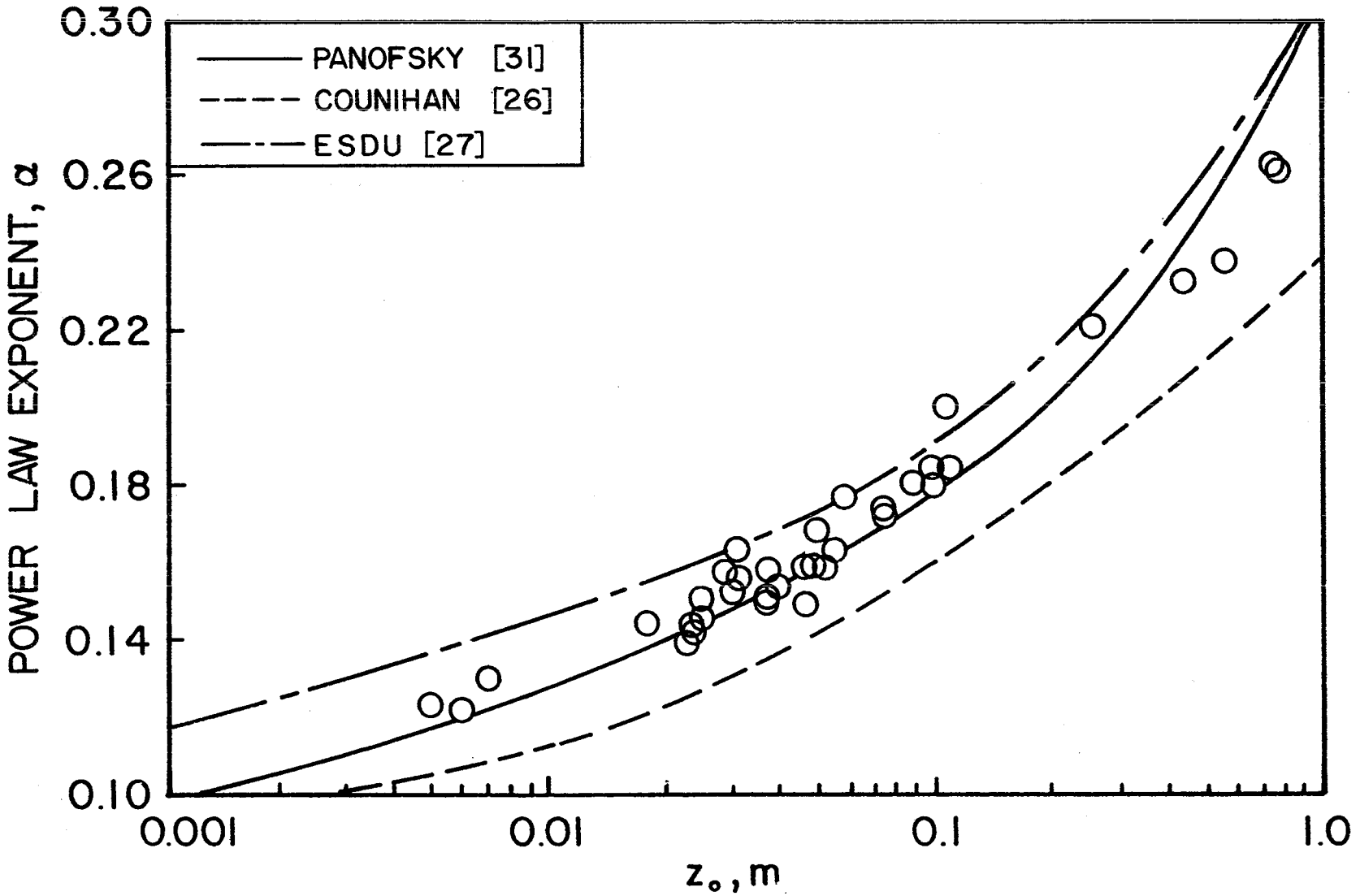

Figure 12. Variation of Power-law Exponent with Roughness Length, Both Based on Velocity Measurements Below 45.7m. Panofsky's Relation (7) Based on z_1=15.2m and z_2=45.7m

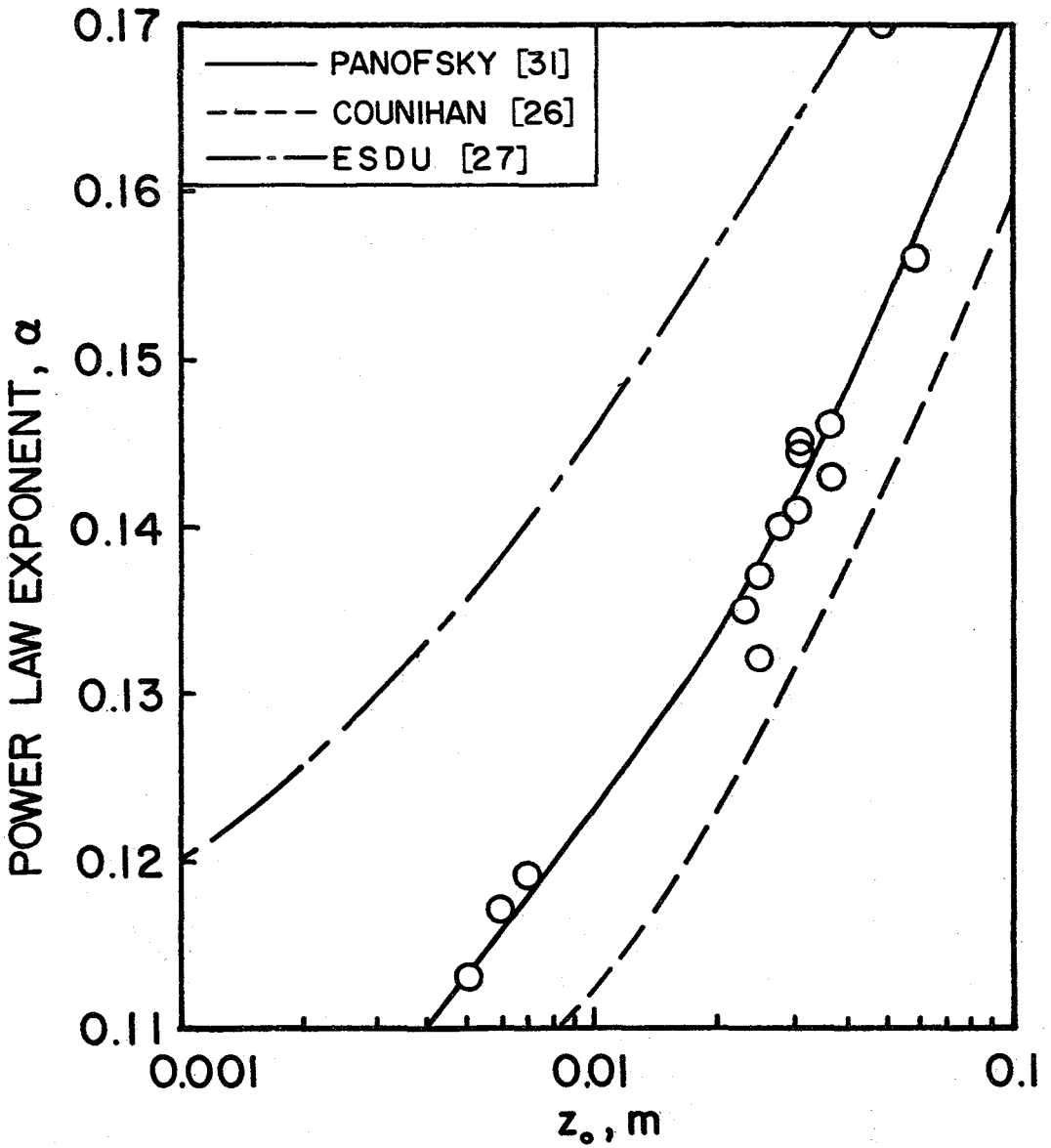

Figure 13. Variation of Power-law Exponent with Roughness Length, Both Based on Velocity Measurements at all Levels. Panofsky's Relation (7) Based on z_1=15.2m and z_2=76.2m

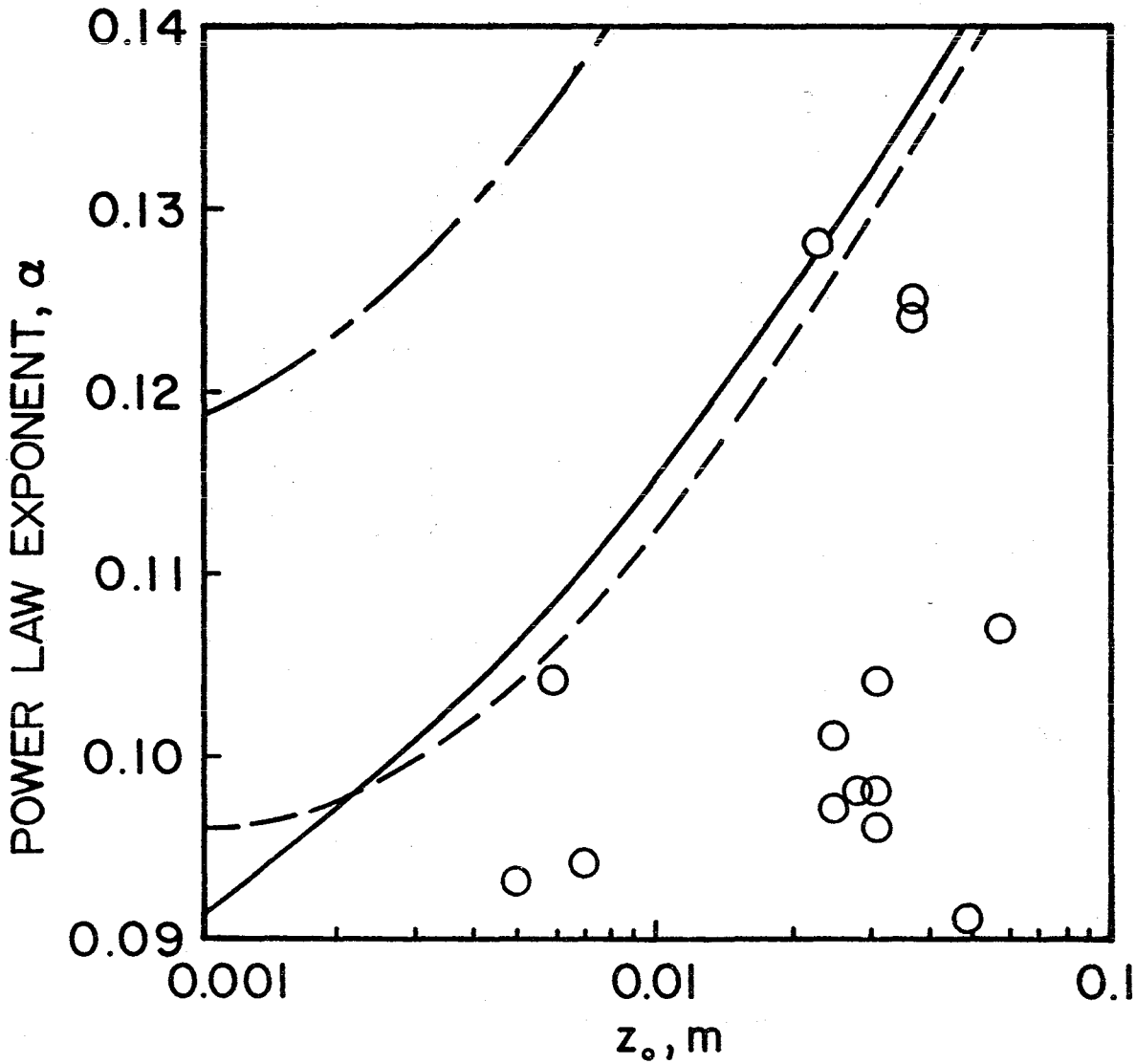

Figure 14. Variation of Power-law Exponent with Roughness Length, Both Based on Velocity Measurements Above 45.7m. Panofsky's relation (7) Based on z_1=45.7m and z_2=76.2m

_____ Panofsky [31] --- Counihan [26] ——— – ——— ESDU [27]

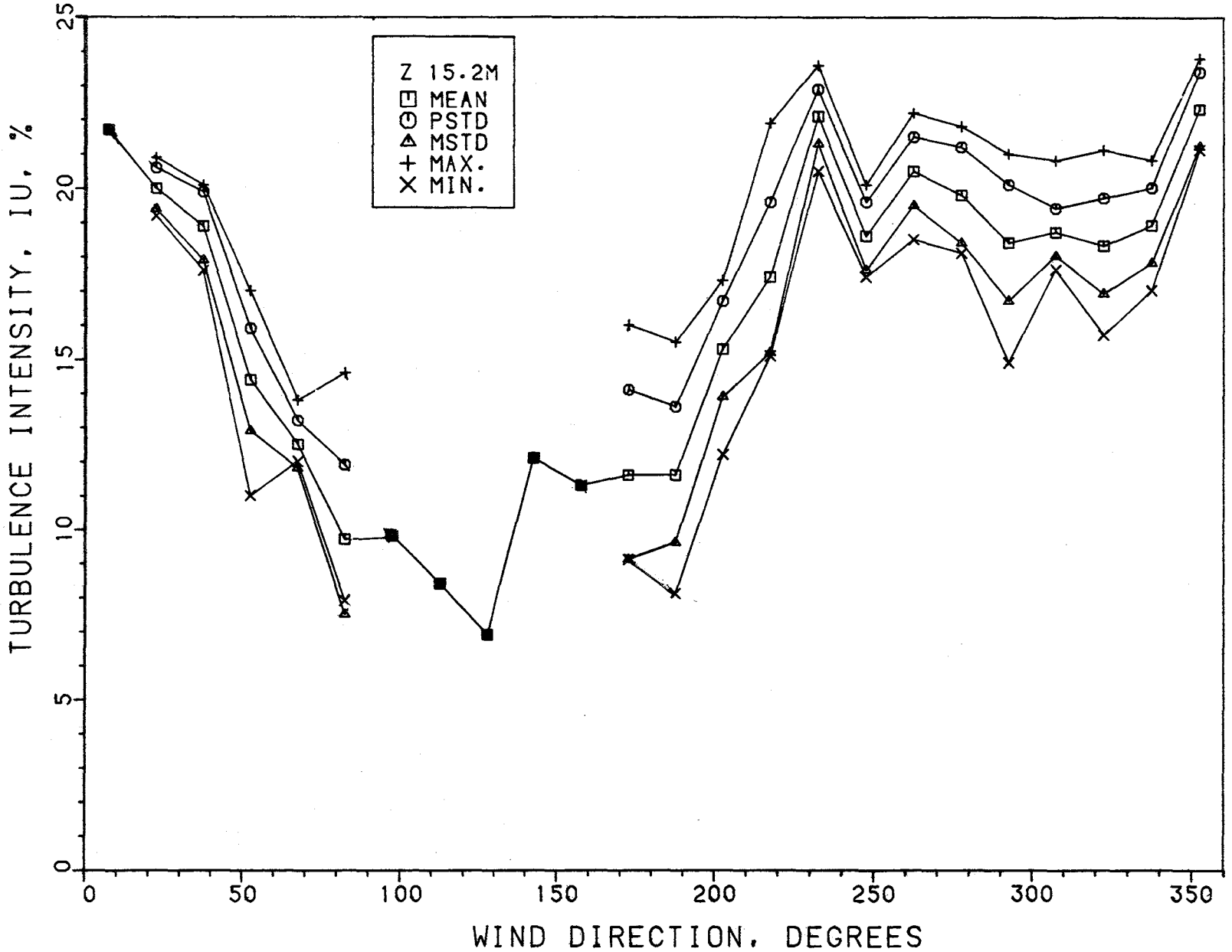

Figure 15a. Variation of Turbulence Intensity, σ_u/U, with Direction, z=15.2m

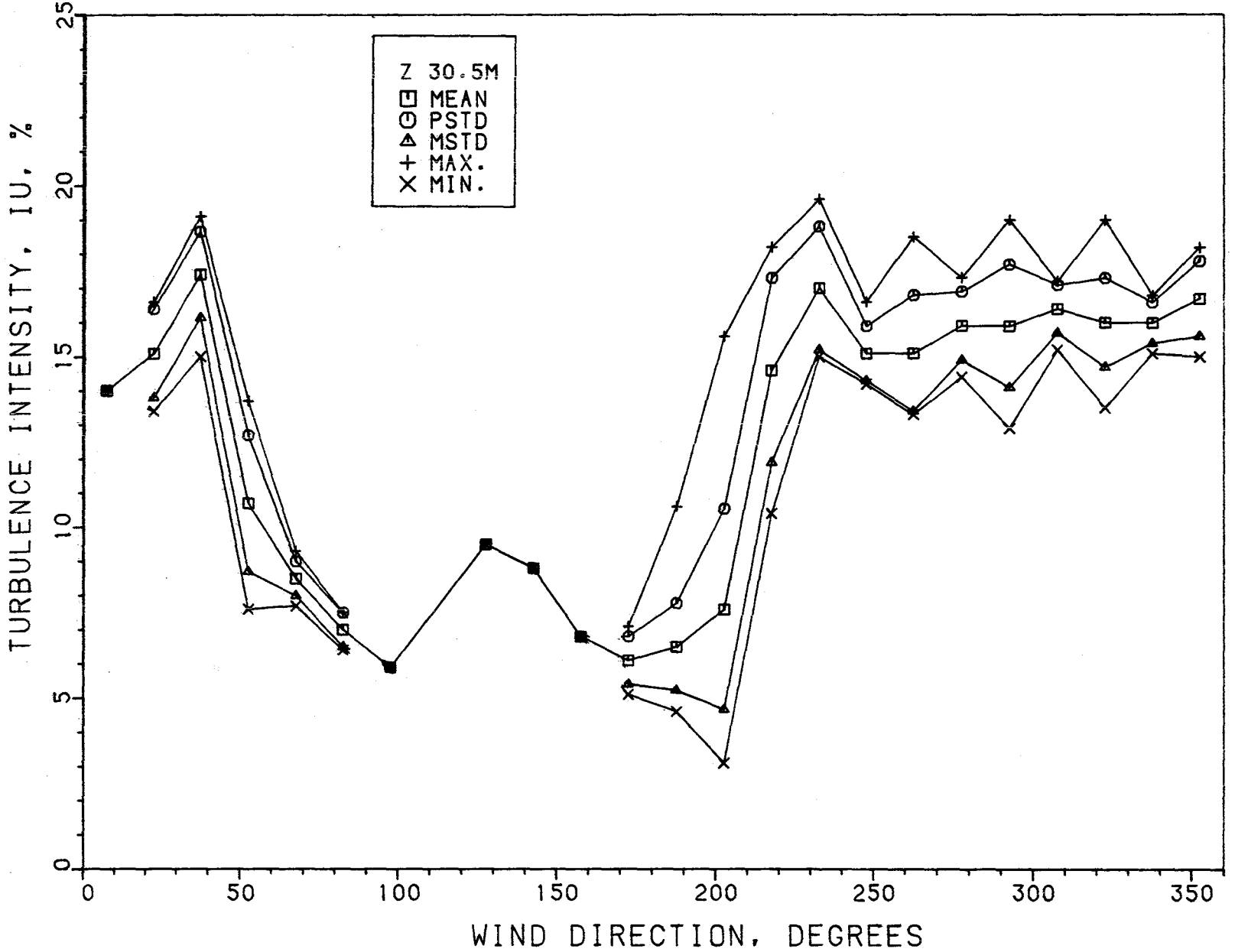

Figure 15b. Variation of Turbulence Intensity, σ_u/U, with Direction, z=30.5m

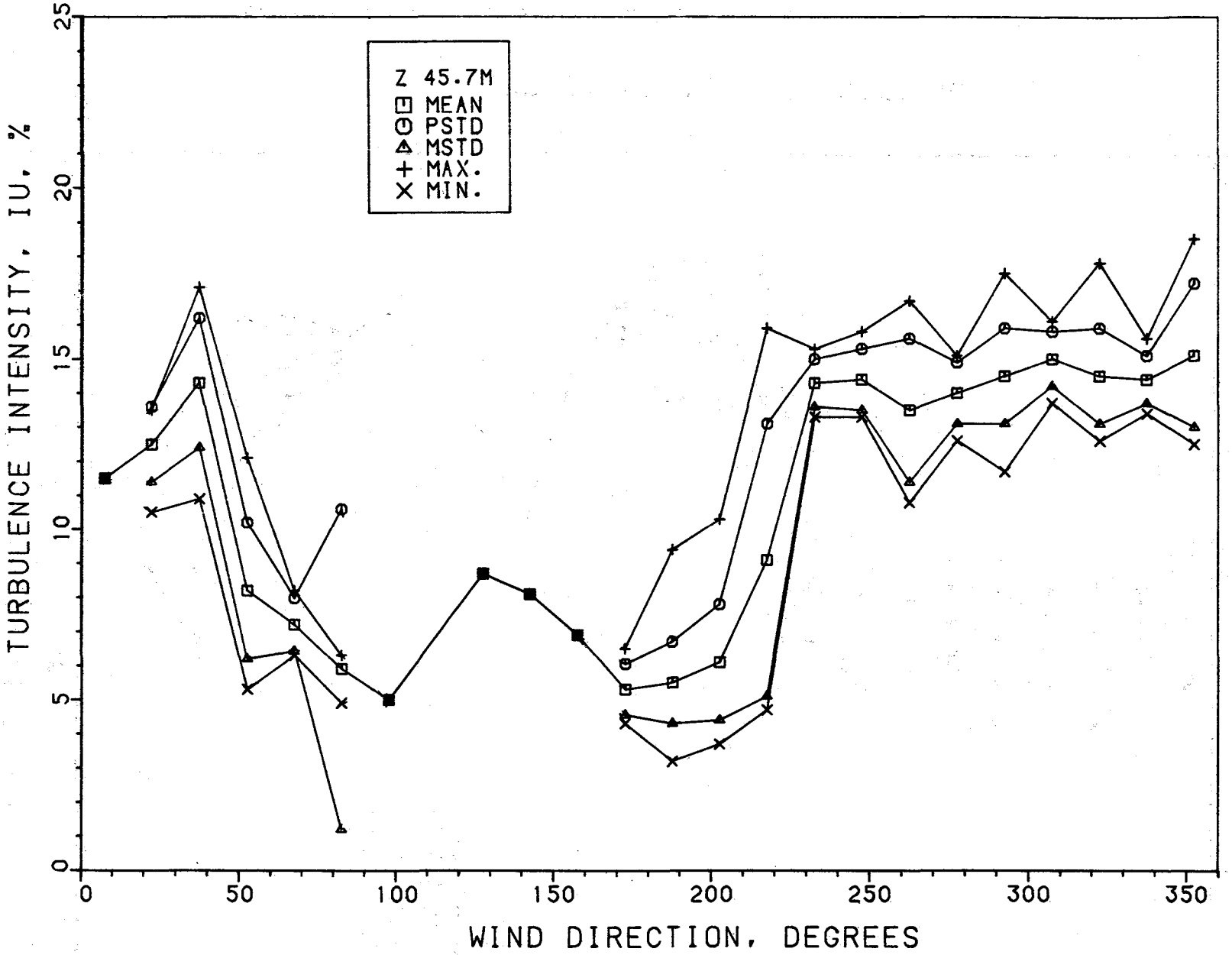

Figure 15c. Variation of Turbulence Intensity, σ_u/U, with Direction, z=47.5m

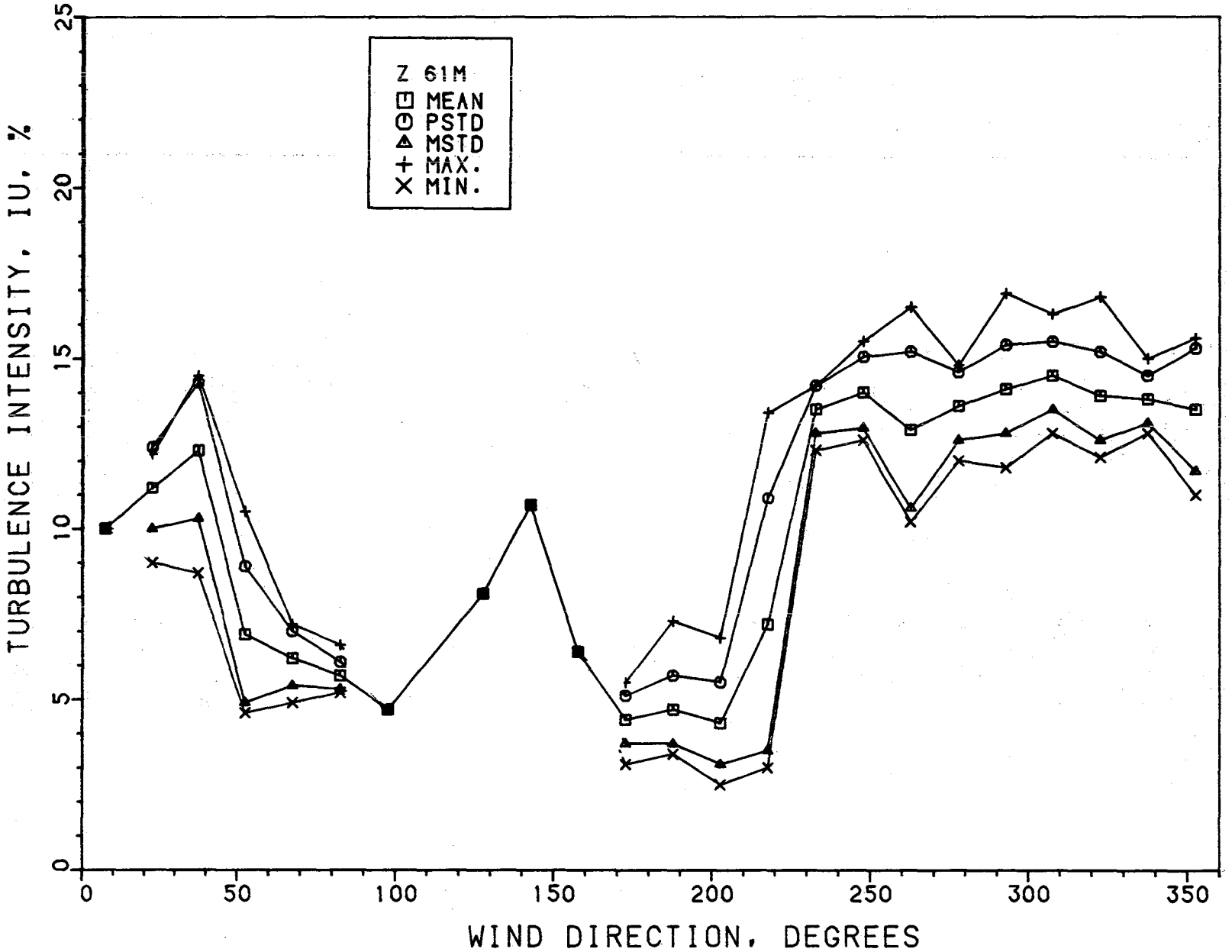

Figure 15d. Variation of Turbulence Intensity, σ_u/U, with Direction, z=61.0m

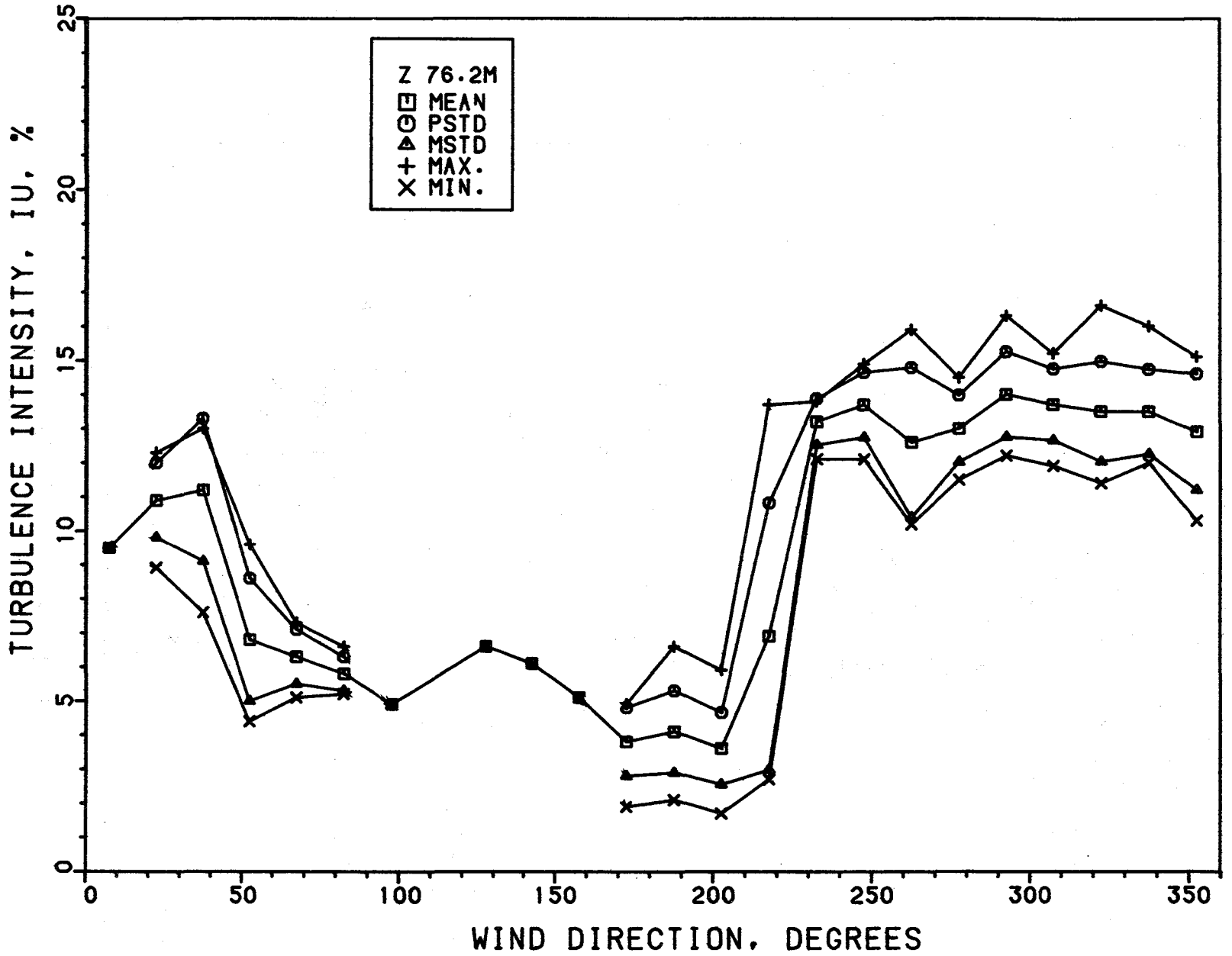

Figure 15e. Variation of Turbulence Intensity, σ_u/U, with Direction, z=76.2m

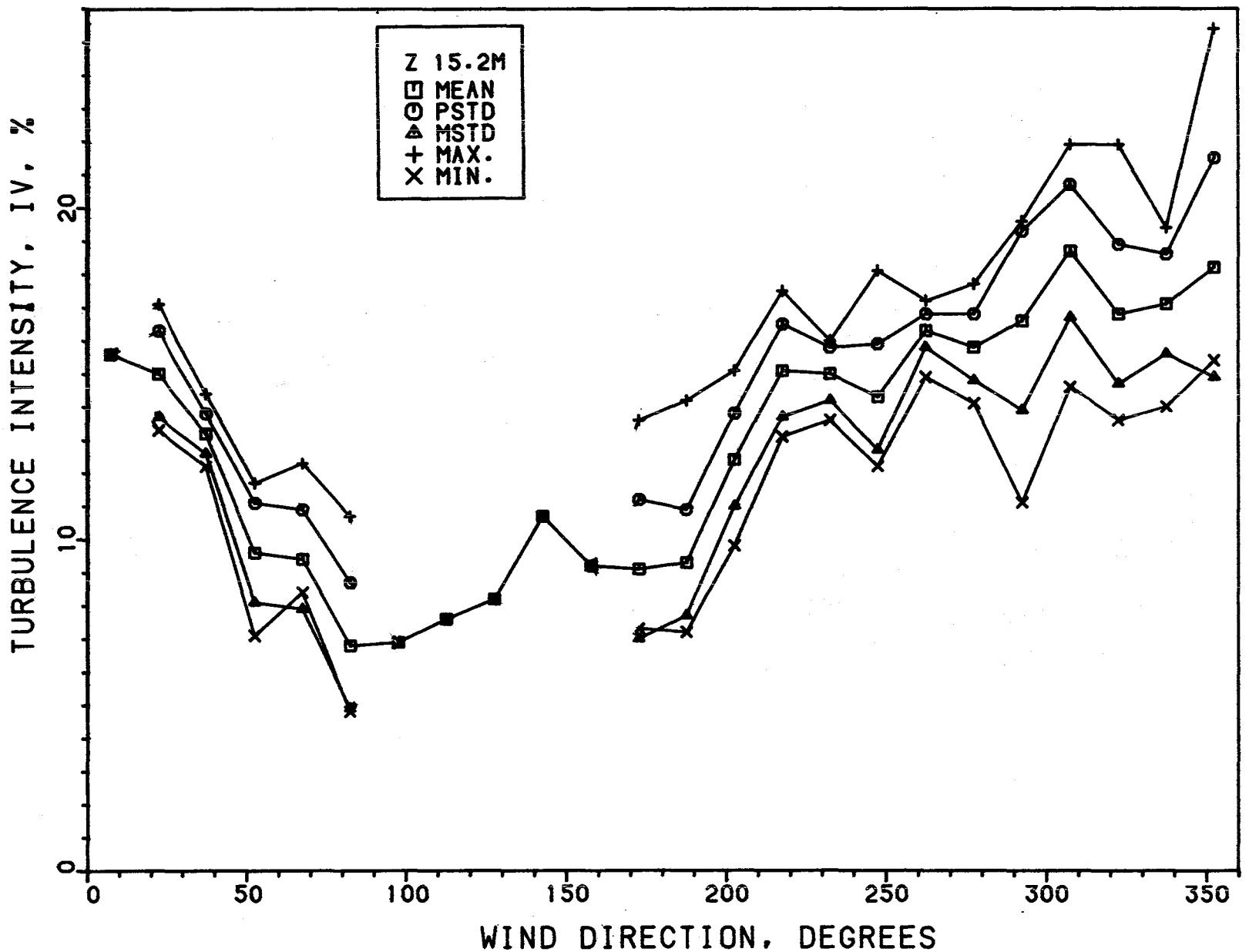

Figure 16a. Variation Turbulence Intensity, σ_v/U, with Direction z=15.2m

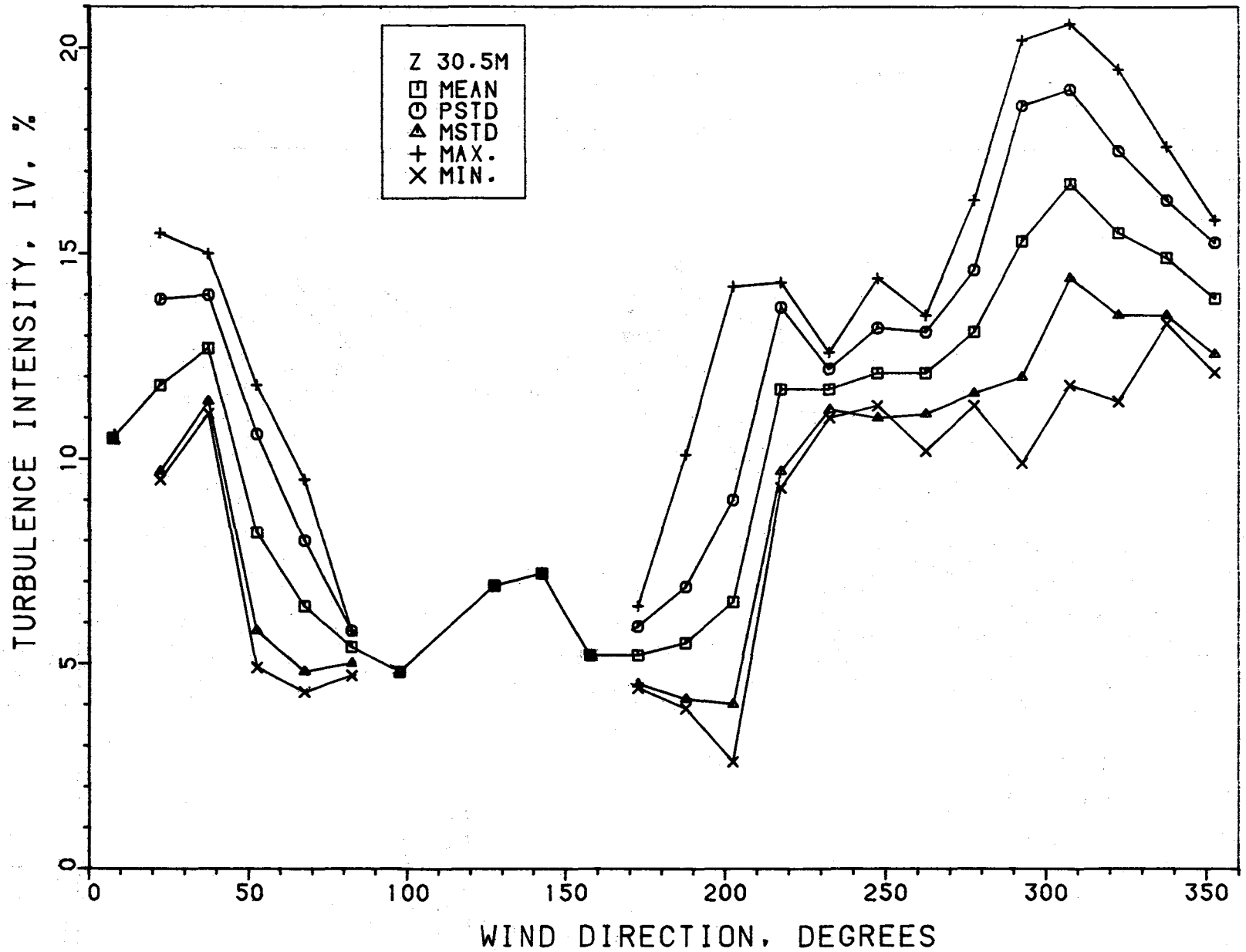

Figure 16b. Variation Turbulence Intensity, σ_v/U, with Direction z=30.5m

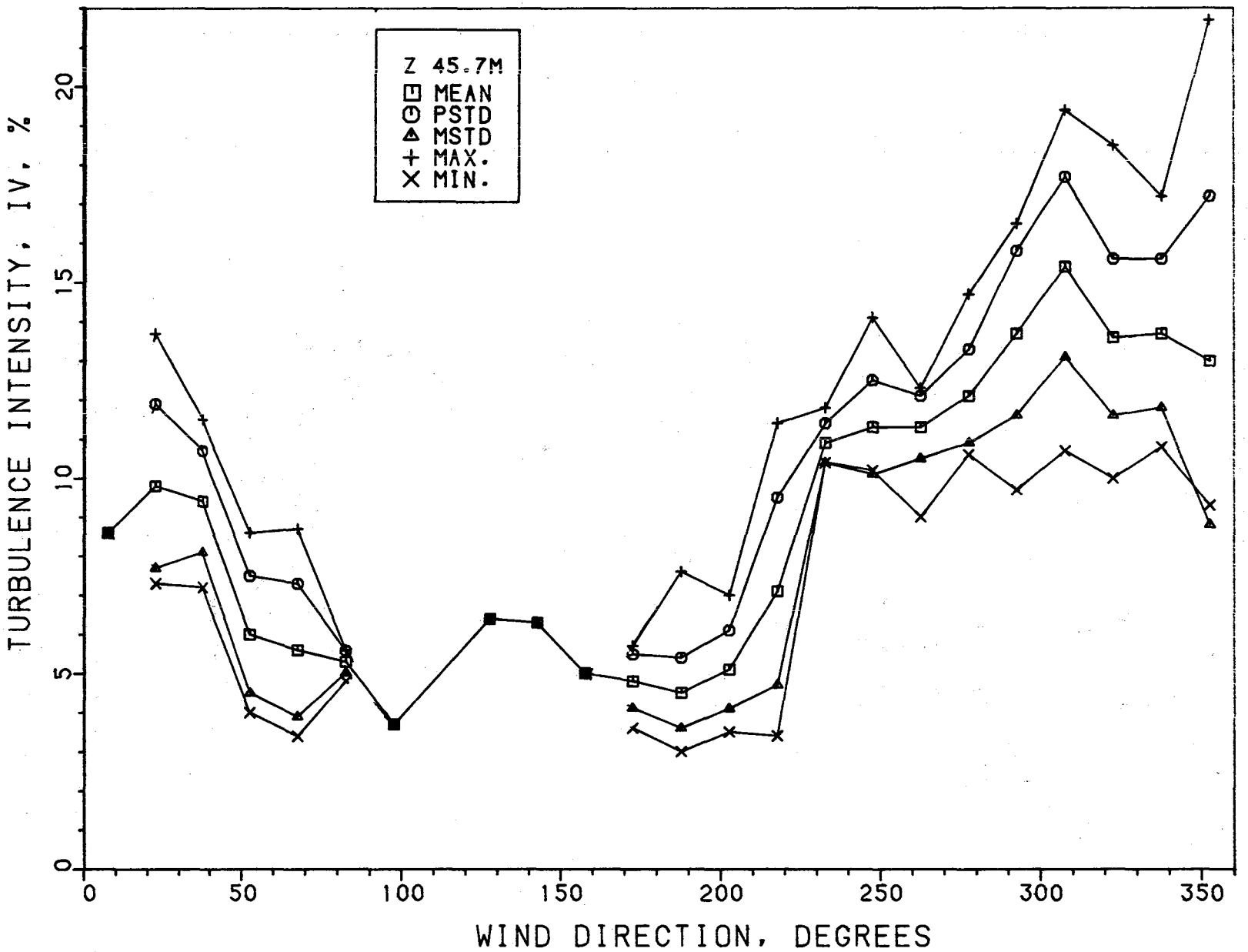

Figure 16c. Variation Turbulence Intensity, σ_v/U, with Direction z=47.5m

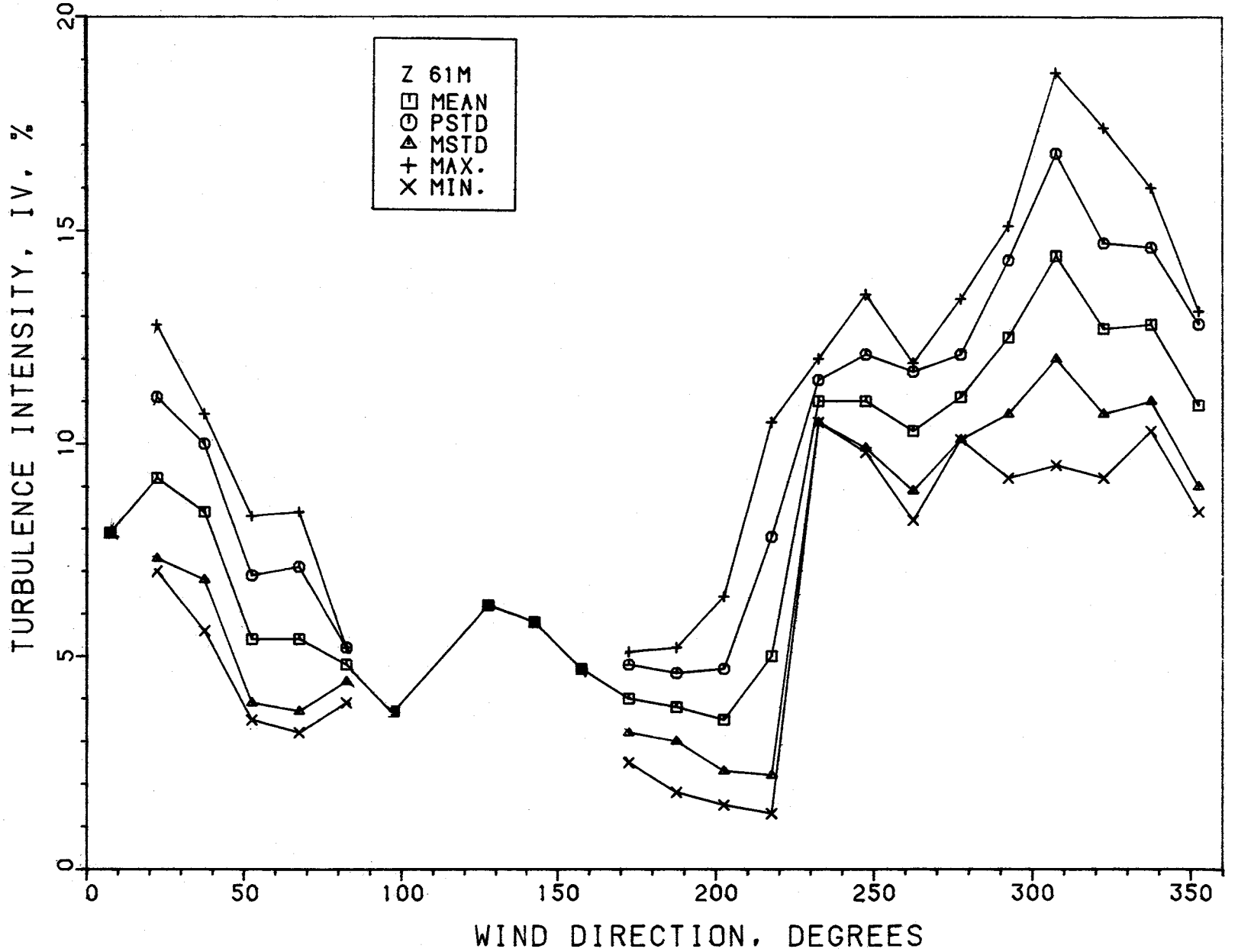

Figure 16d. Variation Turbulence Intensity, σ_v/U, with Direction z=61.0m

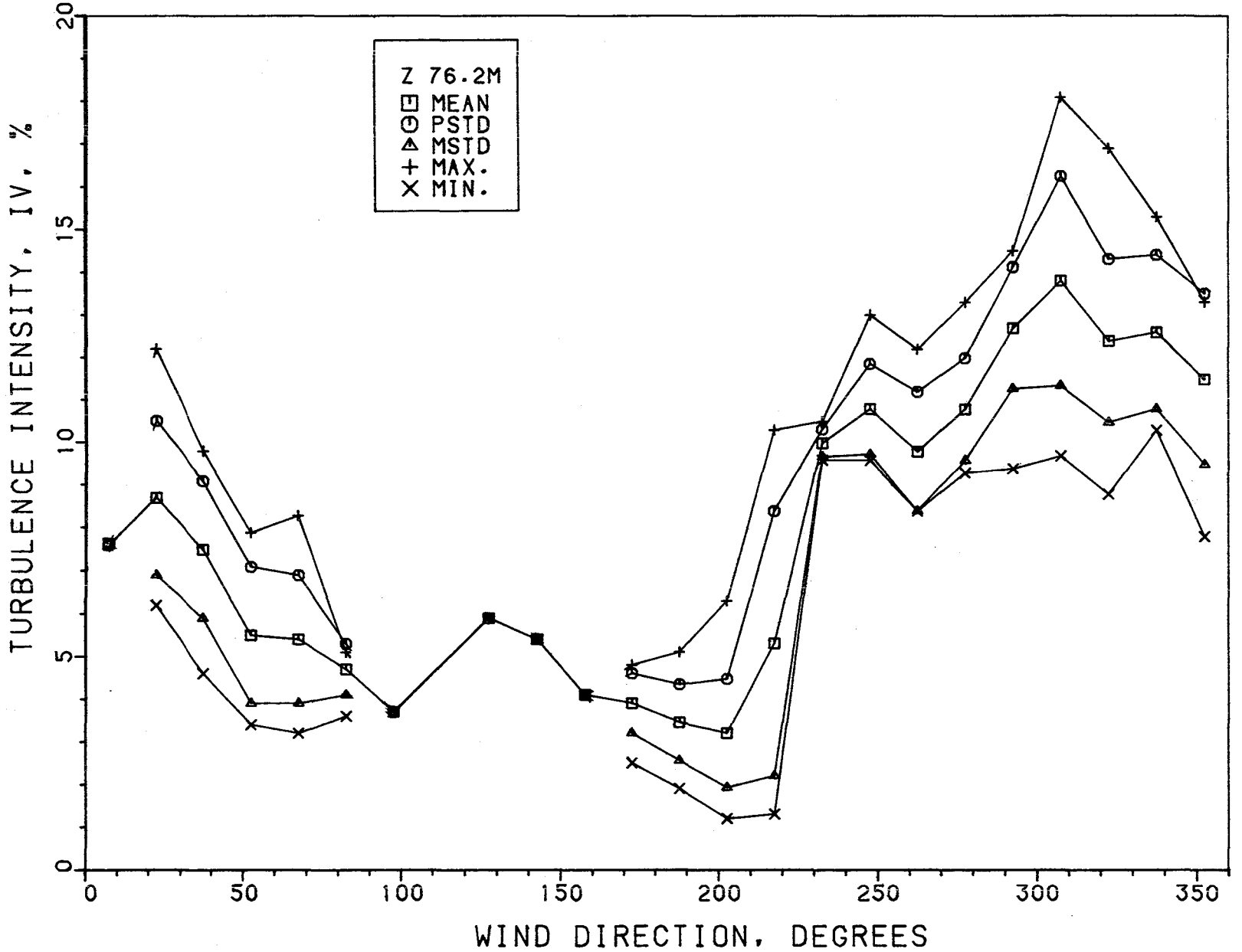

Figure 16e. Variation Turbulence Intensity, σ_v/U, with Direction z=76.2m

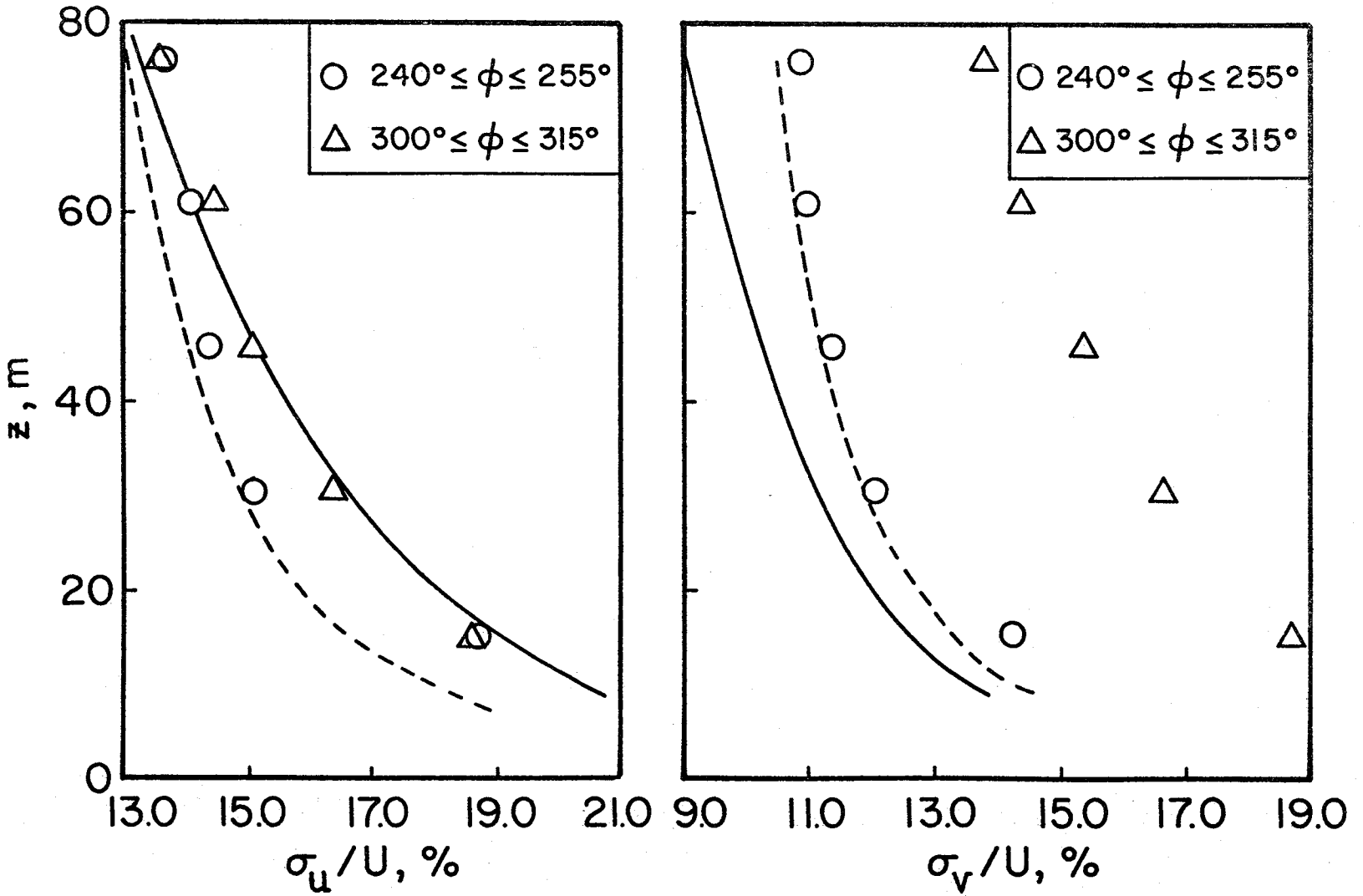

Figure 17. Variation of Average Turbulence Intensities σ_u/U and σ_v/U with Height for Two Wind-Direction Sectors.
——— ESDU [28] ------Teunissen [25]

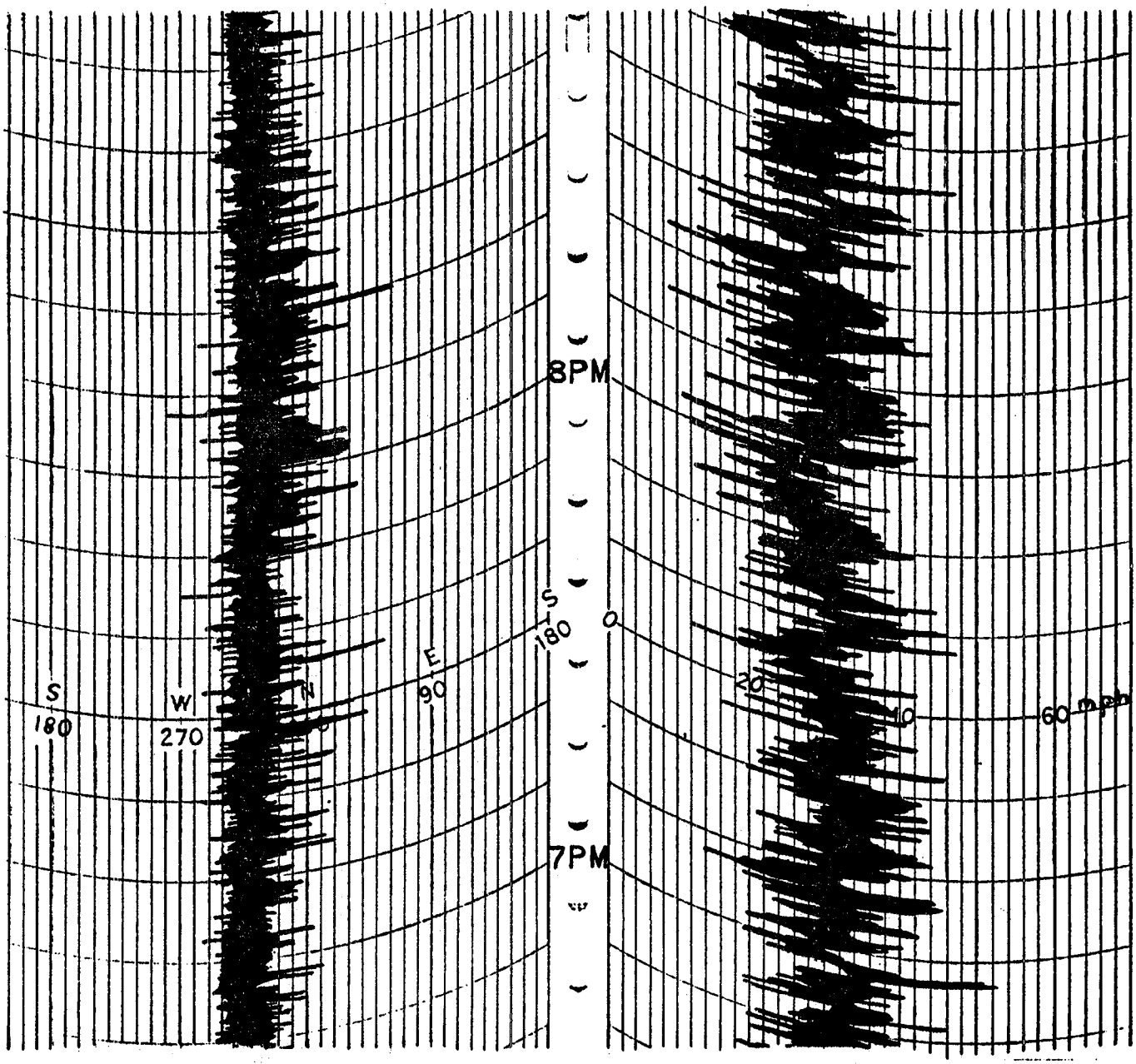

Figure 18. Typical Strong-Wind Aerovane Record of Direction and Speed for Northwest Winds, $\phi \simeq 320°$, $U_{10} \simeq 13$ m/s

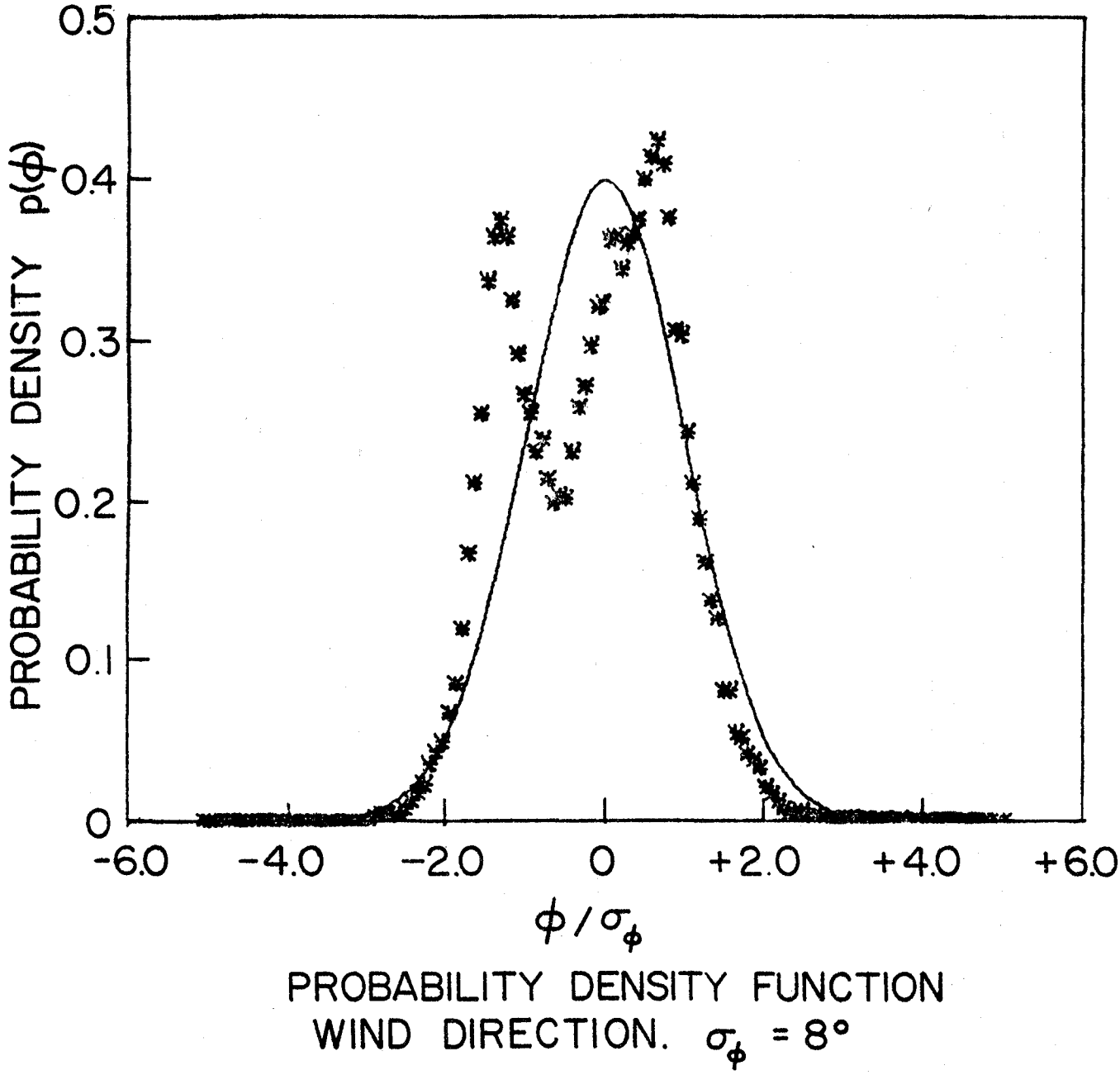

Figure 19. Probability Density Function of Wind-Direction Fluctuations, z=76.2m, σ_ϕ=8°, ϕ=322°
——— Gaussian Distribution Function

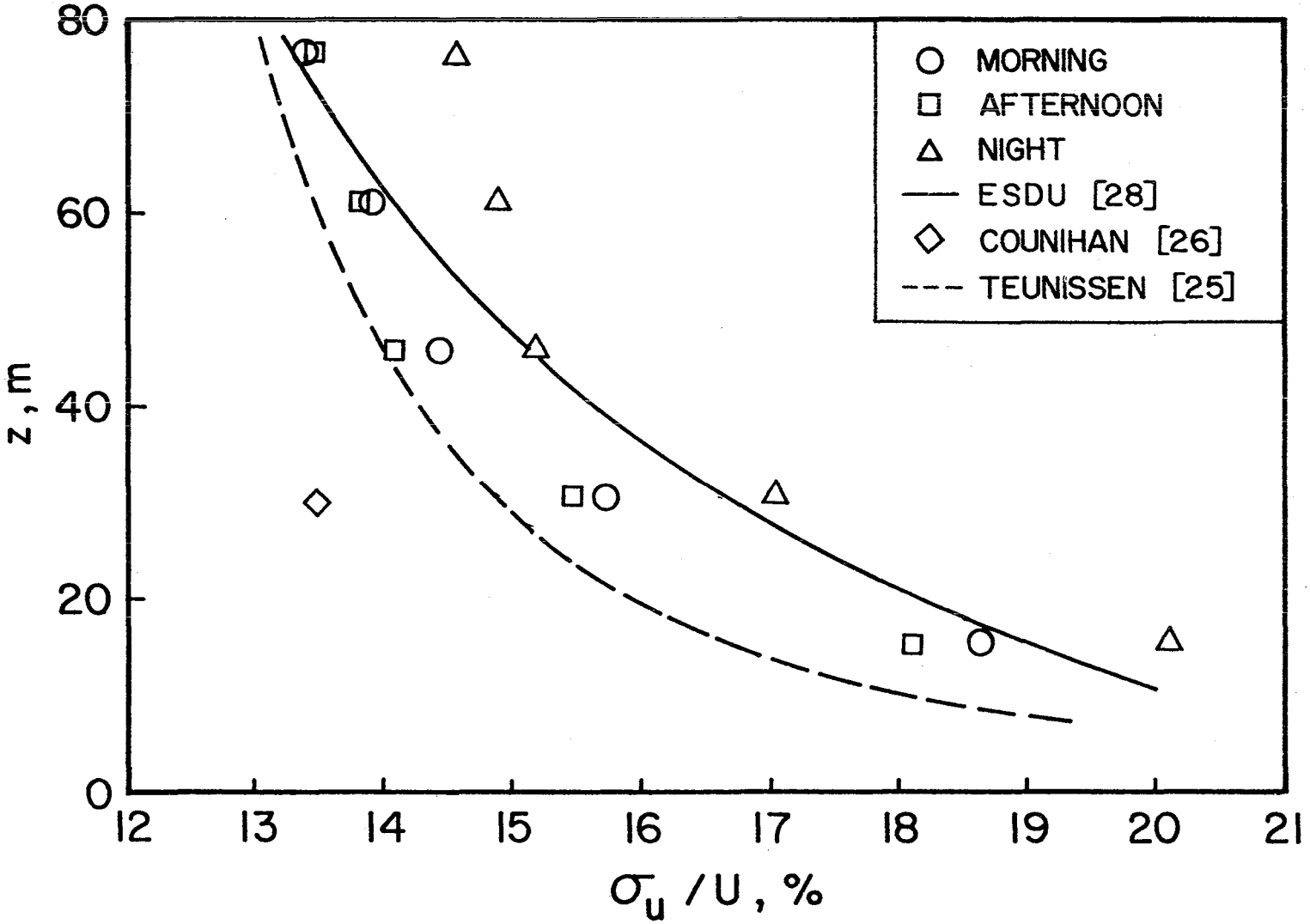

Figure 20. The Variation of the Vertical Distribution of Turbulence Intensity σ_u/U, with Time of Day for Westerly Winds

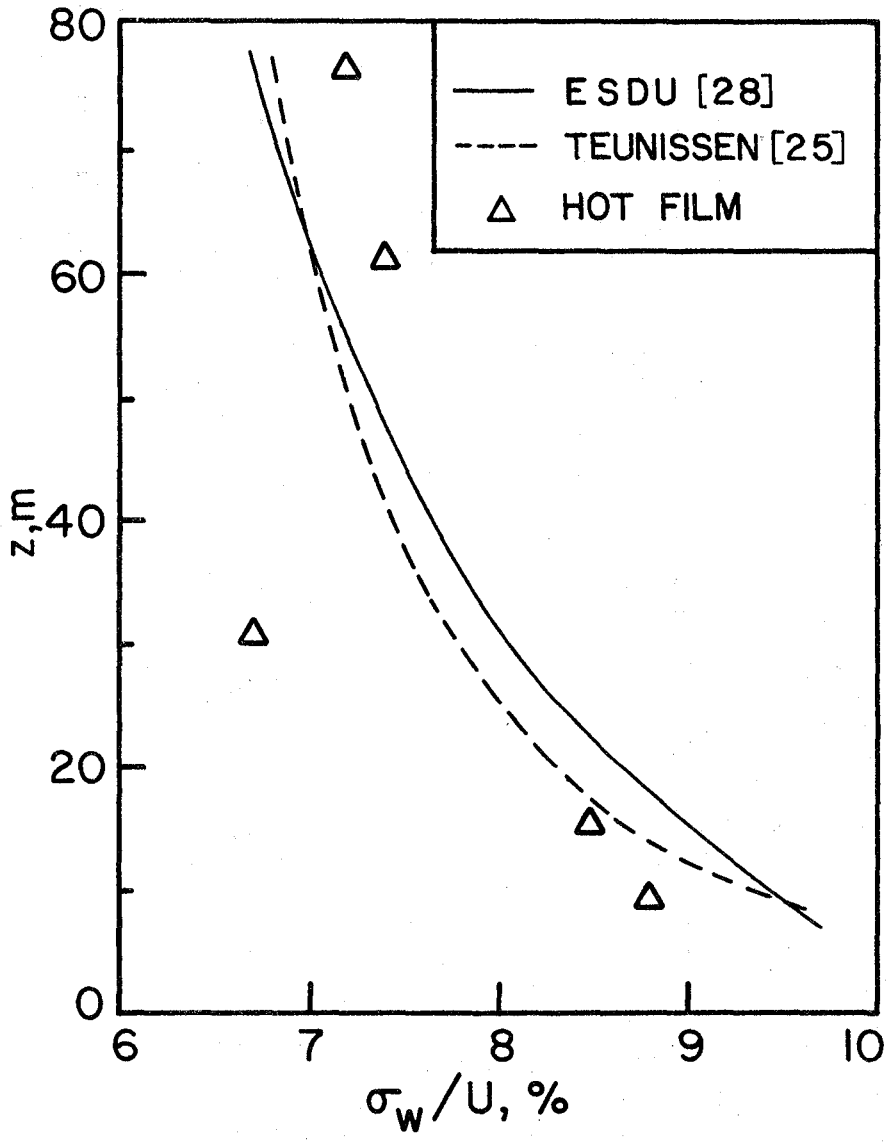

Figure 21. Vertical Distribution of Turbulence Intensity, σ_w/U, for Westerly Winds

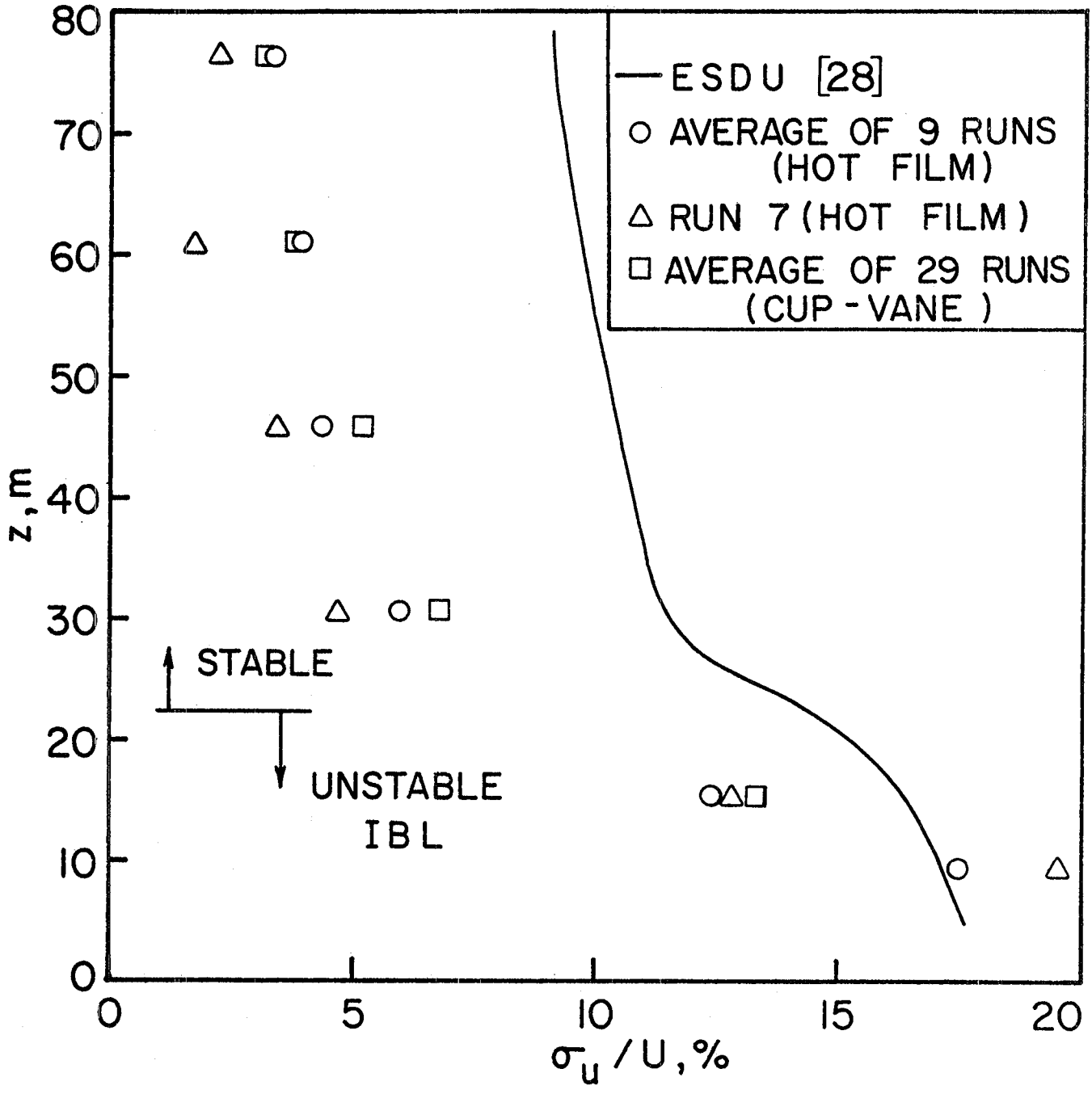

Figure 22. Vertical Distribution of the Turbulence Intensity, σ_u/U, for Southerly Winds

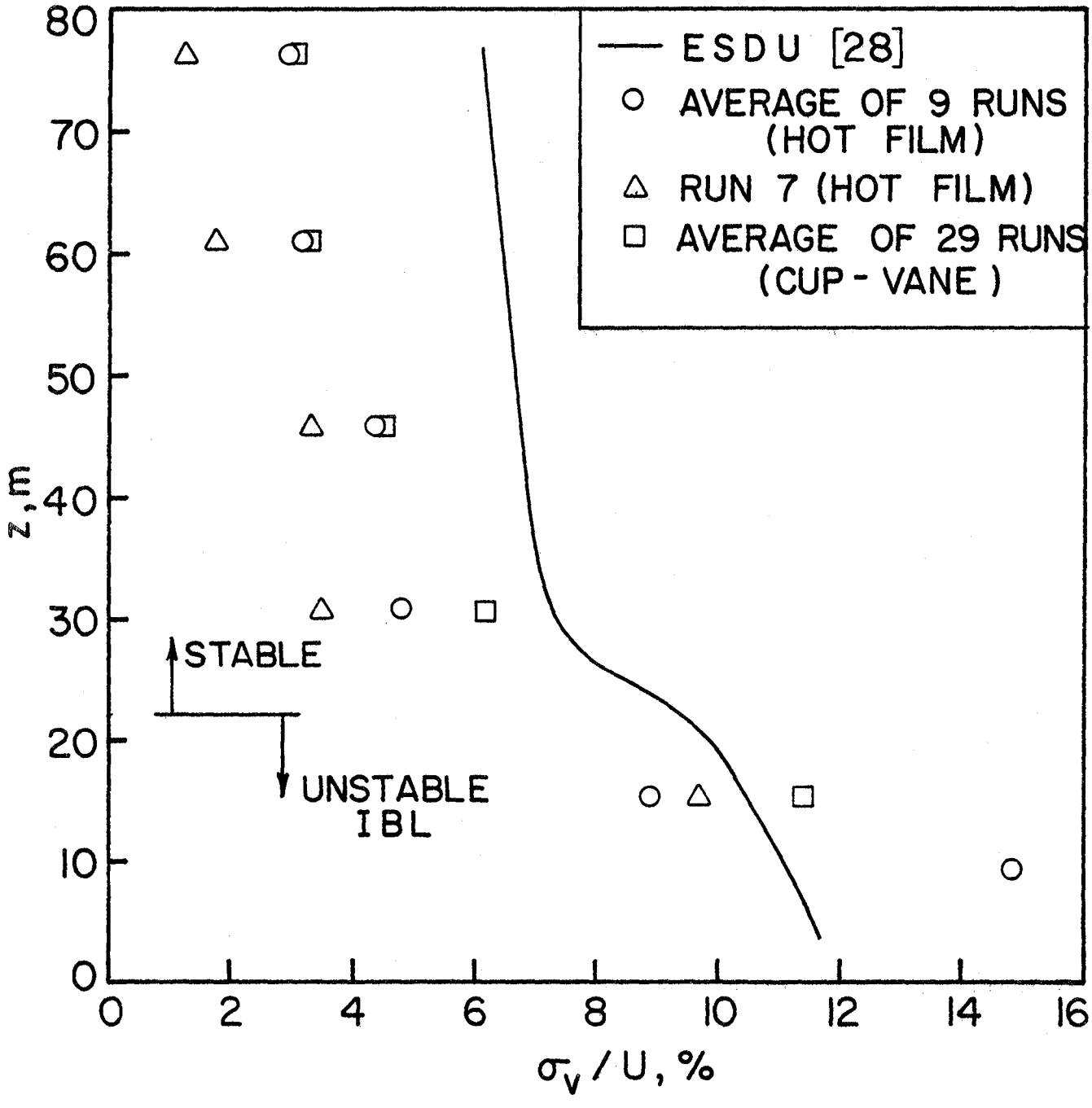

Figure 23. Vertical Distribution of the Turbulence Intensity, σ_v/U, for Southerly Winds

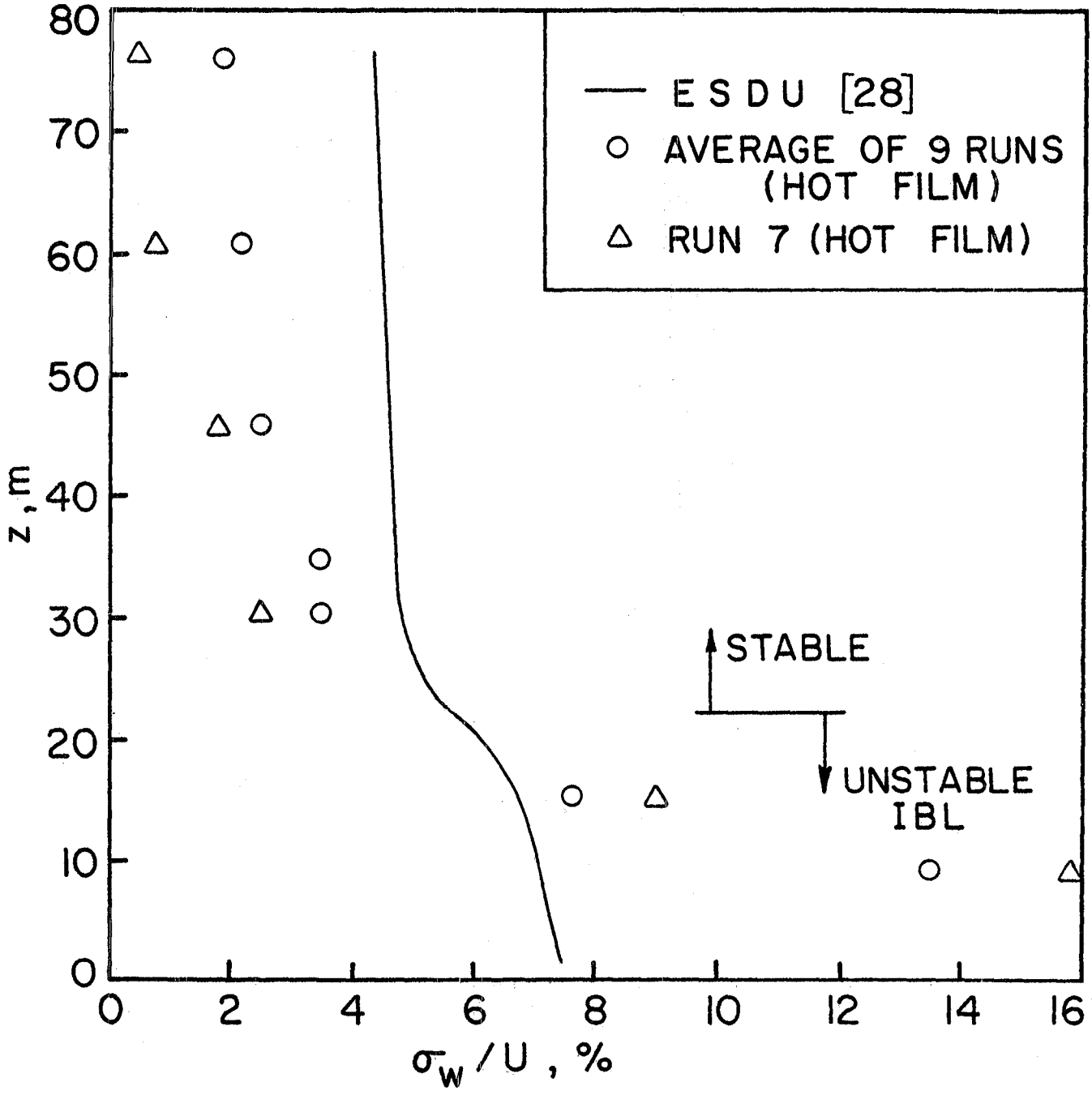

Figure 24. Vertical Distribution of the Turbulence Intensity, σ_w/U, for Southerly Winds

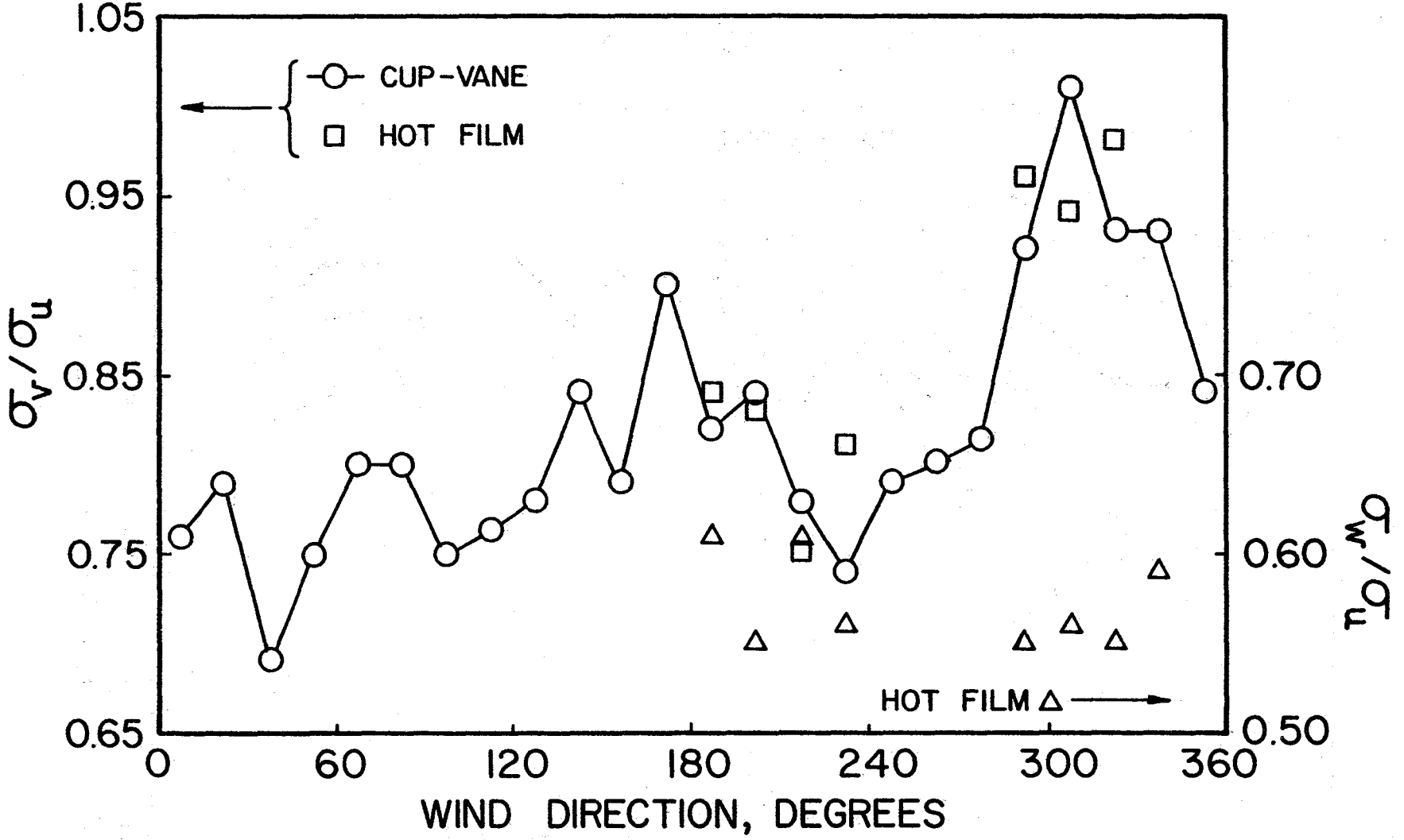

Figure 25. Variation of Ratios of Average Turbulence Intensity with Wind Direction

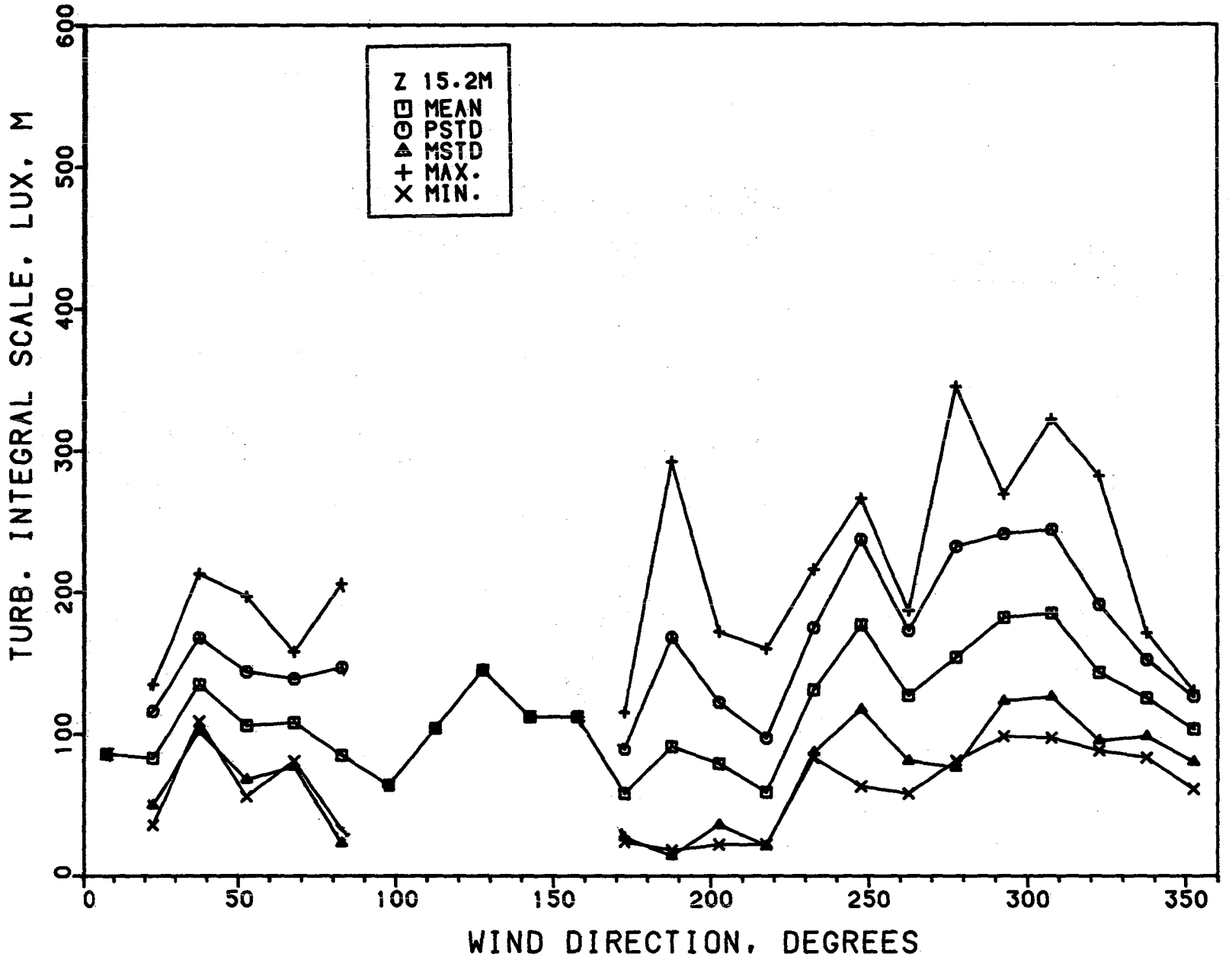

Figure 26a. Variation of Turbulence Integral Scale, L_u^x, with Wind Direction, z=15.2m

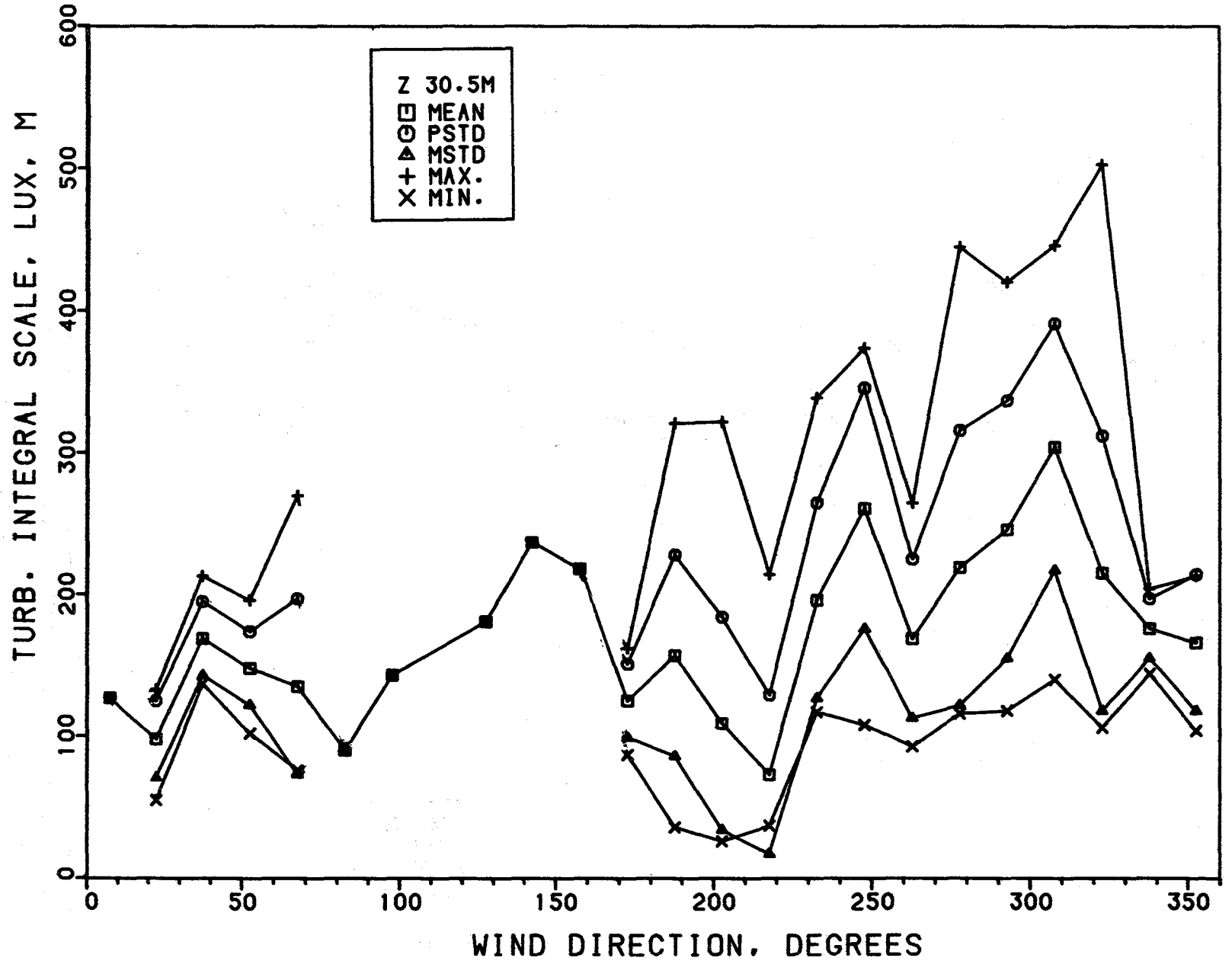

Figure 26b. Variation of Turbulence Integral Scale, L_u^x, with Wind Direction, z=30.5m

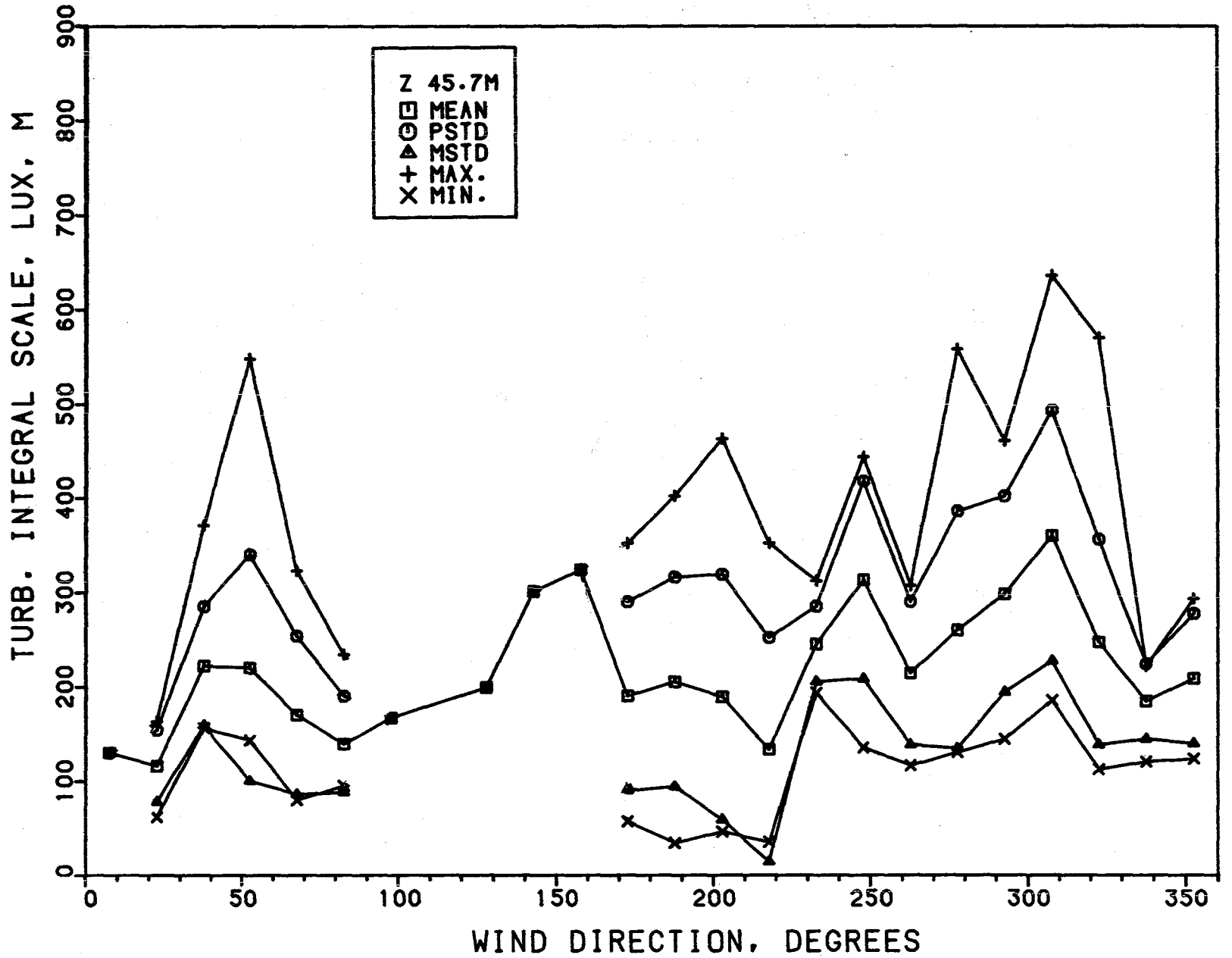

Figure 26c. Variation of Turbulence Integral Scale, L_u^x, with Wind Direction, z=45.7m

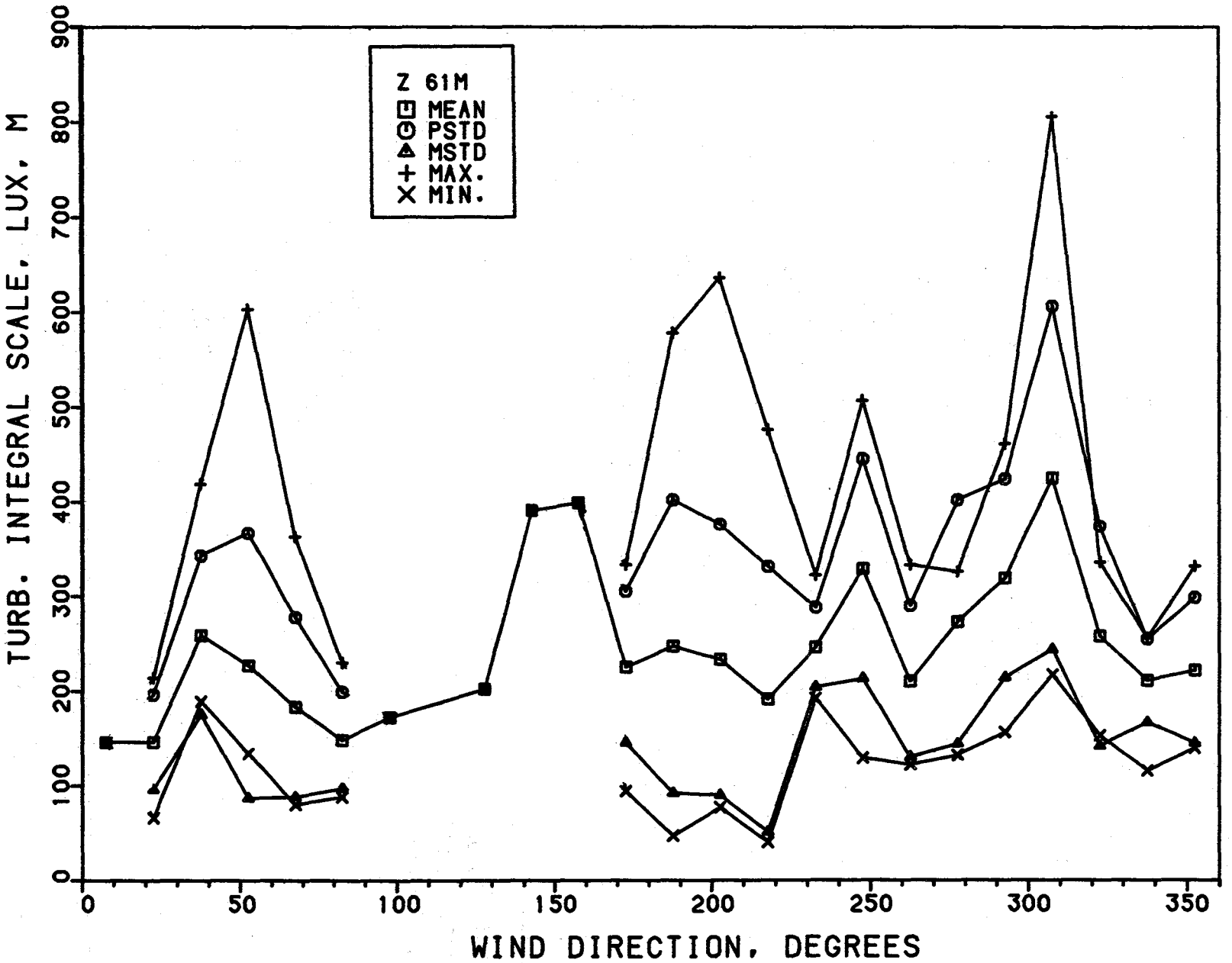

Figure 26d. Variation of Turbulence Integral Scale, L_u^x, with Wind Direction, z=61.0m

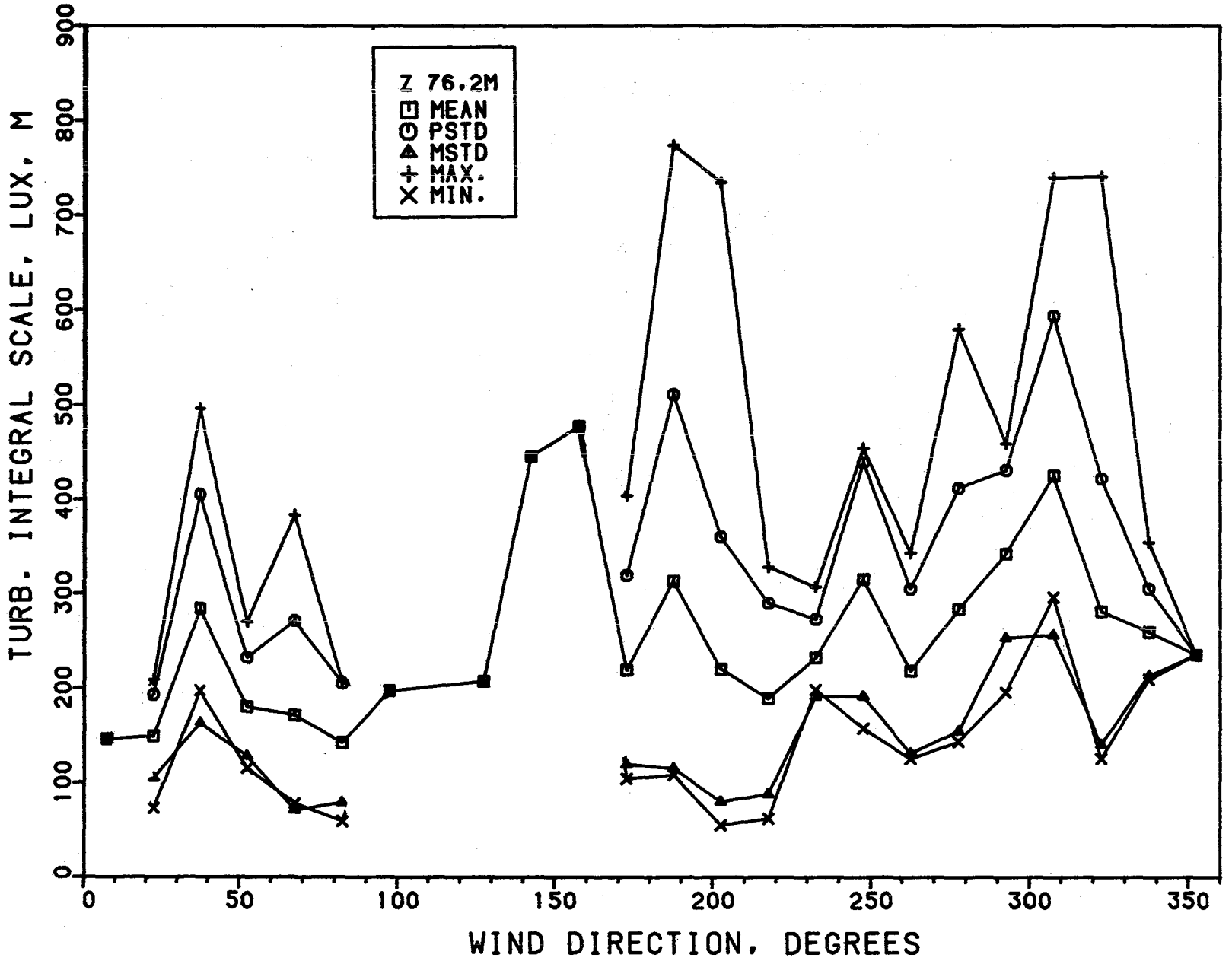

Figure 26e. Variation of Turbulence Integral Scale, L_u^x, with Wind Direction, z=76.2m

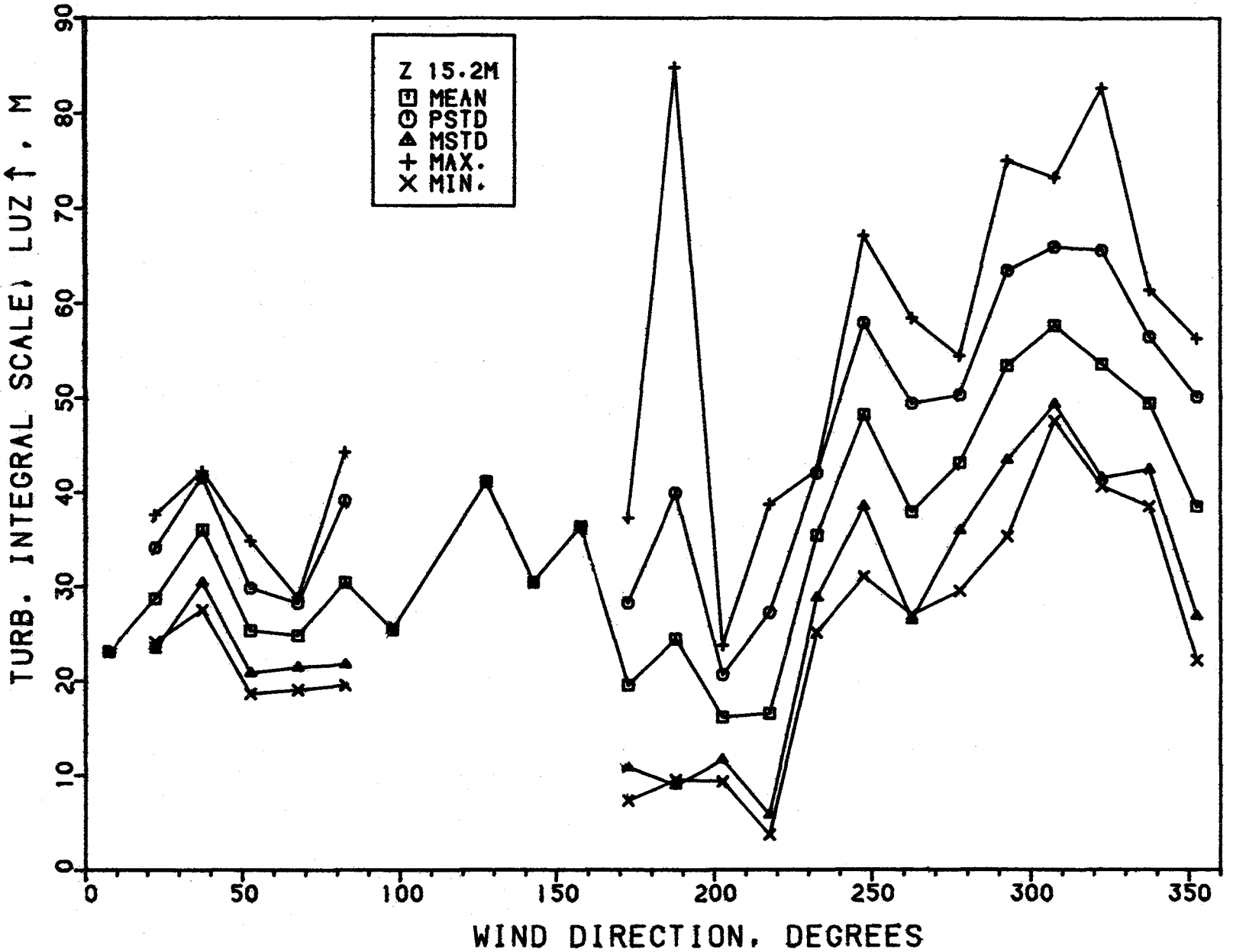

Figure 27a. Variation of Turbulence Integral Scale, $L_u^{z\uparrow}$, with Wind Direction z=15.7m

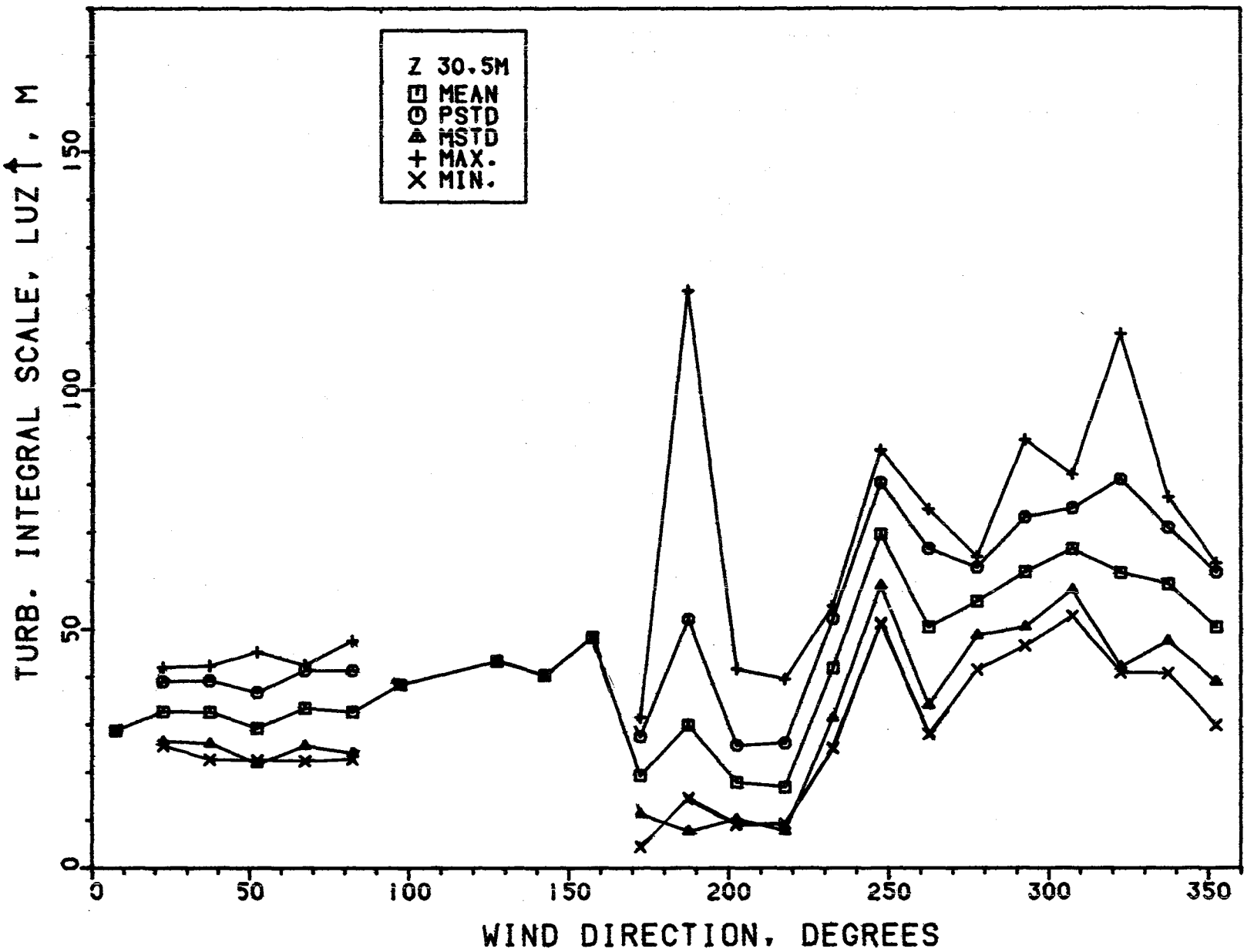

Figure 27b. Variation of Turbulence Integral Scale, $L_u^{z\uparrow}$, with Wind Direction z=30.5m

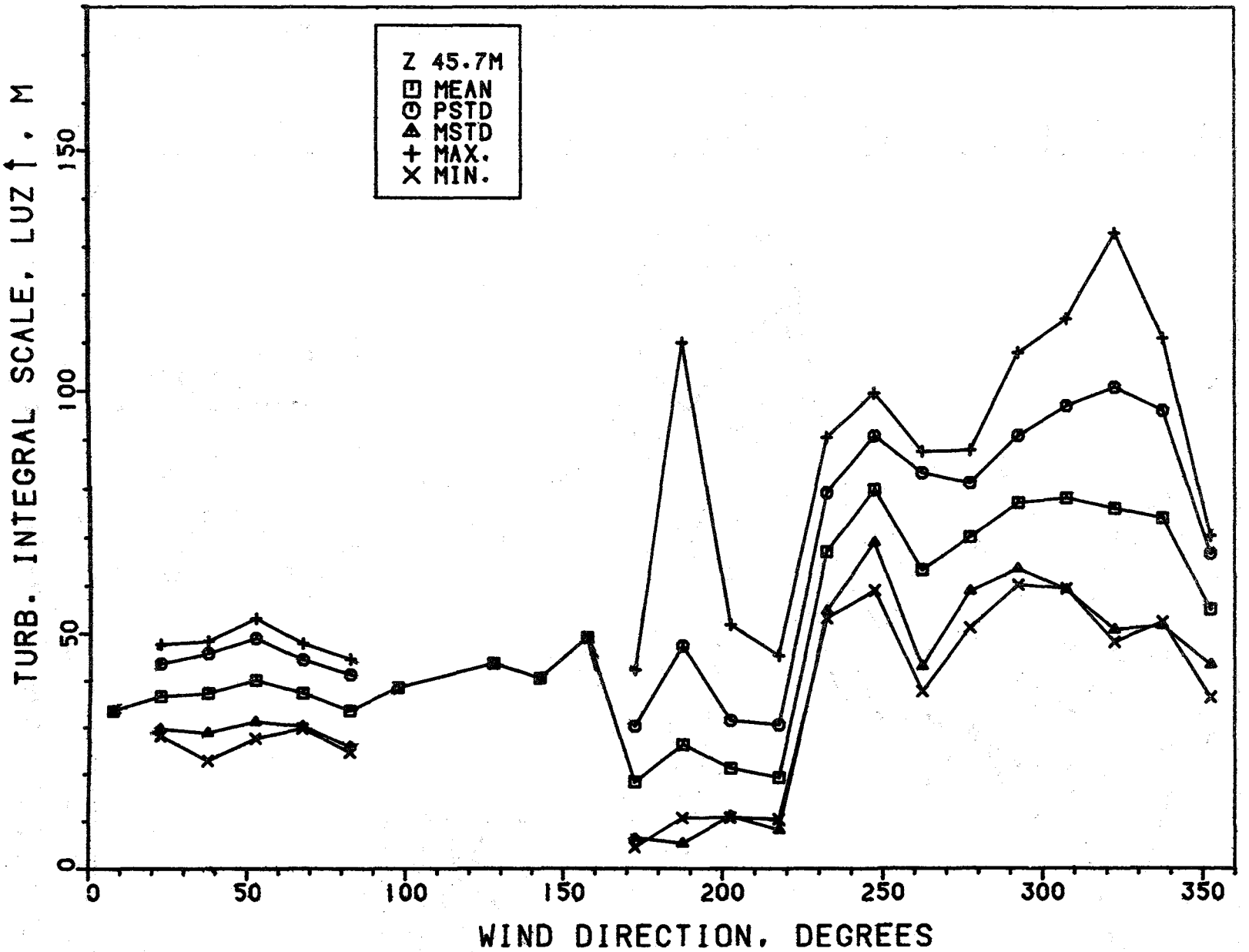

Figure 27c. Variation of Turbulence Integral Scale, $L_u^z\uparrow$, with Wind Direction z=45.7m

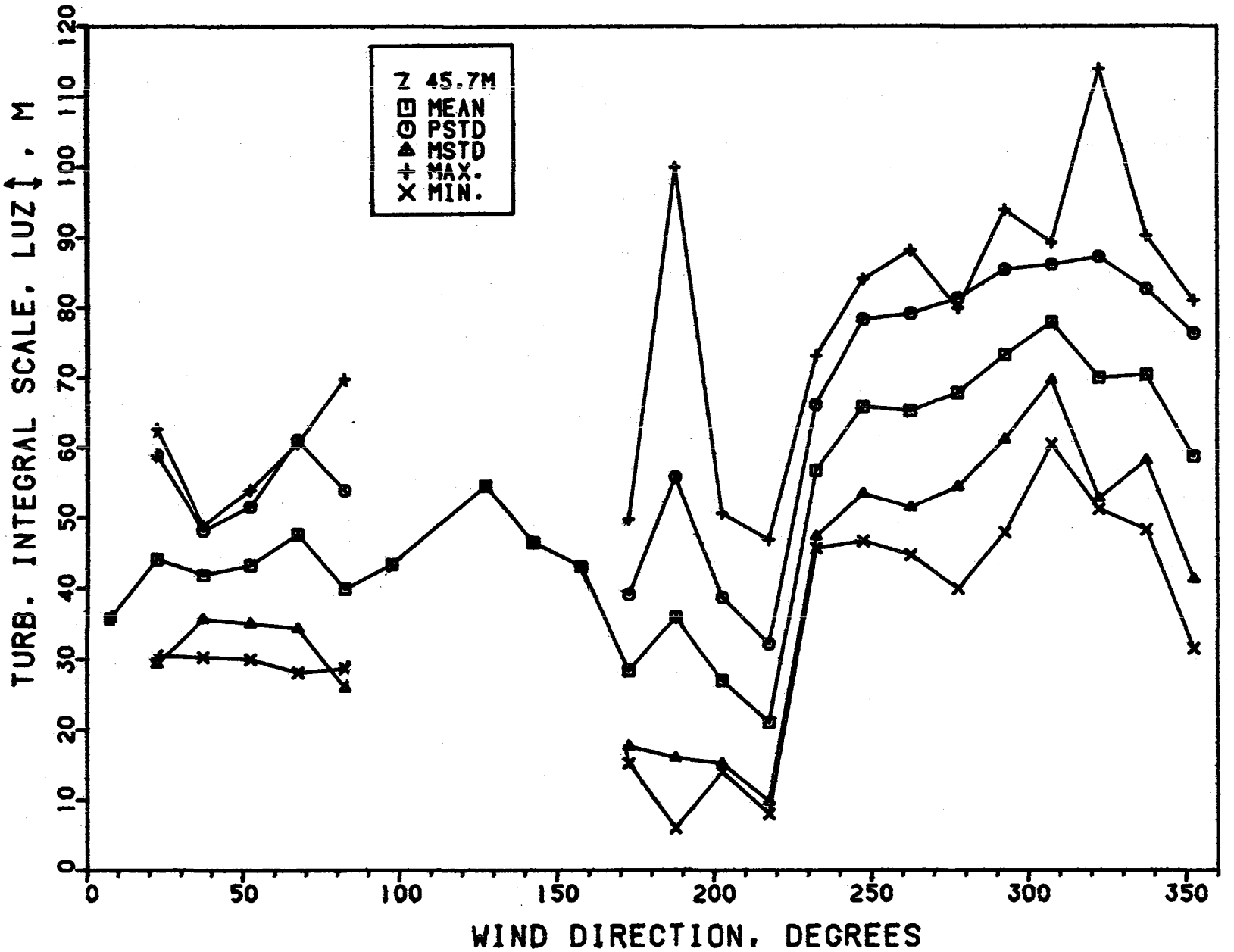

Figure 27d. Variation of Turbulence Integral Scale, $L_{u\downarrow}^{z\uparrow}$, with Wind Direction z=45.7m

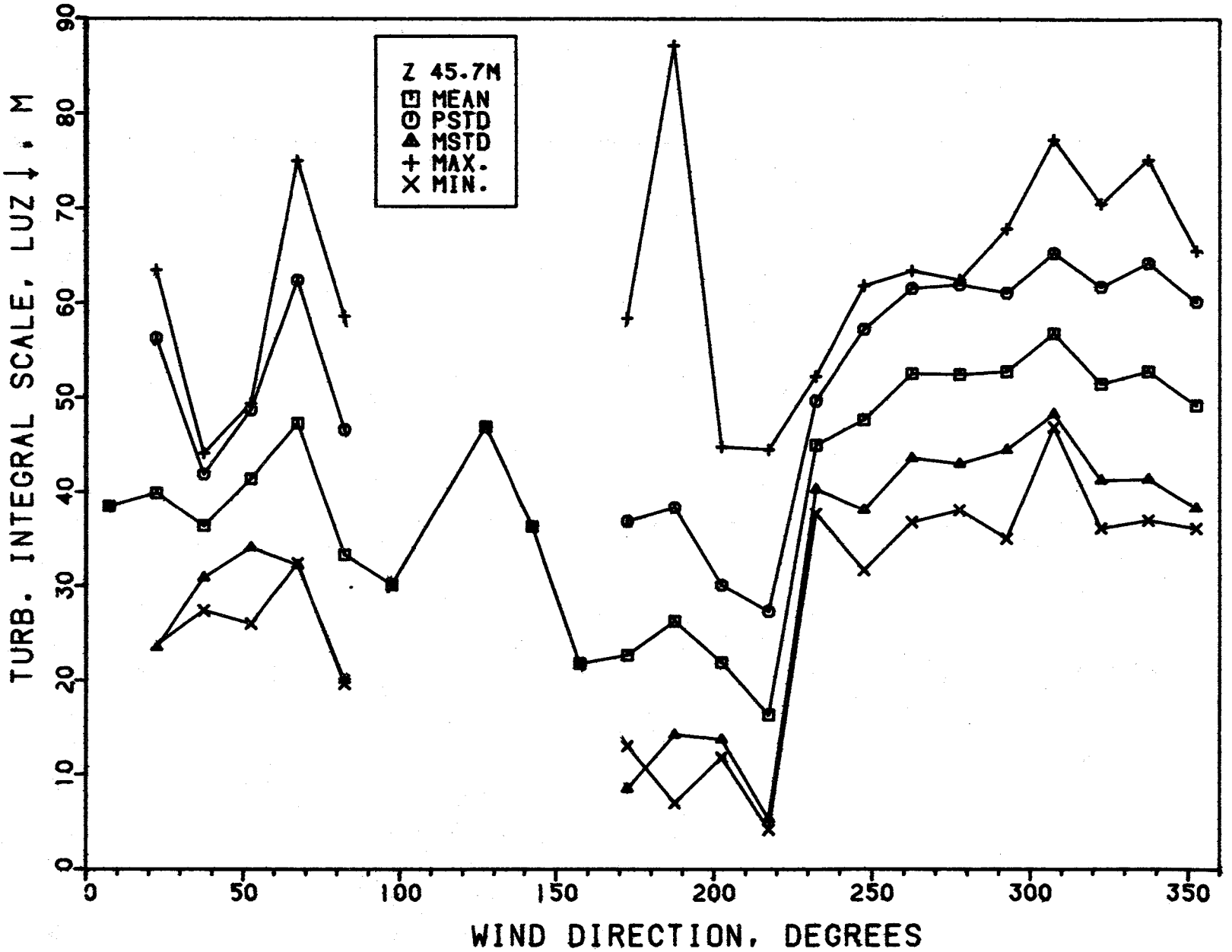

Figure 27e. Variation of Turbulence Integral Scale, $L_u^{z\downarrow}$, with Wind Direction z=45.7m

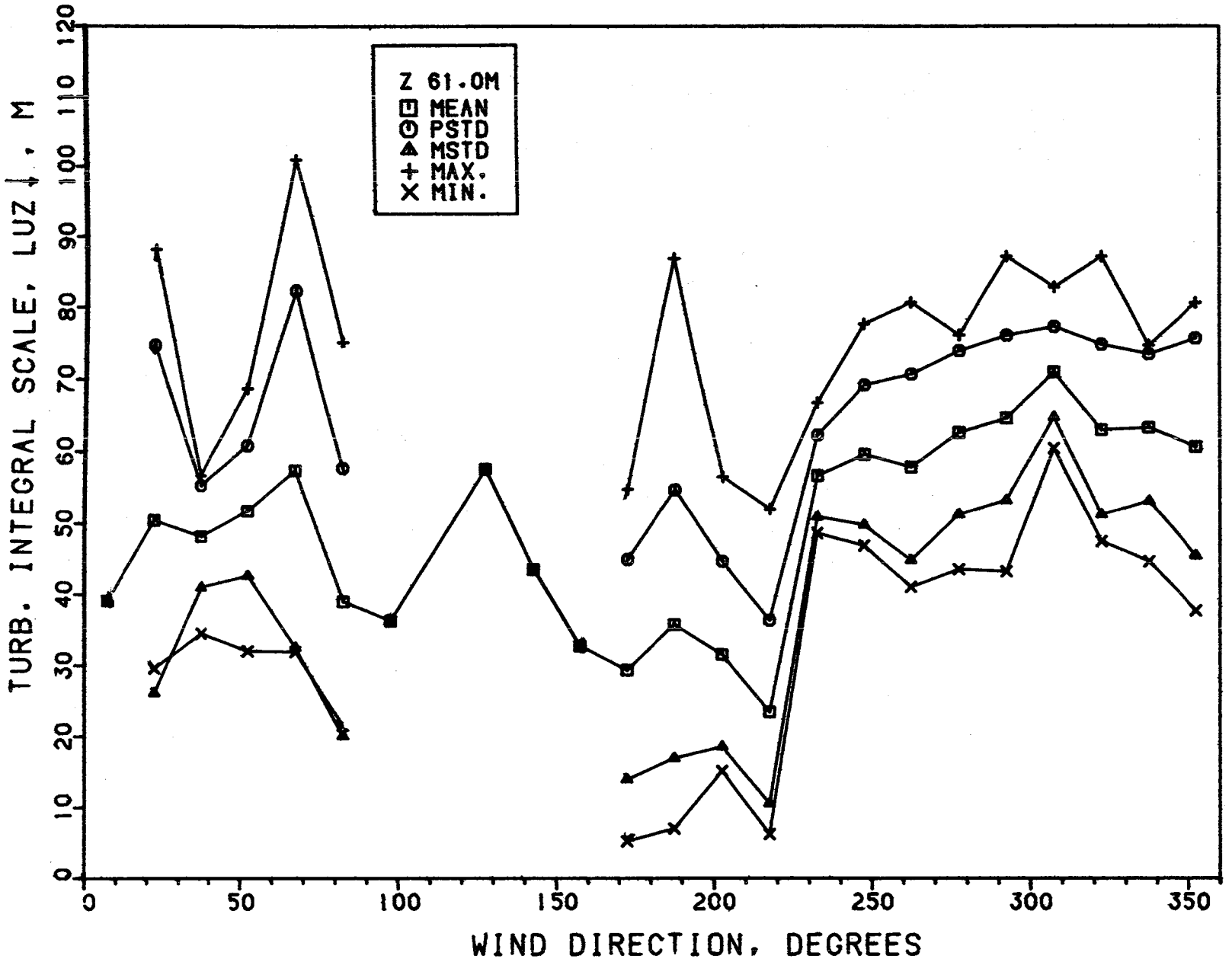

Figure 27f. Variation of Turbulence Integral Scale, $L_u^{z\downarrow}$, with Wind Direction z=61.0m

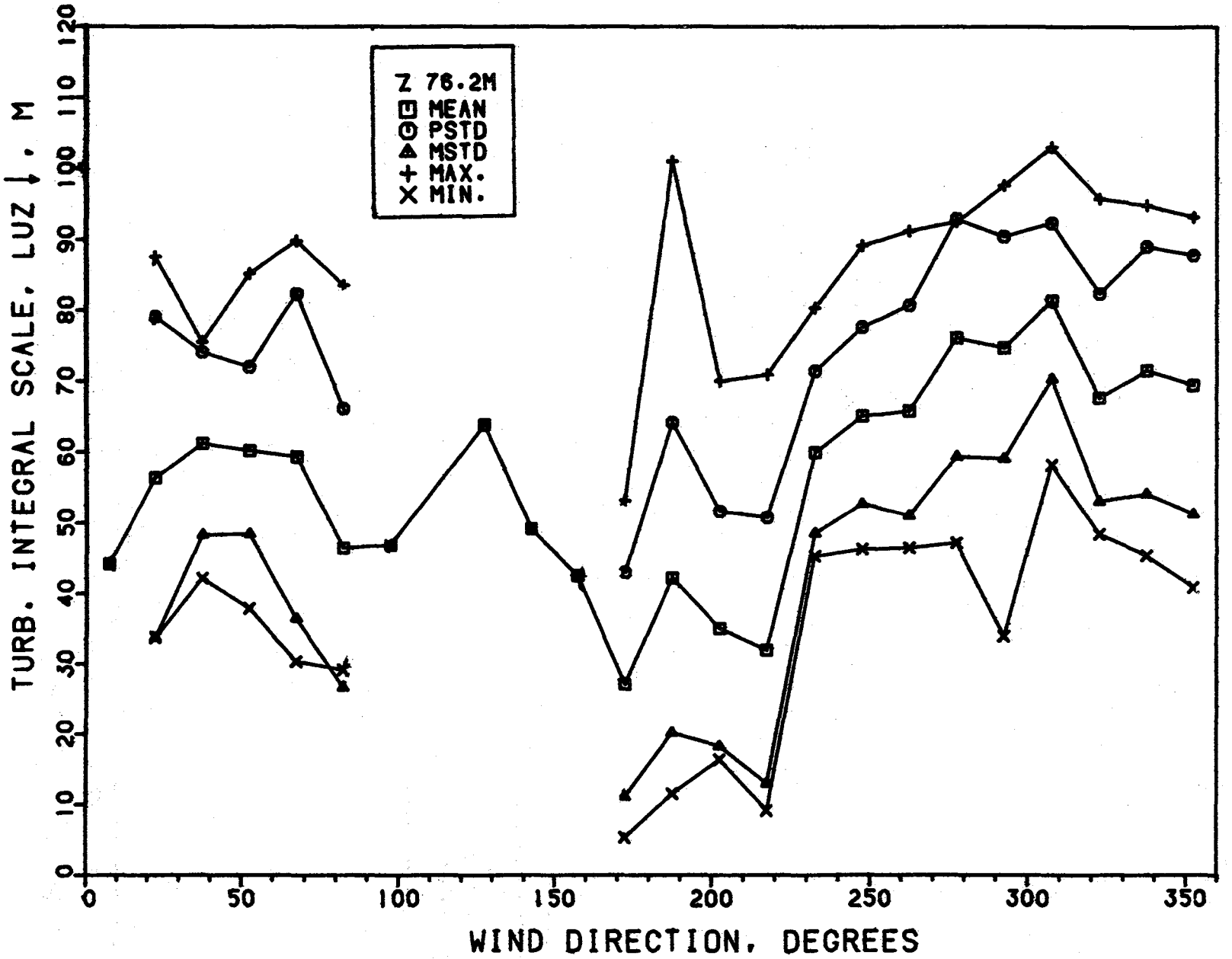

Figure 27g. Variation of Turbulence Integral Scale, $L_u^{z\downarrow}$, with Wind Direction z=76.2m

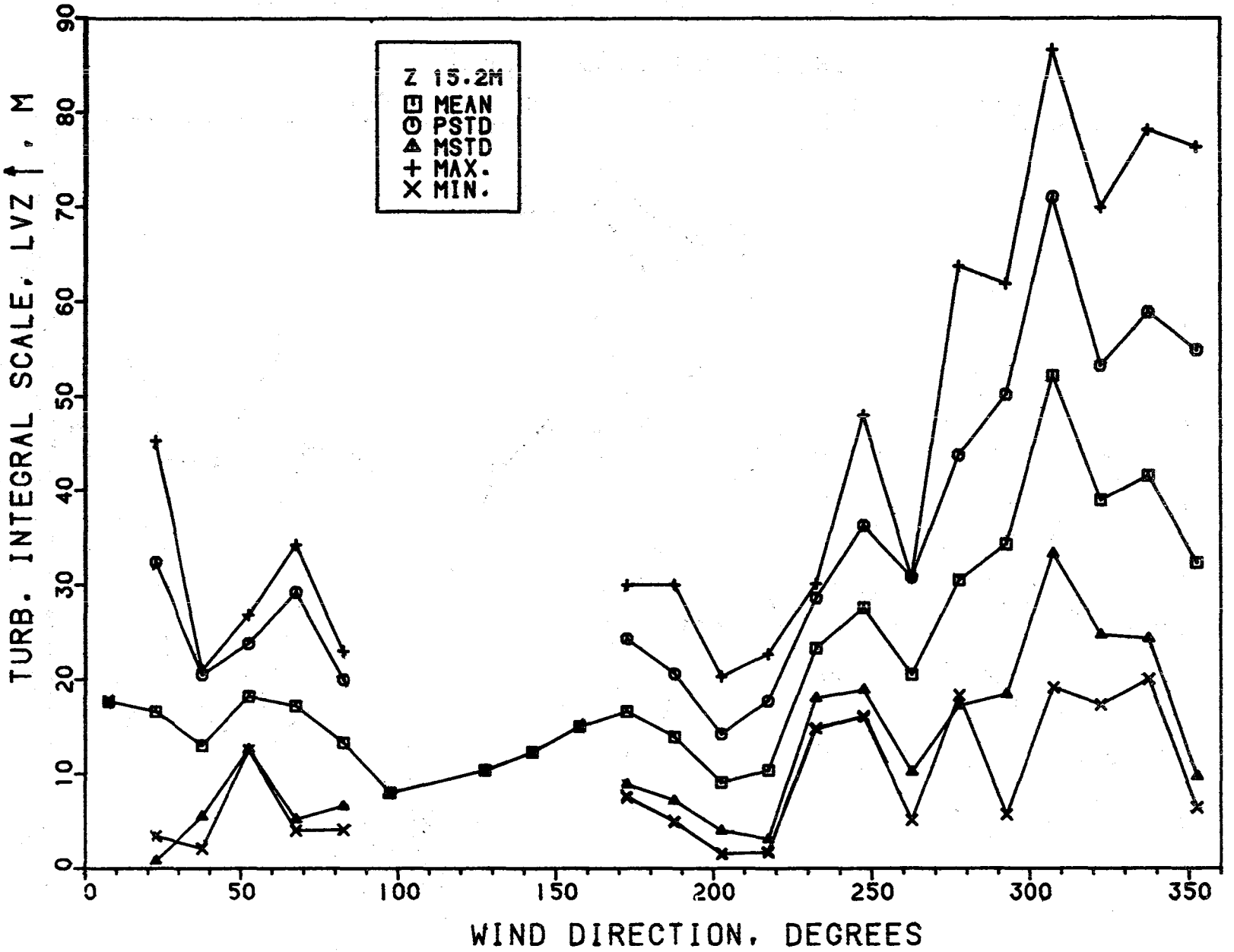

Figure 28a. Variation of Turbulence Integral Scale, $L_v^{z\uparrow}$, with Wind Direction z=15.2m

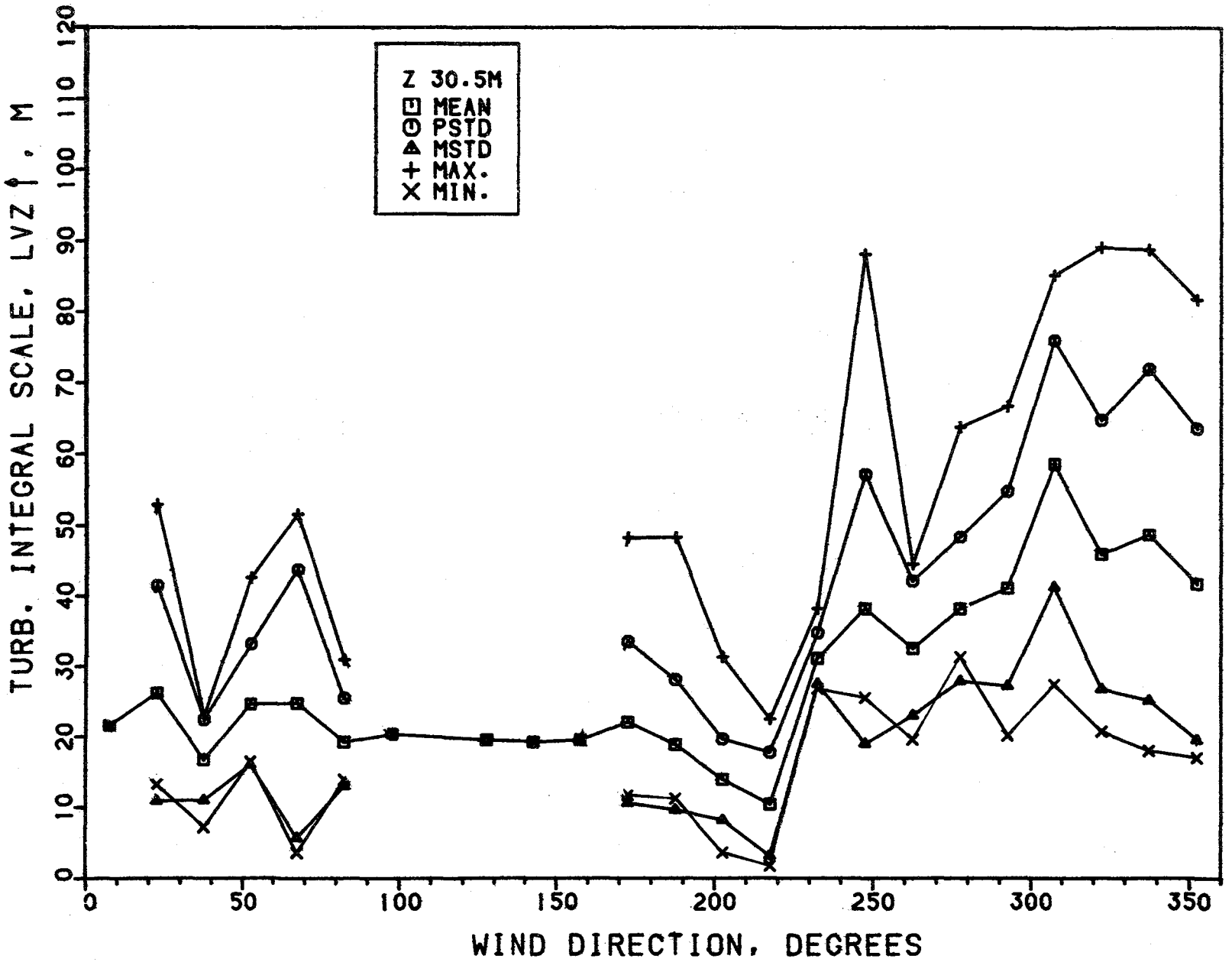

Figure 28b. Variation of Turbulence Integral Scale, $L_v^{z\uparrow}$, with Wind Direction z=30.5m

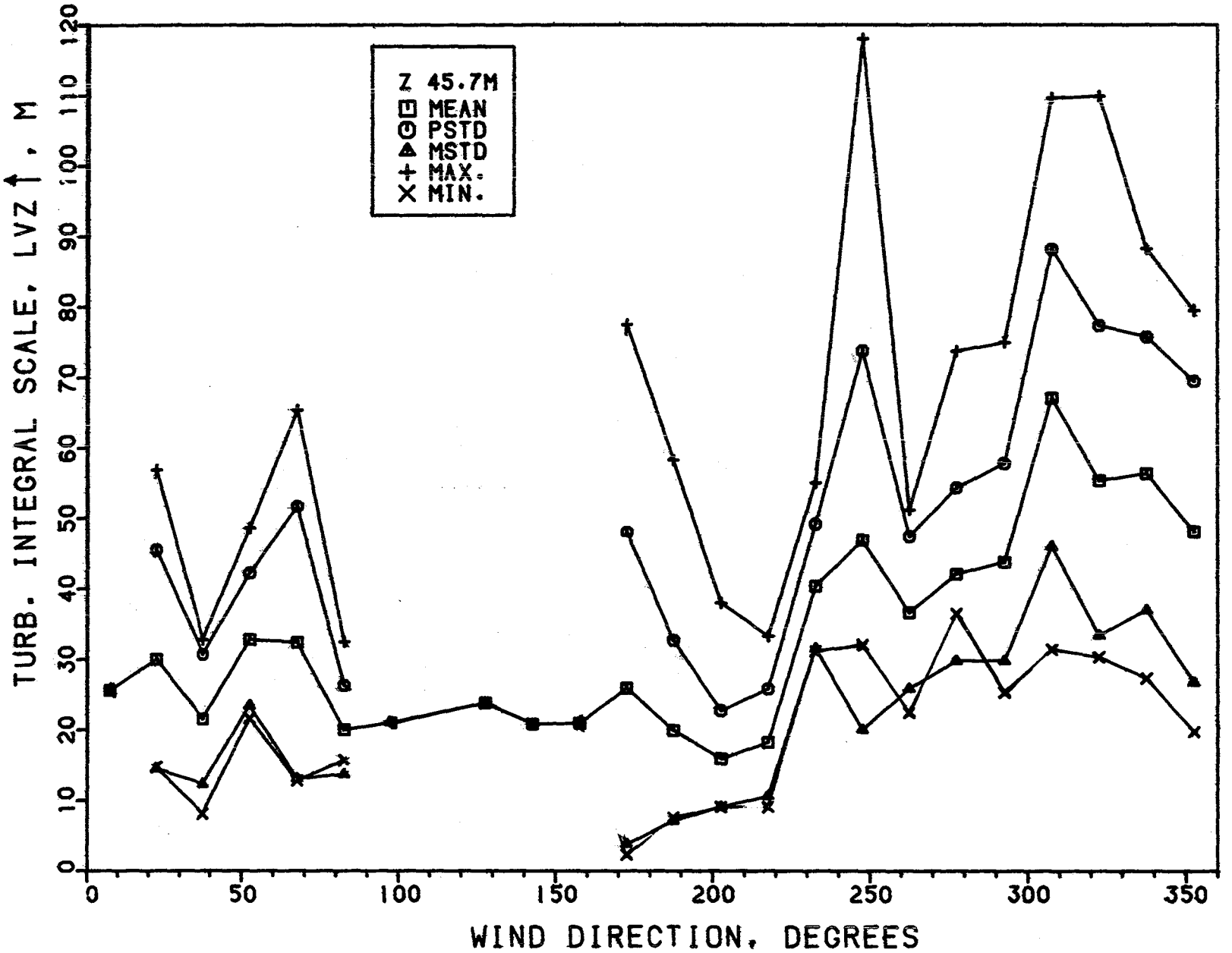

Figure 28c. Variation of Turbulence Integral Scale, $L_v^z\uparrow$, with Wind Direction z=45.7m

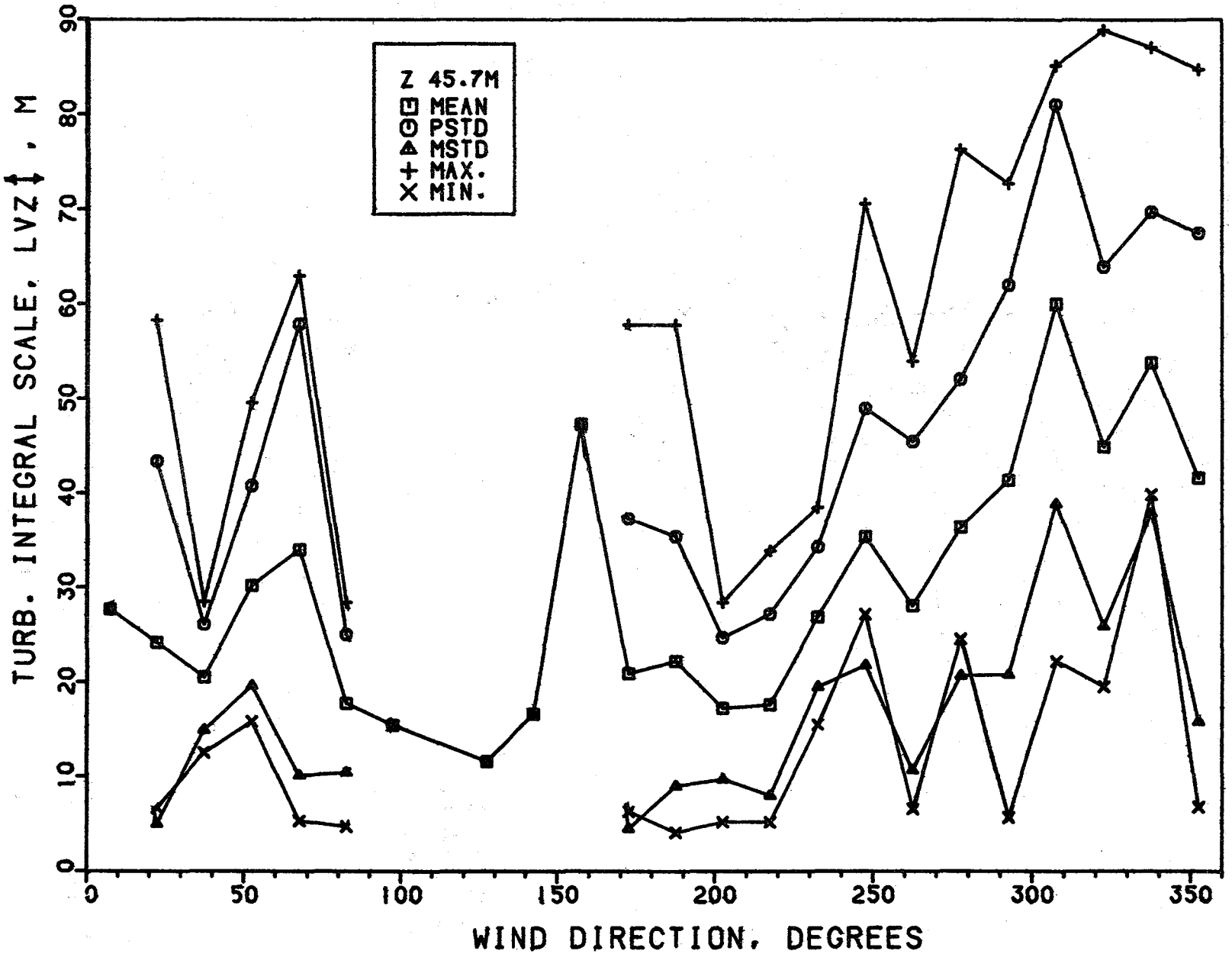

Figure 28d. Variation of Turbulence Integral Scale, $L_{v\updownarrow}^{z}$, with Wind Direction z=45.7m

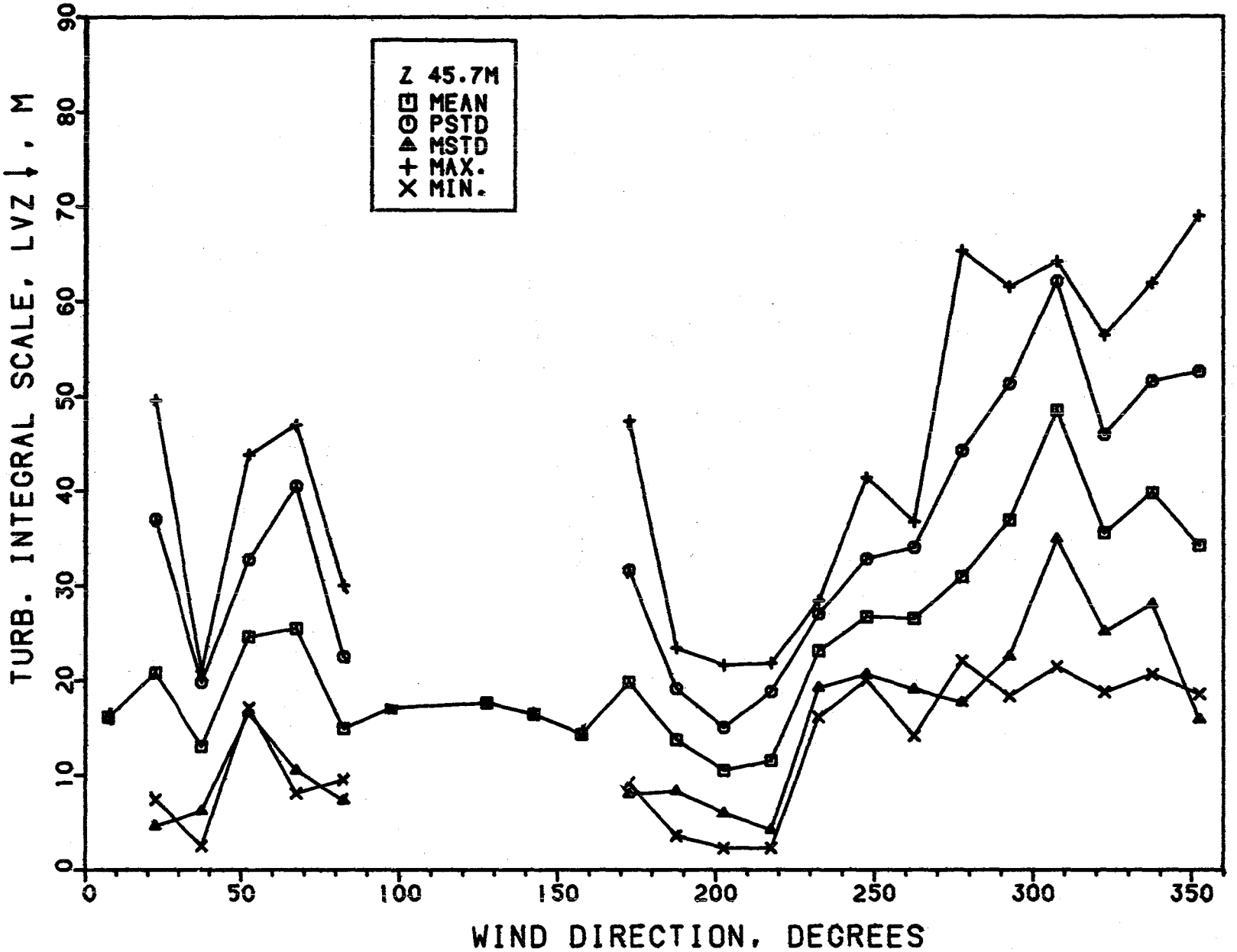

Figure 28e. Variation of Turbulence Integral Scale, $L_v^{z\downarrow}$, with Wind Direction z=45.7m

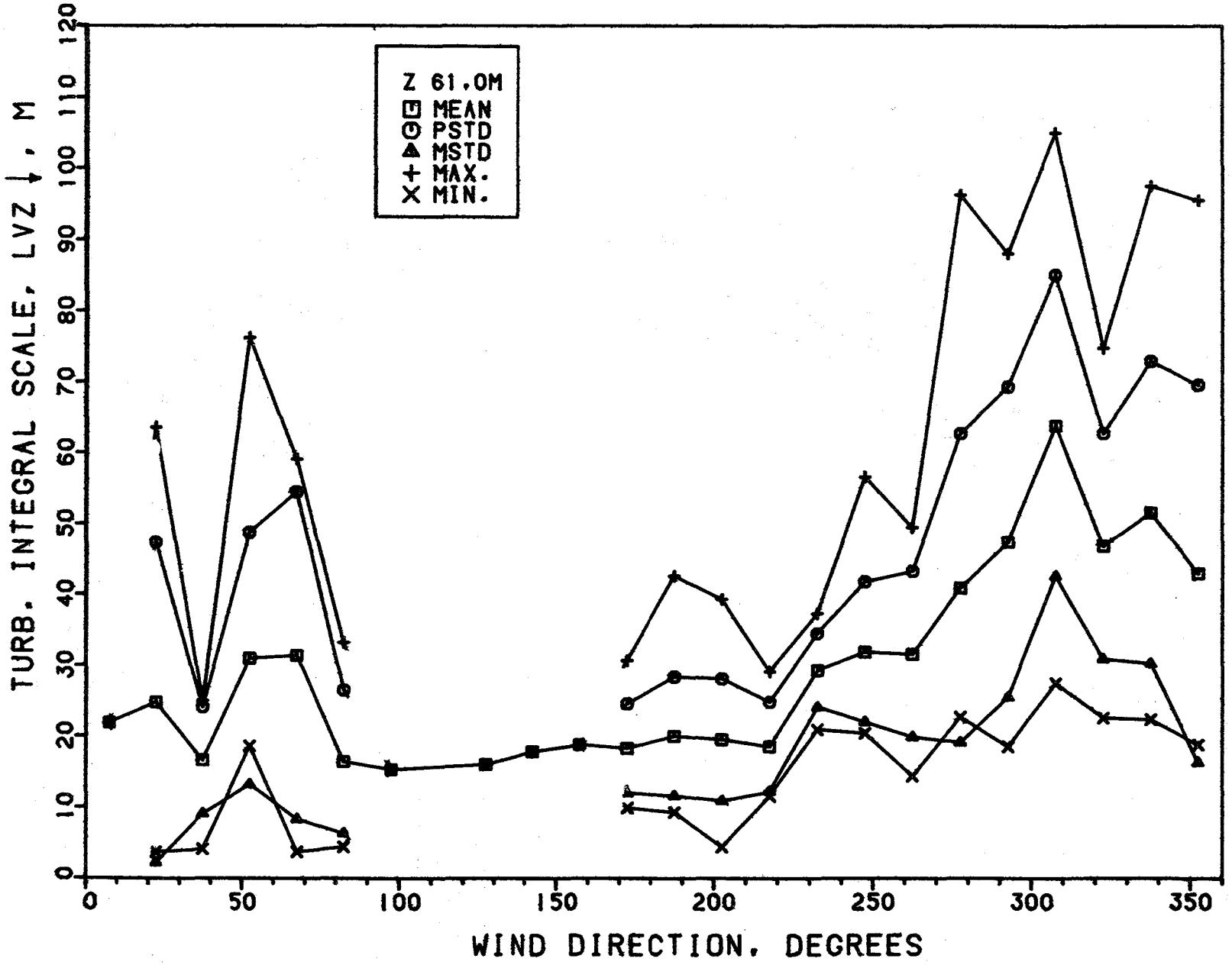

Figure 28f. Variation of Turbulence Integral Scale, $L_v^{z\downarrow}$, with Wind Direction z=61.0m

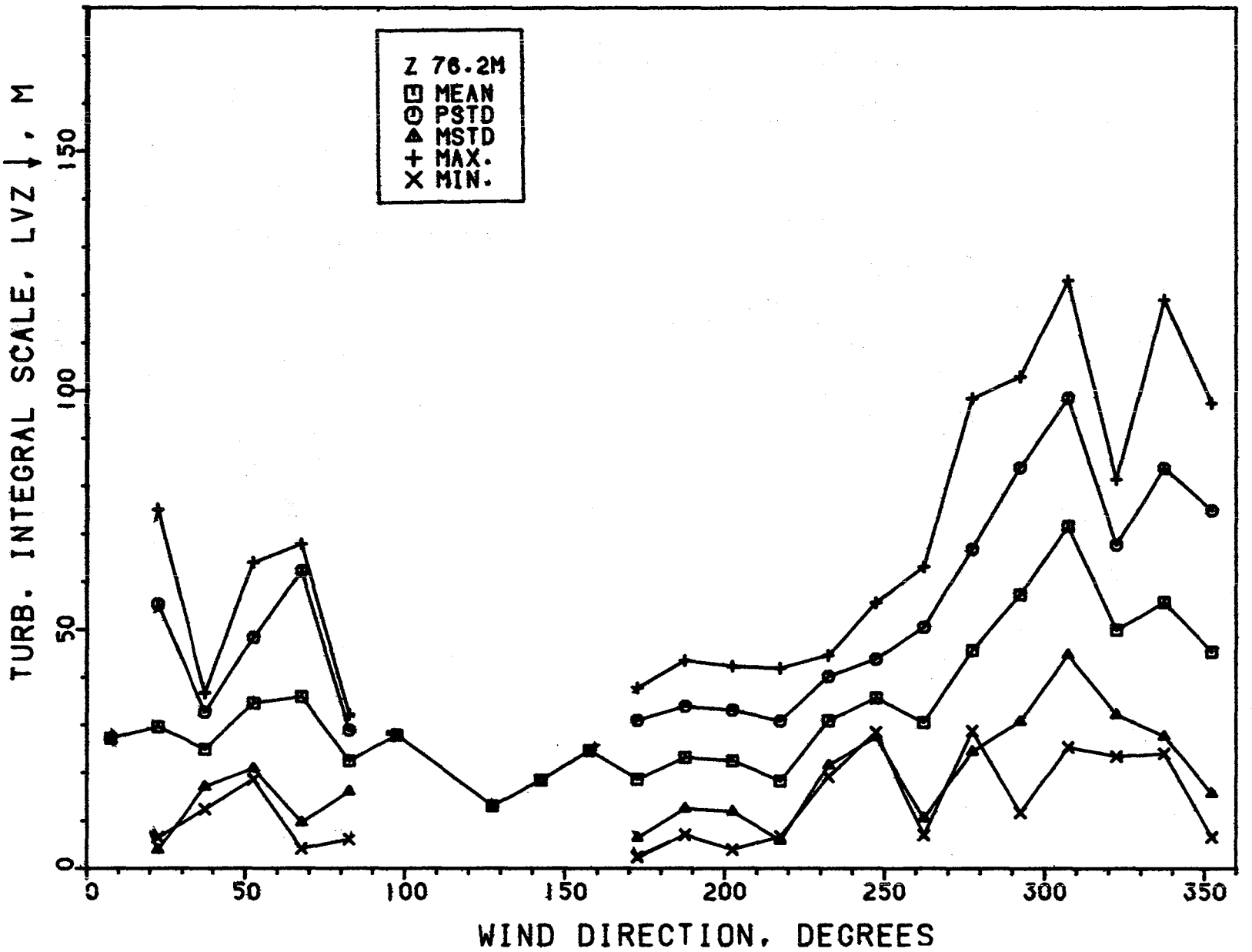

Figure 28g. Variation of Turbulence Integral Scale, $L_v^{z\downarrow}$, with Wind Direction z=76.2m

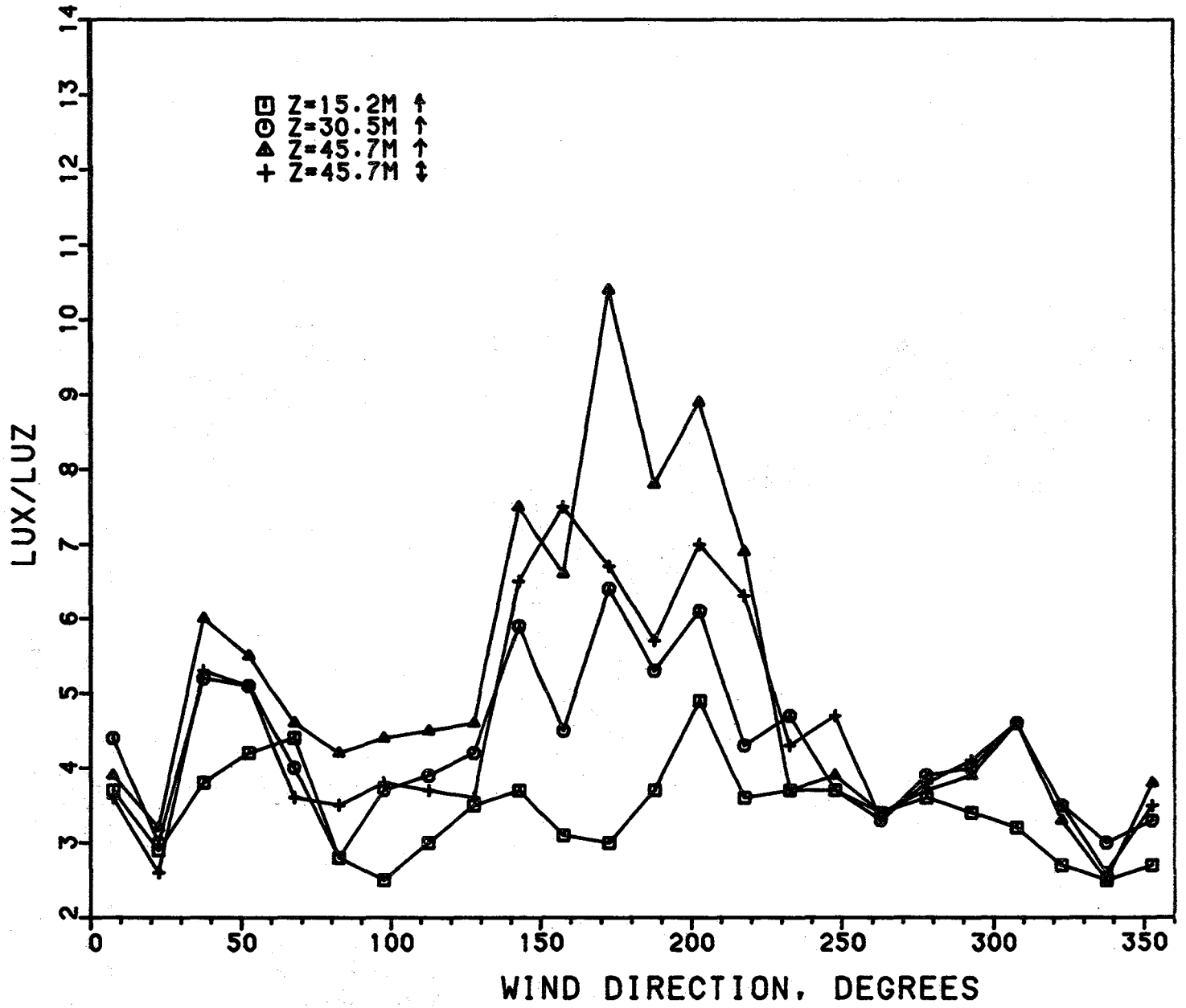

Figure 29. Variation the Integral-Scale Ratio L_u^x/L_u^z for the Three Lowest Observation Levels with Wind Direction. Arrows Indicate the Direction of integration.

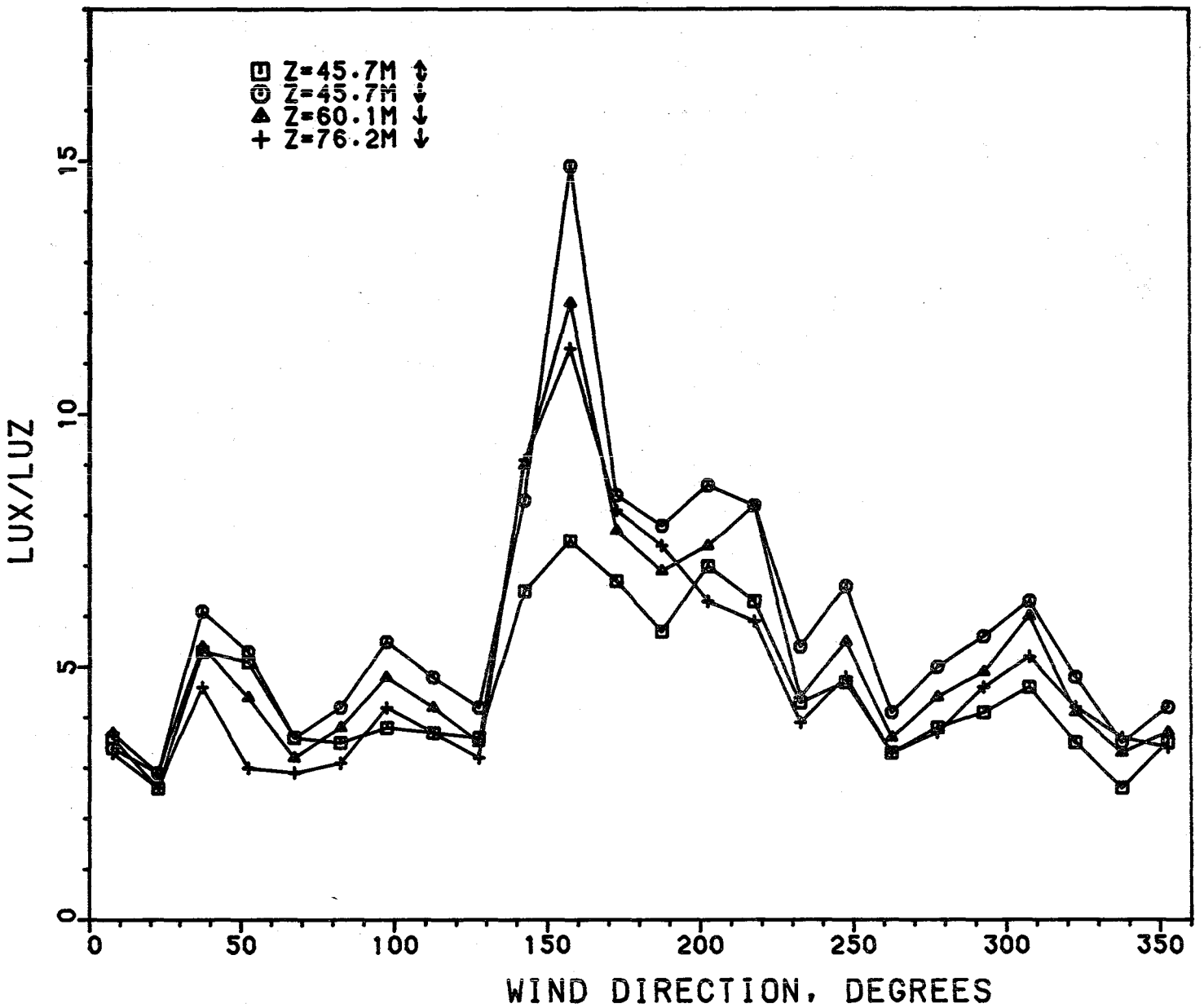

Figure 30. Variation of the Integral-Scale Ratio L_u^x/L_u^z for the Three Highest Observation Levels with Wind Direction. Arrows Indicate the Direction of Integration.

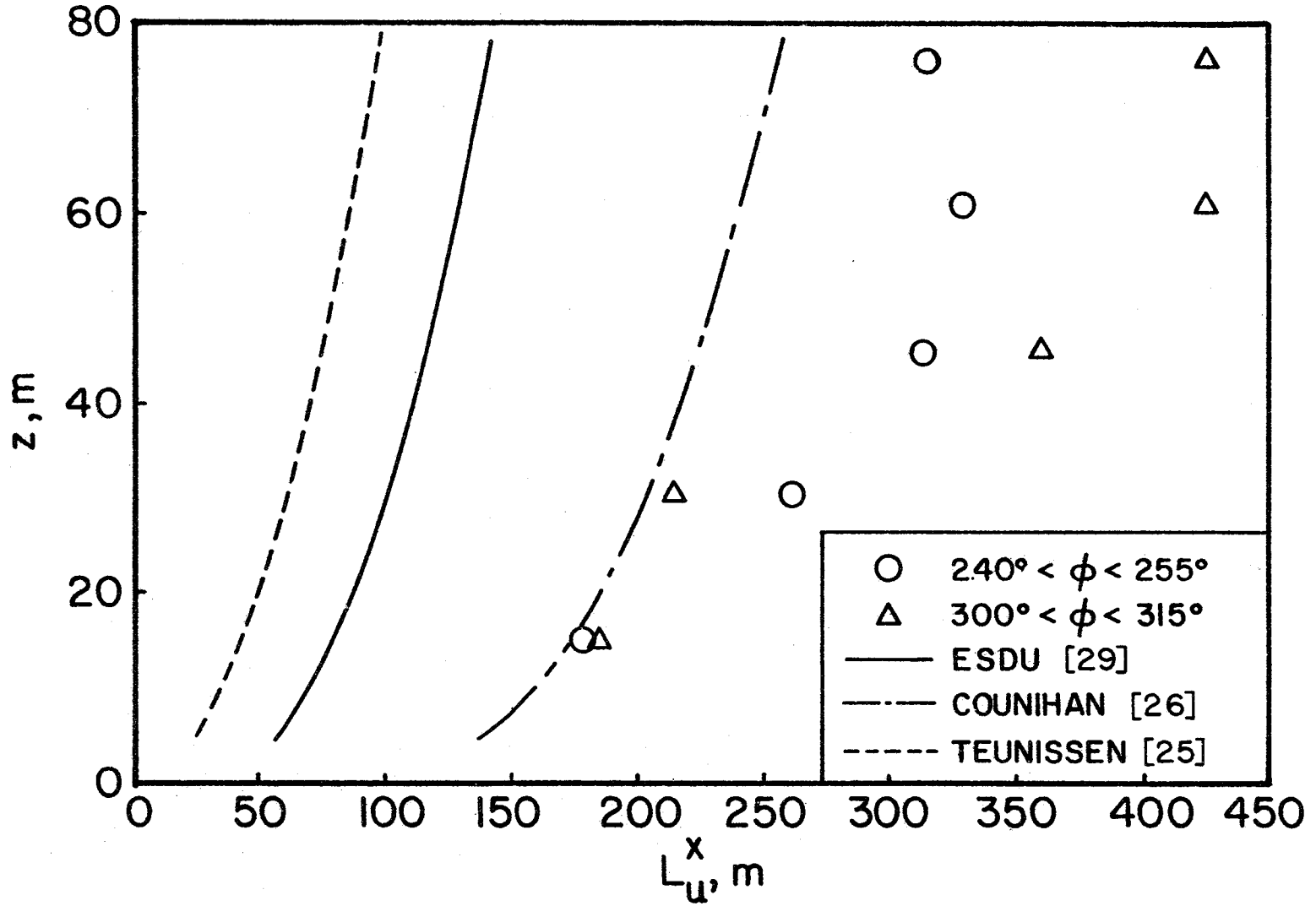

Figure 31. Variation of Average Integral Scales L_u^x (Cup-Vane) with Height for Two Westerly Wind-Direction Sectors

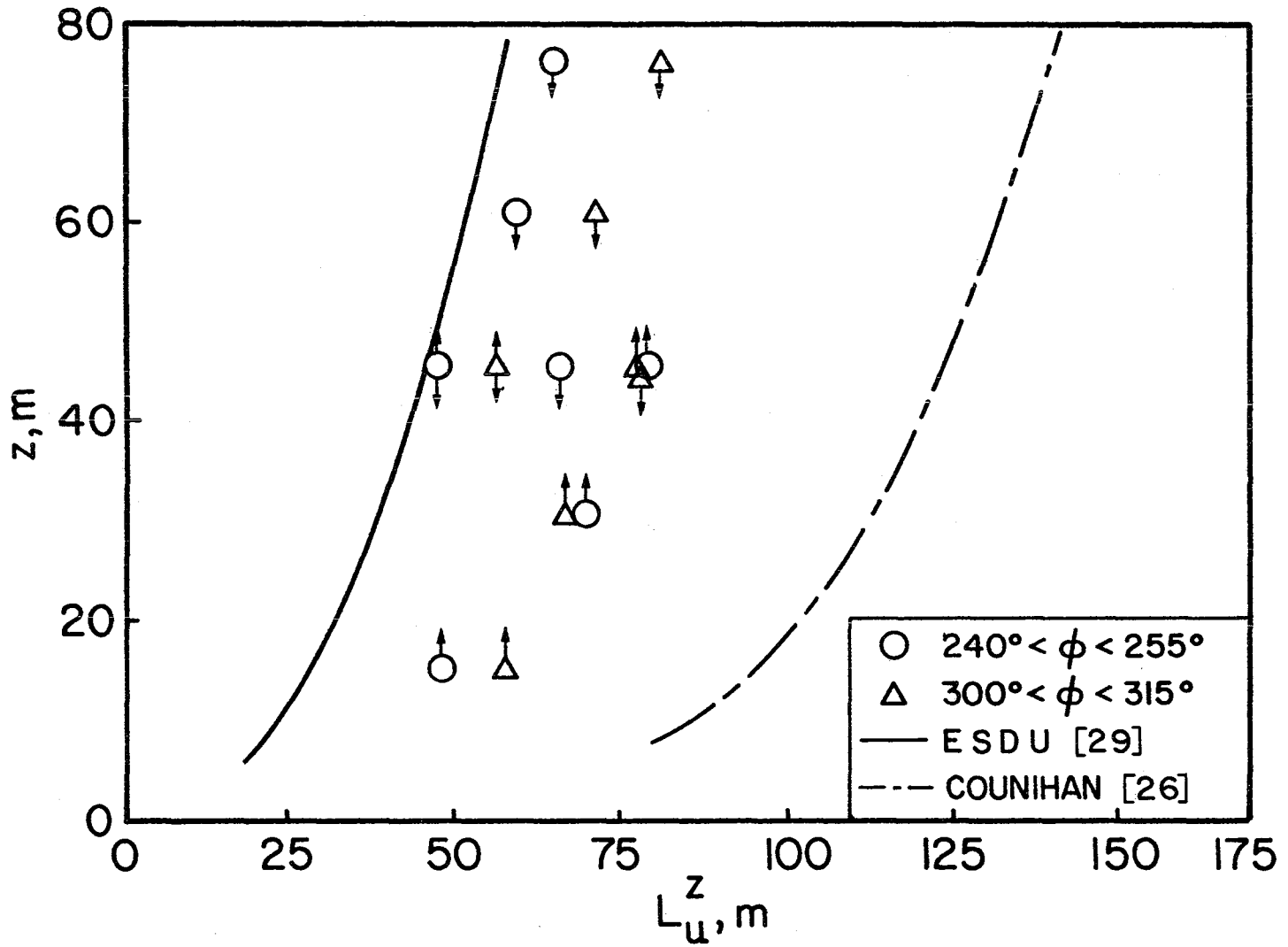

Figure 32. Variation of Average Integral Scales, L_u^z, (Cup-Vane) with Height for Two Westerly Wind-Direction Sectors. Arrows on Symbols Indicate the Direction of Integration

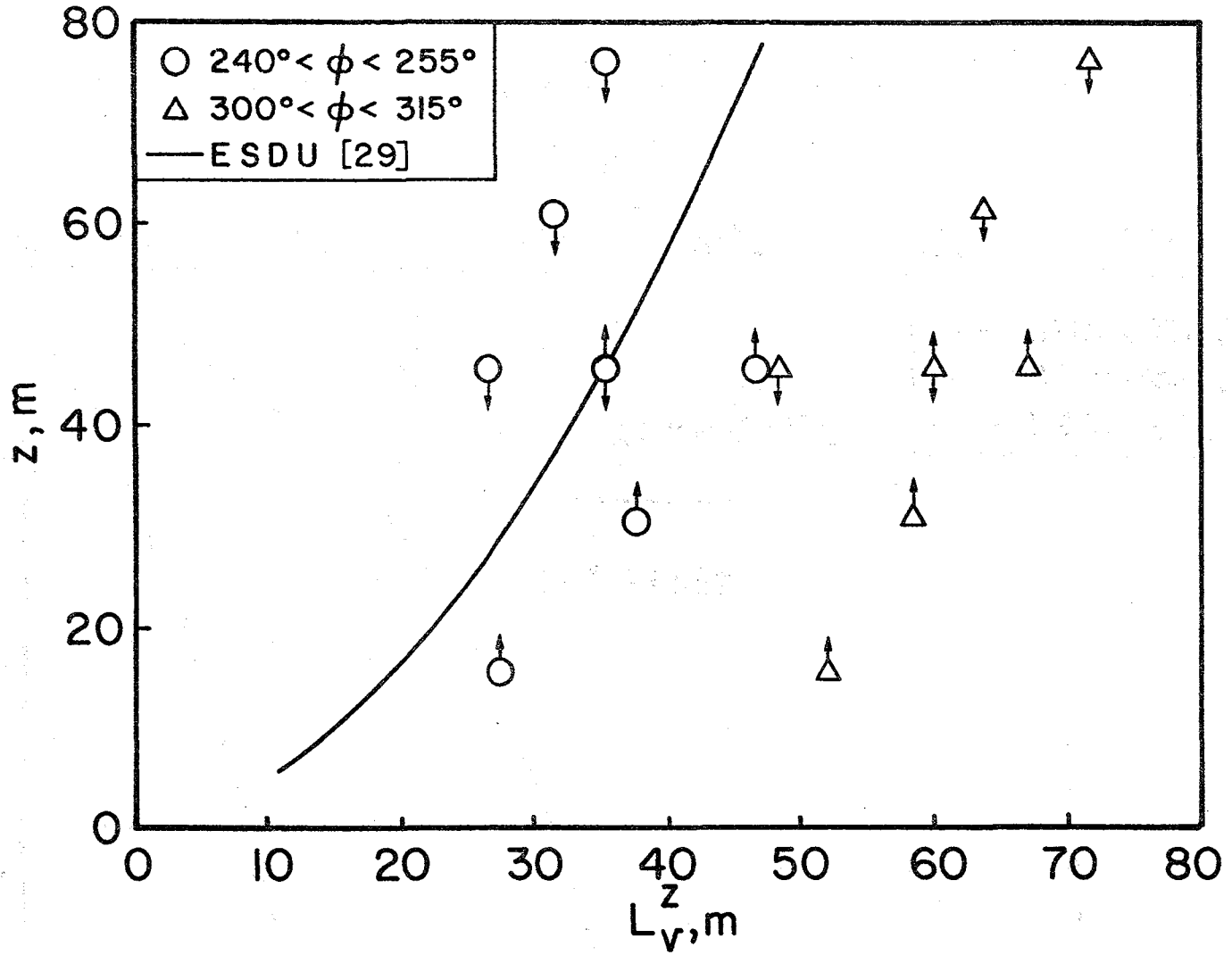

Figure 33. Variation of Average Integral Scales, L_v^z, (Cup-Vane) with Height for Two Westerly Wind-Drecition Sectors. Arrows on Symbols Indicate the Direction of Integration.

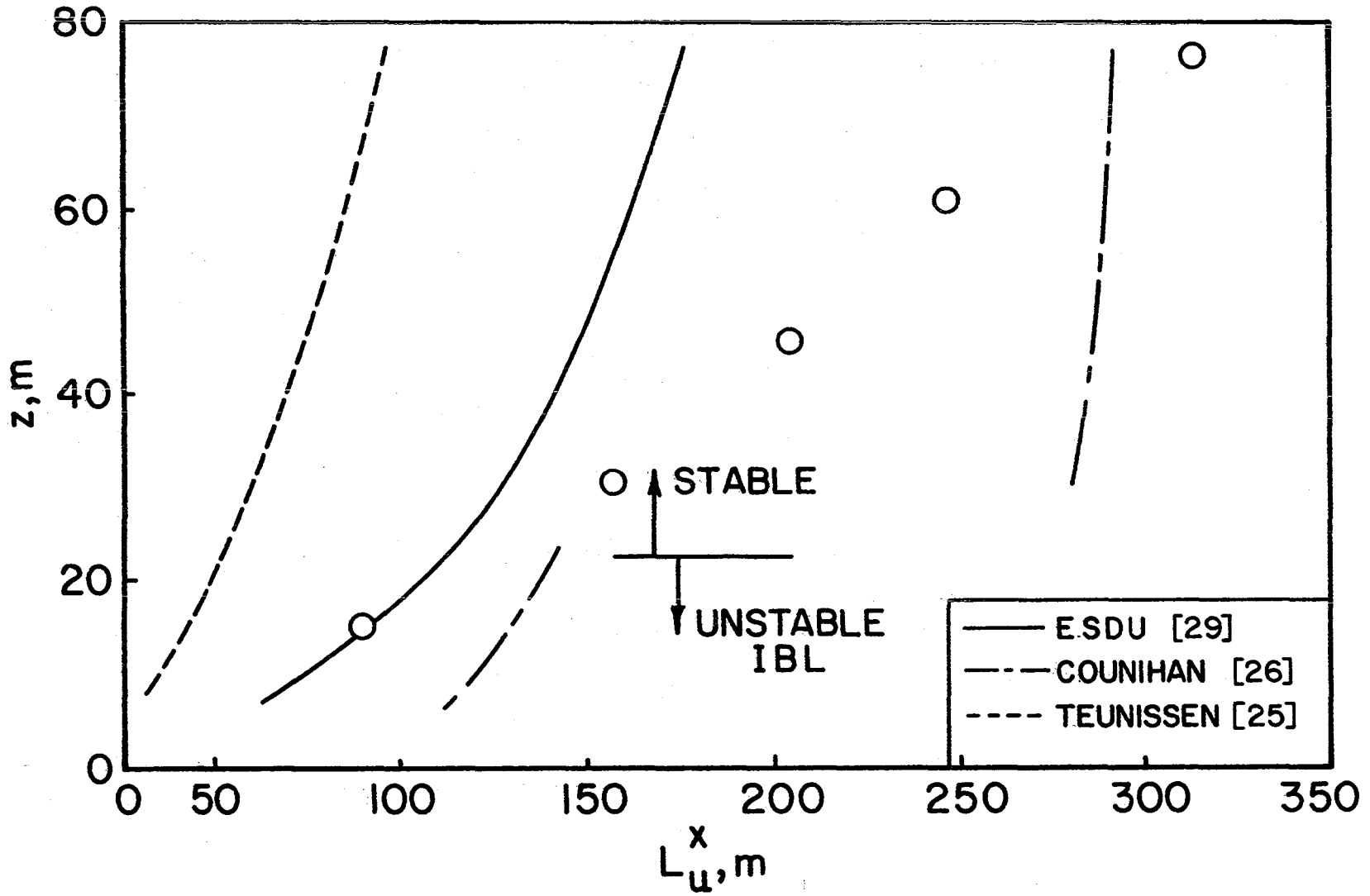

Figure 34. Variation of Average Integral Scales, L_u^x, (Cup-Vane) with Height for Wind-Direction Sector 180°-195° (South Winds) $z<20m \rightarrow z_o \cong 0.01m$ and $z>20m \rightarrow z_o = 0.001m$

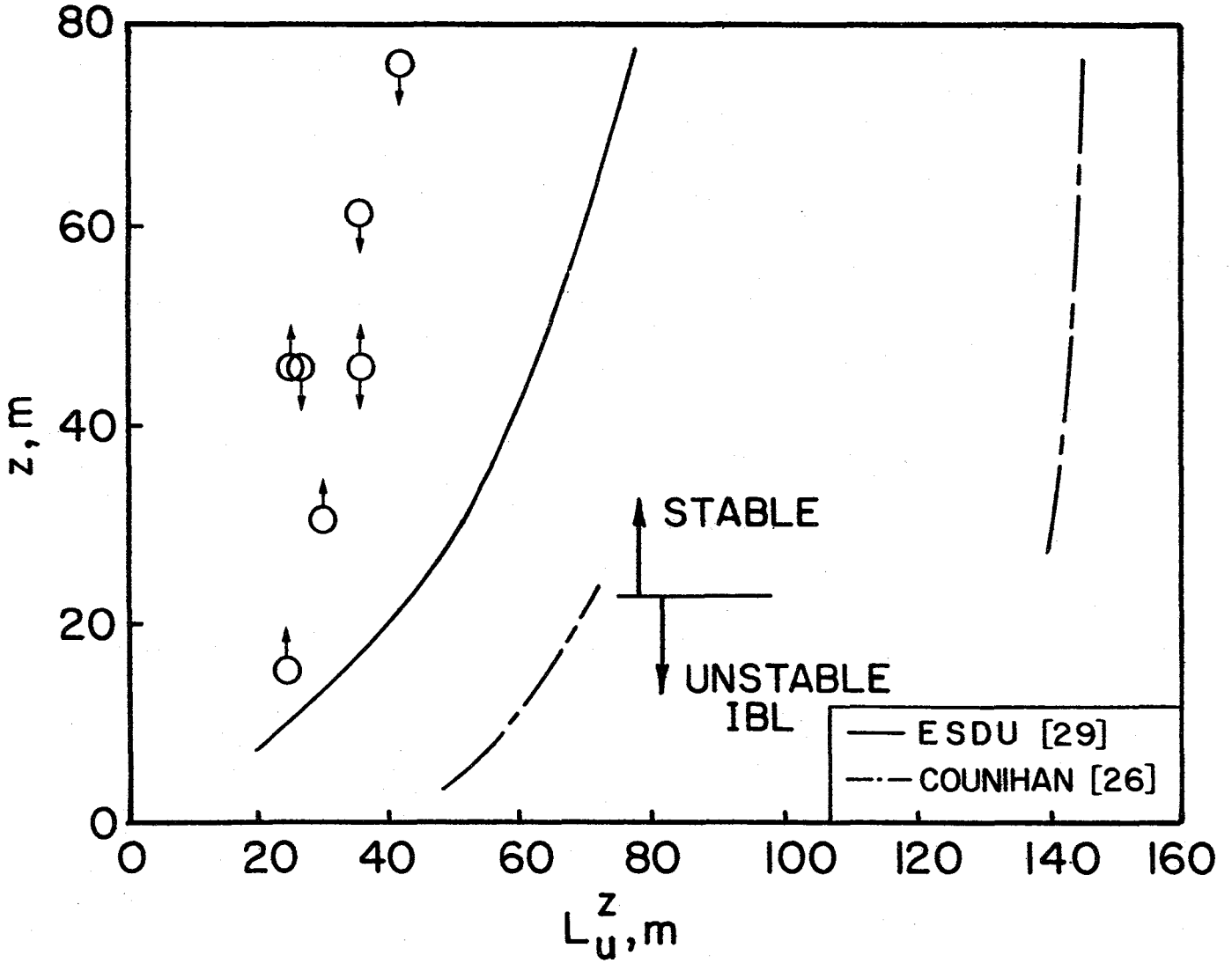

Figure 35. Variation of Average Integral Scales, L_u^z, (Cup-Vane) with Height for Wind-Direction Sector 180°-195° (South Winds). $z<20m \rightarrow z_o=0.01m$ and $z>20m \rightarrow z_o=0.001m$.

Arrows on Symbols Indicate the Direction of Integration

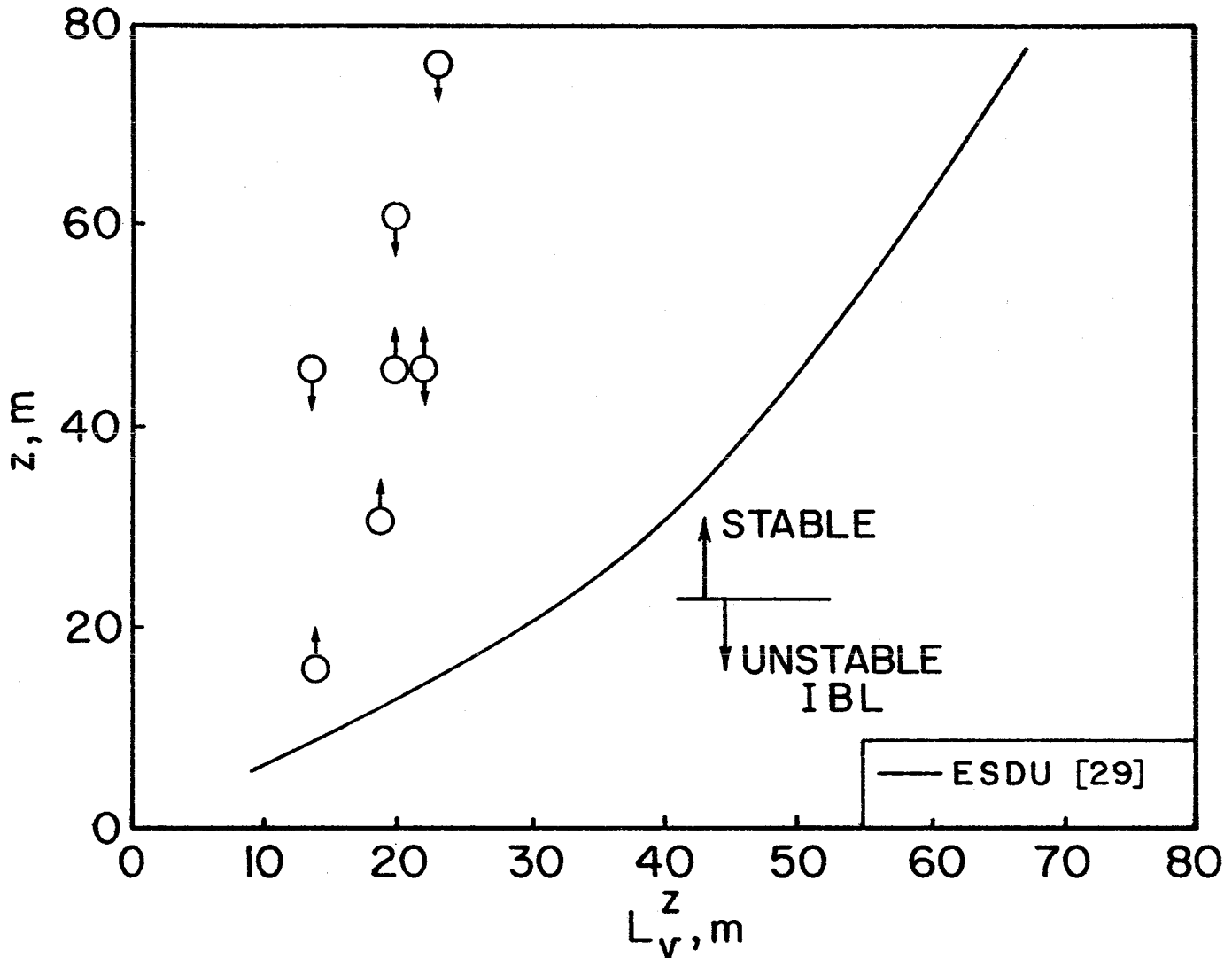

Figure 36. Variation of Average Integral Scales, L_v^z, (Cup-Vane) with Height for Wind-Direction Sector 180°-195° (South Winds) $z<20m \rightarrow z_o=0.01m$ and $z>20m \rightarrow 20m=0.001m$ Arrows on Symbols Indicate the Direction of Integration

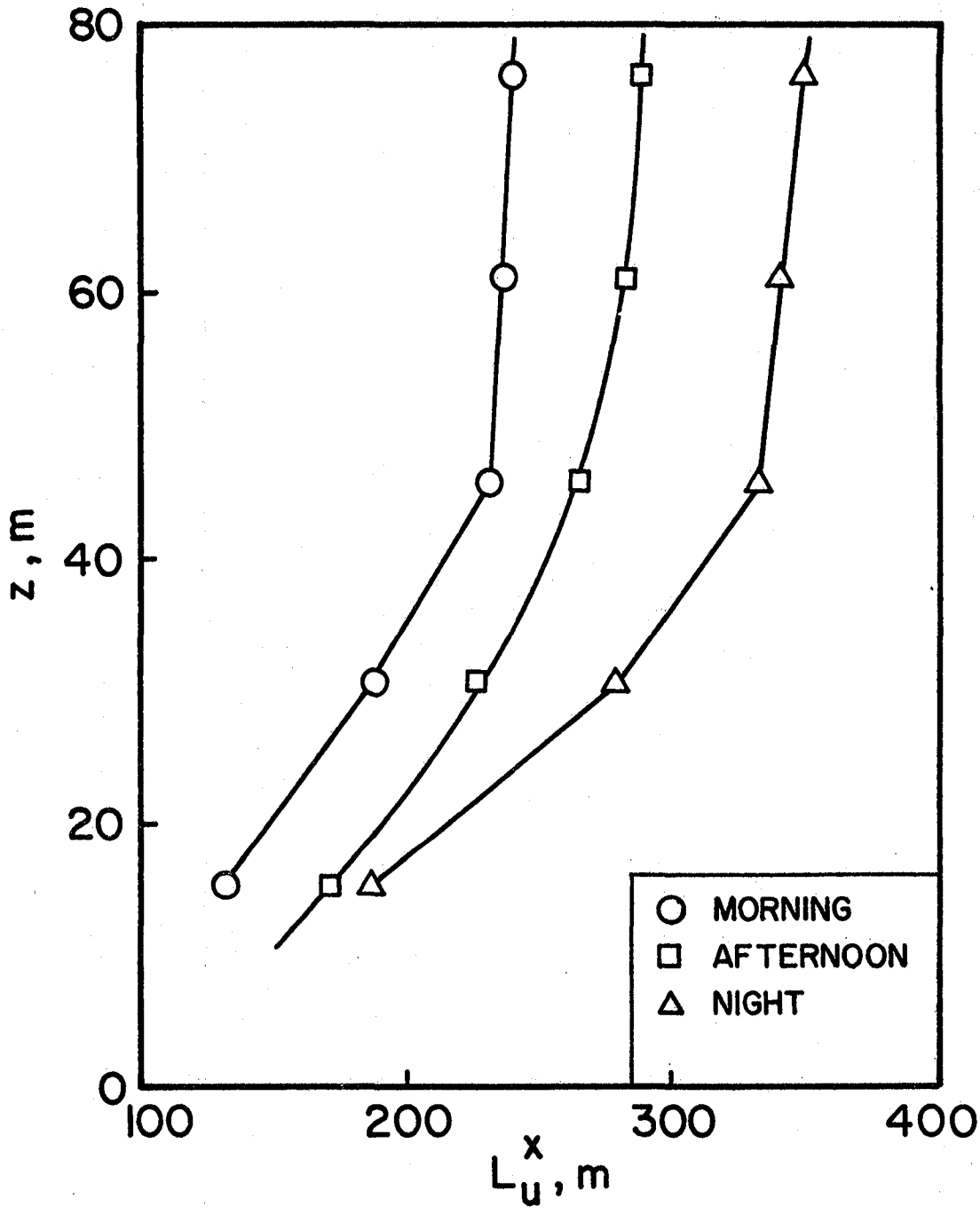

Figure 37. Profiles of Average Integral Scales, L_u^x, for Westerly Winds for Different Times of the Day.

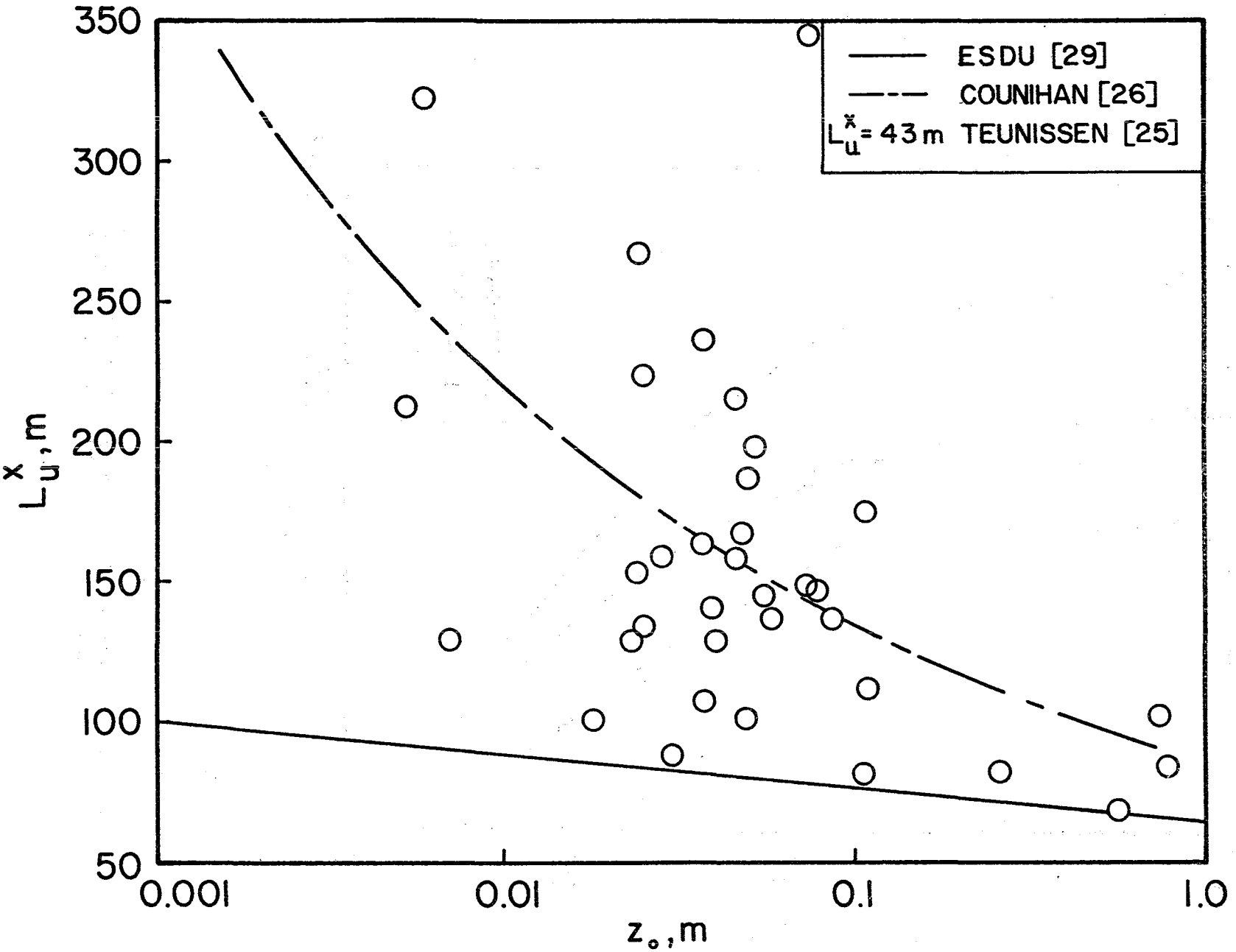

Figure 38. Variation of the Integral Scale, L_u^x, at z=15.2m (50 ft.) with Roughness Length, z_o, for all Data Records with a Westerly Wind Direction and Ri_{15}>-0.1

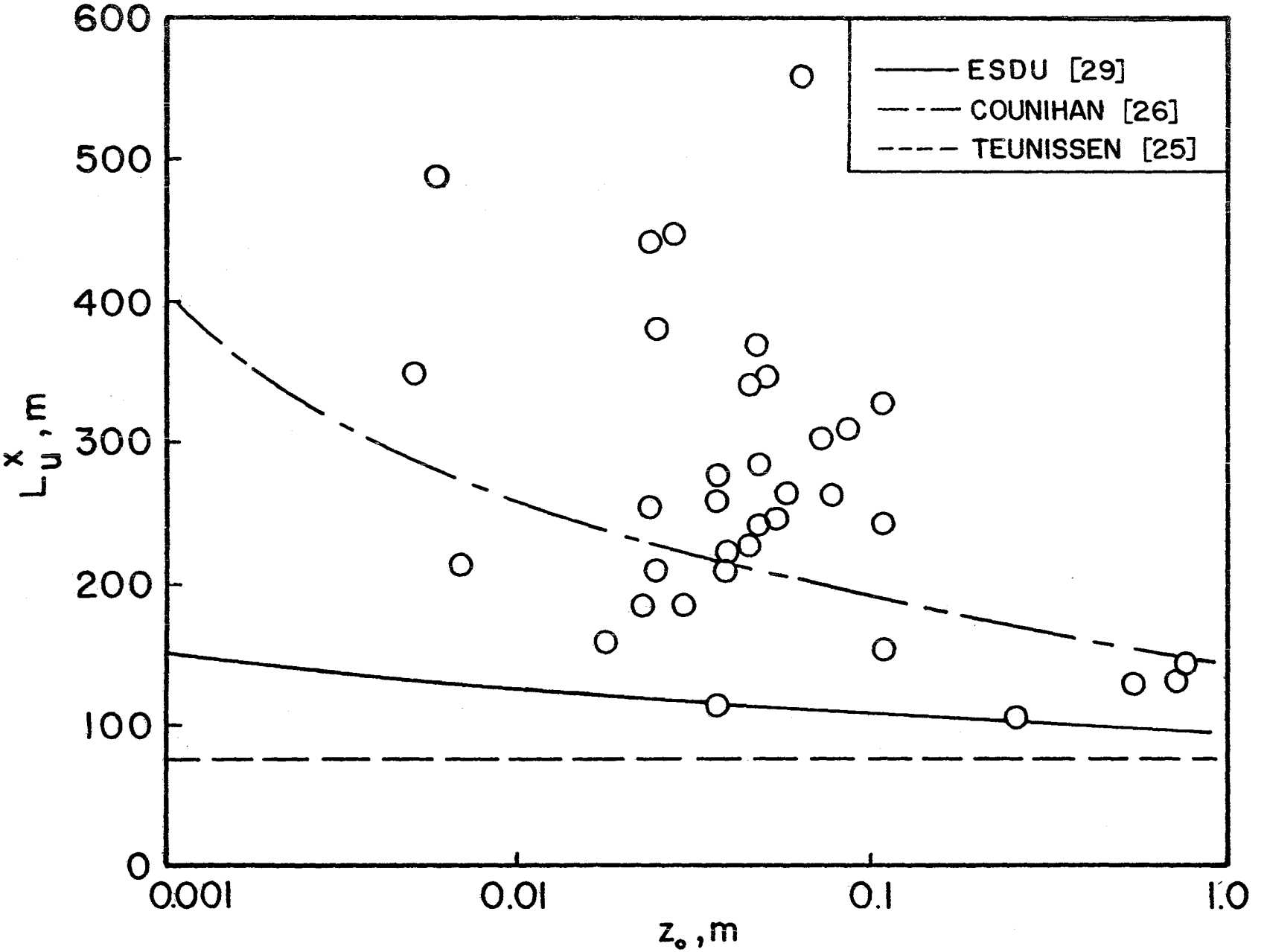

Figure 39. Variation of the Integral Scale, L_u^x, at z=45.7m (150 ft.) with Roughness Length, z_o, for all Data Records with a Westerly Wind Direction and $Ri_{15}>-0.1$

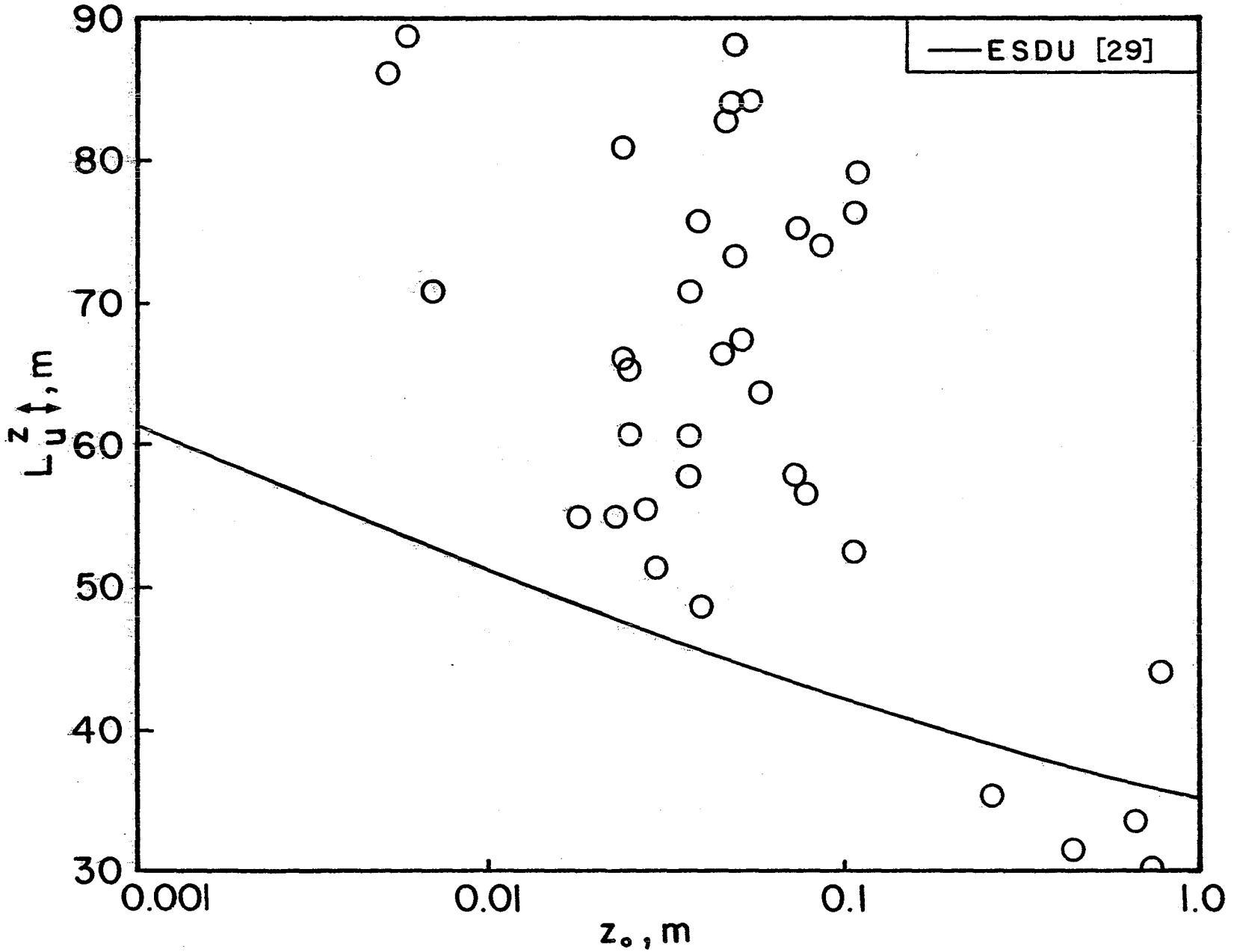

Figure 40. Variation of the Integral Scale, $L^z_{u\updownarrow}$, at z=45.7m (150 ft.) with Roughness Length, z_o, for all Data Records with Westerly Wind Direction and Ri_{15}>-0.1

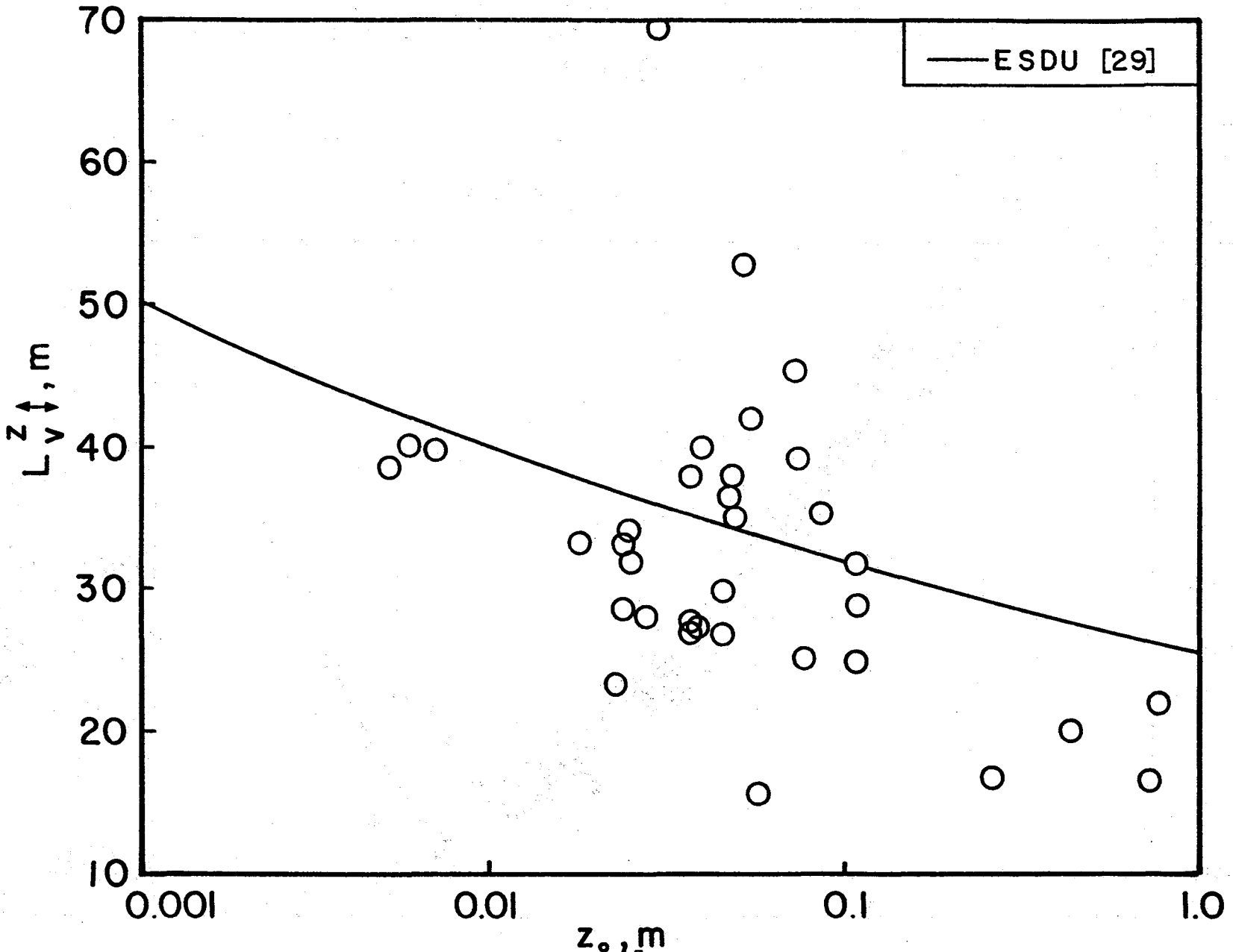

Figure 41. Variation of Integral Scale, $L_v^z\updownarrow$, at z=45.7m (150 ft.) with Roughness Length, z_o, for all Data Records with Westerly Wind Direction and $Ri_{15} > -0.1$

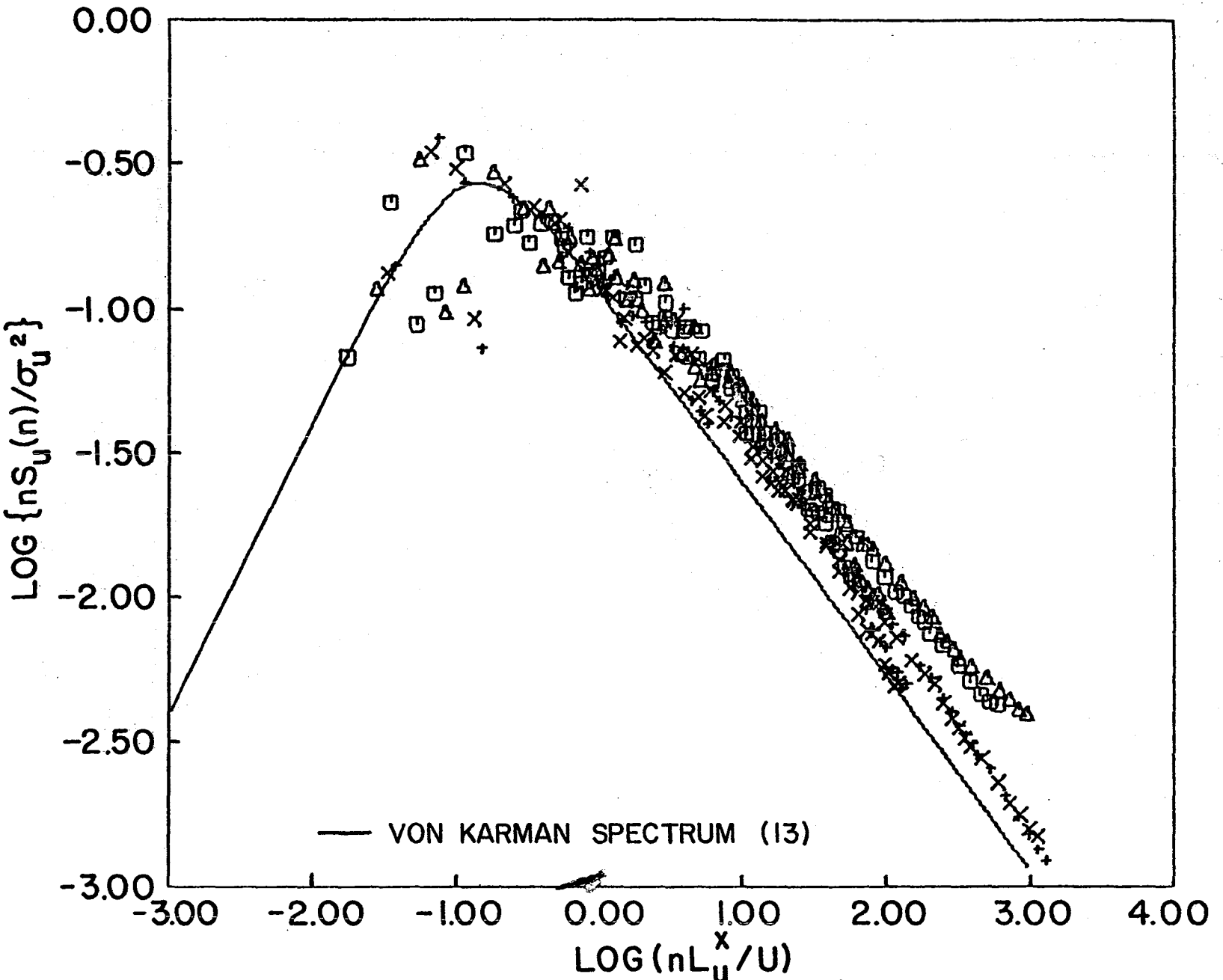

Figure 42. Logarithmic u-Spectra for Run 19, σ_u and L_u^x Obtained in the Middle Frequency Range, L_u^x Obtained Via the Direct Method

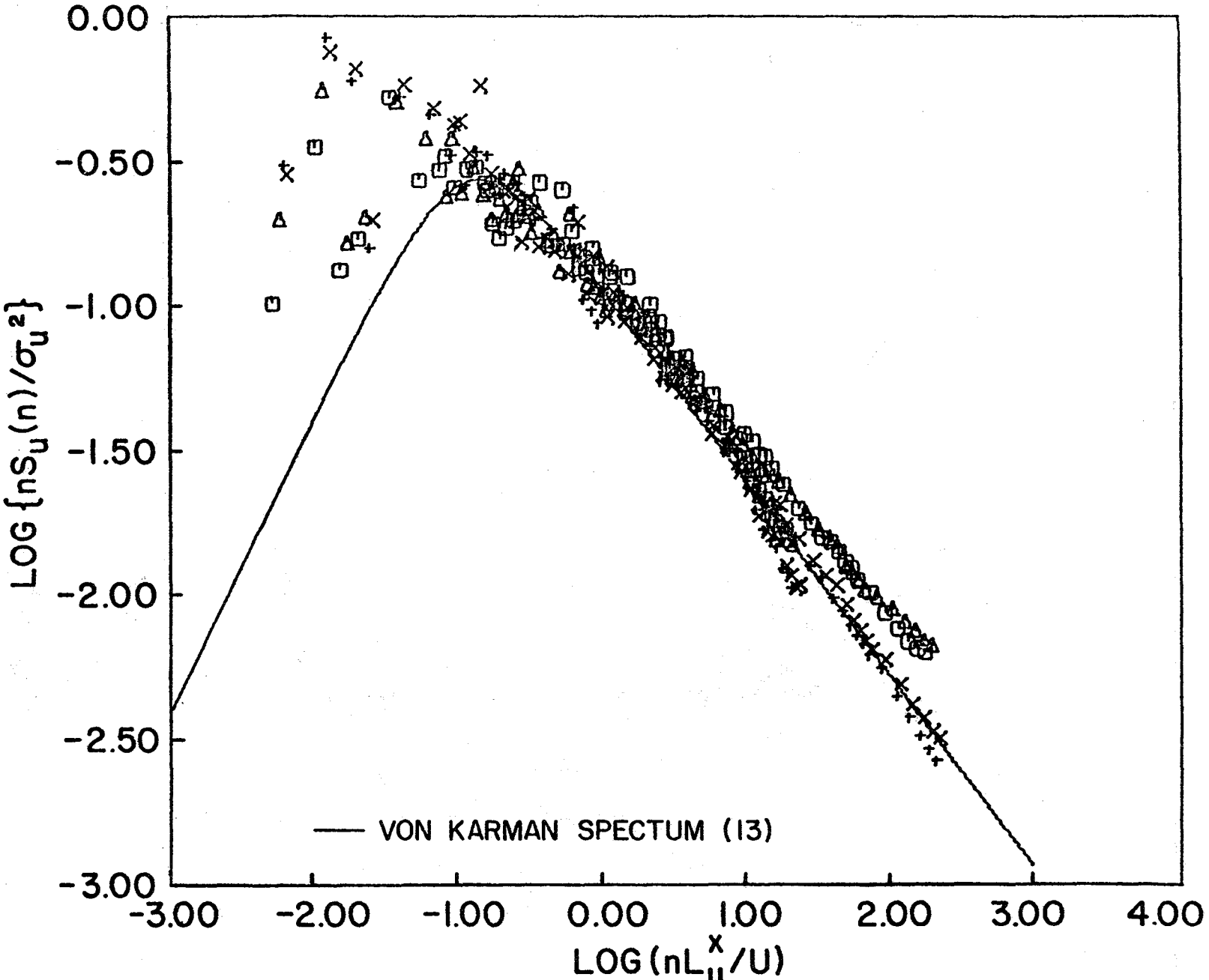

Figure 43. Logarithmic u-Spectra for Run 19, σ_u and L_u^x Obtained in the High Frequency Range, L_u^x Obtained Via the Direct Method

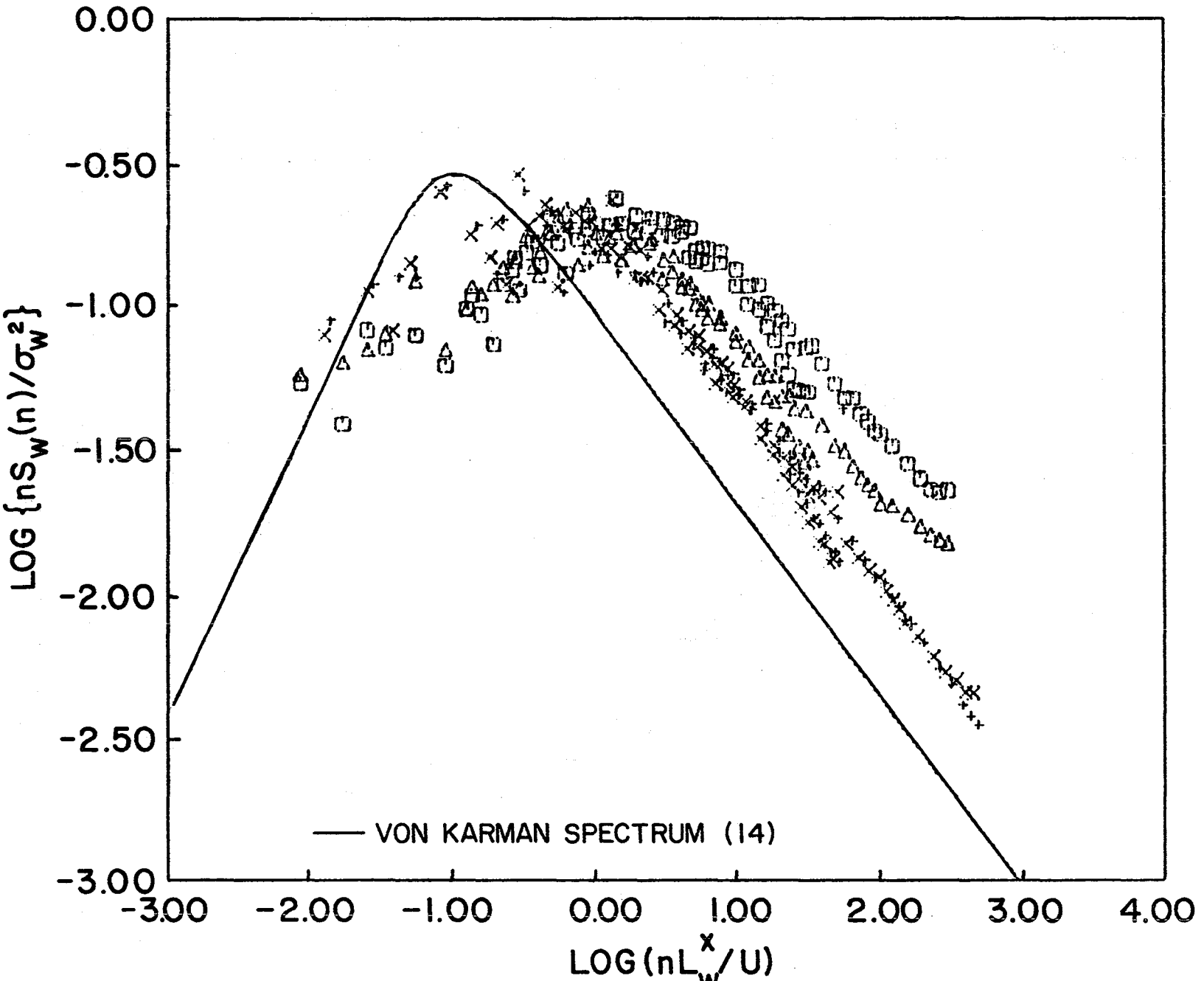

Figure 44. Logarithmic w-Spectra for Run 19, σ_w and L_w^x Obtained in the Middle-Frequency Range, L_w^x Obtained Via the Direct Method

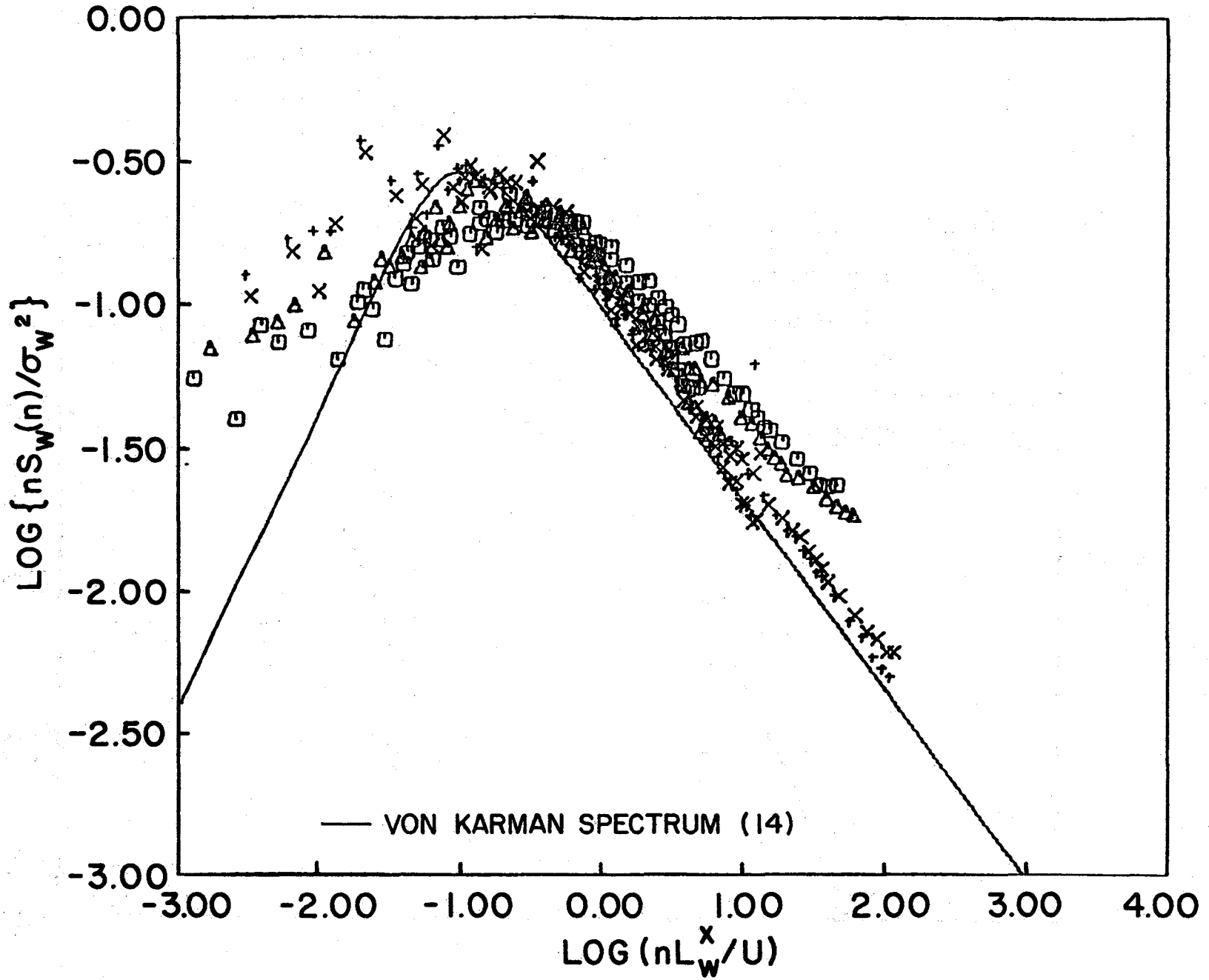

Figure 45. Logarithmic w-Spectra for Run 19, σ_w and L_w^x Obtained in the High-Frequency Range, L_w^x Obtained Via the Direct Method

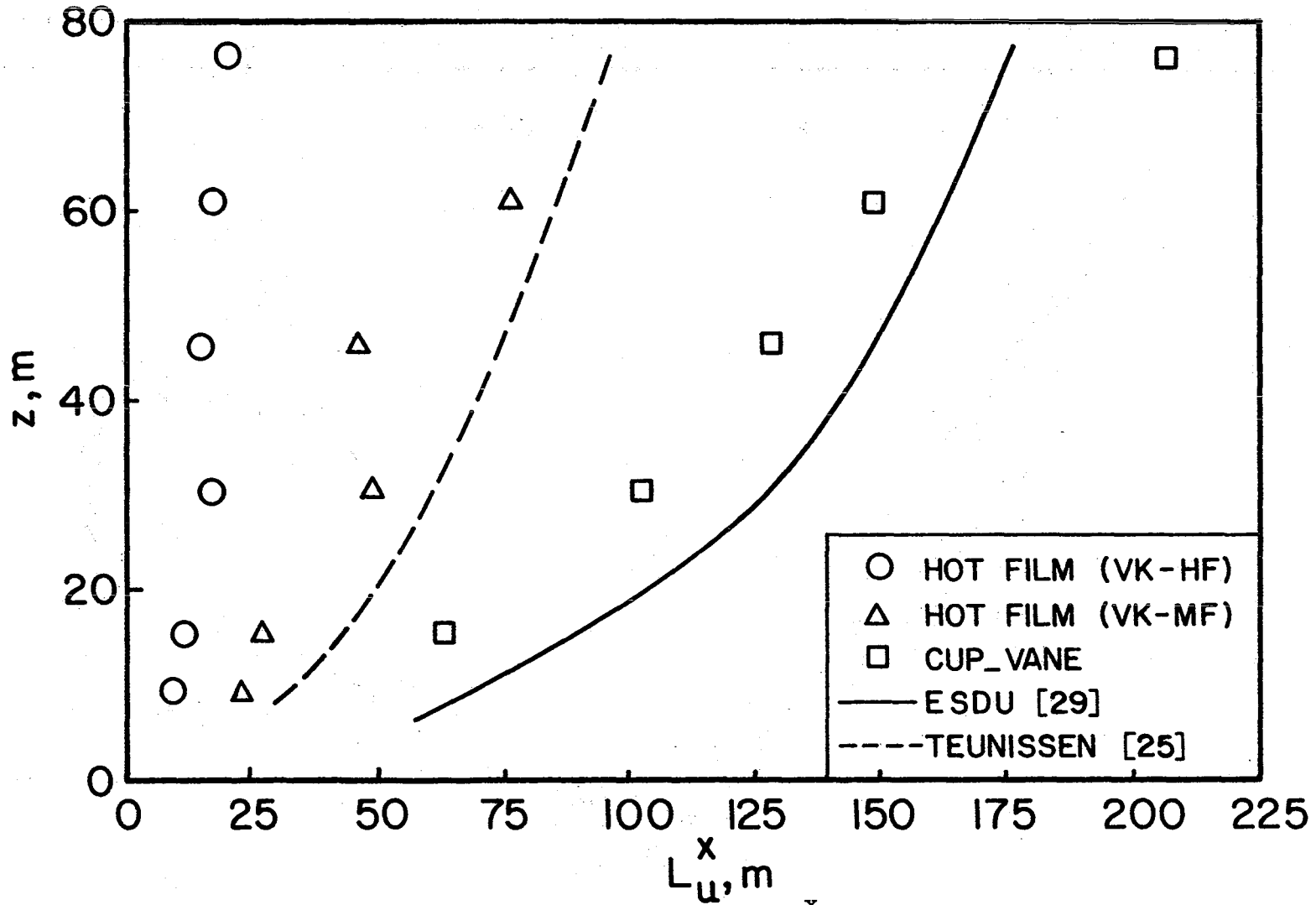

Figure 46. Variation of Average Integral Scales, L_u^x, Obtained with the Hot-Film System (Von Karman Method, High and Middle Frequency Range) and with the Cup-Vane System (Data of the Two Systems Taken Simultaneously), with Height for Southerly Winds

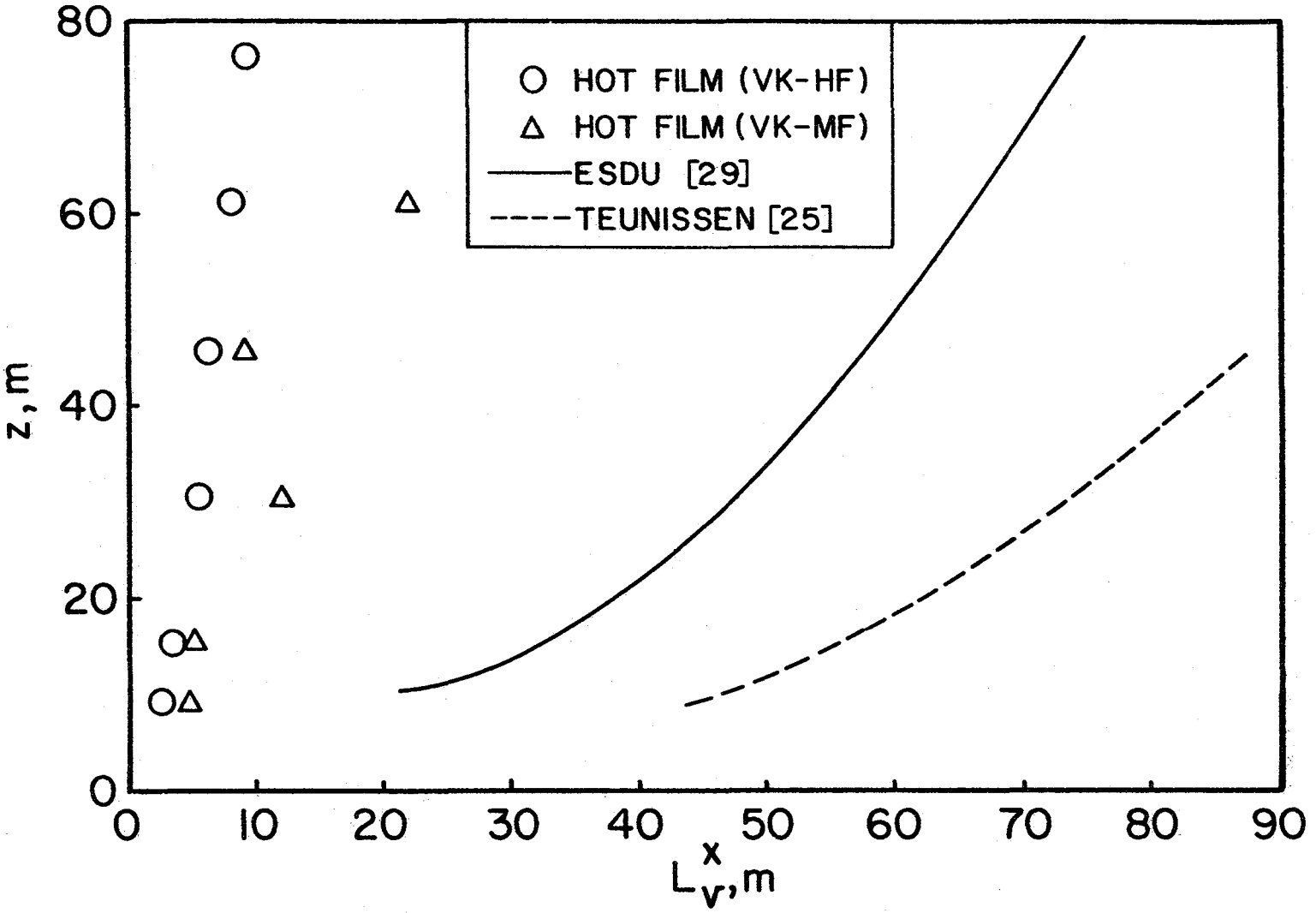

Figure 47. Variation of Average Integral Scales, L_v^x, obtained with the Hot-Film System (Von Karman Method, High and Middle Frequency Range) with Height for Southerly Winds

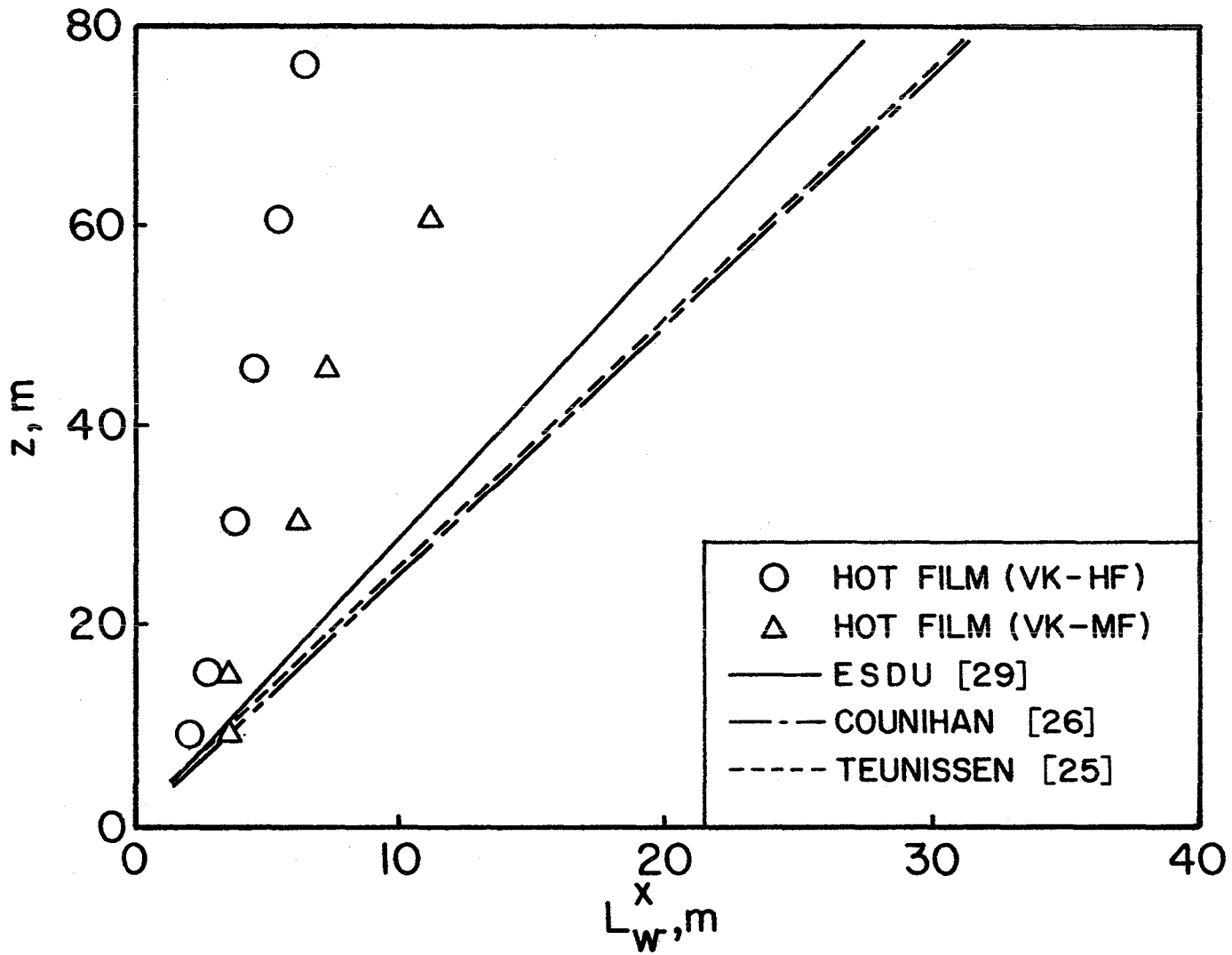

Figure 48. Variation of Average Integral Scales, L_w^x, Obtained with the Hot-Film System (Von Karman Method, High and Middle Frequency Range), with Height for Southerly Winds

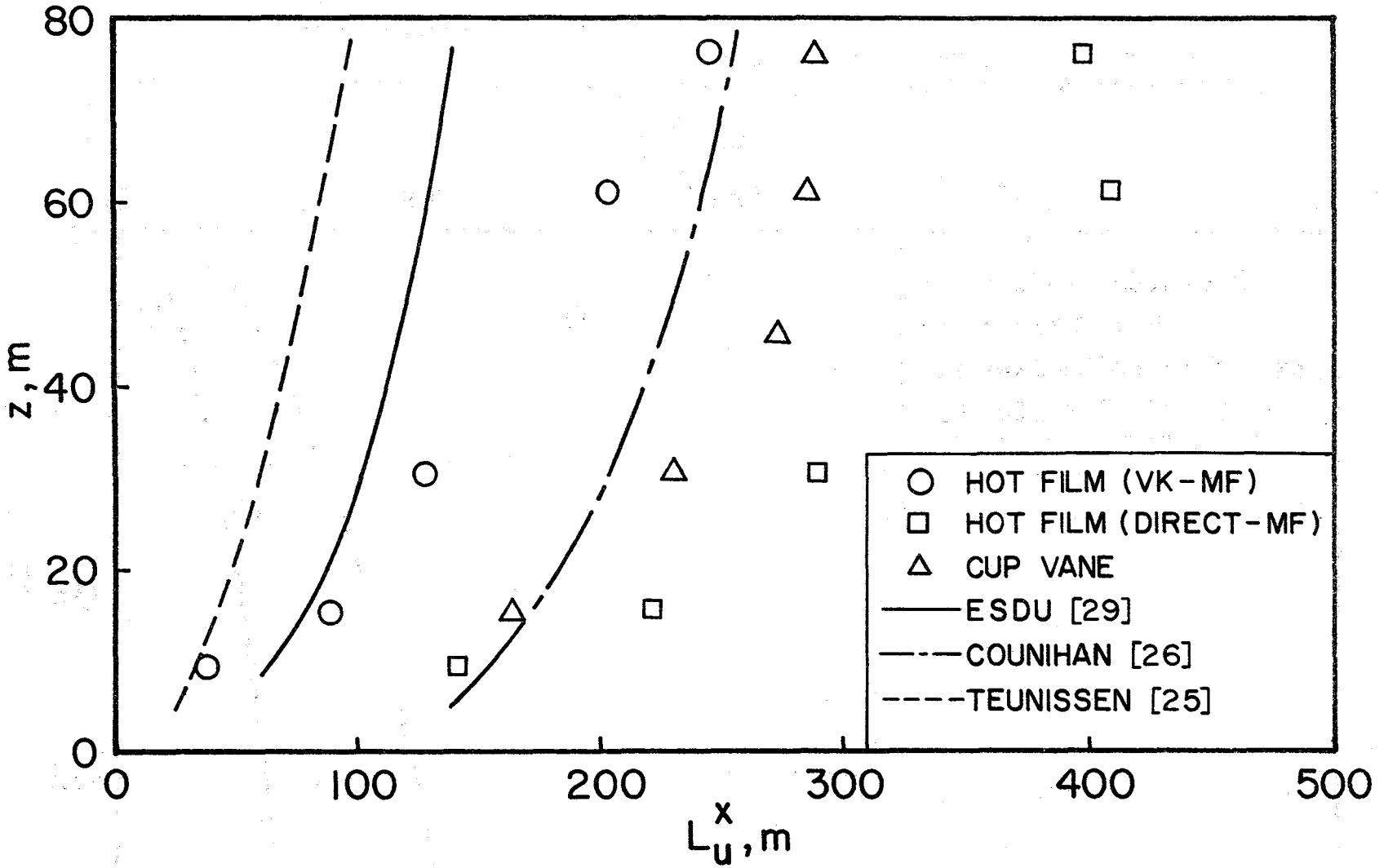

Figure 49. Variation of Average Integral Scales, L_u^x, Obtained with the Hot-Film System (Von Karman and Direct Methods, Middle-Frequency Range) and Cup-Vane System with Height for Northwesterly Winds

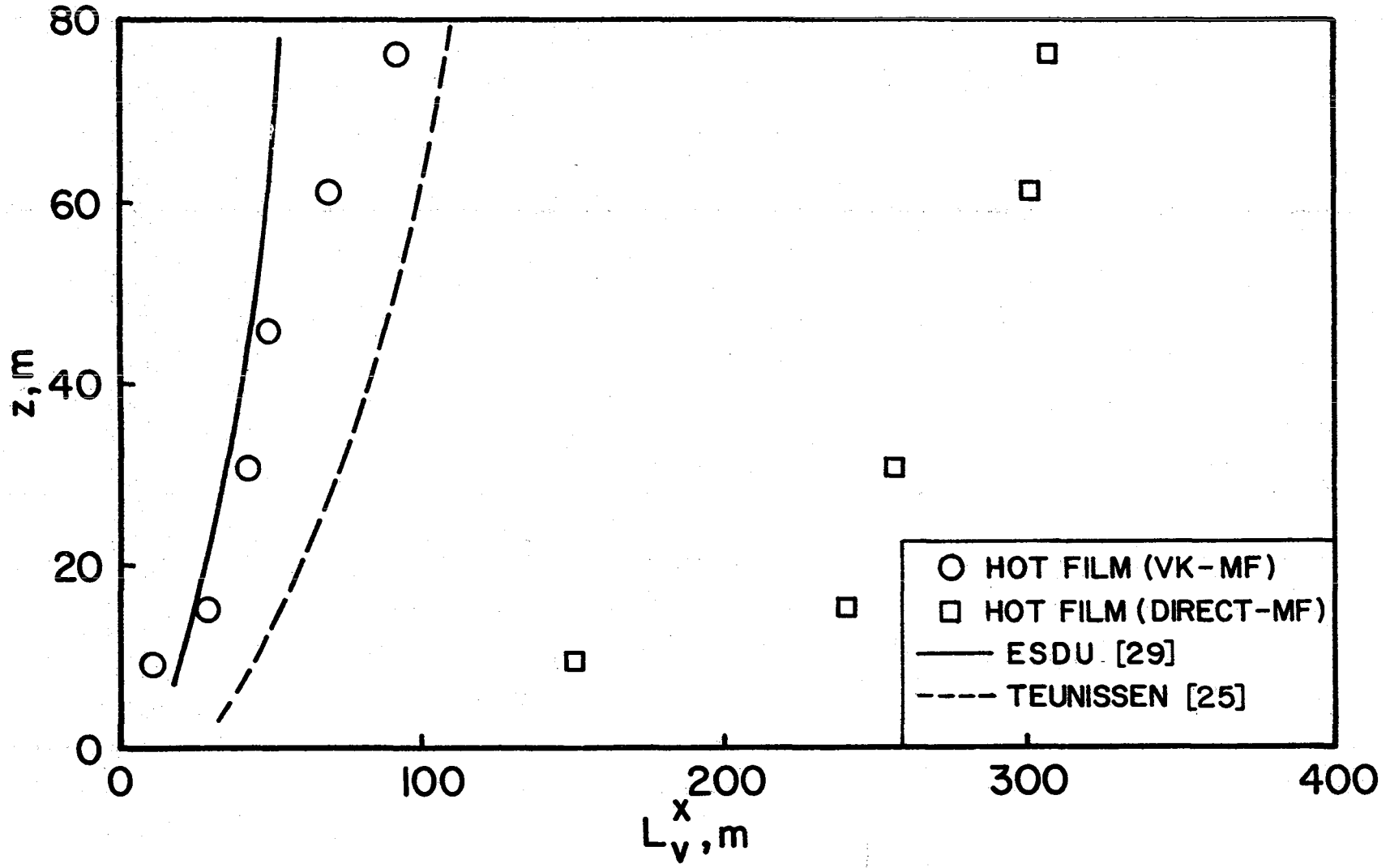

Figure 50. Variation of Average Integral Scales, L_v^x, Obtained with the Hot-Film System (Von Karman and Direct Methods, Middle Frequency Range) with Height for Northwesterly Winds

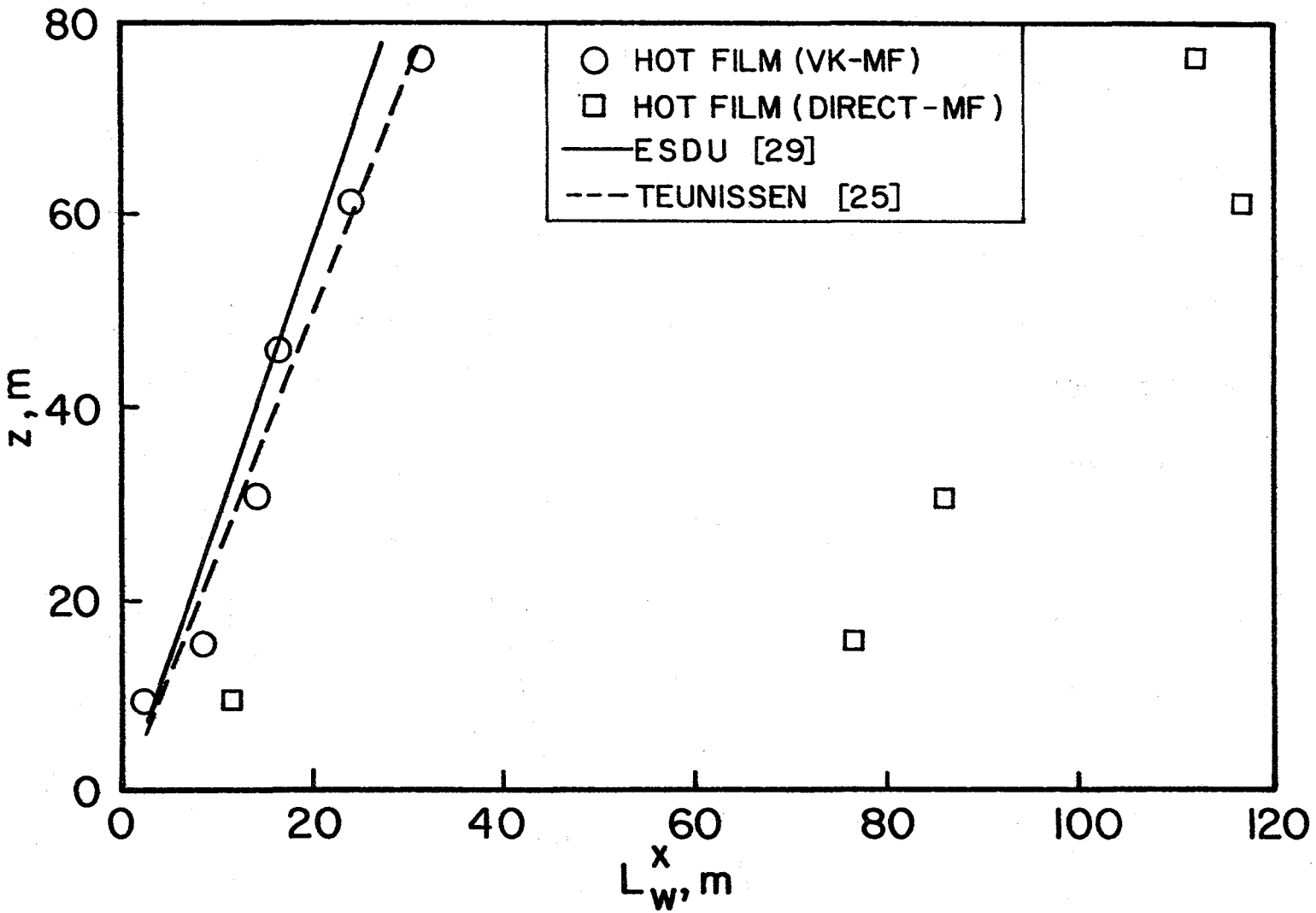

Figure 51. Variation of Average Integral Scales, L_w^x, obtained with the Hot-Film System (Von Karman and Direct Methods, Middle Frequency Range) with Height for Northwesterly Winds

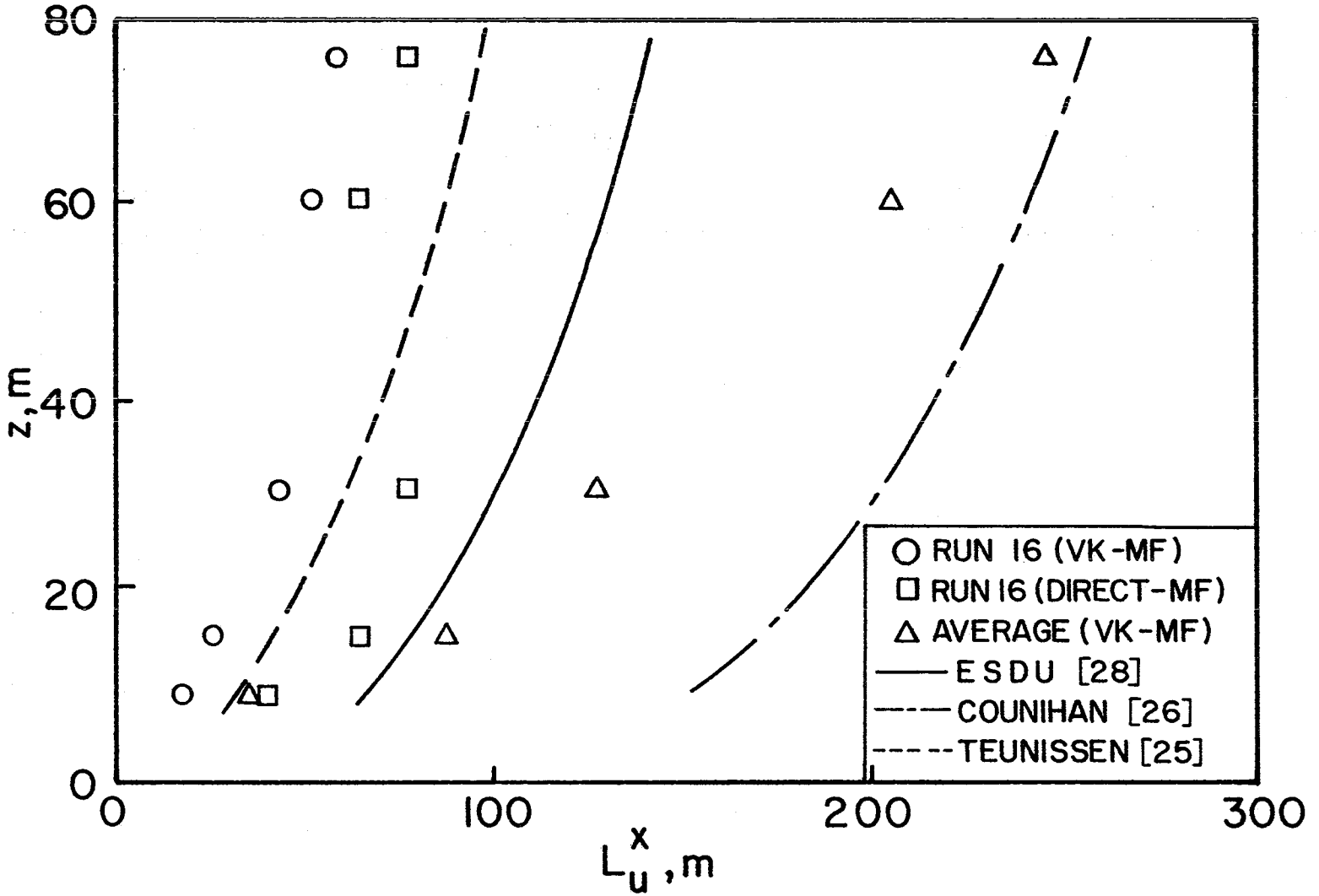

Figure 52. Comparison of Integral Scales, L_u^x, of Record #16. (Evening Run) (Von Karman and Direct Methods, Middle Frequency Range) Against Average of Daytime Hot-Film Runs (Von Karman, Middle Frequency Range) for Northwesterly Winds

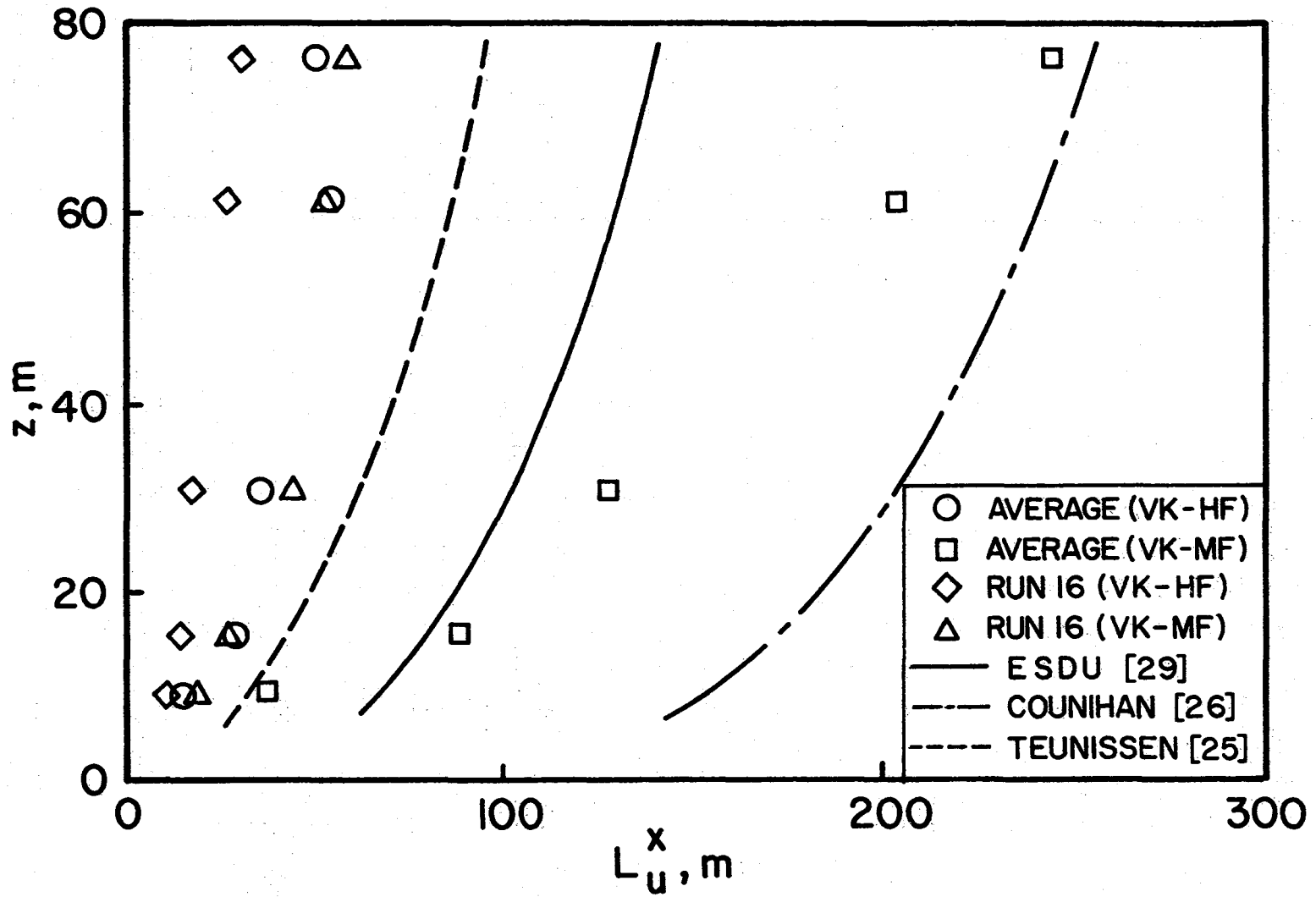

Figure 53. Comparison of Integral Scales, L_u^x, Obtained from the Hot-Film System and Analyzed in the Middle-and High-Frequency Range Using the Von Karman Method for Northwesterly Winds

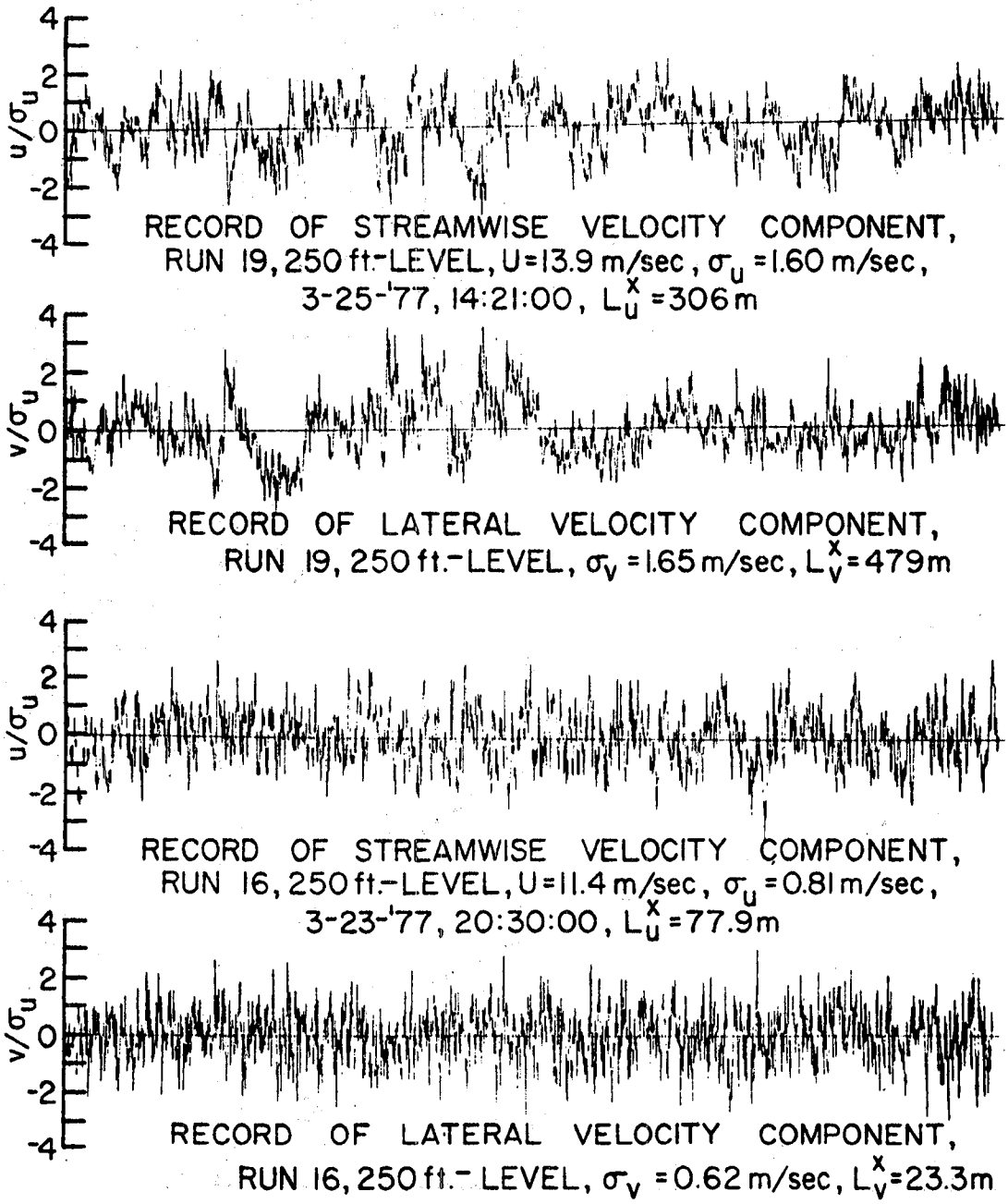

Figure 54. Time Records of Velocity Components. Elapsed Time 55 Minutes.

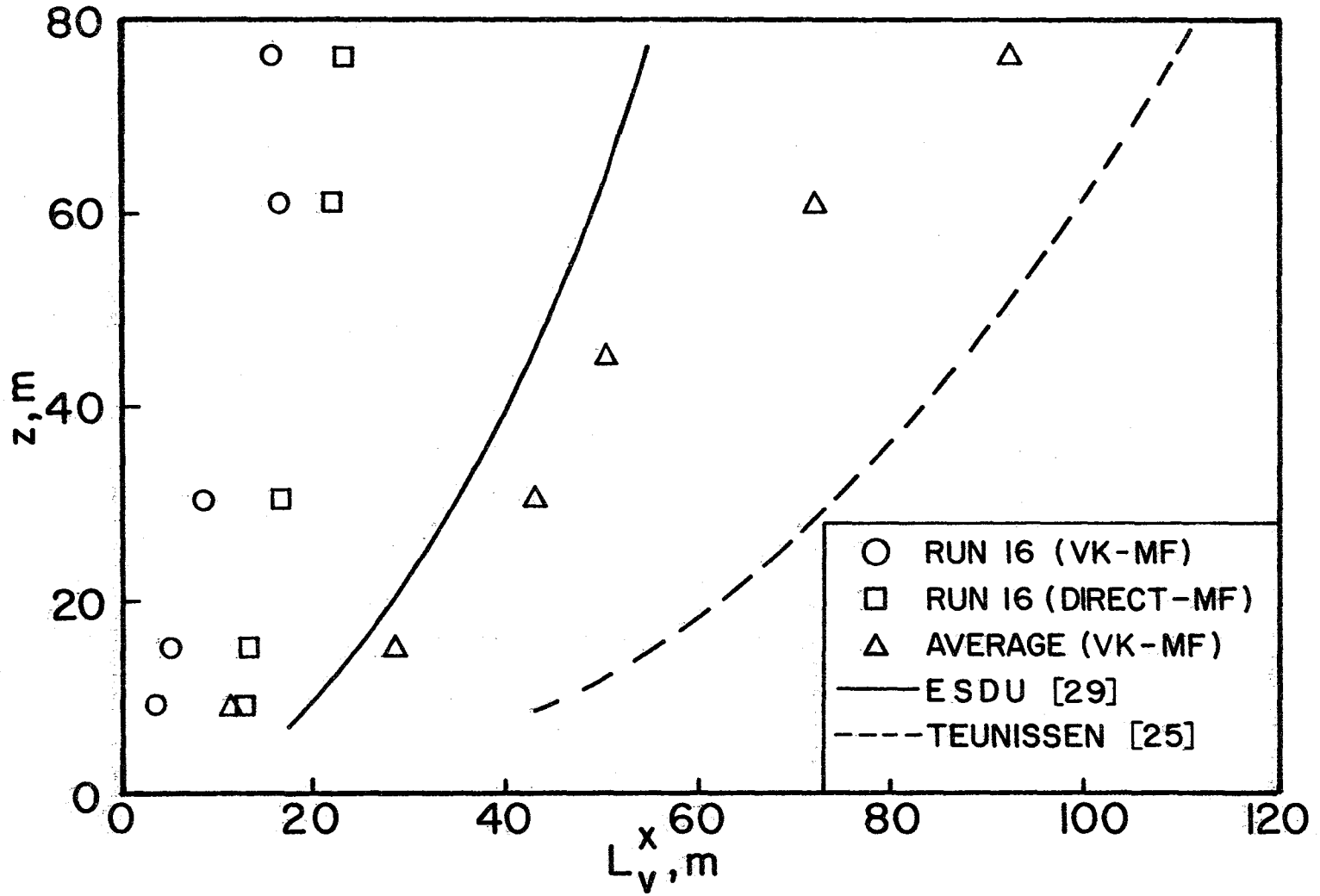

Figure 55. Comparison of Integral Scales, L_v^x, of Record #16 (Evening Run) (Von Karman and Direct Methods, Middle Frequency Range) Against Average of Day Time Hot-Film Runs (Von Karman, Middle Frequency Range) for Northwesterly Winds

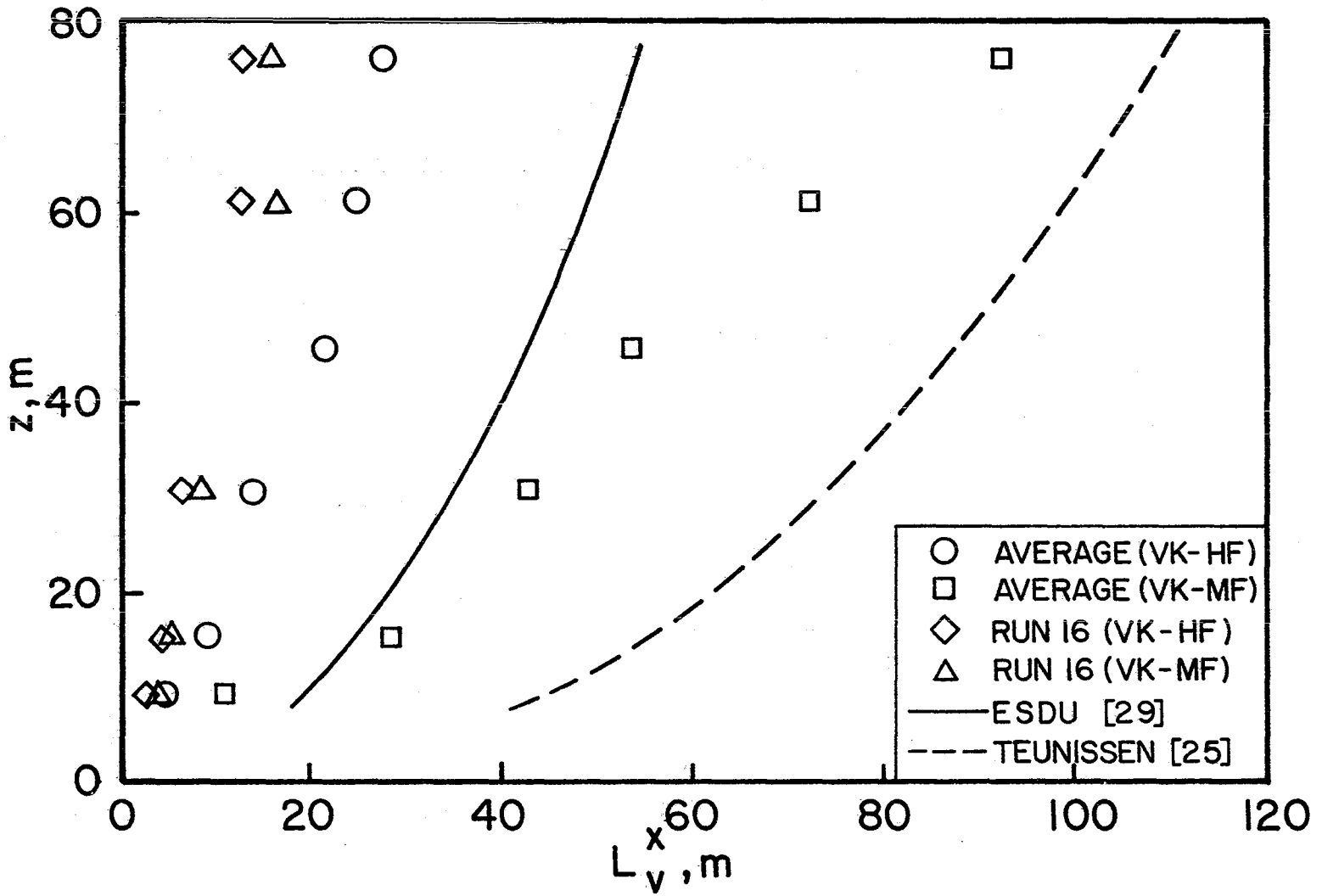

Figure 56. Comparison of Integral Scales, L_v^x, Obtained from the Hot-Film System and Analyzed in the Middle-and High-Frequency Range Using the Von Karman Method, for Northwesterly Winds

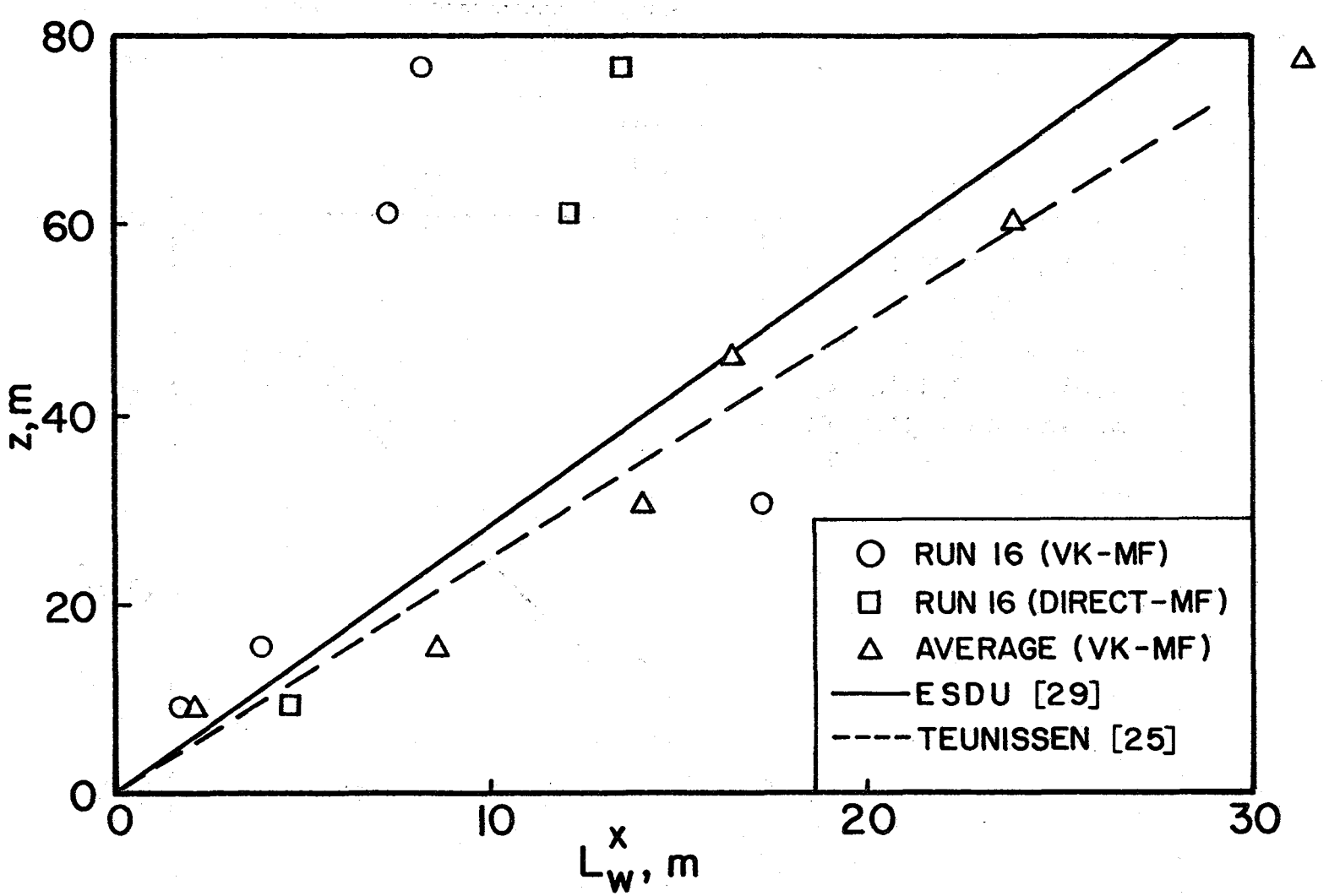

Figure 57. Comparison of Integral Scales, L_w^x, of Record #16 (Evening Run) (Von Karman and Direct Methods, Middle Frequency Range) Against Average of Day Time Hot-Film Runs (Von Karman, Middle Frequency Range)

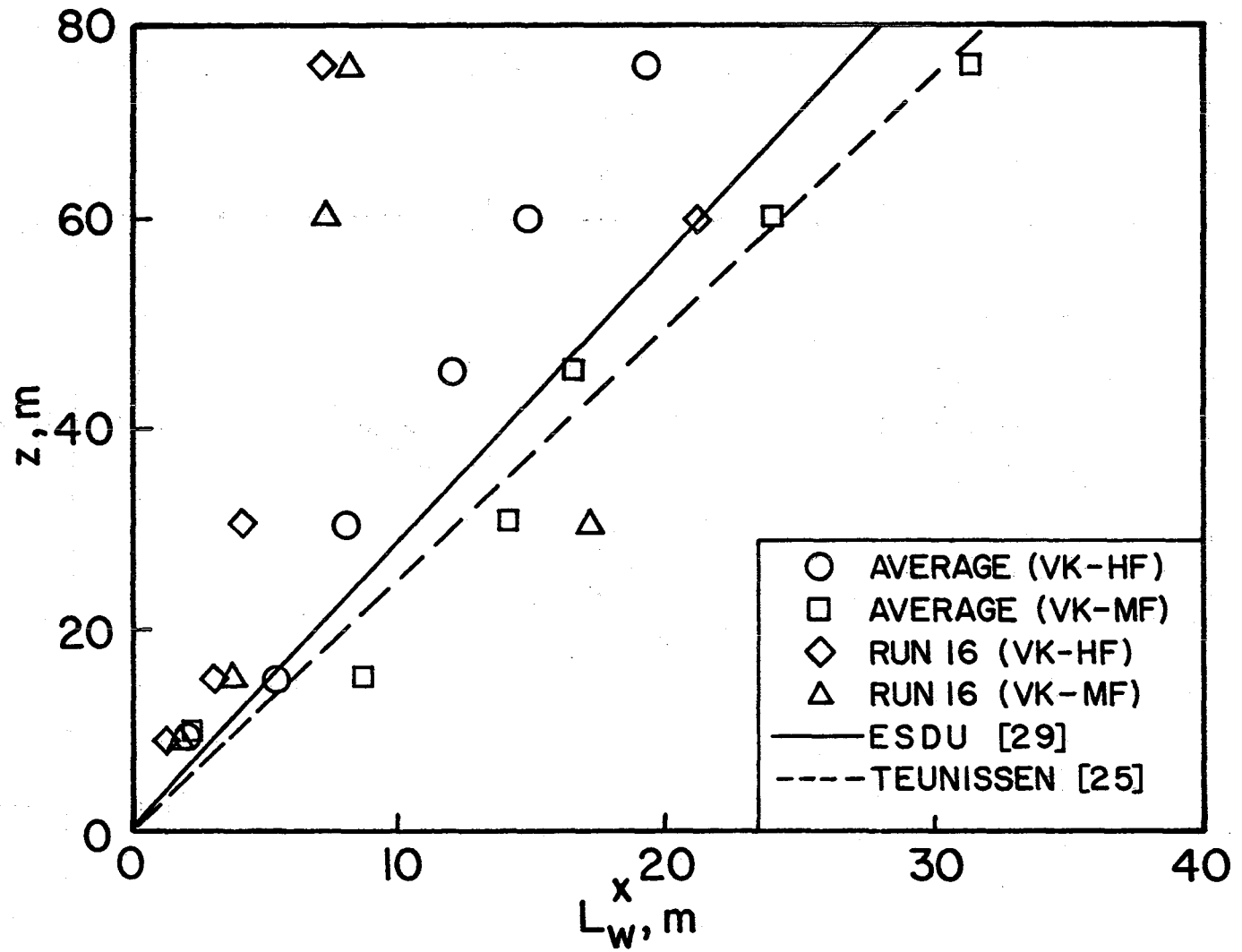

Figure 58. Comparison of Integral Scales, L_w^x, Obtained From the Hot-Film System and Analyzed in the Middle-and High-Frequency Range Using the Von Karman Method for Northwesterly Winds

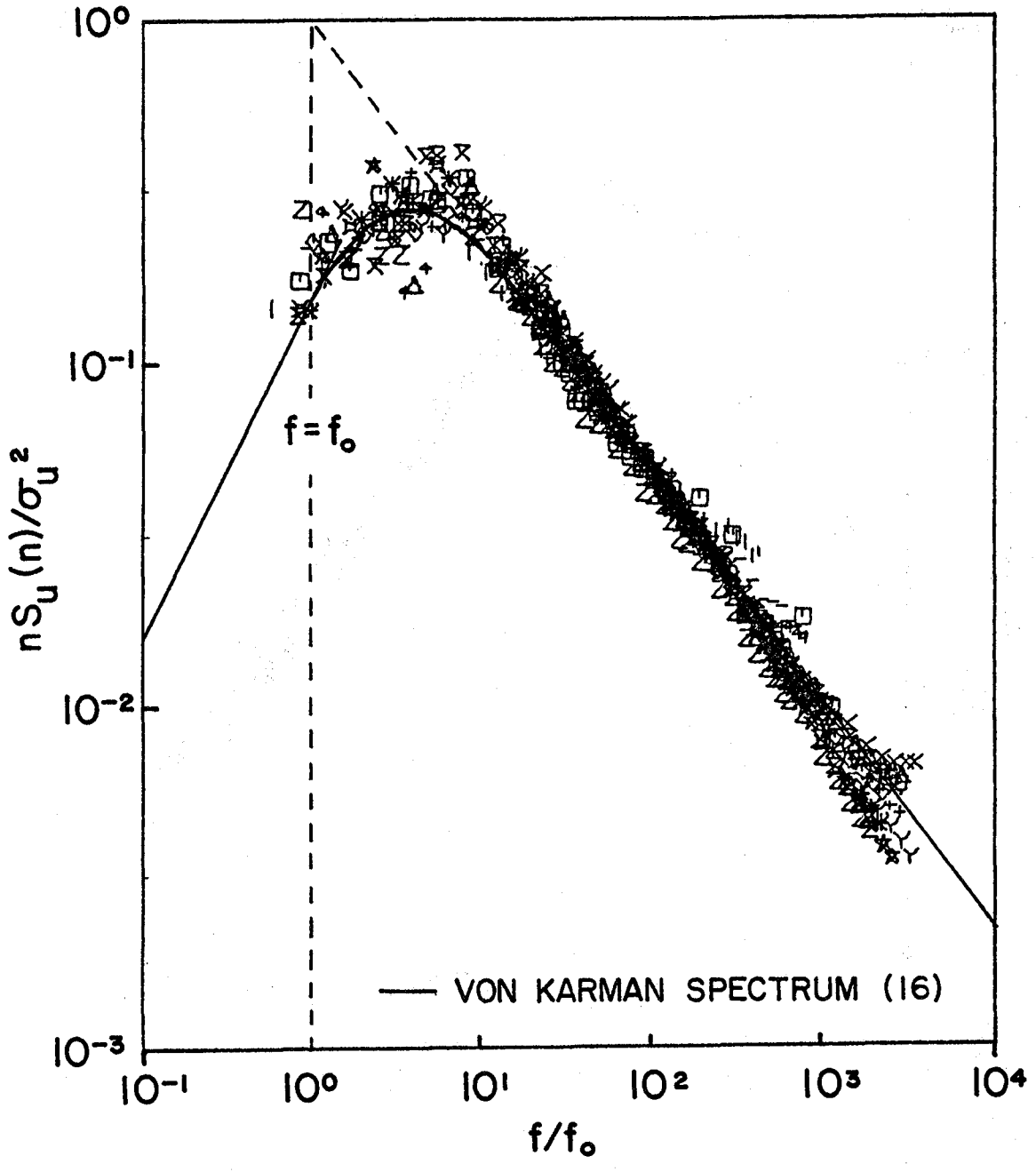

Figure 59a. Logarithmic u-Spectra Versus Modified Reduced Frequency, f/f_o, Analyzed in the High-Frequency Range, South Winds, Unstable Thermal Stratification. $-1.0<z/L<0$

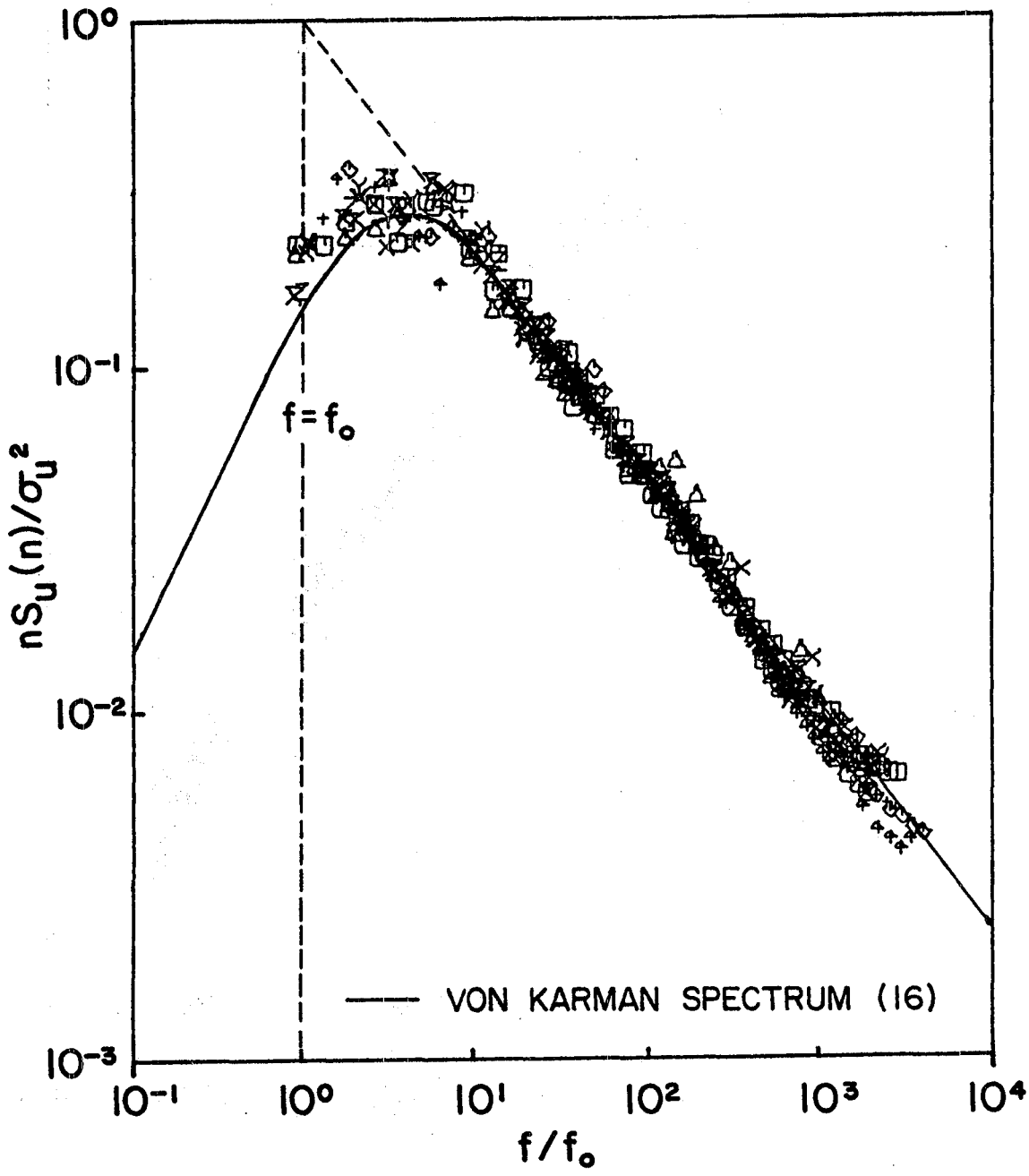

Figure 59b. Logarithmic u-Spectra Versus Modified Reduced Frequency, f/f_o, Analyzed in the High-Frequency Range, South Winds, Stable Thermal Stratification. $0<z/L<+1.0$

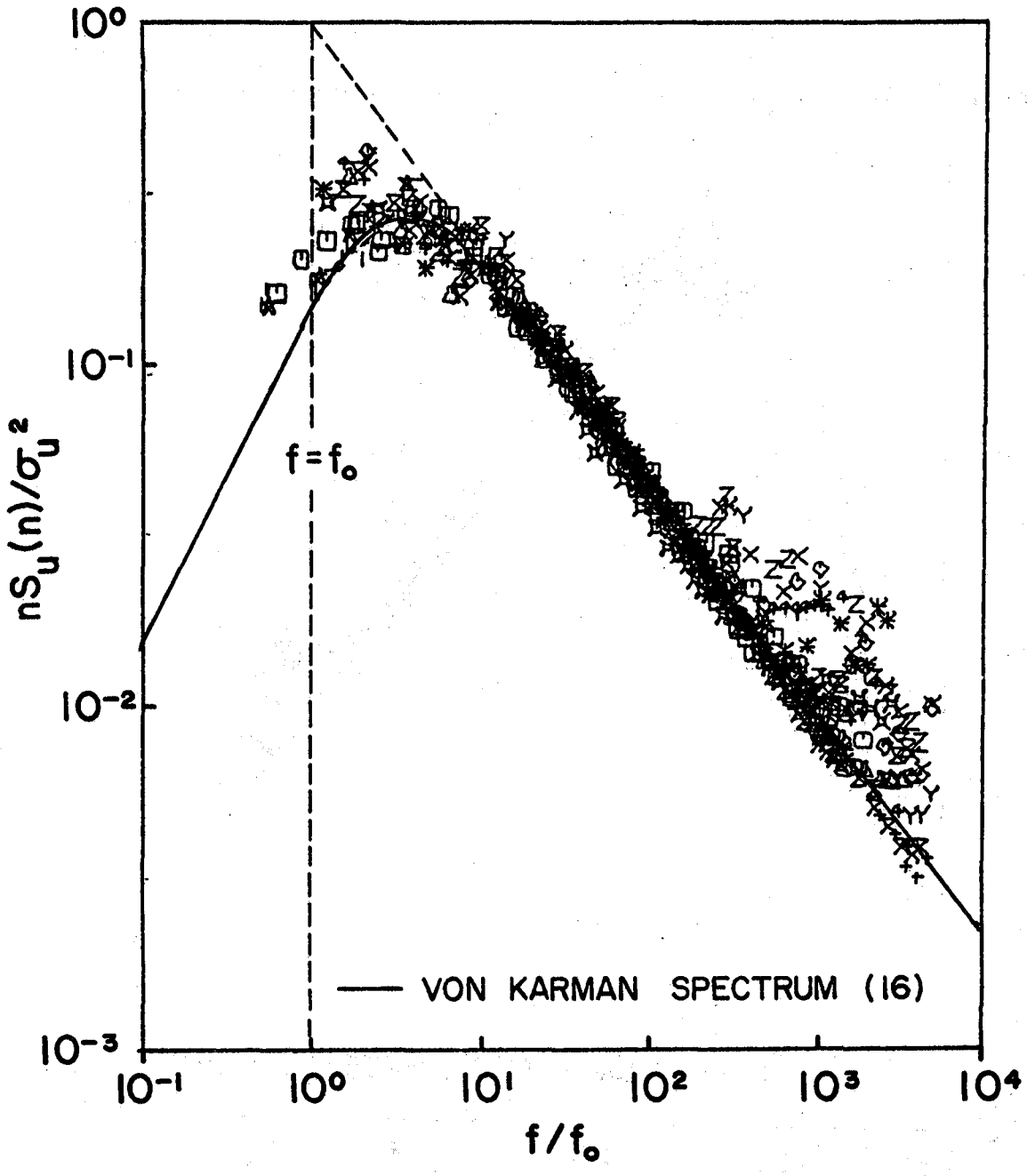

Figure 59c. Logarithmic u-Spectra Versus Modified Reduced Frequency, f/f_o, Analyzed in the High-Frequency Range, South Winds, Extremely Stable Thermal Stratification. $z/L>+1.0$

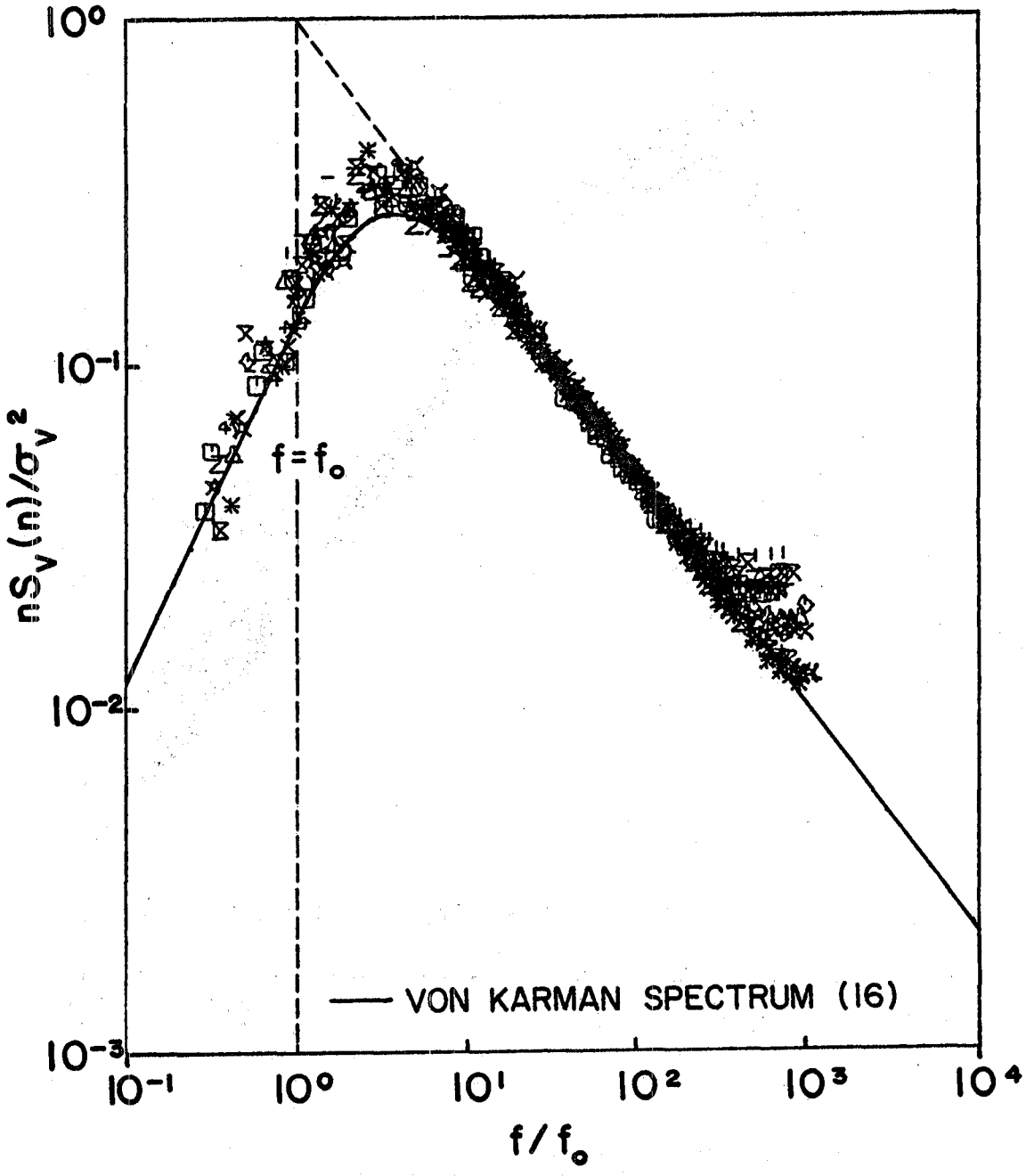

Figure 60a. Logarithmic v-Spectra Versus Modified Reduced Frequency, f/f_o, Analyzed in the High-Frequency Range, South Winds, Unstable Thermal Stratification. $-1.0<z/L<0$

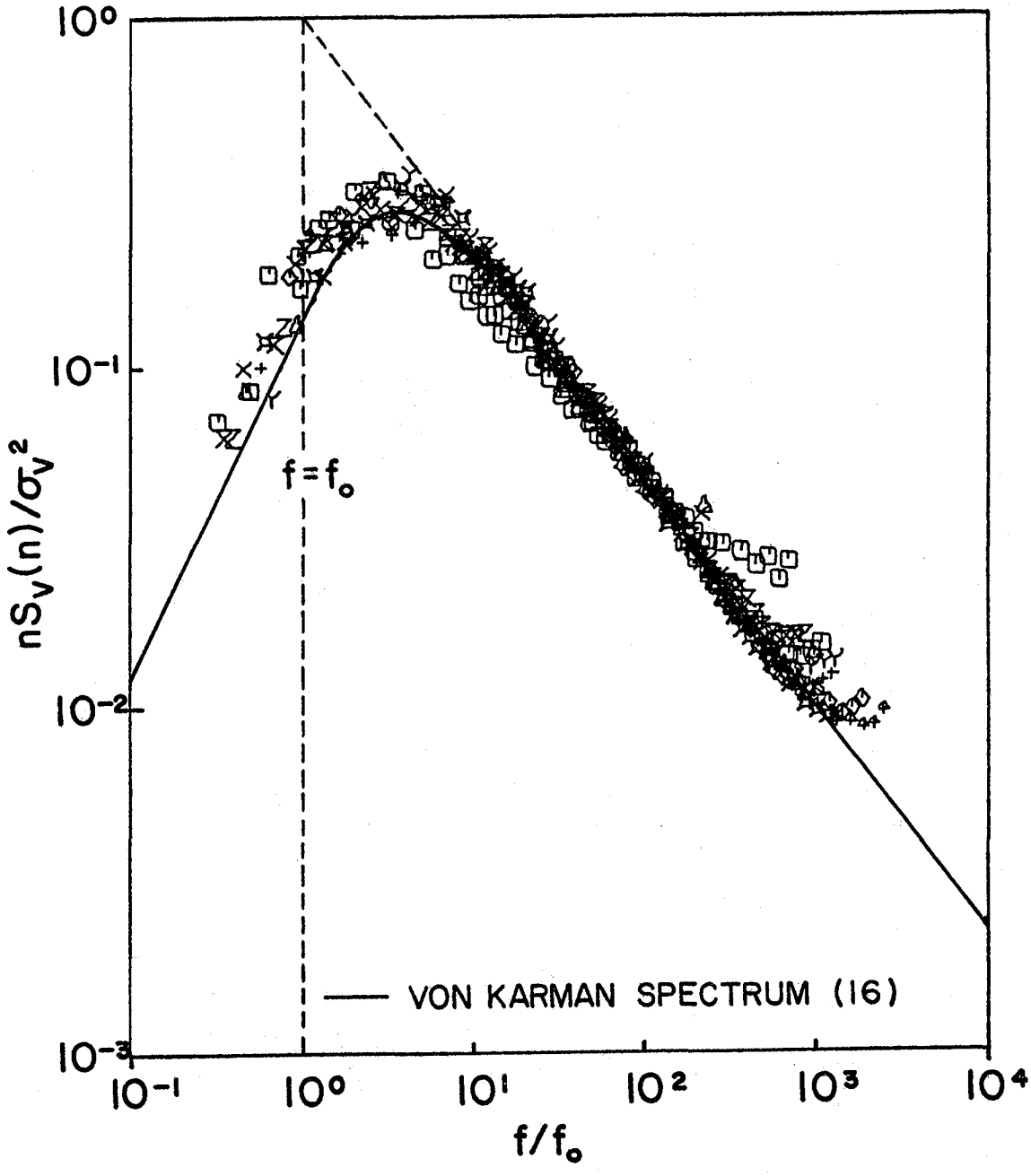

Figure 60b. Logarithmic v-Spectra Versus Modified Reduced Frequency, f/f_o, Analyzed in the High-Frequency Range, South Winds, Stable Thermal Stratification, $0<z/L<+1.0$

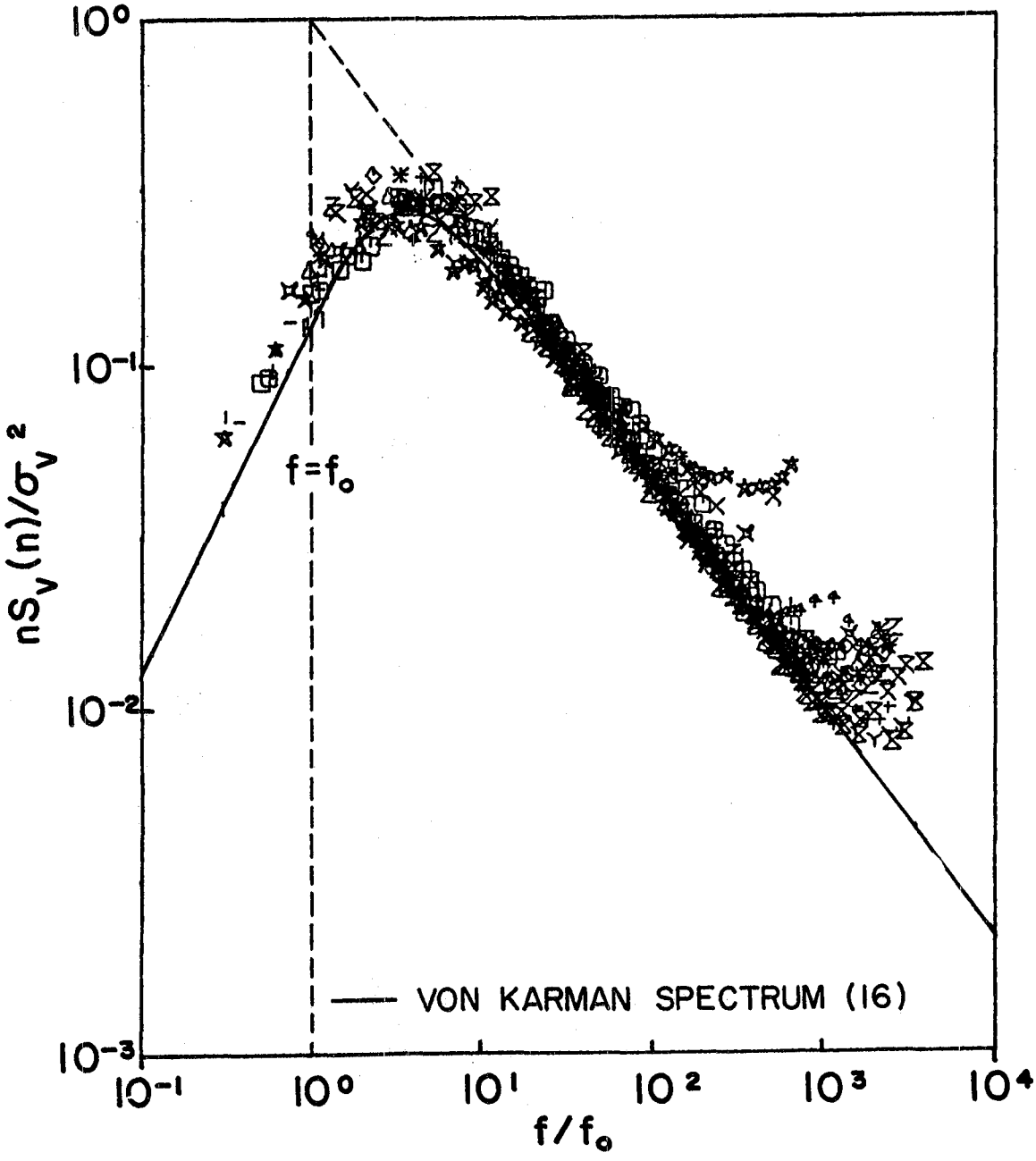

Figure 60c. Logarithmic v-Spectra Versus Modified Reduced Frequency, f/f_o, Analyzed in the High-Frequency Range, South Winds, Extremely Stable Thermal Stratification, $z/L>+1.0$

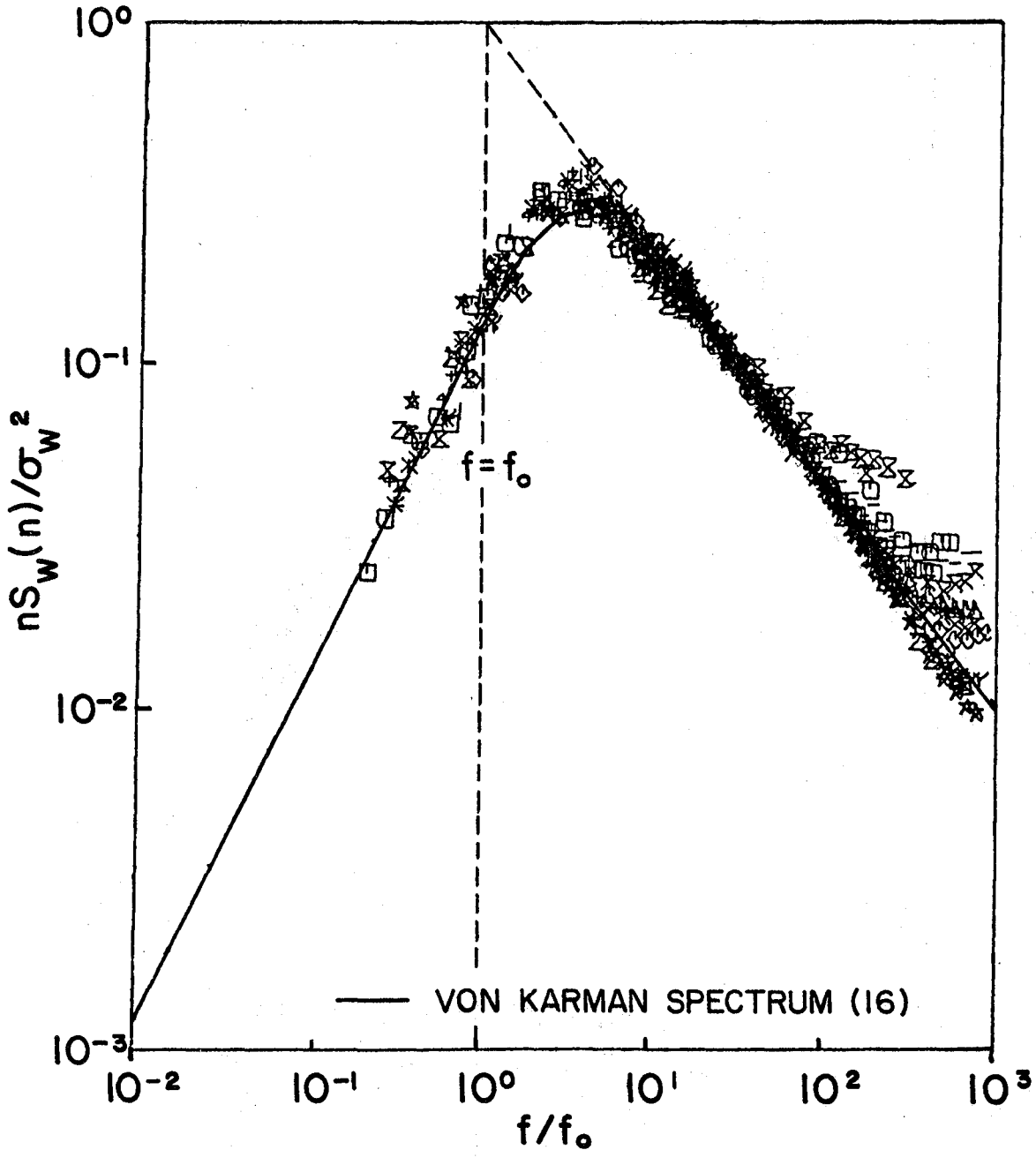

Figure 61a. Logarithmic w-Spectra Versus Modified Reduced Frequency, f/f_o, Analyzed in the High-Frequency Range, South Winds, Unstable Thermal Stratification, $-1.0<z/L<0$

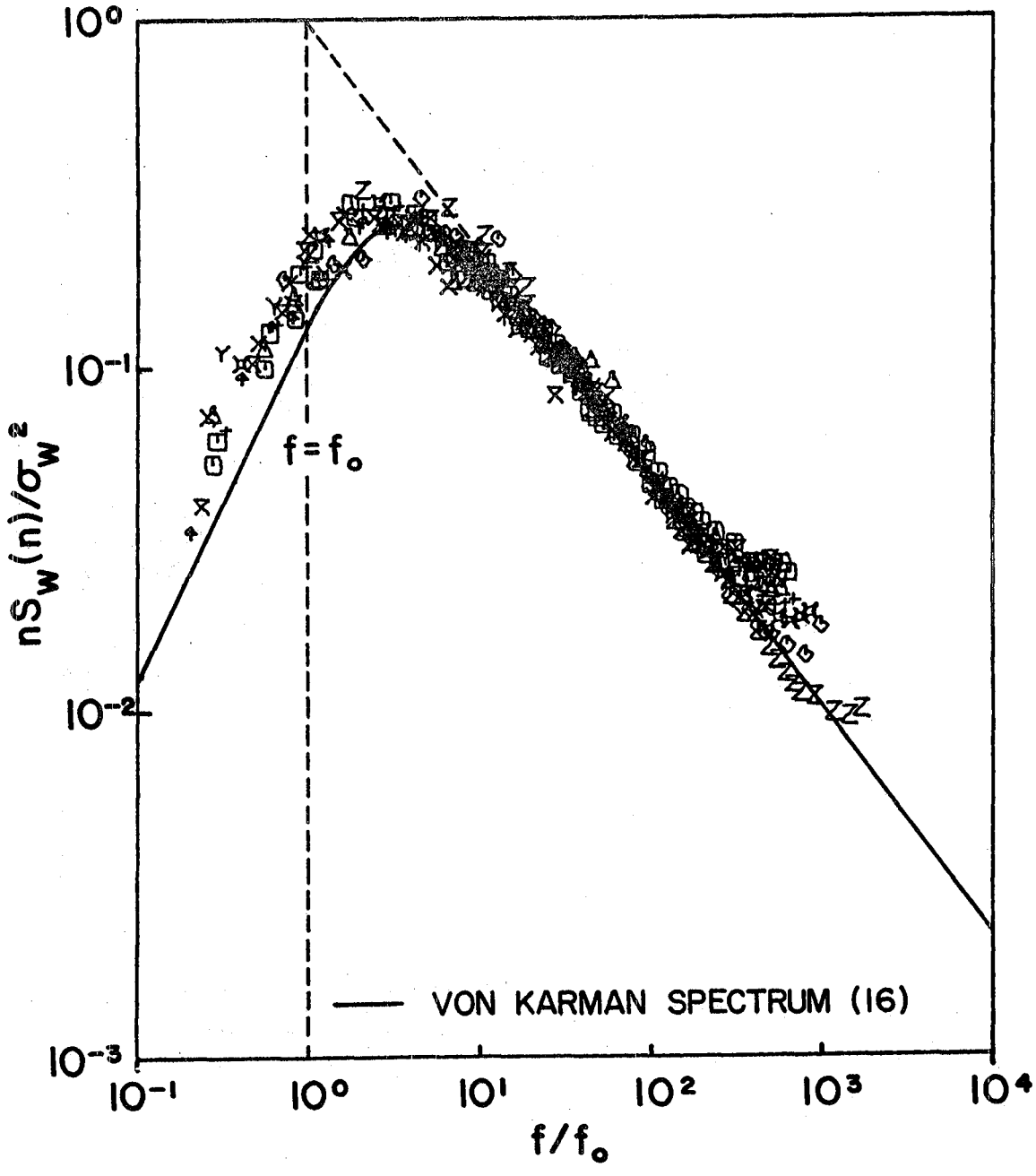

Figure 61b. Logarithmic w-Spectra Versus Modified Reduced Frequency, f/f_o, Analyzed in the High-Frequency Range, South Winds, Stable Thermal Stratification, $0<z/L<+1.0$

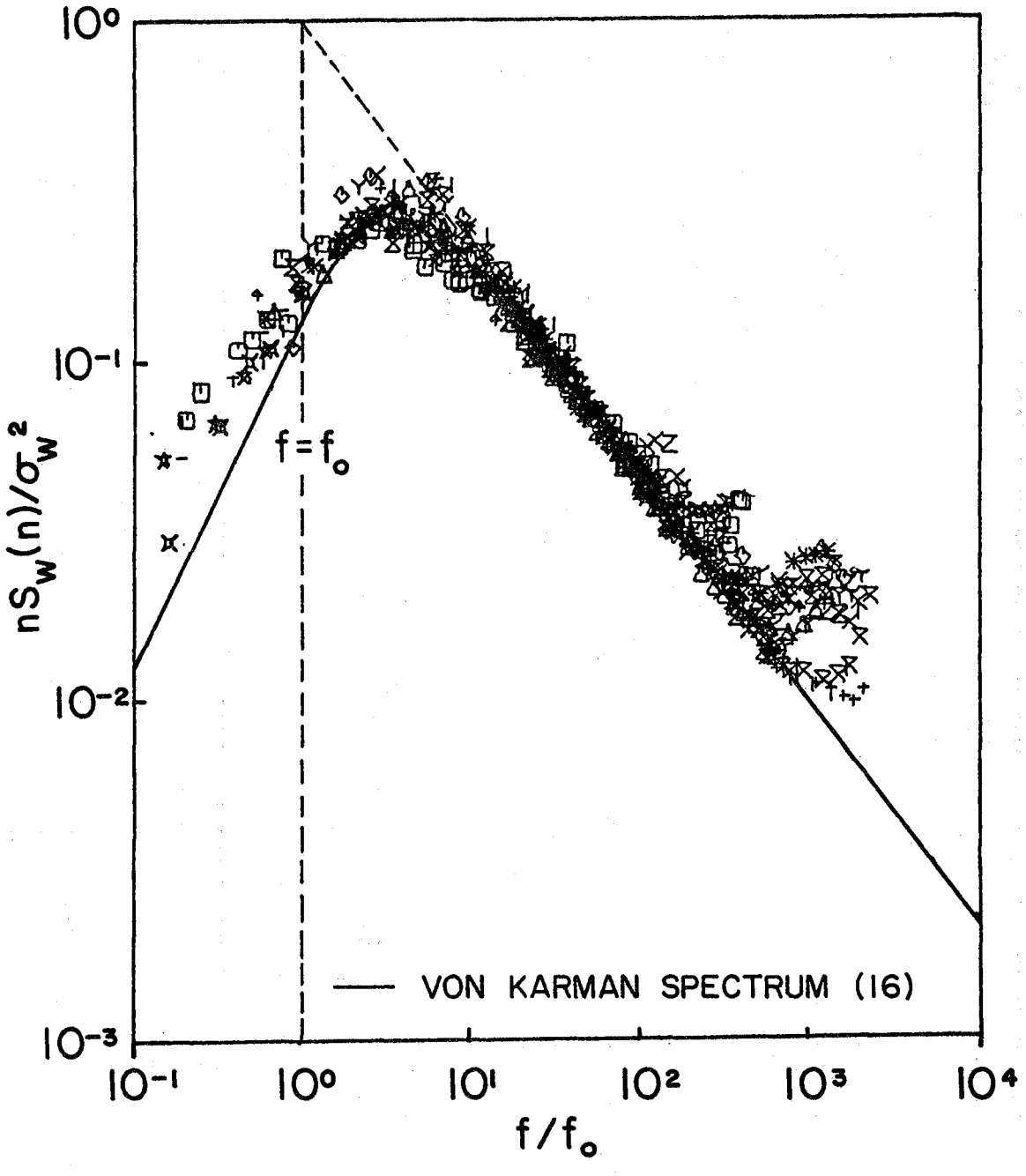

Figure 61c. Logarithmic w-Spectra Versus Modified Reduced Frequency, f/f_o, Analyzed in the High-Frequency Range, South Winds, Extremely Stable Thermal Stratification $z/L>+1.0$

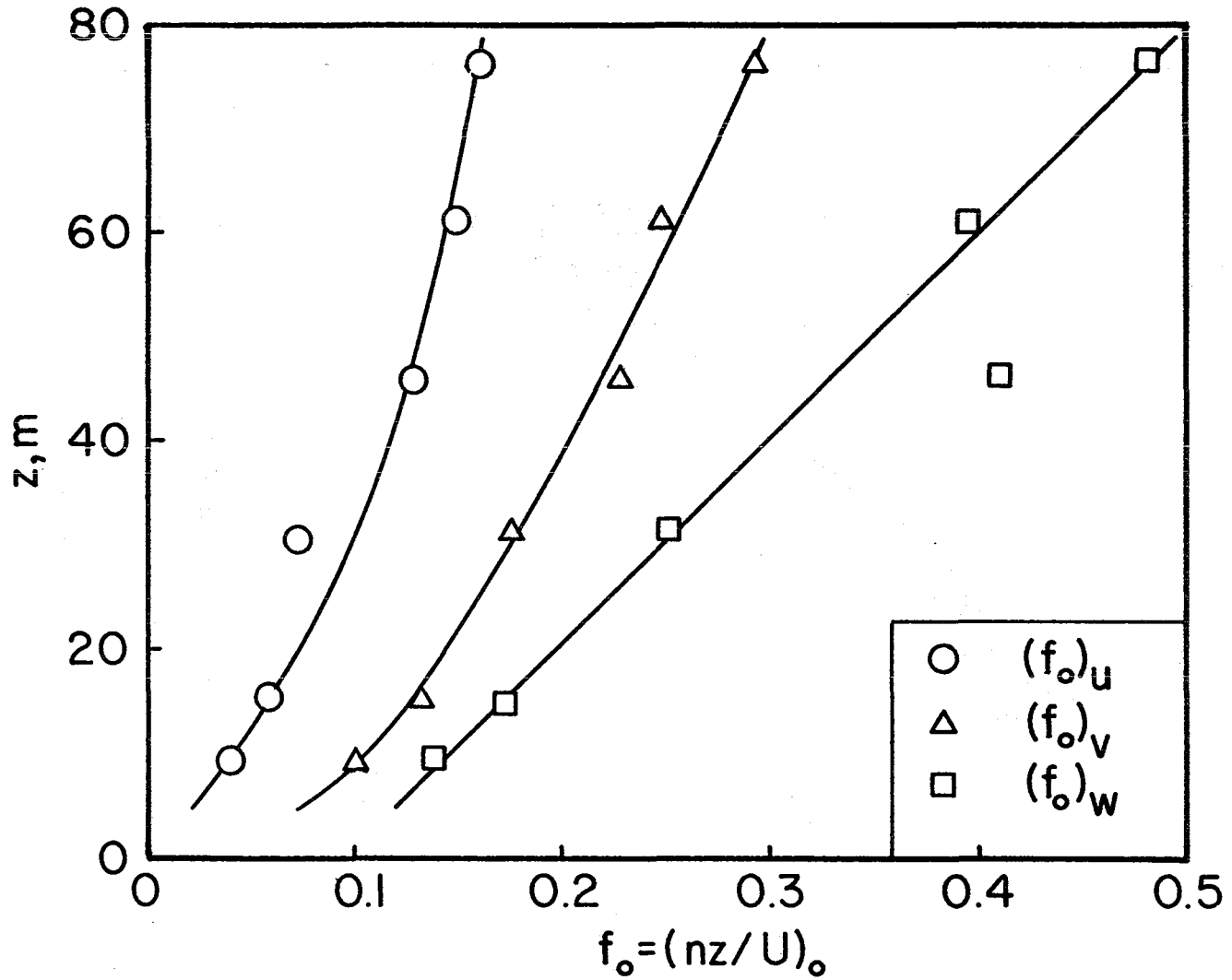

Figure 62. The Vertical Distribution of the Reduced Frequency $(f_o)_i$ with i=u,v,w for Southerly Winds. Data Analyzed in the High-Frequency Range 0.0244<n<100 Hz.

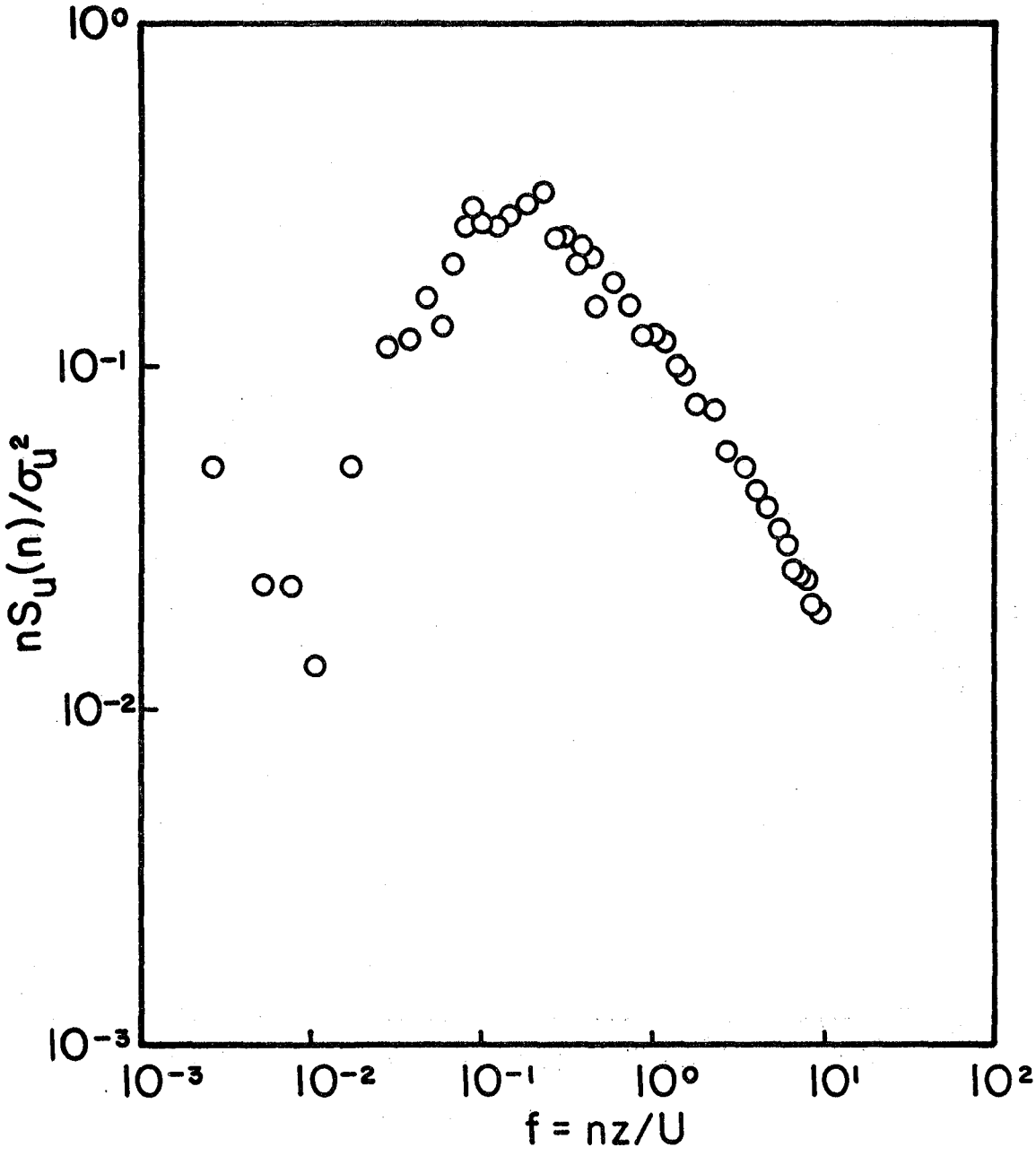

Figure 63. Logarithmic u-Spectrum Versus Reduced Frequency, Analyzed in the Middle-Frequency Range, South Wind, Record #7, z=9.14m

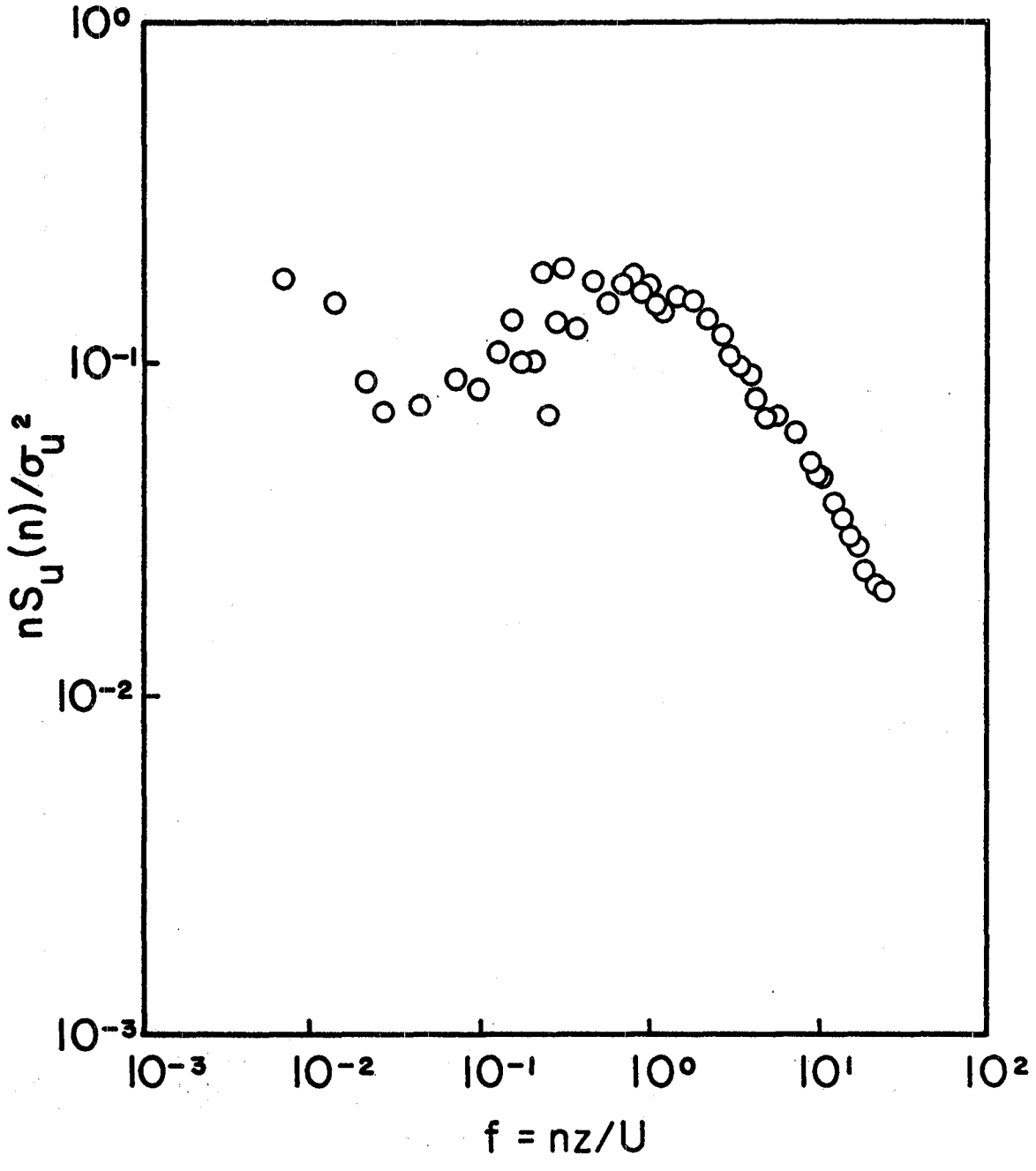

Figure 64. Logarithmic u-Spectrum Versus Reduced Frequency, Analyzed in the Middle-Frequency Range. Southwind, Record #7, z=45.7m

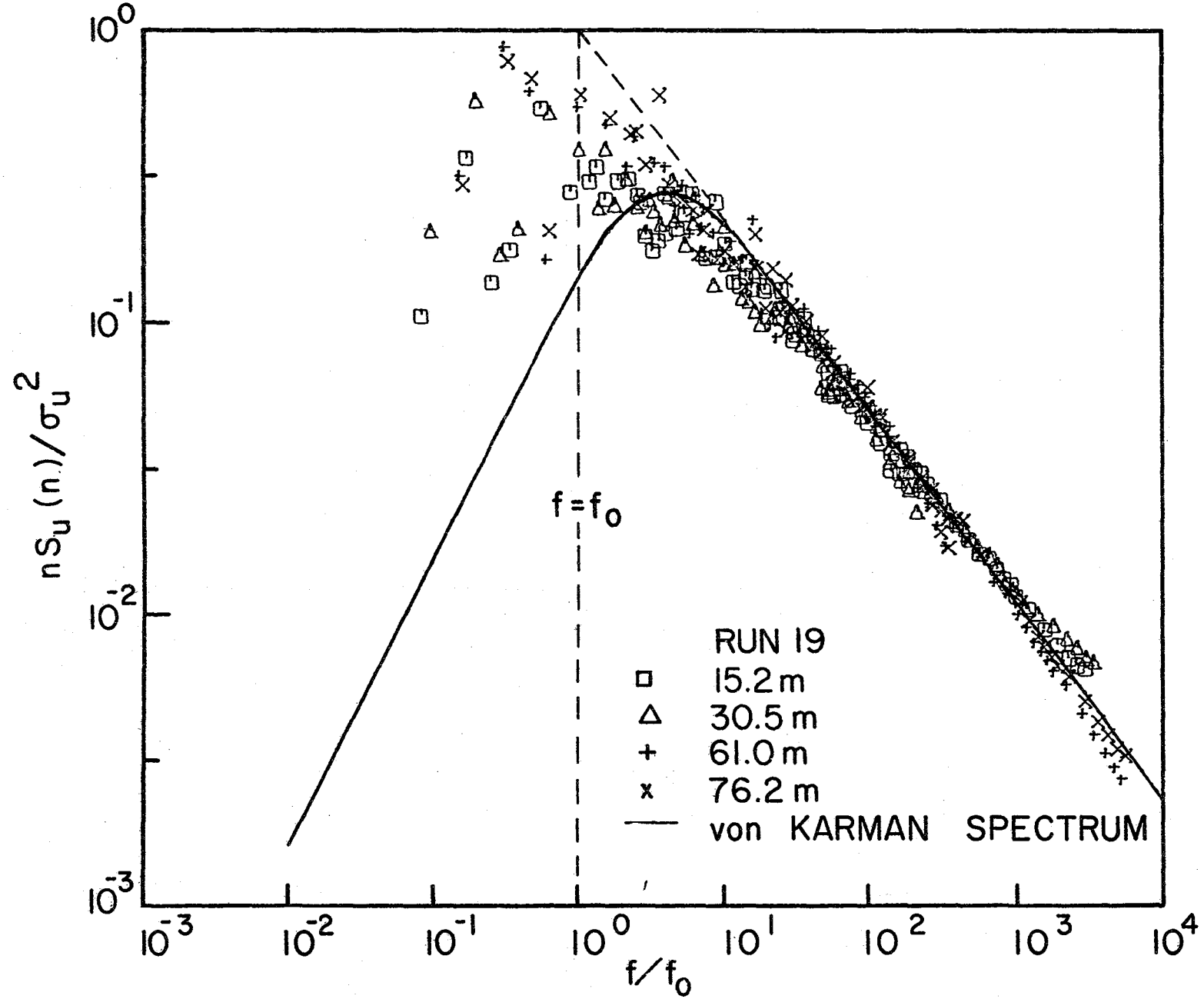

Figure 65. Logarithmic u-Spectra Versus Modified Reduced Frequency, f/f_o, Analyzed in the High and Middle Frequency Range, Northwest Wind, $\phi=301°$

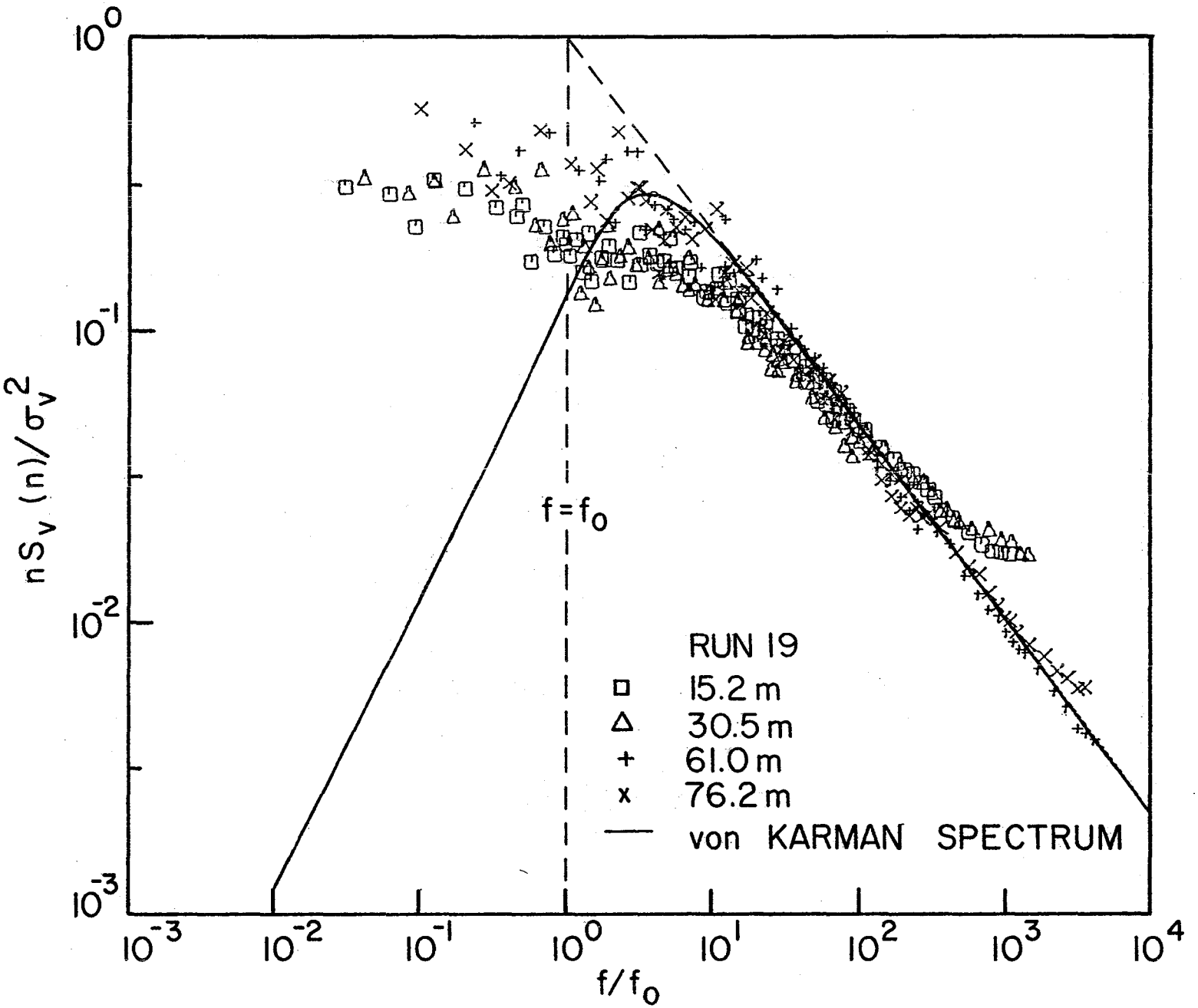

Figure 66. Logarithmic v-Spectra Versus Modified Reduced Frequency, f/f_o, Analyzed in the High and Middle Frequency Range, Northwest Wind, ϕ=301°

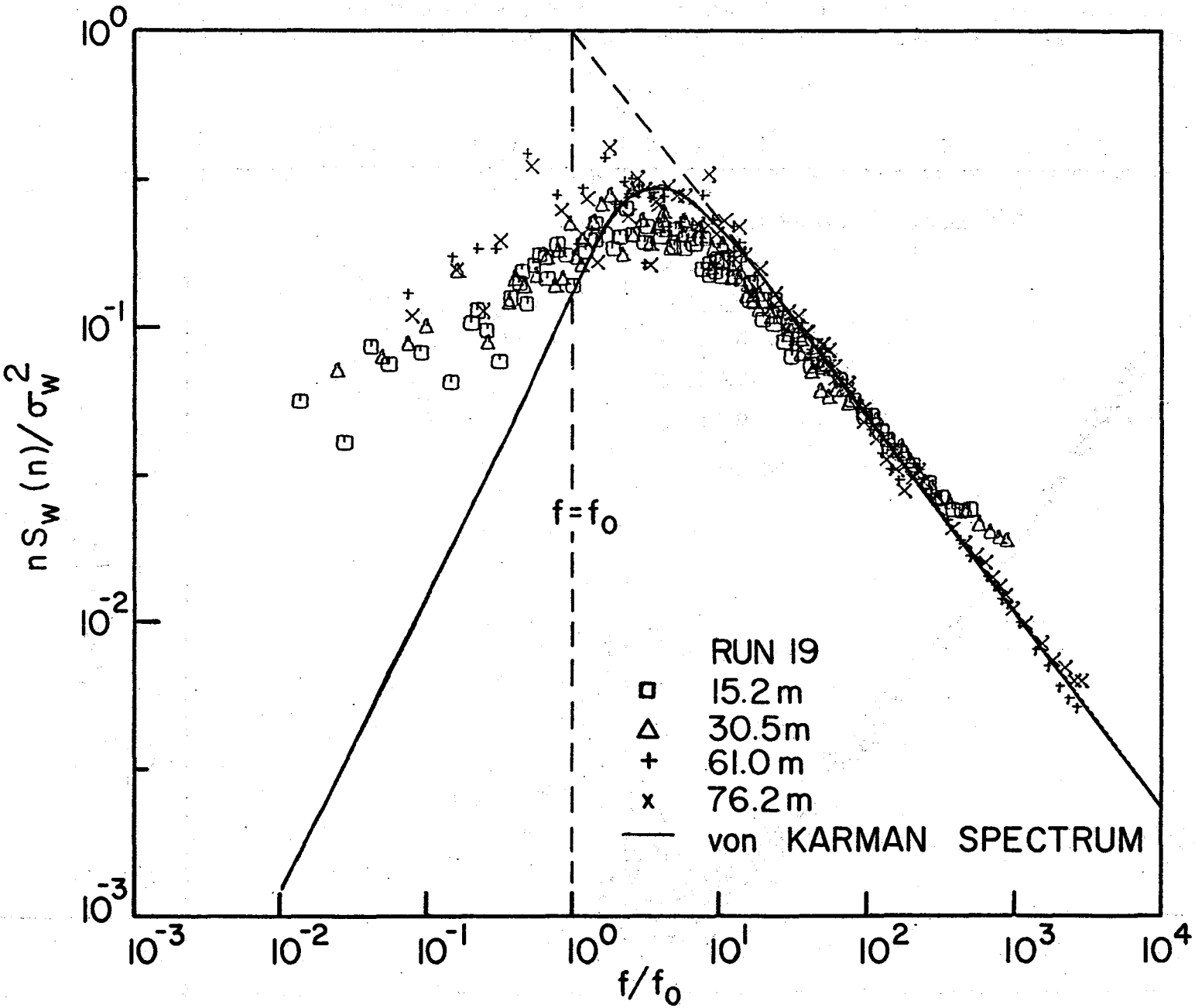

Figure 67. Logarithmic w-Spectra Versus Modified Reduced Frequency, f/f_o, Analyzed in the High and Middle Frequency Range, Northwest Wind, $\phi=301°$

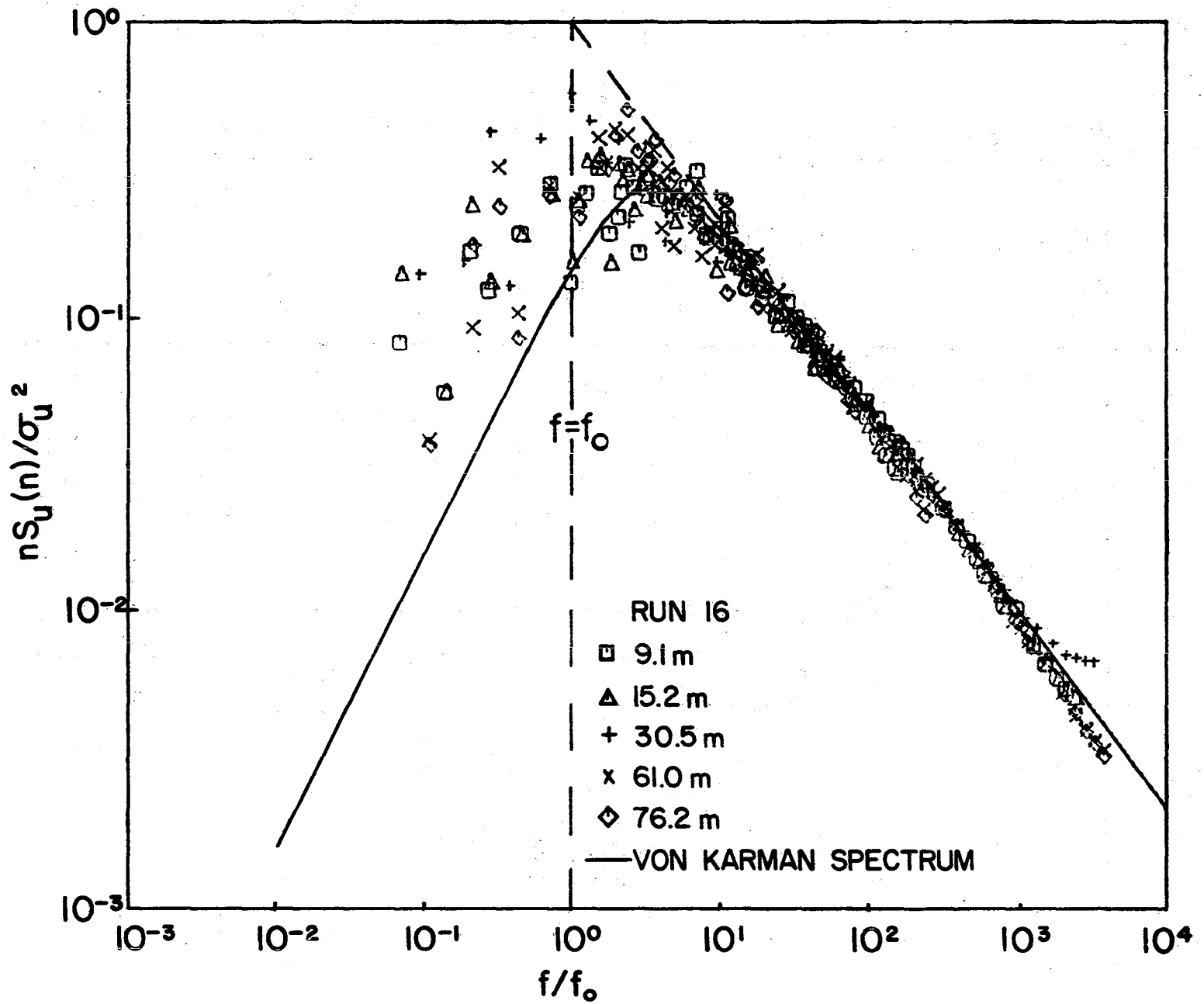

Figure 68. Logarithmic u-Spectra Versus Modified Reduced Frequency, f/f_o, Analyzed in the High and Middle Frequency Range, Evening Run, Northwest Wind, ϕ=292°

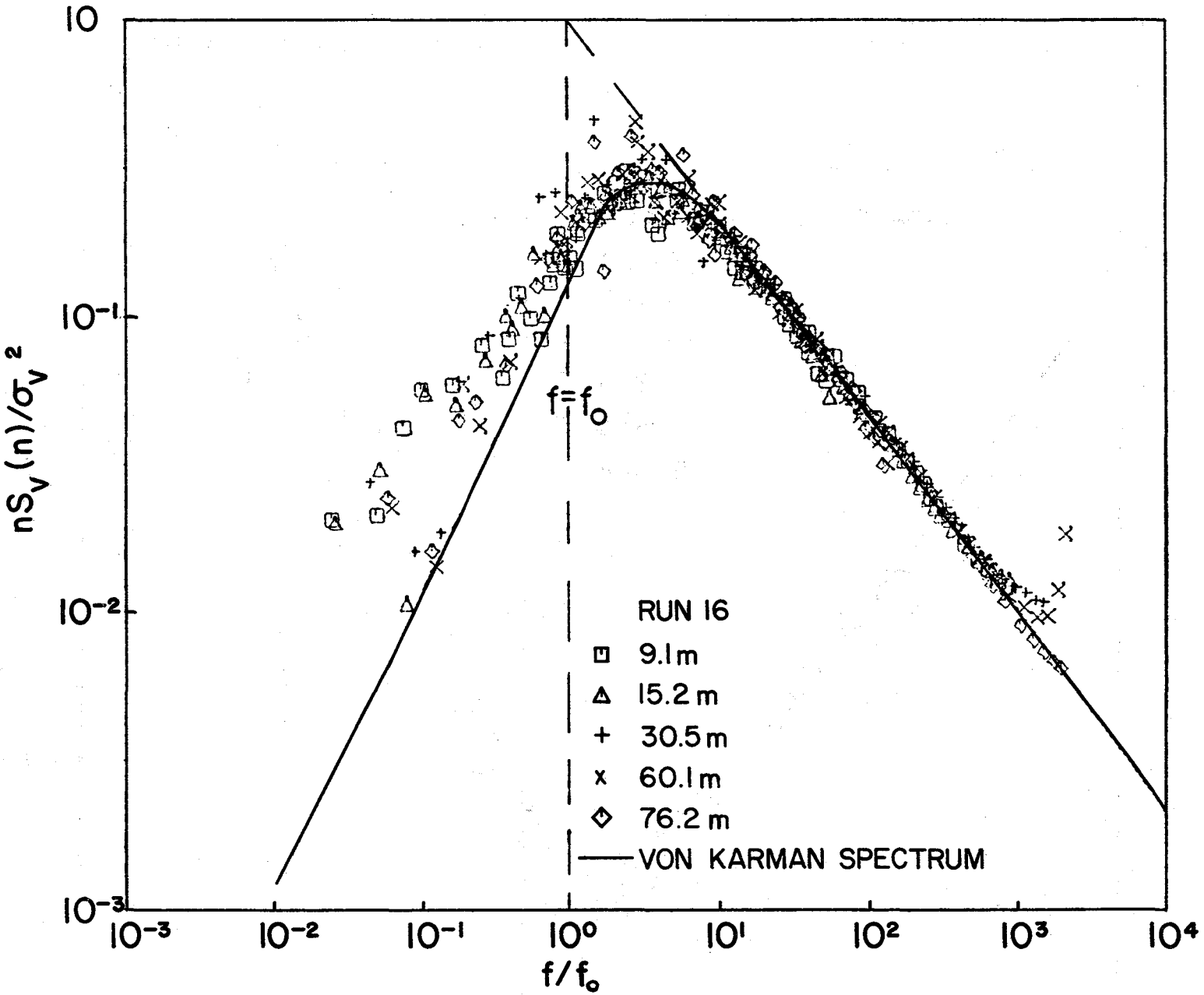

Figure 69. Logarithmic v-Spectra Versus Modified Reduced Frequency, f/f_o, Analyzed in the High and Middle Frequency Range, Evening Run, Northwest Wind ϕ=292°

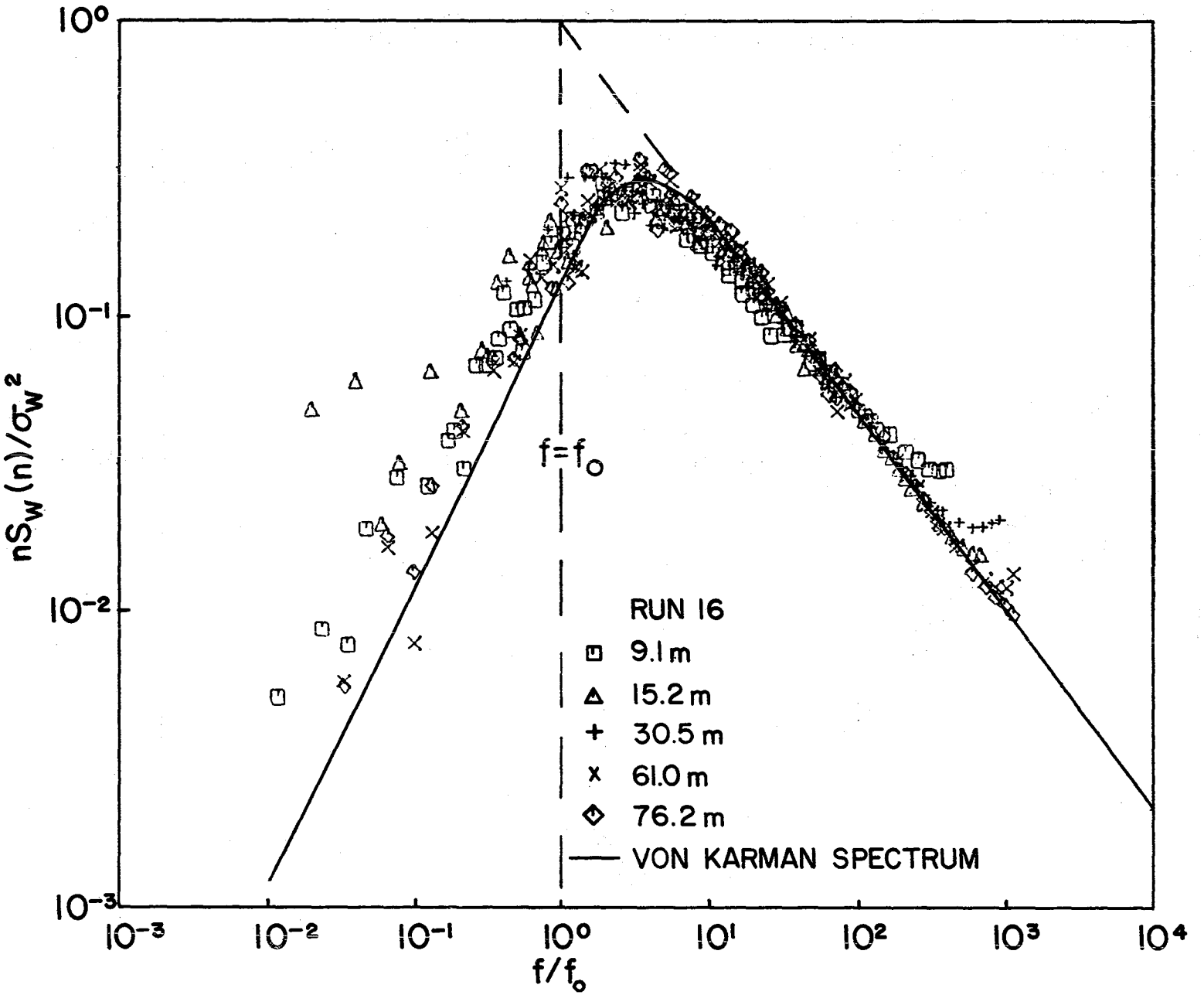

Figure 70. Logarithmic w-Spectra Versus Modified Reduced Frequency, f/f_o, Analyzed in the High and Middle Frequency Range, Evening Run, Northwest Wind, ϕ=292

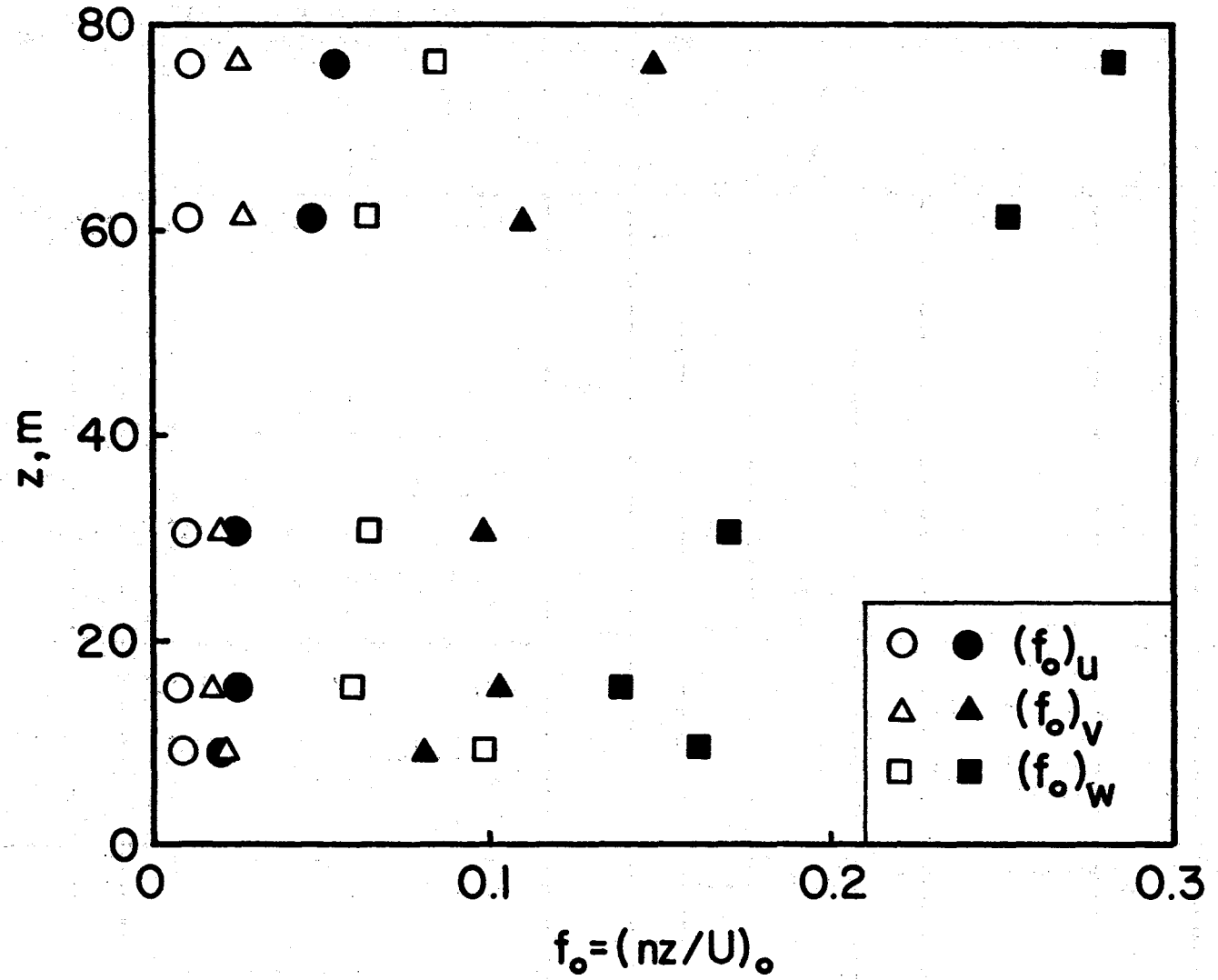

Figure 71. The vertical Distribution of the Reduced Frequency $(f_o)_i$ With i=u,v,w for Westerly Winds. Data Analyzed in the Middle-Frequency Range $0.0015<n<6.25$ Hz. Dark Symbols Denote the Data for the Evening Run 16.

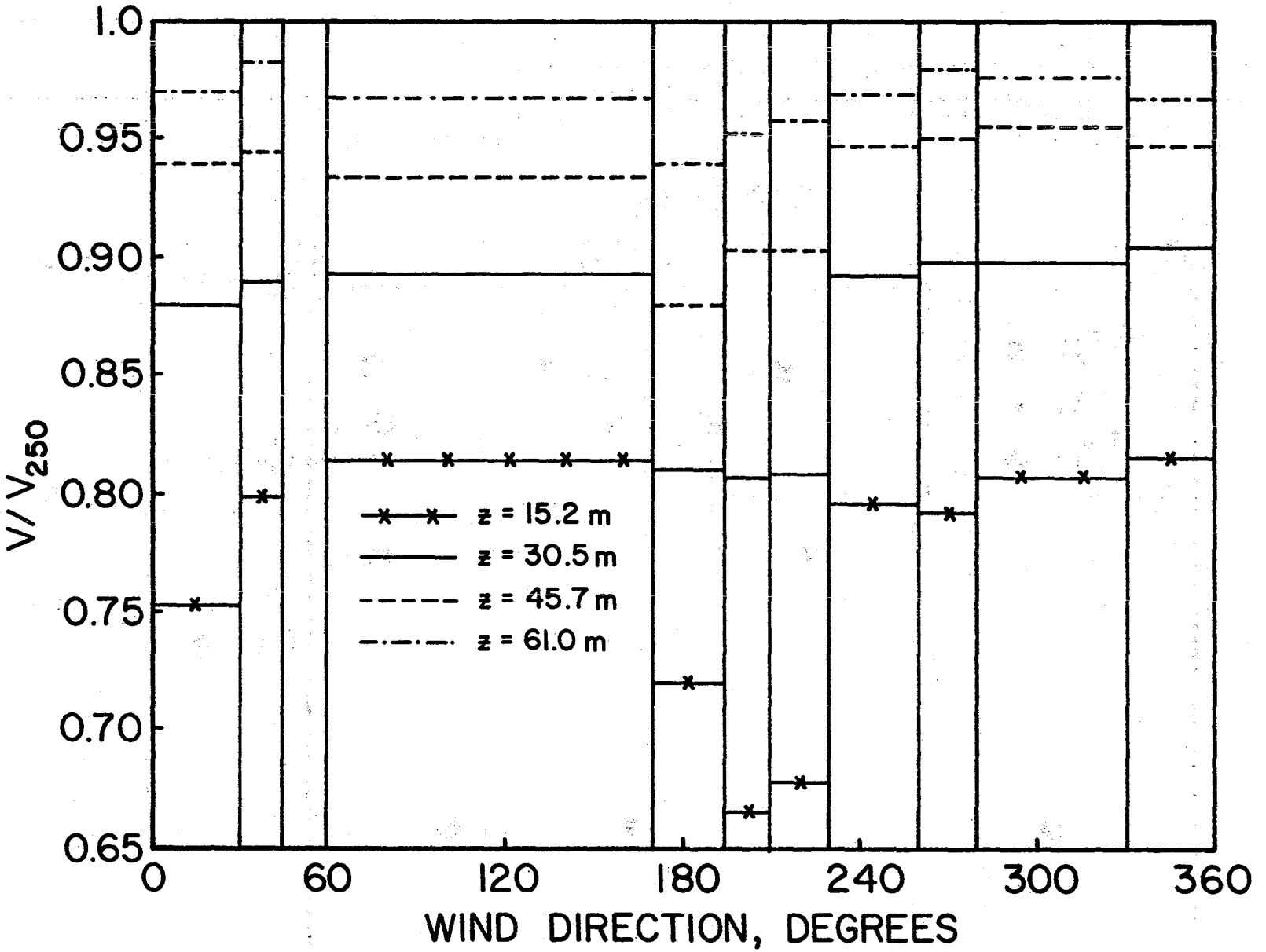

Figure 72. Average Velocity Ratios, V/V250 for Each Wind-Direction Sector with Near-Uniform Upstream Roughness (See Figure 3)

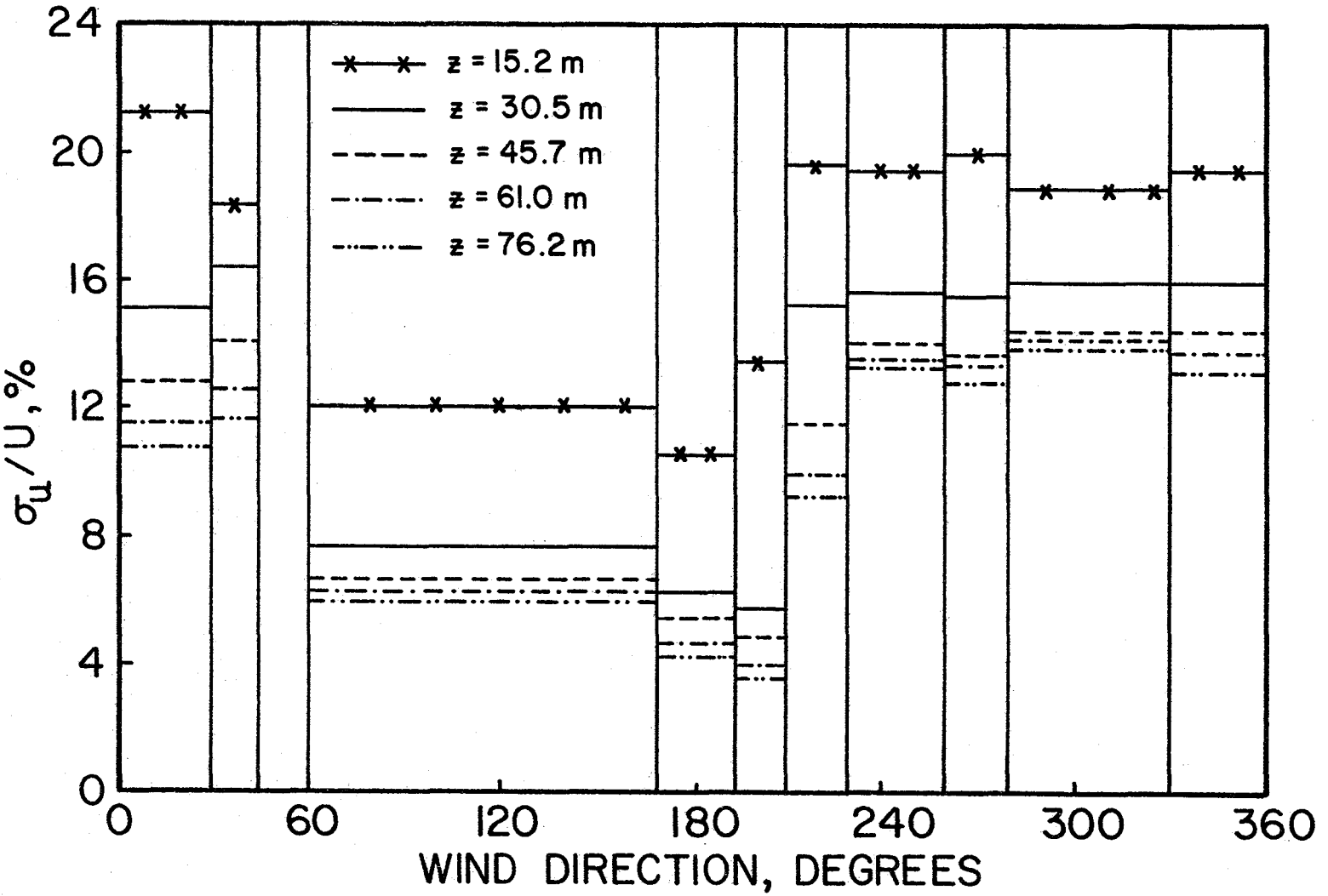

Figure 73. Average Turbulence Intensity, σ_u/U, for Each Wind-Direction Sector with Uniform Upstream Roughness (See Figure 3)

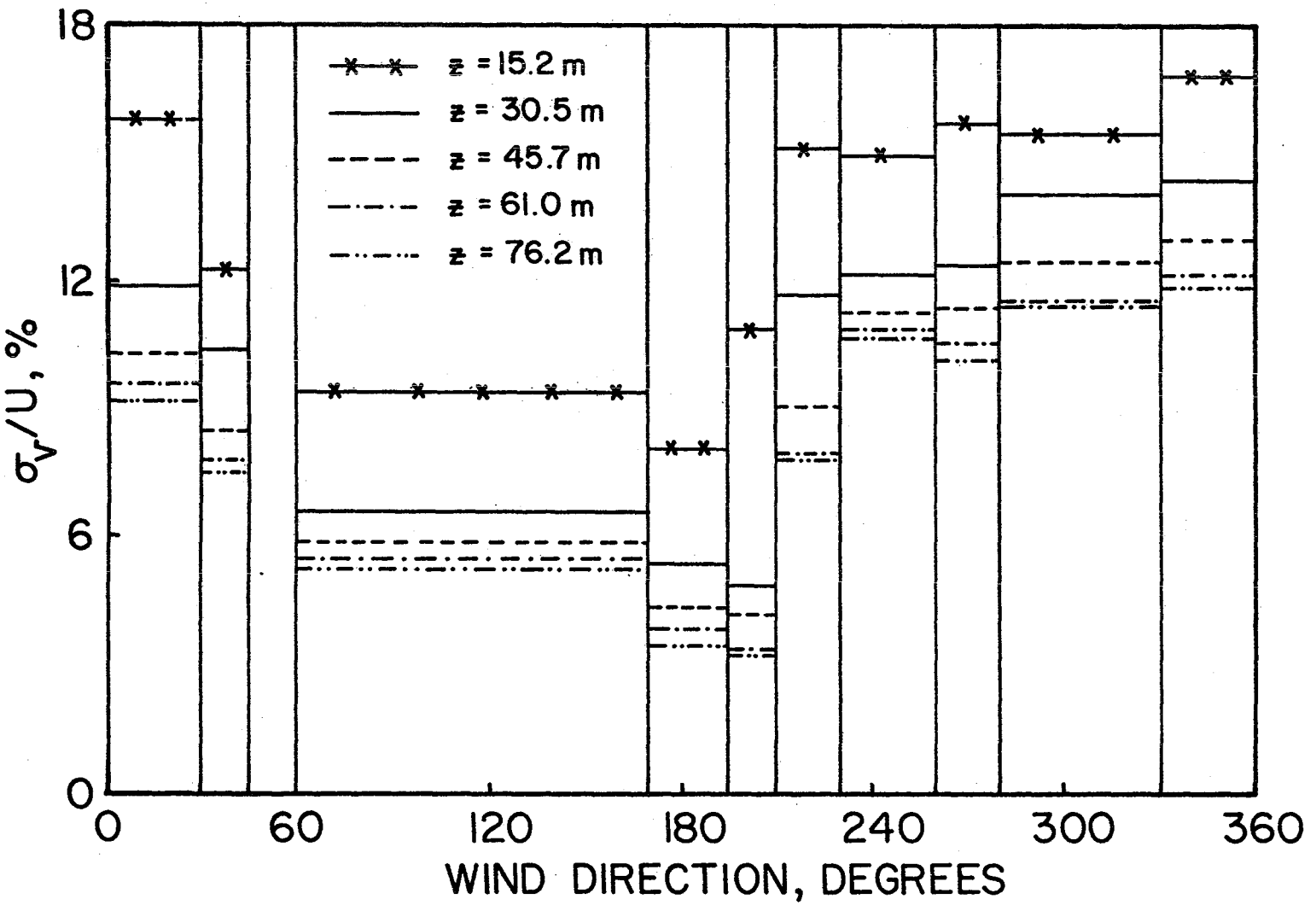

Figure 74. Average Turbulence Intensity, σ_v/U, for Each Wind-Direction Sector with Near-Uniform Upstream Roughness (See Figure 3)

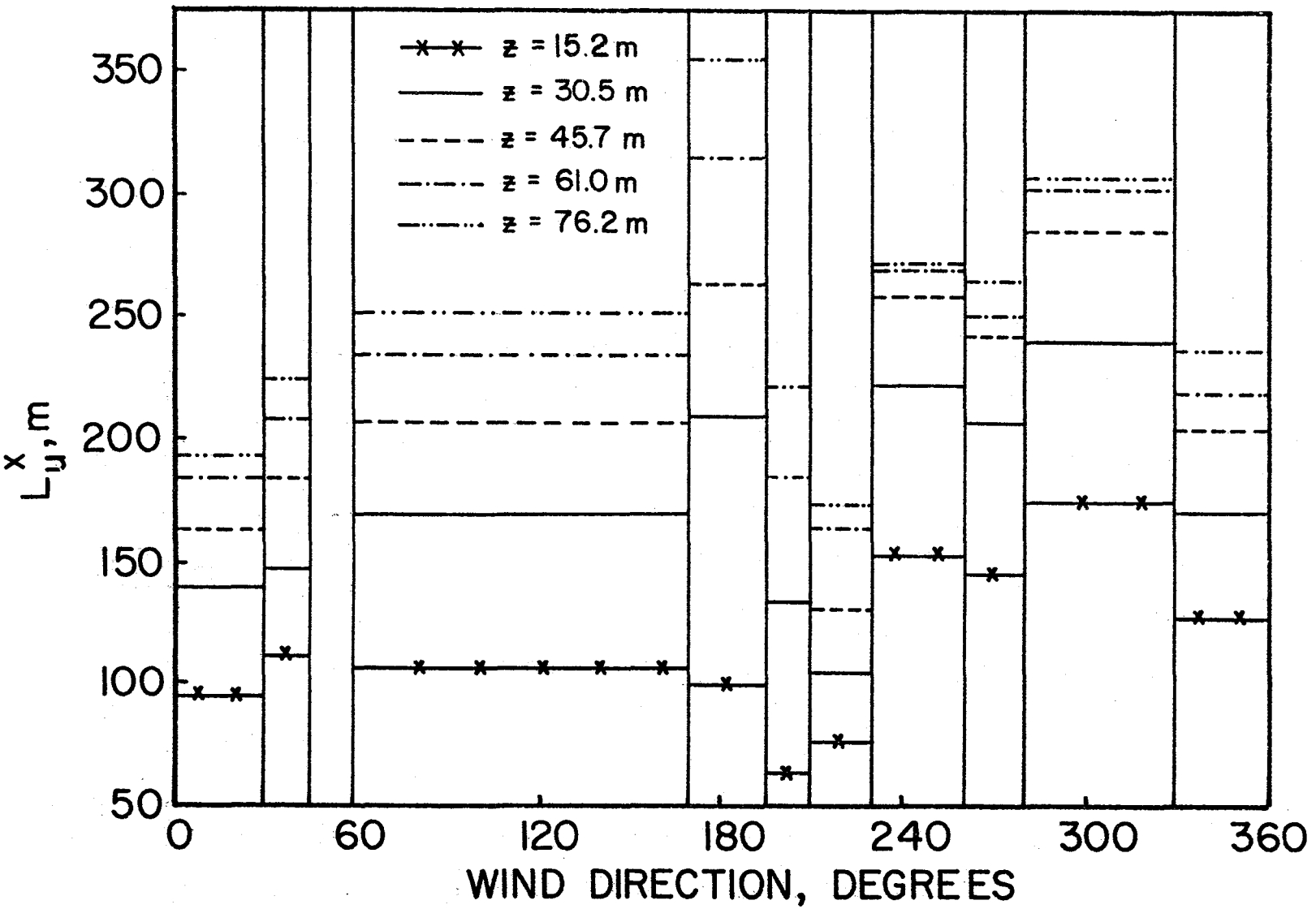

Figure 75. Average Turbulence Integral Scales, L^x_u, for Each Wind-Direction Sector with Near-Uniform Upstream Roughness (See Figure 3)

TABLES

TABLE I. Mean Profile and Turbulence Parameters for Strong Winds Over Near-Uniform Terrain

Cup-Vane Instruments

Data Record	ϕ (deg)	$\bar{U}$ (m/s) at z= 15.2m	$\sqrt{\overline{u^2}}/U_o^*$ at z= 15.2m	L_u^x(m) at 76.2m	U_o^* (m/s)	z_o (m)	α	Ri at z= 15.2m	Type of Profile	Date	Time EST or EDT
158C	241.4	13.5	2.83	303	0.81	0.019	0.131	-0.026	S	2-25-'77	12:37-13:45
158D	244.0	12.9	3.10	149	0.78	0.020	0.137	-0.026	S	2-25-'77	14:02-15:02
158E	247.0	11.6	2.84	201	0.77	0.037	0.146	-0.023	S	2-25-'77	15:02-15:53
153B	288.3	13.3	2.98	393	0.86	0.031	0.164	-0.027	S	12-21-'76	12:22-13:39
153C	291.1	12.5	3.15	420	0.81	0.031	0.146	-0.028	S	12-21-'76	14:30-15:38
153A	291.9	13.2	3.08	429	0.85	0.031	0.140	-0.028	S	12-21-'76	11:14-12:13
168D	297.9	11.4	2.50	342	0.80	0.052	0.157	-0.053	K	3-25-'77	14:12-15:46
168C	312.2	11.2	2.69	639	0.73	0.034	0.150	-0.060	K	3-25-'77	12:38-13:38
128G	316.2	16.8	2.80	191	1.04	0.023	0.136	-0.016	S	8-9-'76	17:07-18:07
128H	316.6	13.9	2.80	125	0.92	0.037	0.150	-0.021	S	8-9-'76	18:07-18:50
144A	317.8	10.9	3.15	167	0.65	0.018	0.140	-0.044	S	10-14-'76	9:58-10:58
169C	319.2	13.1	2.39	319	0.98	0.073	0.173	-0.029	K	3-31-'77	13:27-14:27
163A	323.0	10.6	2.64	201	0.69	0.030	0.152	-0.046	K	3-16-'77	10:53-12:01
169D	323.0	12.2	2.70	236	0.87	0.055	0.163	-0.035	K	3-31-'77	15:09-16:09
128F	340.0	17.1	2.50	209	1.16	0.040	0.160	-0.082	K	8-9-'76	15:08-16:25
Hot-Film Anemometers											
15	294	13.0	2.38	433	0.92	0.082	0.20	-0.039	K	3-23-'77	15:20-16:15
14	296	12.0	2.79	426	0.85	0.070	0.17	-0.040	S	3-23-'77	13:30-14:25
19	301	11.6	2.57	306	0.78	0.040	0.16	-0.046	K	3-25-'77	14:21-15:16
17	304	12.5	2.61	541	0.87	0.049	0.15	-0.041	S	3-24-'77	12:27-13:22
18	322	11.9	2.36	397	0.90	0.073	0.18	-0.025	K	3-24-'77	16:25-17:20
16	292	7.1	1.03	78	0.94	0.741	0.25	-0.0014	S	3-23-'77	20:30-21:25

Note: Type of Profile: S-single logarithmic profile, K-kink in profile.

* U.S. GOVERNMENT PRINTING OFFICE: 1981-740-145/2192

End of Document